國 立 成 功 大 學

太空與電漿科學研究所

碩士論文

National Cheng Kung University

Institute of Space and Plasma Science

Master Thesis

400 MW脈衝功率系統之開發

Development of a 400 MW pulsed-power system

研究生:鄭名城

指導教授:張博宇 博士

中華民國一百零八年七月

國立成功大學

碩士論文

400 MW脈衝功率系統之開發

Development of a 400 MW pulsed-power system

研究生：鄭名城

本論文業經審查及口試合格特此證明

論文考試委員：陳孝輝

曲宏宇

張博彥

指導教授：張博彥

系(所)主管：陳昭志

中　華　民　國　108　年　7　月　3　日

摘要

本實驗正在建置使用平行板電容庫的脈衝功率系統(Pulsed-power system using parallel plate capacitor bank，簡稱 PPCB)。平行板電容庫是使用兩個對稱的翼(Wing)的電容器所組成，目前已經建置了系統的一半，稱之南翼(South wing)。南翼的電容器使用 5 個並聯的一磚電容器(One-brick)，每一磚電容器有 0.5μF,所以共有 2.5μF。目前電容器充電至 20 kV 儲存 500 J 的能量存去做測試。平行版電容庫使用低電感的軌道間隙開關(Rail-gap switch)作為主要開關，並由馬克斯機(Marx generator)產生的快速升降的高壓脈衝訊號來觸發軌道間隙開關。

使軌道間隙開關產生多通道放電(Multichannel discharge)的觸發訊號需要有 5 kV/ns 的上升速度。我們使用多階觸發系統(Multistep-triggering system)中的三級馬克斯機(3-stage Marx generator)來產生所需要的高壓觸發源，其輸出上升(下降)速度為-7.7±1.4 kV/ns 的-40 kV 高壓脈衝訊號。

南翼放電的量測結果經曲線擬合後得到的峰值電流為 59.2 ± 0.7 kA、電流上升時間為 1280 ± 10 ns、南翼總電感為 265±2 nH（含 53 nH 負載）、軌道間隙開關的電感值為 60 ± 20 nH、瞬時功率為 363 MW，系統觸發訊號的延遲時間不準度(Jitter)為 11 ns，是小於電流上升時間的 1%。也就是說，我們可以在 1%的精度內同步即將完成的北翼和南翼。 因此，我們預計在不久的將來使用完整的 PPCB 時，可以提供峰值約為 120 kA 的脈衝電源。

關鍵字: 平行版電容庫；脈衝功率系統；軌道間隙開關；多通道放電；馬克斯機；電漿噴流

doi:10.6844/NCKU201900671

Abstract

A pulsed-power system using parallel plate capacitor bank (PPCB) is being built. Parallel-plate capacitor bank is a symmetrical structure which has two wings of capacitors connected in parallel. Half of the PPCB has been built, called the south wing. The other one is called the north wing and will be built in near future. Each wing consists of 5-brick of capacitors connected in parallel where a single brick is formed by two 1-uF capacitors connected in series. Total capacitance of the south wing is 2.5 uF. Capacitors of south wing are charged to 20 kV storing 500 J of energy. The low-inductance rail-gap switch is used. The fast-rising high-voltage pulse signal generated by the Marx generator is used to trigger the rail-gap switch.

To trigger the rail-gap switch forming the multichannel discharge, the fast trigger pulse with a rising speed > 5 kV/ns is needed. We use a 3-stage Marx generator in a multistep-triggering system to provide a high voltage trigger pulse with a falling speed of 7.7 ±1.4 kV/ns.

We have tested the performance of the south wing. The curve-fitting results showed that the total inductance of the south wing was 265 ±2 nH (with a 53-nH load), the inductance of the rail-gap switch was 60 ±20 nH and the inductance of the one-brick capacitor was 120 ±30 nH. The south wing provided a peak current of 59.2 ±0.7 kA with a rising time of 1280 ±10 ns and power was 363 ±7 MW. The jitter of the peak current respect to the trigger pulse was only 11 ns, 1% of the rise time. Therefore, we can synchronize the north wing and the south wing within the accuracy of 1% once the north wing is also constructed. Therefore, we are expecting a peak current of ~120 kA when the full PPCB is built in the near future.

Key word: Parallel-plate capacitor bank, pulsed-power system, Rail gap switch, multichannel, Marx generator, plasma jet

doi:10.6844/NCKU201900671

致謝

這本碩士論文能夠順利完成，特別感謝我的指導教授　張博宇老師。在這兩年，嚴謹紮實的實驗訓練、細心的指導實驗與口頭報告。在每一次來來回回的修改中，我與實驗室的夥伴們都在平凡的過程中有非凡的進步與成長。感謝老師豐富我的專業知識，也時時刻刻在實驗室分享人生歷程、告誡我們為人處世的眉角。有您，有更好的我們。

感謝同居同學們的互相加油打氣，特別感謝我的實驗室夥伴　陳國益，您讓我學會很多專業技能與技術，願您在北京順順利利。感謝學弟　謝知叡，您熟練的程式語言技巧，是我學習的模範。感謝老師、畢業的學長姐們與即將留美的宜霖、學妹宛儀、準新人學弟柏維，感謝您們攜手合作，讓我們在ＰＧＳ實驗室中建立起脈衝功率系統。

感謝台南的鄉親與商家，在我設計實驗室的架構與選購零件時的專業建議，感謝有您們，讓我在實驗室兩年間的進度有段脫稿的精彩演出。

感謝我的父母阿喜與阿蘭、大哥阿竣與小弟阿傑。自我南下離開故鄉，是您們支持與鼓勵，我才有機會繼續升學讀碩士，完成我的碩士學位。

doi:10.6844/NCKU201900671

Contents

摘要……………………………………………………………………..………..i
Abstract…………………………………………………………………..………..i i
致謝………………………………………………………………………..………..i i i
Content……………………………………………………………………………….iv
List of tables…………………………………………………………………vii
List of figures……………………………………………………………………….ix

Chapter 1 Introduction……………………………………………...…………1
1.1 Pulsed-power system….…………………………………………………...…1
1.2 An application of the pulsed-power system……………………..…………2
1.3 Existing components in our laboratory…………....………………………3
1.3.1 The high voltage DC power supply………………….…………4
1.3.2 The trigger pulse generator……………………………………..…5
1.3.3 Spark-gap switches……………………………………………….6
1.4 An application in our lab…...……………………………………….…………9
1.5 The goal…………………………………………………………….…….…10
Chapter 2 The pulsed-power system using Parallel-plate Capacitor Bank…...14
2.1 The Parallel-Plate Capacitor Banks (PPCB)……………….…………………..16
2.1.1 Dumped and divider resistors for PPCB……………………..…….20
2.1.2 Stands for PPCB……………………...……………………………25
2.1.3 Mylar films for the PPCB…………………………..………………26
2.1.4 Ground fence……….………….……………………….……….....…26
2.2 The south wing pulsed-power system……………………….…………………27
Chapter 3 Compressed air systems……………………………………………29
3.1 Dry air using the compressed gas cylinder…….……………………………29
3.2 A compressed gas system using a compressor…………………….…………33
Chapter 4 Pneumatic high voltage relay………………………………………37
4.1 Requirements of relays……………...…………………………………37
4.2 Design of relays……….………….……………………………………39
4.2.1 The air cylinder holder…….……………………………………40
4.2.2 The rod of the pneumatic valve………………………………………41
4.2.3 The supporting frame……………………..………………………42
4.2.4 The spring supporting frame…….………...……………………44
4.2.5 Operation of relays…………………………………………………46
Chapter 5 Multistep triggering system………………………………………47
5.1 Multistep triggering system……………………………………………47

doi:10.6844/NCKU201900671

5.1.1 The battery-powering trigger-pulse generator…………………48
5.2 The Marx generator……………………………………………………49
5.3 Optimization of the Marx generator…………………………………52
5.4 Experimental Results……………..……………………………………53
Chapter 6 The rail-gap switch testing……………………………………59
6.1 Rail-gap switches………………………………………………………59
6.2 Experimental setup……………….……………………………………64
6.3 Analysis method…………………………………………….…………67
6.4 Experimental Results…………………………………………………69
Chapter 7 The south wing pulsed power system testing…………………..……74
7.1 The south wing…………………………………………………………74
7.2 Experimental setup……………….……………………………………75
7.3 Analysis method………………………….....…………………….77
7.4 Jitter of the south wing…………………………………………………80
7.5 Summaries……………………..…………………………………86
Chapter 8 Optimization of the south wing…………………..…………………87
8.1 Shorter electrodes for the rail gap switch……………..…………………87
8.2 The design of the experiment…………….…………………….………89
8.3 Data analysis……………....……………………....…………………90
Chapter 9 The negative output of the south wing……..……..…………………94
9-1 The measurement method of the experiment…..………..…………95
9-2 The negative output result……..…………………………….….………96
Chapter 10 Summary ………………………….…………………………..…100
Bibliography…………………………………………………………………………103
Appendix…………………………………………………………………………104
A1 Circuit diagram of the trigger pulse generator...……………104
A2 Drawings of the normally open (NO) relay………………………..105
A3 Drawings of the normally closed (NC) relay…..…..………………..123
A4 Drawings of Trigatron………………………..………………..140
A5 Drawings of the round electrode…...………….…………………..148
A6 Operation of the pulsed-power system…………………….…..149
A7 Manufactures…………………………………………………...153
A8 Folder position……………………………………………..………155

doi:10.6844/NCKU201900671

A9 Picture of the discharge…………………..……..…..…………….157

doi:10.6844/NCKU201900671

List of tables

Table 1.1: Switches were a prototype made by former students in our lab [2][3]……………………………………………………………………….……...7

Table 1.2: Paschen's curve of three spark gap switches[2][3].…………..………8

Table 1.3: Expected parameter of PPCB and the south wing. And my goal is testing the south wing pulsed-power system, and capacitors are charged to 20 kV.……………………………………………………………….…………12

Table 2.1: The parameter of component and calculation methods in each component. The inductance of capacitor and rail gap switch is unknown and used assumed values.…………………………….............................…19

Table 2.2: The different situation of the south wing pulsed-power system working by each relay..………...……………………………………………22

Table 2.3: Equivalent circuit diagram and conditions in each experimental state……………………………………………………………………………23

Table 2.4: Resistance of each resister……………………………………….…25

Table 3.1: Flowmeter parameter reference table using 7000 cm^3 volume..….31

Table 3.2: Flowmeter parameter reference table using 14000 cm^3 volume…31

Table 3.3: Open operation of the flowing dry air using the cylinder..…………..32

Table 3.4: Closed operation of the flowing dry air using the cylinder..……....33

Table 3.5: Open operator of the compressor system.…………………….…….35

Table 3.6: Closed operator of the compressor system..…………………….……..36

Table 4.1: Relay status during the experiment and suitable relays..…………..38

Table 5.1: The various parameters experiments..………………………….…....53

Table 5.2: Fitting data of five times experiment and the result of an average and the standard deviation is shown..…………………………………….….………..58

Table 6.1: The discharge experiment with N-brick..…………………..………72

Table6.2: The parameter of 5-brick capacitor with a rail-gap switch..………....73

Table 7.1: The discharge parameters in each experiment and the calculated

doi:10.6844/NCKU201900671

inductance and resistance..……………………..…………………………....79

Table 7.2: Curve fitting parameters with N-brick capacitors…………………..80

Table 7.3: The rise speed and the rise time of the Marx generator in this experiment.…………………………………………..……………………...83

Table 7.4: The three delay time are shown, fitting range of P_cur is 10% to 90% of the half period.……………………………………………..……………..85

Table 7.5: The jitter by using the point P_cur which fitting range is 25% to 75% of the half period.……………………………………………..……………..86

Table 8.1: All combined experiments are tested...……………………………..90

Table 8.2: Each delay time and jitter of all experiments..…………………......90

Table 8.3: The period of RLC oscillation and the percentage of jitter in a quarter cycle those are analyzed from all experiments.…………………..…………....91

Table 8.4: The total inductance of each experiment..…………………………..92

Table 8.5: The peak current of each experiment.…………………………….....93

Table 8.6: Estimate the power efficiency and power of the south wing pulsed-power system using the average of the experimental data..……………..…...93

Table 8.7 The falling speed and the falling time in each experiment..……..…....93

Table 9.1: Analysis result of the peak current, total inductance, and Marx signal……………………………………………………………………………..98

Table 9.2: Analysis result of the delay time and jitter…………………………..98

Table 10.1: The result of the south wing..…………………………………..102

doi:10.6844/NCKU201900671

List of figures

Figure 1.1: the basic pulsed-power system. ……………………………………1

Figure 1.2: The RLC circuit……………………………………………………..2

Figure 1.3: (a) The z-pinch. (b)-(c) Process of a capillary z-pinch…………….3

Figure 1.4: Input-Output diagram of High voltage DC power system…………..5

Figure 1.5: Schematic of using the receiver and the transmitter to connect the trigger pulse generator and the function generator.[3]…………………………6

Figure 1.6: the Fundamental conical-wire arrays design of the laboratory…..…9

Figure 1.7: The using conical-wire arrays to generate plasma jets and balls with different materials [5]……………………………………………………….…10

Figure 1.8: the parallel-plate capacitor bank pulsed-power system…………..11

Figure 1.9: half of the parallel-plate capacitor bank pulsed-power system…….12

Figure 2.1: Part tree of the PPCB pulsed-power system……….……………..15

Figure 2.2: The “Brick ” design of PPCB and capacitors of one wing…..……..17

Figure 2.3: A mixing side view and circuit of the PPCB pulsed power system...18

Figure2.4: The south wing pulsed-power system with two relays to change state………………………………………………………………………………21

Figure 2.5: (a)Two different size pipes are fixed by plastic spacers. (b) After injecting the Styrofoam, press the pipe to prevent the Styrofoam from filling out. (c) The surface of the column after the Styrofoam is solidified. (d) the Styrofoam is supplied from the company of Norway……………………………………..25

Figure 2.6: Mylar layout………………………………………………….………26

Figure 2.7: The supporting frame of the grounded fence...…………………….27

Figure 2.8: The experimental setup diagram of the south wing pulsed-power system..…………………………..…………………………….…………………28

Figure 3.1: The architecture of the flowing dry air system to supply dry air for switch and Marx..………………………………………………………………29

Figure 3.2: Picture components..………………………………………………32

doi:10.6844/NCKU201900671

Figure 3.3: Air compressor is used to push relays and supply gas to the dryer…34

Figure 3.4: Air compressor is used to push relays and supply gas to the dryer. 34

Figure 4.1: Simple PPCB circuit diagram with two switches…………………37

Figure 4.2: The normally closed relay and the normally open relay..……..……38

Figure 4.3: The relay design is a combination of four parts……………………40

Figure 4.4: The constitution of the pneumatic valve holder..…………………41

Figure 4.5: The constitution of the rod of the pneumatic valve. On the left is the NO relay and on the right side is the NC relay..…………………...…………42

Figure 4.6: The constitution of the rod of the support frame. On the left is the NO relay and on the right side is the NC relay..………………………………43

Figure 4.7: Sections of two relays. (a)and(b) is section of the NO relay in different deep. (c)and(d) is section of the NC relay in different deep…..………43

Figure 4.8: The distance between two electrodes is bigger than 22.3 mm. On the left is the NO relay and on the right side is the NC relay.………………………44

Figure 4.9: The constitution of the rod of the spring support frame. On the left is the NO relay and on the right side is the NC relay..…………………………..…45

Figure 4.10: Special design of the spring frame for strong contact….…………45

Figure 4.11: NO relay and NC relay in deactivated and activated…………..…46

Figure 5.1: the operation of the multistep trigger system is shown….…………48

Figure 5.2: The trigger-pulse generator using a 24 V battery.…………………..…49

Figure 5.3: The charging and discharging of the Marx generator………………50

Figure 5.4: A Trigatron switch has a trigger pin embedded in one of the electrodes……………………………………………………………….……50

Figure 5.5: The (a) the top view of the Marx generator. (b) the circuit diagram of the Marx generator.………………………………………………………51

Figure 5.6: the pulse waveform of the Marx generator…..……………….……52

Figure 5.7: (a) The Marx with blockers. (b) Without blockers…………………53

Figure 5.8: Blocker(Red) or not blocker(Black)….……………………………55

doi:10.6844/NCKU201900671

Figure 5.9: 1 kΩ(Red) and 100 Ω(Black)..……………………………….………56

Figure 5.10: the experiment of three different gap distance..…………………56

Figure 5.11: 10 mm gap distance experiments: the data of disk is red. The data of the M8 cap nut is gray….……………………………………………………57

Figure 5.12: 18 mm gap distance experiments: the data of disk is red. The data of the M8 Nut is gray…..……………………………………………………57

Figure 5.13: the five data point used to fit the falling speed of the voltage..……58

Figure 6.1: (a)A rail gap switch has long electrodes to encourage multichannel. (b)A typical mounting arrangement for an electrically triggered rail gap.[8] 60

Figure 6.2: Schematics of the rail gap switch.…………………………………61

Figure 6.3: Relative position relationship of components in the rail gap switch.62

Figure 6.4: Spacer A with the gap distance between the knife edge and the electrode with a high voltage terminal and other gap distance are 7 mm and 14 mm……………………………………………...…………………………63

Figure 6.5: The test data of the rail gap switch with a ratio of 6 mm to 3 mm…..63

Figure 6.6: Spacer B consists of three different thickness plate. The mid palate is 5 mm, which is the same as a knife edge………………………...………64

Figure 6.7: Architecture diagram of the N-brick discharge experiment……..…66

Figure 6.8: The discharge experiment of the one-brick capacitor and the rail-gap switch. The blue data is the voltage of the capacitor. The red data is current……………………………………………………………………..…67

Figure 6.9: The transmission line……………………………………………69

Figure 6.10: The discharge experiment with the one-brick capacitor..…………70

Figure 6.11: The discharge experiment with the two-brick capacitor.…………70

Figure 6.12: The discharge experiment with the three-brick capacitor.……..…71

Figure 6.13: The discharge experiment with the four-brick capacitor…………71

Figure 6.14: The discharge experiment with the five-brick capacitor..……..…72

Figure 6.15: The average data of each experiment is used to fit the curve..……73

doi:10.6844/NCKU201900671

Figure 6.16: The peak current of each experiment……………………………73

Figure 7.1: The composition of the south wing pulsed-power system……..….75

Figure 7.2: The load consisted of 8 straight wire connected in parallel……..…75

Figure 7.3: Experimental setup to test the discharge in the south wing..….……76

Figure 7.4: The output signal of discharge experiments……………….…………77

Figure 7.5: South wing discharge experiment using the one-brick capacitor……………………………………………………………….……………78

Figure 7.6: South wing discharge experiment using the three-brick capacitor…..……………………………………………………………………78

Figure 7.7: South wing discharge experiment using the five-brick capacitor...78

Figure 7.8: The average value of the inductance obtained by each experiment and the result of curve fitting…………………………………………………79

Figure 7.9: The peak current of N-brick experiment in the south wing……….80

Figure 7.10: There are three significant waveforms in the pulse signal from the Marx generator……………………………………………….………………82

Figure 7.11: The region extremum defines two reference points. Defines the range of usage data for the third reference point…..…………………………82

Figure 7.12: The rising(falling) time and the rising(falling) speed of the Marx generator are defined……………………………………………………………83

Figure 7.13: The current data is used to define the point P_{cur}……….………….84

Figure 7.14: Each data provided 5 points and those are used to find the delay time..…………………………………………………………...………84

Figure 8.1: (a)~(c) The scar on the rail-like electrode are dense in specific locations. (d) The scar is dense on the end of the knife edge..…………….………88

Figure 8.2: Top view: The rail-like electrode with 350 mm and 300 mm and the knife edge with 300 mm…..……………………………………………………88

Figure 8.3: The round electrode and the disk electrode for the Marx generator………………………………………………………….…...…89

Figure 9.1: Setup of the negative output of the south wing..…………………94

doi:10.6844/NCKU201900671

Figure 9.2: Measuring instrument configuration diagram..............................…95

Figure 9.3: the voltage signal of the point between ‘‘Test 1’’ and ‘‘Ground.’’.…96

Figure 9.7: Trigger, voltage and current signal analysis result of the new electrode………………………………………………………………….…98

Figure 9.8: Record of delay time for each experiment…………………………98

Figure 9.9: The voltage signal of capacitors and the load……………..………99

Figure 10.1: The parallel plate capacitor bank pulsed-power system……...…100

Figure 10.2: (a) The rail-gap switch used in our lab. (b) The Marx generator used in our lab...……………………………...…………………………101

doi:10.6844/NCKU201900671

Chapter 1 Introduction

Pulsed-power system provides a tremendous power output by releasing the stored energy in a short period. The technology is widely used in medical, material science researches and semiconductor fabrication such as phase-contrast x-ray radiography, x-ray (tomographic) microscopy, EUV lithography, etc. In this chapter, we will introduce the general pulsed-power system in section 1.1. In section 1.2, an application is introduced. In section 1.3, the existing components in our laboratory: the high voltage power supply, the trigger pulse generator, three types of spark gap switches, are introduced. Those are built by former students. In section 1.4, applications in our lab in the future are introduced. In section 1.5, the goal of this thesis will be given.

1.1 Pulsed-power system

As shown in Figure 1.1, capacitors as the energy bank are charged by high voltage power supply and stored the energy over a relatively long time. When the trigger-pulse generator sends a trigger signal to activate the switch, the energy in the energy bank is delivered to the load with high instant power. A pulse forming line between the switch and the load may be used if a specific pulsed shape is needed.

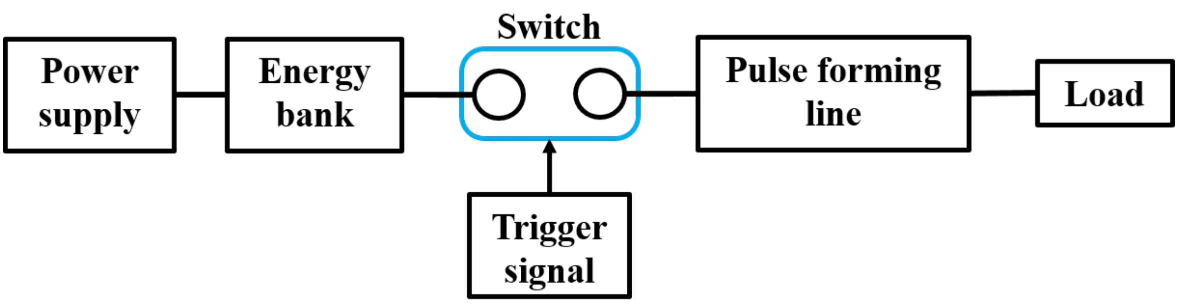

Figure 1.1: the basic pulsed-power system.

doi:10.6844/NCKU201900671

Shown in Figure 1.2 is a simplified system circuit diagram of any pulsed-power systems. The output of this simple pulsed-power system follows RLC oscillation, particularly under-dumped RLC in our case. The equation of the output current is

$$\boldsymbol{I_{(t)}} = \frac{\boldsymbol{V_{charge}}}{\sqrt{\frac{L}{C}-(\frac{R}{2})^2}} \boldsymbol{e^{-\frac{R}{2L}t}}\ \boldsymbol{sin}\ [(\sqrt{\frac{1}{LC}-\left(\frac{R}{2L}\right)^2})\boldsymbol{t}].$$

It shows that the amplitude and the frequency are determined mostly by the capacitance and inductance of the system. The amplitude is inversely proportional to the $\sqrt{L/C}$ and the frequency is inversely proportional to $\sqrt{LC}$ for R→0. It is used to control the characteristics of the energy to fulfill the electrical requirements of the load.

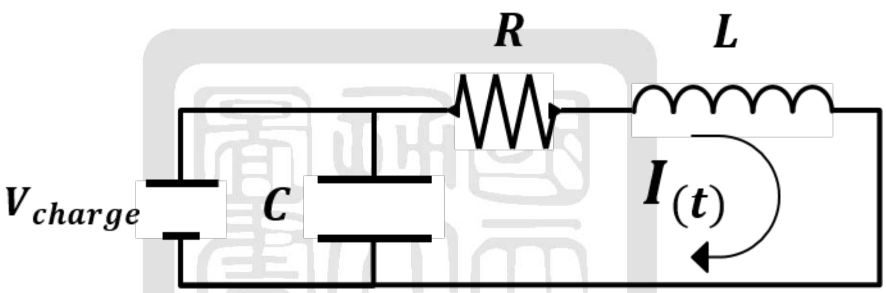

Figure 1.2: The RLC circuit.

1.2 An application of the pulsed-power system

Pulsed-power systems are experimental platforms for many applications. One of them is to generate a soft x-ray laser using a capillary z-pinch. When a high current flows through preionized gas, magnetic fields in the azimuth direction are generated as shown in Fig 1.3(a). The plasma is pinched, compressed, and heated due to the Lorentz force in the radial direction. It is called a z-pinch. If the gas is pinched in a relatively long capillary, as shown in Fig 1. 3(b)-(d), the plasma which acts as a pumped gain media can be compressed uniformly along the capillary reaching a high temperature in the order 100s eV using a pulsed current of 23 kA with a pulse width of 120 ns [1]. If argon gas is used, Ne-like Ar lasing at 46.9 nm [1], which is

doi:10.6844/NCKU201900671

in the range of soft x ray, can be generated in the hot plasma. Therefore, a soft x-ray laser in both ends of the capillary is implemented. It can potentially be used for x-ray (tomographic) microscopy, EUV lithography, etc.

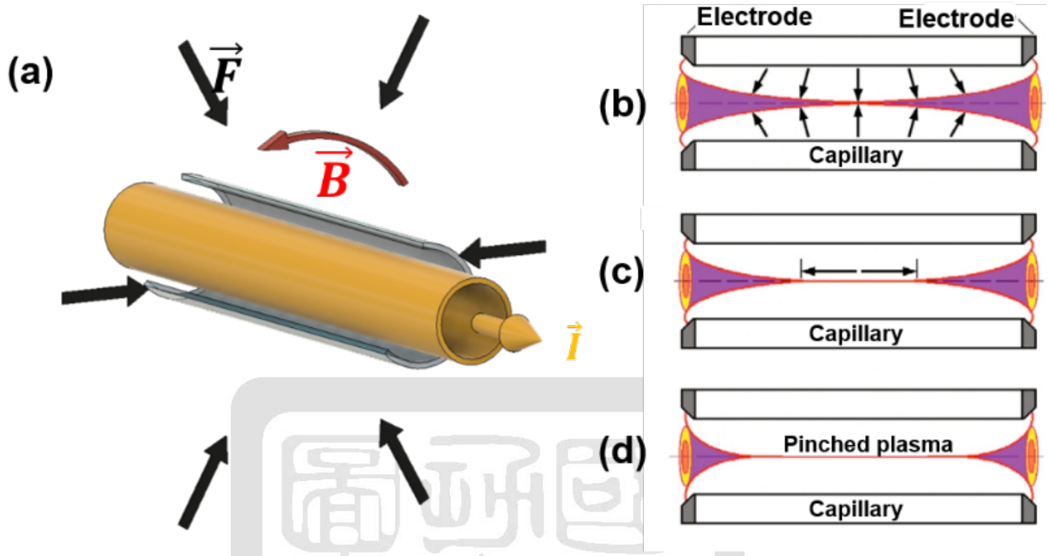

Figure 1.3: (a) The z-pinch. (b)-(c) Process of a capillary z-pinch.

1.3 Existing components in our laboratory

To build a pulsed power system, we have developed a high voltage DC power supply, a trigger-pulse generator and three different kinds of spark gap switch in our laboratory. The high voltage DC power supply is used to charge capacitors. The trigger-pulse generator is used to generate a high voltage pulse signal to trigger the spark gap switch. Three different kinds of switches were developed in the laboratory with different shape of electrodes. The Paschen's curves of these switches were measured. I will use those switches in a Marx generator for a fast trigger-pulse generator introduced in Chapter 5.

doi:10.6844/NCKU201900671

1.3.1 The high voltage DC power supply

The high voltage DC power supply system was built and used to charge capacitors in our pulsed-power system. For details, please refer to Reference [3]. This system consists of a low voltage DC power supply[DC-5050A], a pulse generator [SPIK2000A-03], a transformer [500-30k-02] and a voltage doubler. The input-output diagram is shown in Figure 1.4.

The low voltage power supply provides a low voltage DC current with a voltage up to 500 V and a power up to 2500W to the pulse generator. The pulse generator converts the DC current to AC pulses. The voltage of pulses is multiplied 60 times by the transformer, i.e., the amplitude up to 30 kV. Finally, the output voltage is doubled and rectified to a high voltage DC current by the voltage doubler with a voltage up to 60 kV. The power range of the transformer is 1500 W so that the whole system can provide a 60 kV DC current with limited power at 1500 W.

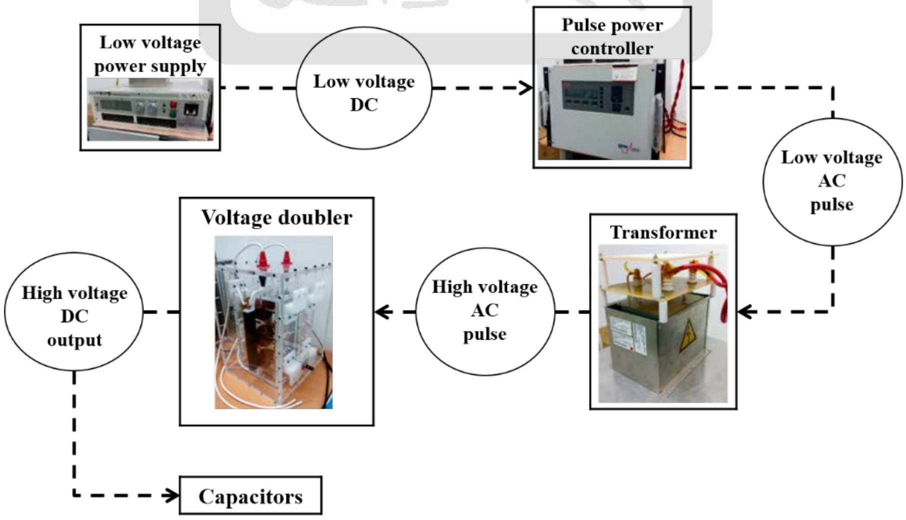

Figure 1.4: Input-Output diagram of High voltage DC power system.

doi:10.6844/NCKU201900671

1.3.2 The trigger pulse generator

The trigger pulse generator provides a -17 kV pulse with a rise time of 55.0 ± 0.4 μs. It was developed by former student Mei-Feng Huang. We found that an electromagnetic pulse (EMP) is generated after the spark gap switch is discharged. Reverse currents which are generated by the activation of the spark gap switch may flow back to our function generator. In either case, our function generator was toasted during the discharge.

Therefore, the former student Sheng-Hua Yang built an optical system in the trigger pulse generator to protect the upstream instruments. As shown in figure 1.5, the TTL signal from the function generator is converted to an optical signal by the transmitter and propagate, through a fiber. The optical signal is converted back to the electrical signal for triggering the trigger pulse generator.

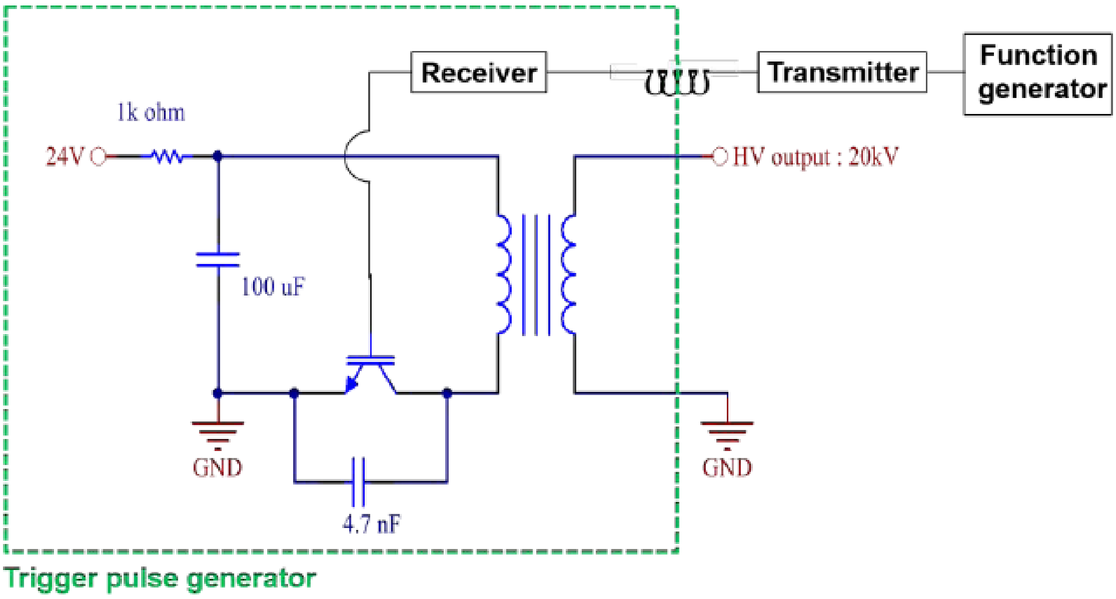

Figure 1.5: Schematic of using the receiver and the transmitter to connect the trigger pulse generator and the function generator.[3]

doi:10.6844/NCKU201900671

1.3.3 Spark-gap switches

The spark gap is a high voltage switch which consists of two electrodes in a cavity filled with gas. Two electrodes with gap in between can hold the high voltage so that no current can flow through the gap. In this case, it is open. If the voltage between the electrodes is high enough, the gas is ionized between the gap. This ionized gas is forming a path to generator a lightning-like arc, which we call a “breakdown.” The voltage when the breakdown occurs is called the “breakdown voltage.” At this moment, the switch is closed. Therefore, controls of the breakdown phenomenon of the spark gap switch can be used as a high voltage switch.

The main factors influencing the breakdown voltage are the gas pressure and the gap distance between two electrodes. It is described by Paschen's curve expressed as[4]

$$\mathrm{V} = \frac{apd}{\ln(pd) + b}$$

where p is the gas pressure, d is the distance of the gap, and both a and b are constants. These constants are related to gas composition.

There are three different kinds of spark gap switches in our lab as shown in Table 1.1 Those switches were a prototype made by former students in our lab, Mei-Feng Huang and Sheng-Hua Yang[2][3]. The electrode of the fundamental self-breakdown switch uses the M8 cap nut with gas of nitrogen or air. Other shapes of electrodes are the same, called the disk electrode. Either brass or stain less steel were used. We are now fixed on using stainless steel, SUS304 particularly.

We will use the M8 cap nut and the disk electrode in the Marx generator so that Paschen's curve of those, as shown in Table 1.2, will be used for setting gap distance of each spark-gap switch of on the Marx generator.

doi:10.6844/NCKU201900671

Table 1.1: Switches were a prototype made by former students in our lab [2][3].

	The fundamental self-breakdown switch	**The self-breakdown switch**	**The controlled breakdown switch**
Top view	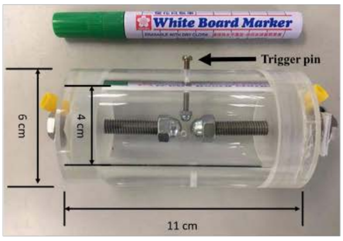	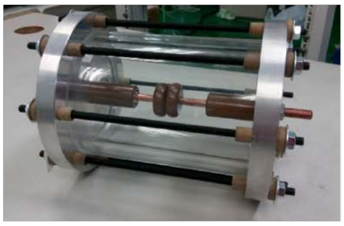	
Electrode	M8 Round head cap nut is used.	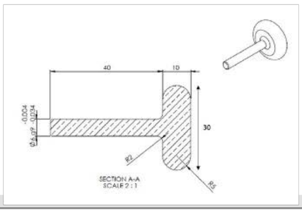	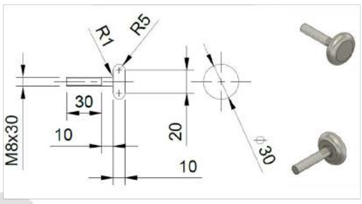

doi:10.6844/NCKU201900671

Table 1.2: Paschen's curve of three spark gap switches[2][3].

	Discharge characteristics
The fundamental self-breakdown switch	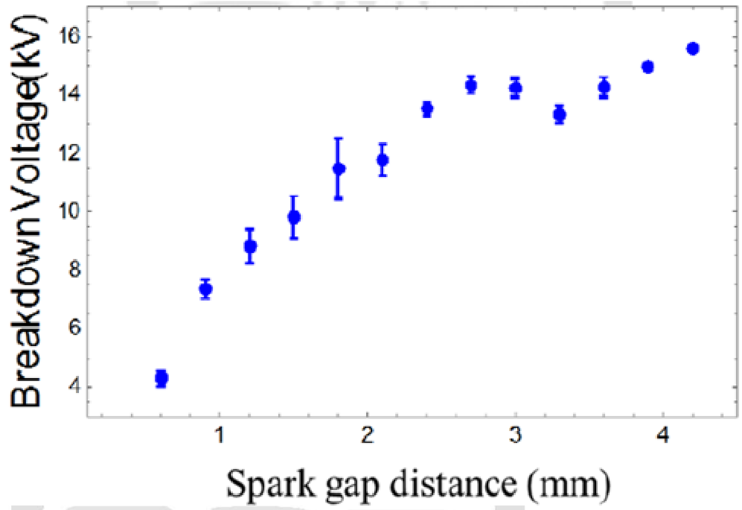
The self-breakdown switch	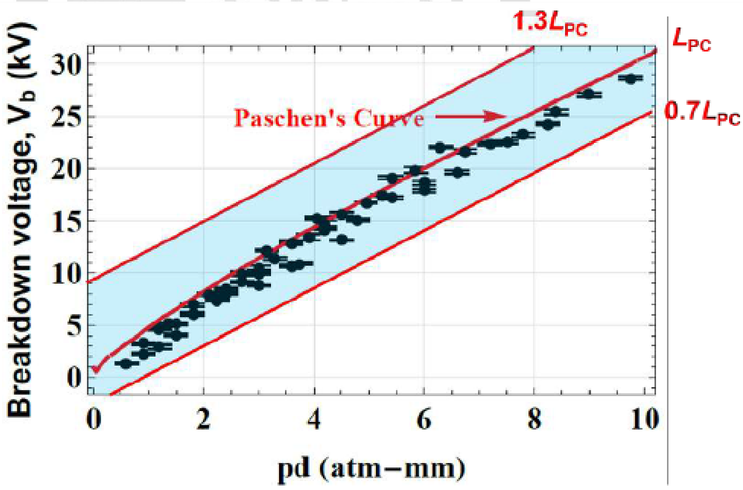
The controlled breakdown switch	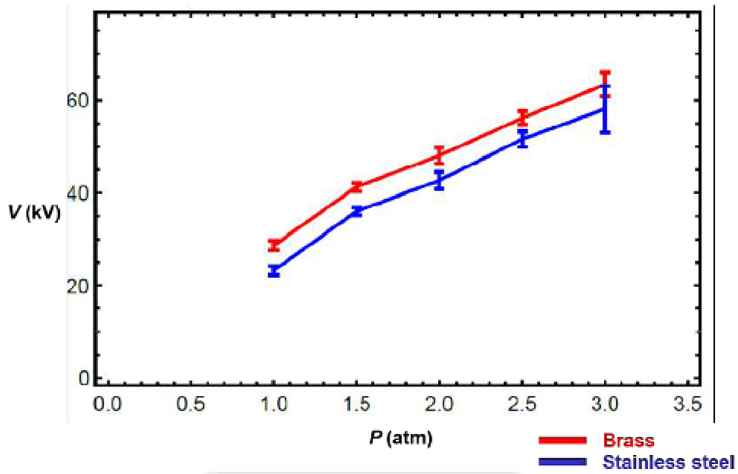

doi:10.6844/NCKU201900671

1.4 An application in our lab

There are many applications using a pulsed-power system. Because the soft x-ray introductanced in section 1.2, we also plan to conduct other experiments on the system. The pulsed-power system is an excellent platform to study plasmas in astrophysics events. It can be used to generate supersonic plasma jets which occurred in astrophysical environments. One application in our lab is to simulate interactions of solar winds with the plants where solar winds can be simulated by plasma jets. To generate supersonic plasma jets, conical-wire arrays is used to be the load in the pulsed-power system, as shown in Figure 1.6. It will be the project of junior students in our lab.

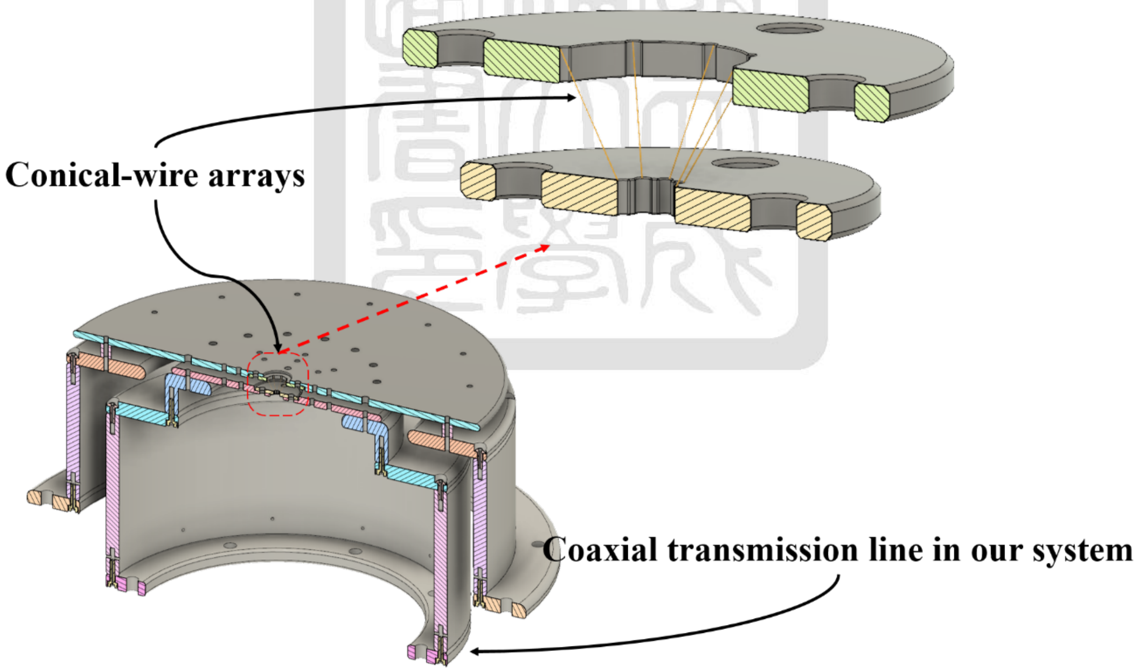

Figure 1.6: the Fundamental conical-wire arrays design of the laboratory

An obstacle on the path of the supersonic plasma jet will be used to simulate a planet. Three different materials will be used for the obstacle to simulating the Earth, Moon, and Mars. The insulated ball will be used to simulate the Moon. The

doi:10.6844/NCKU201900671

conductive ball will be used to simulate the Mars. A small magnet will be used to simulate the Earth. As shown in Figure 1.7, research of interactions between supersonic plasma jets and three balls with different materials will be conducted for simulating interactions between solar winds and planets in the experiments.

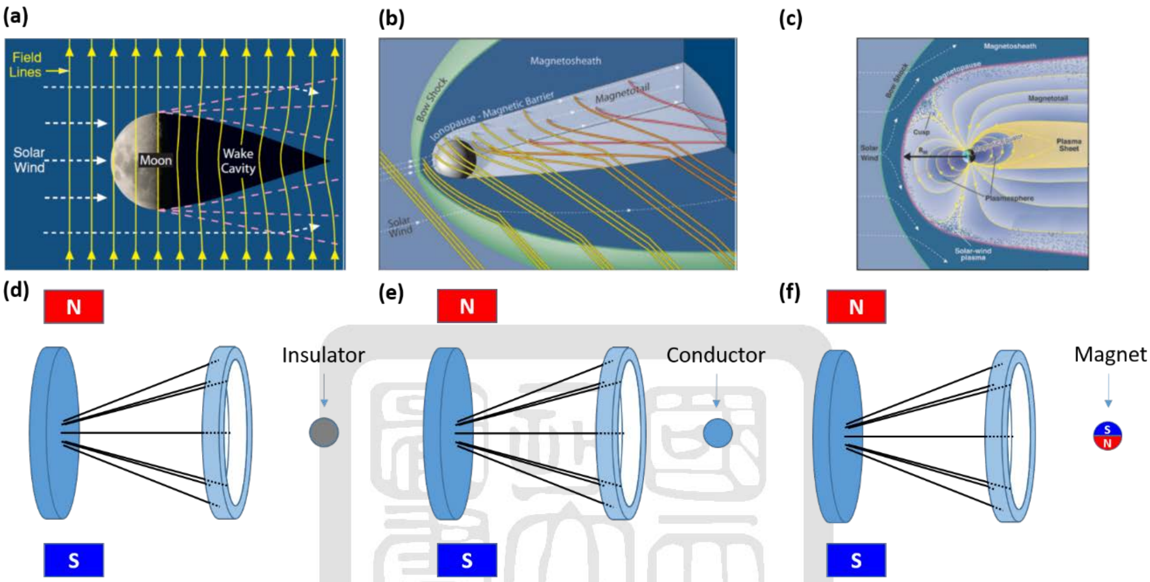

Figure 1.7: The using conical-wire arrays to generate plasma jets and balls with different materials to simulate the interaction between solar winds and planets[5]

1.5 The goal

The pulsed-power system being built is shown in Figure 1.8. Capacitors were charged to 20 kV right now and the voltage will be raised to 50 kV in the furture. That the total capacitance and the stored energy of the system are 5 μF and 6.25 kJ when it is charged to 50 kV. The estimated rise time and the output peaking current are ~1.3 us and ~300 kA, respectively.

The whole system is divided into two identical parts, called a single wing,as shown in Figure 1.8 and1.9. One single wing, the south wing, particularly, will be built first.

doi:10.6844/NCKU201900671

As shown in Table 1.3, the total capacitance of the south wing is 2.5 μF. When capacitors are charged to 20 kV, the energy of the south wing is 500 J. The estimated rise time and the output current are ~1.3 us and ~60 kA, respectively. After the south wing is built, the north wing will be built so that PPCB is completed and an expected total current of 150 kA is delivered. Once the charging voltage is raised to 50 kV, the system will be operated under full specifications. In this thesis the goal is to build the south wing.

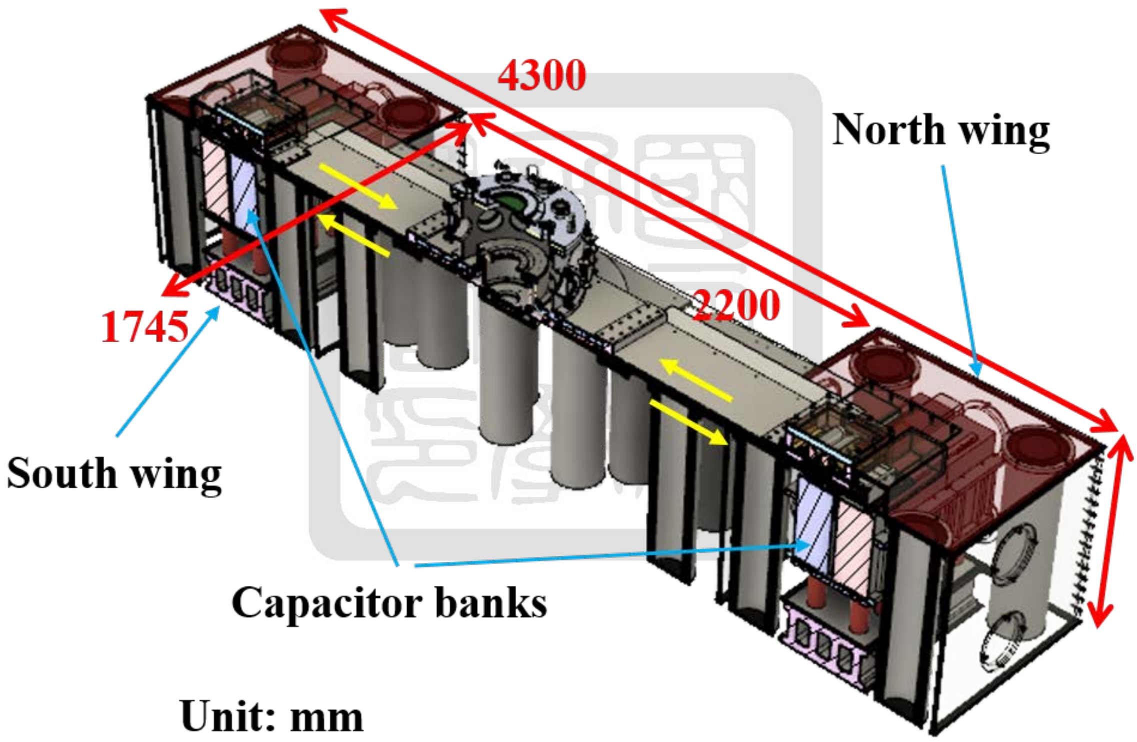

Figure 1.8: the parallel-plate capacitor bank pulsed-power system.

doi:10.6844/NCKU201900671

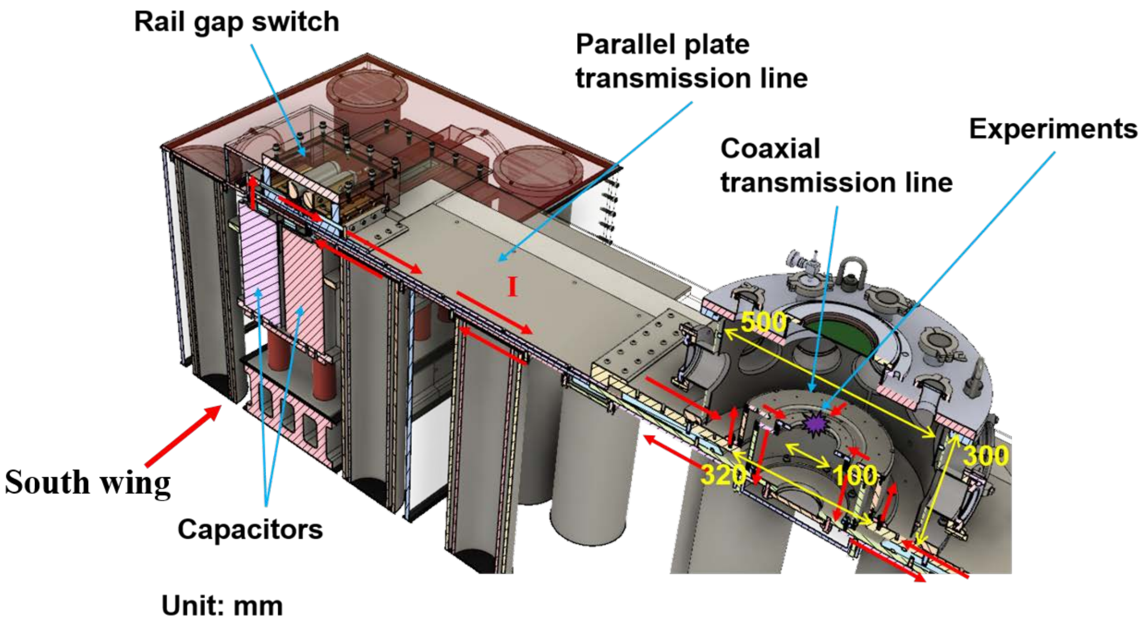

Figure 1.9: half of the parallel-plate capacitor bank pulsed-power system.

Table 1.3: Expected parameter of PPCB and the south wing. And my goal is testing the south wing pulsed-power system, and capacitors are charged to 20 kV.

	South wing	PPCB	
# of capacitor	10	20	
Capacitance/each	1 uF	1 uF	
Total Capacitance	2.5 uF	5 uF	
Voltage	20 kV	20 kV	50 kV
Total energy	0.5 kJ	1 kJ	6.25 kJ
Rise time	1.3 us	1.3 us	
Peak current	~75 kA	~150 kA	~300 kA
Power	~0.4 GW	~5 GW	~ 0.8 GW

This thesis is structured as following. In chapter 2, the organization and construction of PPCB are introduced. In chapter 3, the compressed air systems for the PPCB pulsed-power system are introduced. In chapter 4, the homemade relays for PPCB are introduced. In chapter 5, the fast trigger pulse generator for triggering the

doi:10.6844/NCKU201900671

rail-gap switch is inducted. The rail-gap switch is introduced in chapter 6 and shows the discharge of the rail-gap switch with N-brick capacitors. In chapter 7, we test that the discharge of the fast trigger pulse generator and the rail gap switch are connecting with the south wing pulsed-power system. In chapter 8, we optimize the south wing for smaller jitter. The summary is concluded in Chapter 9.

doi:10.6844/NCKU201900671

Chapter 2 The pulsed-power system using Parallel-plate Capacitor Bank

We are building a pulsed-power system using the parallel plate capacitor bank(PPCB). Shown in Figure 2.1 is the part tree of PPCB showing all components it contents. The small pulsed-power system in the multistep triggering system and the high voltage DC power supply have been built by the senior students in the laboratory. Those devices will be reviewed in this chapter.

In section 2.1, the composition and design of PPCB are introduced. We built stand supports the system and the grounded fence surrounding the system ourselves. They are introduced in section 2.2 and section 2.3, respectively. In section 2.4, Mylay layout is introduced. Finally, the south wing of PPCB which is being built in this work is shown in section 2.2.

doi:10.6844/NCKU201900671

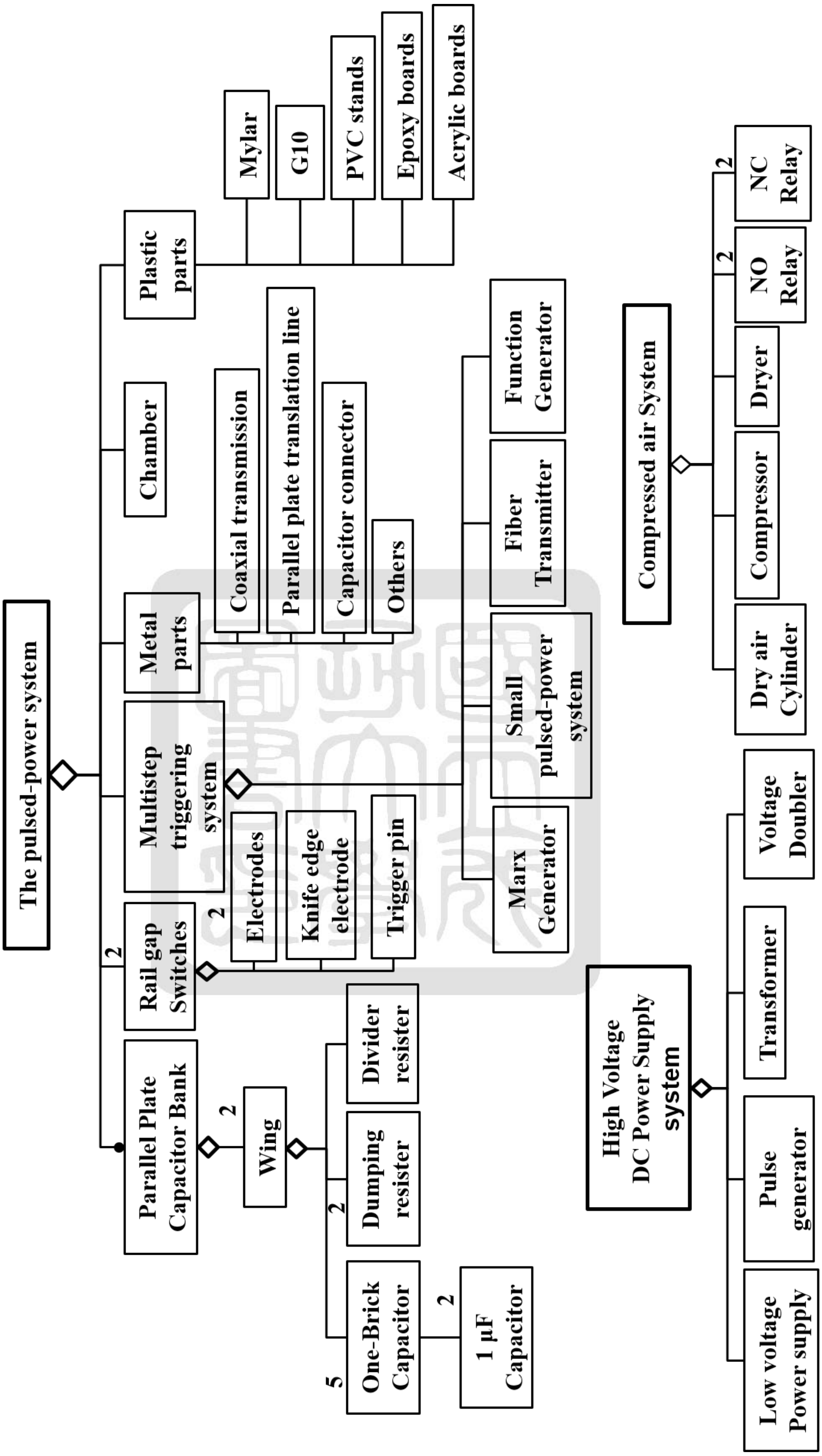

Figure 2.1: Part tree of the PPCB pulsed-power system

doi:10.6844/NCKU201900671

2.1 The Parallel-Plate Capacitor Banks (PPCB)

A parallel plate capacitor banks(PPCB) is one way to implement a pulsed-power system.[3] As shown in Fig 2.3, PPCB has a symmetrical energy bank with two wings, called the north wing and the south wing, connected in parallel. Each wing is connected with a rail gap switch and a pair of aluminum plates. Twenty Mylar films with thickness of 3.76 mm are used for insulating each pair of aluminum plates, forming a parallel-plate transmission line. It is why we called it ‘‘Parallel Plate Capacitor Banks(PPCB)’’ pulsed-power system.

The PPCB stores electrical energy in twenty capacitors, each capacitor has a capacitance of 1 uF. One brick, the fundamental unit, is formed by connecting two capacitors serially. Thus, the capacitance of one brick is 0.5 μF. Each wing has five bricks connected in parallel, so its capacitance is 2.5 μF, as shown in Figure 2.2. As shown in Figure 2.3, PPCB has two wings connected in parallel. Thus, the total capacitance is 5 μF. Components in each wing are assembled in an acrylic box filled with dry air to keep the internal environment in low humidity. The inductance of the one-brick capacitor will be measured indirectly. Testing results will be given in the following chapters.

The inductance of the PPCB significant influence the peak value and the rise time of the discharge current. The inductance of the capacitor and rail gap switch is unknown and used assumed values. Parameters of components, calculation methods, and calculated inductance are shown in Table 2.1. The calculation of the peak current is as below:

The total inductance of PPCB is: $\frac{8}{2}+\frac{70+22+3}{2}+14+\frac{100}{10}+\frac{50}{2}\cong 100$ nH.

doi:10.6844/NCKU201900671

The total capacitance of PPCB : $\frac{1\ \mu F * 10}{2} = 5\ \mu F$

The impedance of PPCB : $\sqrt{\frac{100nH}{5\mu F}} = 0.14\ \Omega$

Peak current of PPCB: I_{peak} is = 140 kA for V = 20 kV,

I_{peak} is = 350 kA for V = 50 kV,

	The design diagram	Equivalent Circuit	Equivalent parameter
One-Brick capacitor	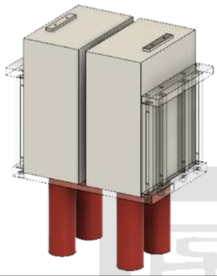	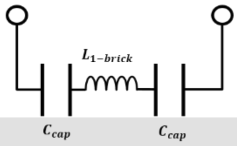	Capacitance: $\frac{C_{cap}}{2} = 0.5\ \mu F$ Inductance: $L_{1-Brick}$
One-Brick capacitor (The wing)	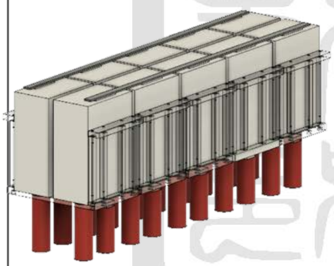	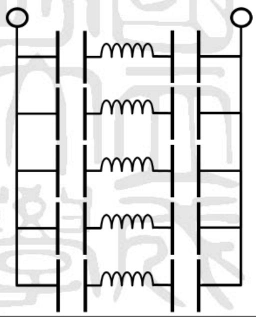	Capacitance: $\frac{C_{cap}}{2} * 5 = 2.5\ \mu F$ Inductance: $\frac{L_{1-Brick}}{5}$

Figure 2.2: The “Brick ” design of PPCB and capacitors of one wing is five-brick capacitors connected in parallel.

doi:10.6844/NCKU201900671

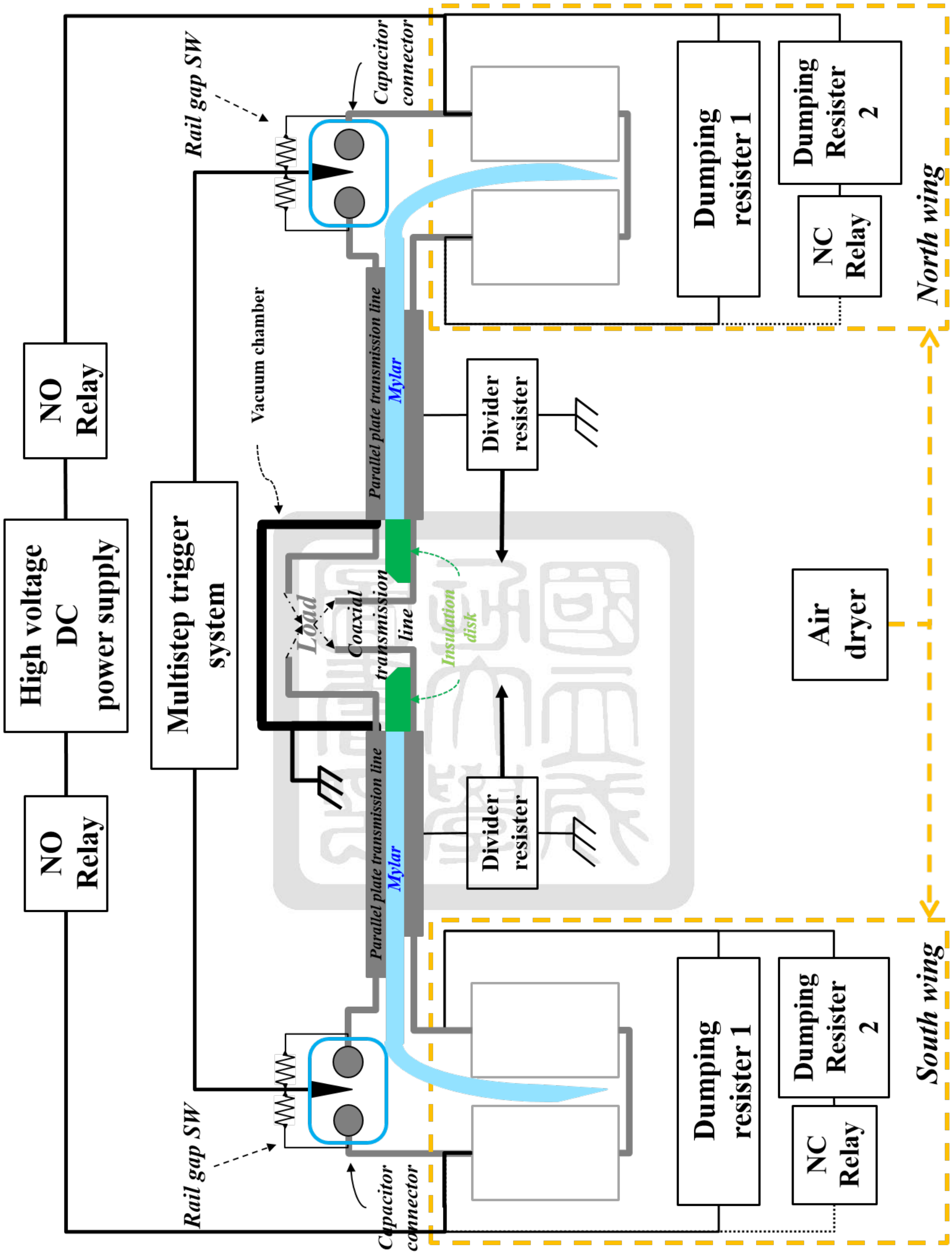

Figure 2.3: A mixing side view and circuit of the PPCB pulsed power system

doi:10.6844/NCKU201900671

Table 2.1: The parameter of component and calculation methods in each component.

	Components in PPCB	Calculated model	Theoretical inductance
Parallel plate transmission line	**Top: 825*600*10 [mm] (l*w*T)** **Down: 960*600*10 [mm] (l*w*T)** 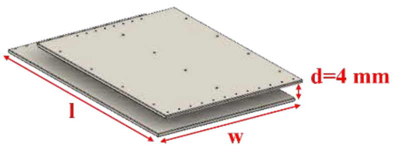	**l=960, w=600, d=3.76 [mm]** 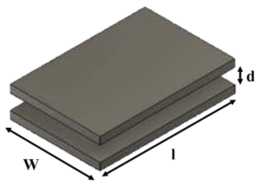	$L = \mu \frac{ld}{w}$ L_{pptl}= 8 nH
Capacitor connector		**a: l=45, w=305, d=380 [mm]** **b: l=20, w=320, d=278 [mm]** **c: l=10, w=1220, d=278 [mm]** 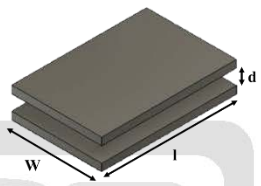	$L = \mu \frac{ld}{w}$ L_a= 70 nH L_b= 22 nH L_b= 3 nH
Coaxial transmission line	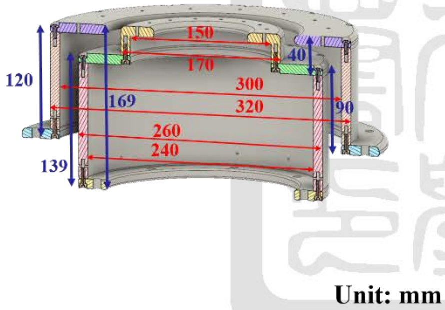	**l=170, D=300, R=200 [mm]** 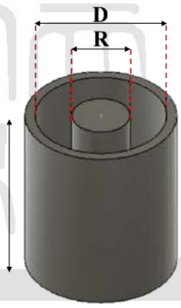	$L = \frac{\mu l}{2\pi} \ln(\frac{D}{R})$ L_{ctl}= 14 nH
One-Brick capacitor	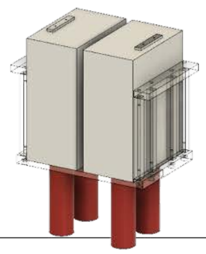		The inductance of one-brick capacitor is an unknown number $L_{1-brick}$. Here we assume that is 100 nH.
Rail gap switch	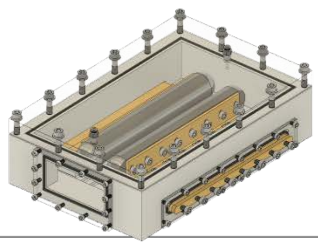		The inductance of the rail gap switch is an unknown number L_{sw} . Here we assume that is 50 nH.

doi:10.6844/NCKU201900671

2.1.1 Dumped and divider resistors for PPCB

Capacitors of each wing have two dumped resistors connected in parallel, as shown in Figure 2.4. One of the dumped resisters is used to release energy in 15 mins; the other is connected with a normally closed (NC) relay in series to release energy immediately using pneumatic valve. Each wing also has a five hundred to one (500:1) divider resistor to measure the output voltage signal. Most importantly, the plate of the parallel-plate transmission line and chamber is grounded for safety. When the rail-gap switch is triggered, the ground terminal of capacitors becomes –HV. The divider resistor is required to provide the –HV output to the load.

In order to estimate the resistance, we first analyze the various states of the system and simplify its circuit to get the equivalent circuit. The equivalent circuit is used to obtain reasonable numbers of each resister. Two wings have the symmetrical specification of all components and they are connected in parallel. The symmetrical design of PPCB makes it easy to analyze the resistance of dumped resistors used in PPCB.We only need to analyze the various states of a single wing.

As shown in Table 2.3, we draw the simple circuit diagram in the south wing for different states, as shown in Table 2.2. The state is changed by using high-voltage relays. Those relays are different switches and introduced in Chapter 4. In this section, we only discuss whether it is open or closed in the electrical circuit.

The four states of the system are shown in Table 2.3 and each state follows:

(1) Initial state: This state is for protecting users and the high voltage power supply. Any remaining energy in capacitors is dumped using the dumped resister 2. Thus, the NO relay is used to separate the HV power supply and capacitors. The NC relay is used so that energy is dumped through dumped resistor 2.

doi:10.6844/NCKU201900671

(2) Charging state: Capacitors being charged by the high voltage power supply. Therefore, the NO relay is used to forming a closed contact so that the HVP is connected to capacitors. The NC relay should open so that energy is not dumped.

(3) In experiment state: After charging, the power supply is isolated from the circuit of the system. Thus, both the NO and the NC relays are open.

(4) End state: The NC relay is closed and the remaining energy of capacitors is reduced by the dissipated through resistor 2. Note that energy can still be dissipated through dumped resistor 1 in 15 mins. If the NC relay is malfunction and remains open.

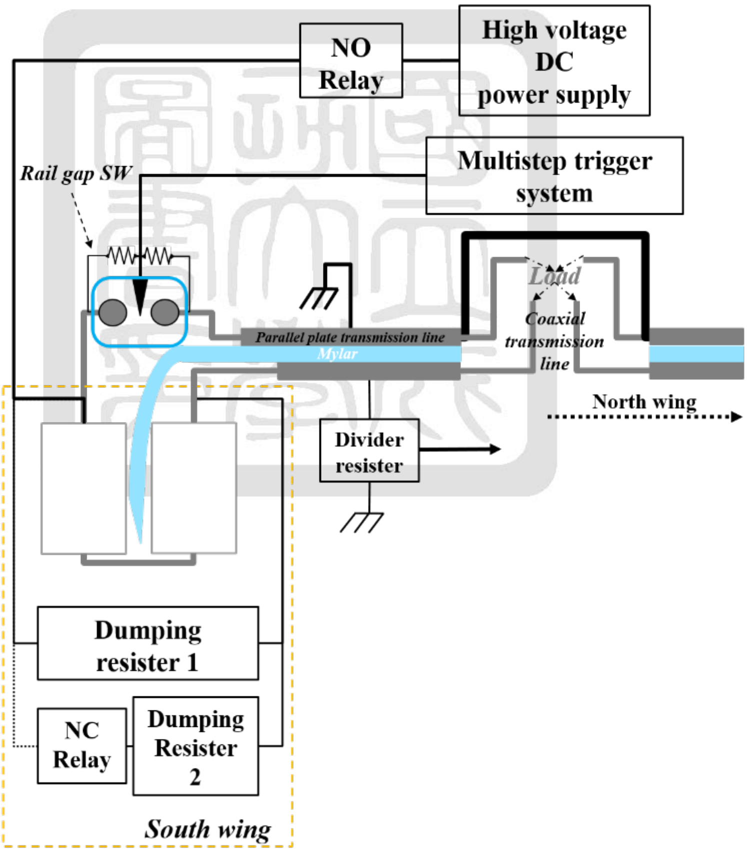

Figure2.4: The south wing pulsed-power system has two relays to change state.

doi:10.6844/NCKU201900671

Table 2.2: The different situation of the south wing pulsed-power system working by each relay.

System status	States of the relay	
	NO relay	*NC relay*
Initial state	Open	Closed
Charging	Closed	Open
In experiment	Open	Open
End	Open	Closed

As shown in Table 2.3, the equivalent circuits and resistance requirements in each state are given.

(1) Initial state: the energy of capacitors is mainly dumped by the dumped resistor 2. So the condition is

$$R_{D1} \gg R_{D2} \ .$$

(2) Charging state: The voltage of capacitors should be charged to V_0, but charging voltage is divided by R_{D1}, R_{div} and R_{load}. So, the equivalent resistance of R_{div}andR_{load} should be much smaller than R_{D1} ($\frac{R_{load}*R_{div}}{R_{load}+R_{div}} \ll R_{D1}$). In most cases R_{load} is from wires and much smaller than R_{div}. On the other hand, the charging current goes through R_{load}. It needs to be dumped loads. Further, there will be a leak current through R_{D1} and R_{load}. Therefore, the power supply needs to be able to supply enough power. In other words, the power supply needs to be able to provide a current $I_{load} > \frac{V}{R_{D1}}$. As a result,

$$R_{D1} \gg R_{div} \gg R_{load}$$

doi:10.6844/NCKU201900671

(3) In experiment state: all components are connected in parallel. The energy of capacitors should mainly input to the load. Therefore, the condition is given by

$$R_{D1} \gg R_{div} \gg R_{load} \ .$$

(4) End state: it will be the same as the initial state where the load should be burned out so that $R_{load} \rightarrow \infty$.

Table 2.3.: Equivalent circuit diagram and conditions in each experimental state.

Initial State	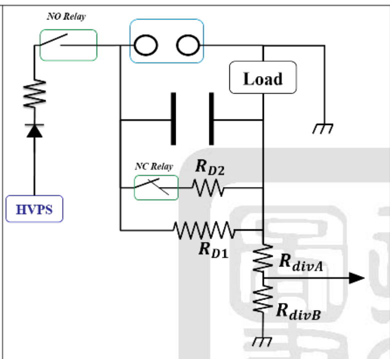	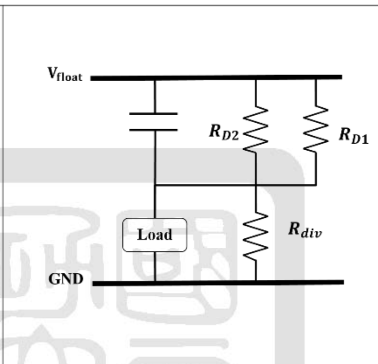	$R_{D1} \gg R_{D2}$
Charging	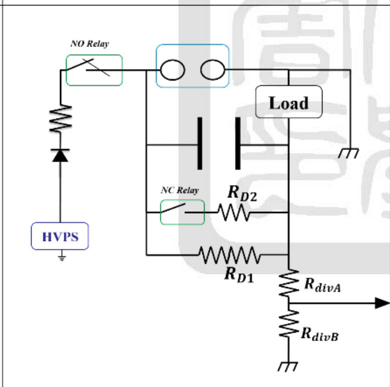	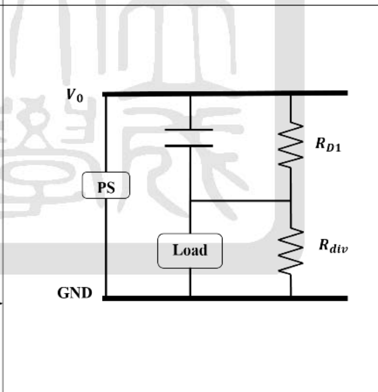	$R_{D1} \gg R_{div} \gg R_{load}$
In experiment	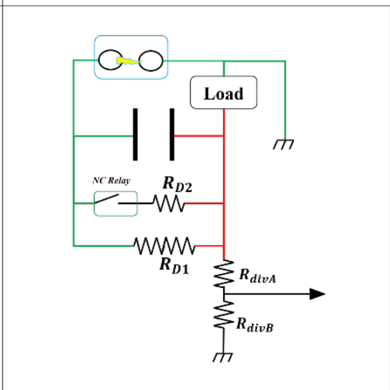	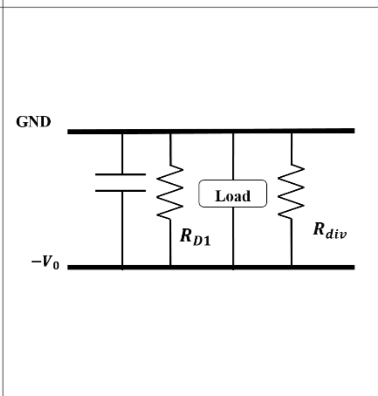	$R_{D1} \gg R_{div} \gg R_{load}$
	Circuit diagram	**Equivalent Circuit**	**Result**

doi:10.6844/NCKU201900671

To calculate the resistance, we use the RC damping formula

$$V(t) = V_0 e^{-\frac{t}{RC}},$$

and we define the safe voltage as 10 V. V_0 is charging voltage. Charging voltage V_0 is 20 kV. C is capacitance. The capacitance of the south wing is 2.5 uF. R is resistance and will be determained. Substituting V(t)=10 into this formula and take the natural logarithm from the voltage ratio. The time of disspating the energy of capacitors follows the formula:

$$\Delta t = RC * \ln(\frac{V_0}{10}) \text{ (s) or } R = \frac{\Delta t}{C*\ln(\frac{V_0}{10})} \ (\Omega)$$

(1) R_{D1}: It is the last protection if everything inculding relays goes wrong. We design R_{D1} such that dumps all energy in 15 mins. Therefore, by setting $\Delta t = 15$ mins, resistance is 47 MΩ. For convenience, we use five 10MΩ resistors connected in series form a 50 MΩ. So Δt is about sixteen minutes. During the Charging state, the lower value of the current is 0.4 mA for charging to 20 kV. In the future, our laboratory will increase the charging voltage to 50 kV, and Δt is about 18 mins. When charging voltage is 50 kV, the current from the HVPs needs to be greater than 1 mA for a single sing.

(2) R_{D1}: The conditions of the charging state and in experiment state are the same

$$R_{D1} \gg R_{div} \gg R_{load} \ .$$

R_{D1} is 50 MΩ, and R_{load} is assumed to1 Ω. The resistance of the divider resistor is between 50 MΩ and 1 Ω. Resistance on the order of MΩ is reasonable. Therefore, the divider resistor is formed by a 5-MΩ resistor and a 500-Ω resistor connecting in series. It sent a voltage signal with ratio 1/500 of the capacitor voltage for the oscilloscope.

doi:10.6844/NCKU201900671

(3) R_{D2}: The dumped resister 2 is a 1 kΩ, 1500 W resistor [TE1500B1K0J]. The time of dessipating the remaining energy of capacitors is ~20 ms. On the other hands, the current through R_{div} is $2\text{x}\,10^{-7}$ times relative to that through the load. In other words, I_{div}~0.02 A during the discharge.

Table 2.4: Resistance of each resister

Resisters	Resistance	Made
Dumping resister 1 (R_{D1})	50 MΩ	10 MΩ *10
Dumping resister 2 (R_{D2})	1 kΩ	1kΩ ±5% 1.5kW
Divider resister (R_{div})	50500 Ω	(1 MΩ*5)+ (100 Ω *5)

2.1.2 Stands for PPCB

We use low-cost materials to make stands to support the PPCB. PVC pipes with 6 and 8 inches in diameter are used. As shown in Figure 2.5 (a) and (c), each 6-inch pipe is inserted at the center of each 8-inch pipe. The spacers are used to make sure the 6-inch pipe is at the center of the 8-inch pipe. The space between the two pipes is filled with Styrofoam to increase the strength of the stand.

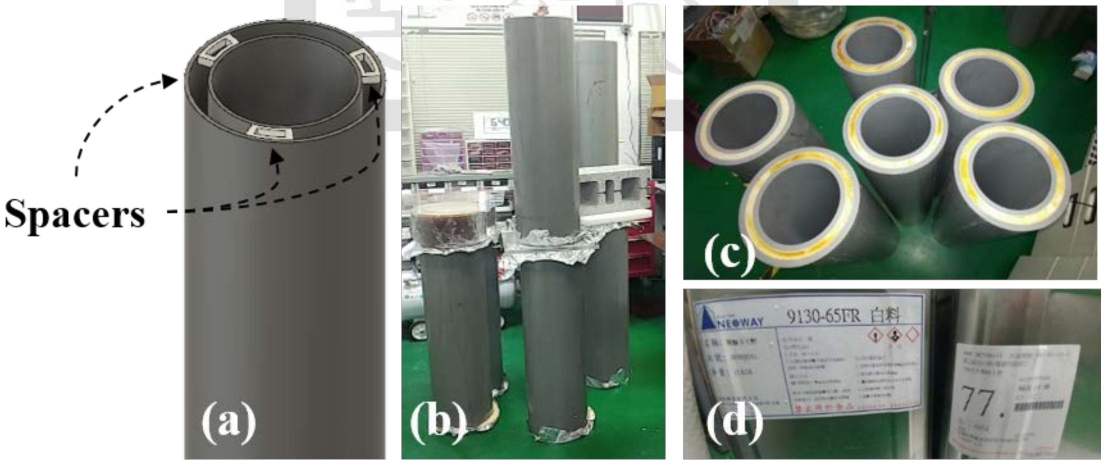

Figure 2.5: (a)Two different size pipes are fixed by plastic spacers. (b) After injecting the Styrofoam, press the pipe to prevent the Styrofoam from filling out.

doi:10.6844/NCKU201900671

(c) The surface of the column after the Styrofoam is solidified. (d) the Styrofoam is supplied from the company of Norway.

2.1.3 Mylar films for the PPCB

Twenty Mylar films are stacked on each other for insulating the aluminum plates of the parallel-plate transmission line, as shown is Figure 2.6. The thickness of the film is 0.188 mm so that the total thickness is 3.76 mm. The dielectric strength is 400 kV/cm so that the breakdown voltage is 150 kV. Mylar film was cut into 360 cm long and 100 cm wide. At the middle of the Mylar films, a circle hold of 600~605 mm in diameter is cut. The suggested way is the upper layer uses Maylar with a smaller diameter ~600 mm and the lower layer uses a larger diameter 605 mm.

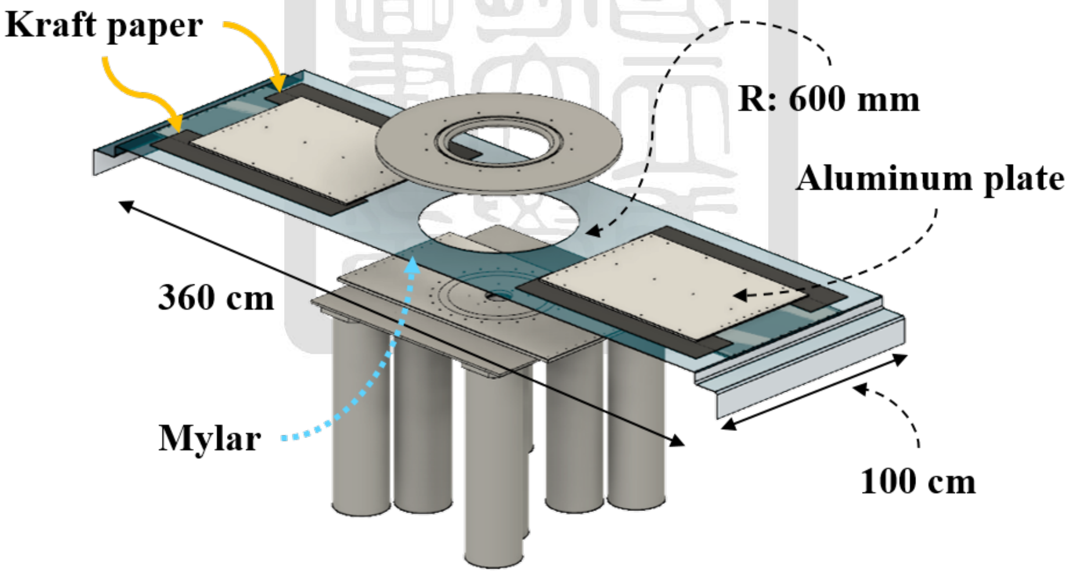

Figure 2.6: Mylar layout.

2.1.4 Ground fence

Our PPCB is an experimental device with high voltage discharge. Protecting laboratory personnel is essential. We built a grounded fence around the entire system

doi:10.6844/NCKU201900671

to isolate experimenters and the system. Therefore, any high voltage power will be connected to the ground when it arcs through the air unexpectedly.

As shown in Figure 2.7, the supporting frame of the grounded fence is composed of slotted steel angles and bridge latched with different length. Latched bridges have latches to connect with the lotted steel angles. The interior size of the grounded fence is 14.5 feet in length, 8 feet in width and 2.4 meters in height. The weld welded-mesh was paved on the interior surface of the supporting frame. It is than connected to the earth ground.

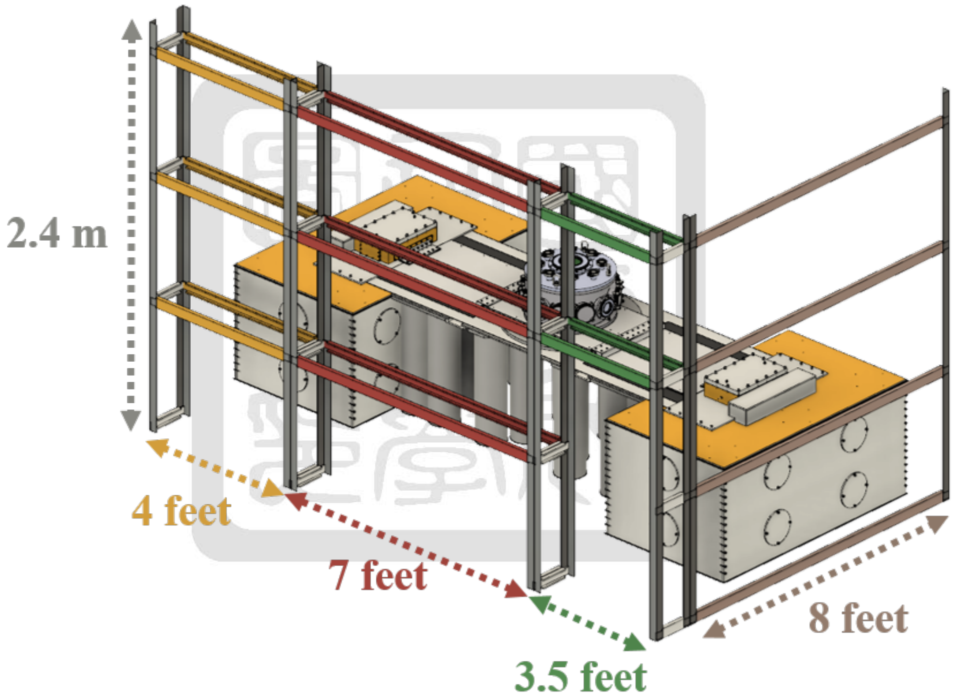

Figure 2.7: The supporting frame of the grounded fence.

2.2 The south wing pulsed-power system

Shown in Figure 2.8, it is the experimental setup of the south wing pulsed-power system. The high voltage DC power supply connected with a diode and a 1 kΩ resistor. When it is ready to be discharged, the NO relay is used to separate the high voltage DC power supply from the south wing. The capacitors are connected to two

doi:10.6844/NCKU201900671

dumped resistors, which are used to dissipate the residual energy of the capacitor. One of the dumped resistors of 50 MΩ is directly connected with capacitors in parallel. The other dumped resistor with 1 kΩ and NC relay are connected in series. They are connected with capacitors in parallel. The 1 kΩ resistor is used to dissipate the residual energy of the capacitor immediately. The air compressor is used to control the NO and NC relays.

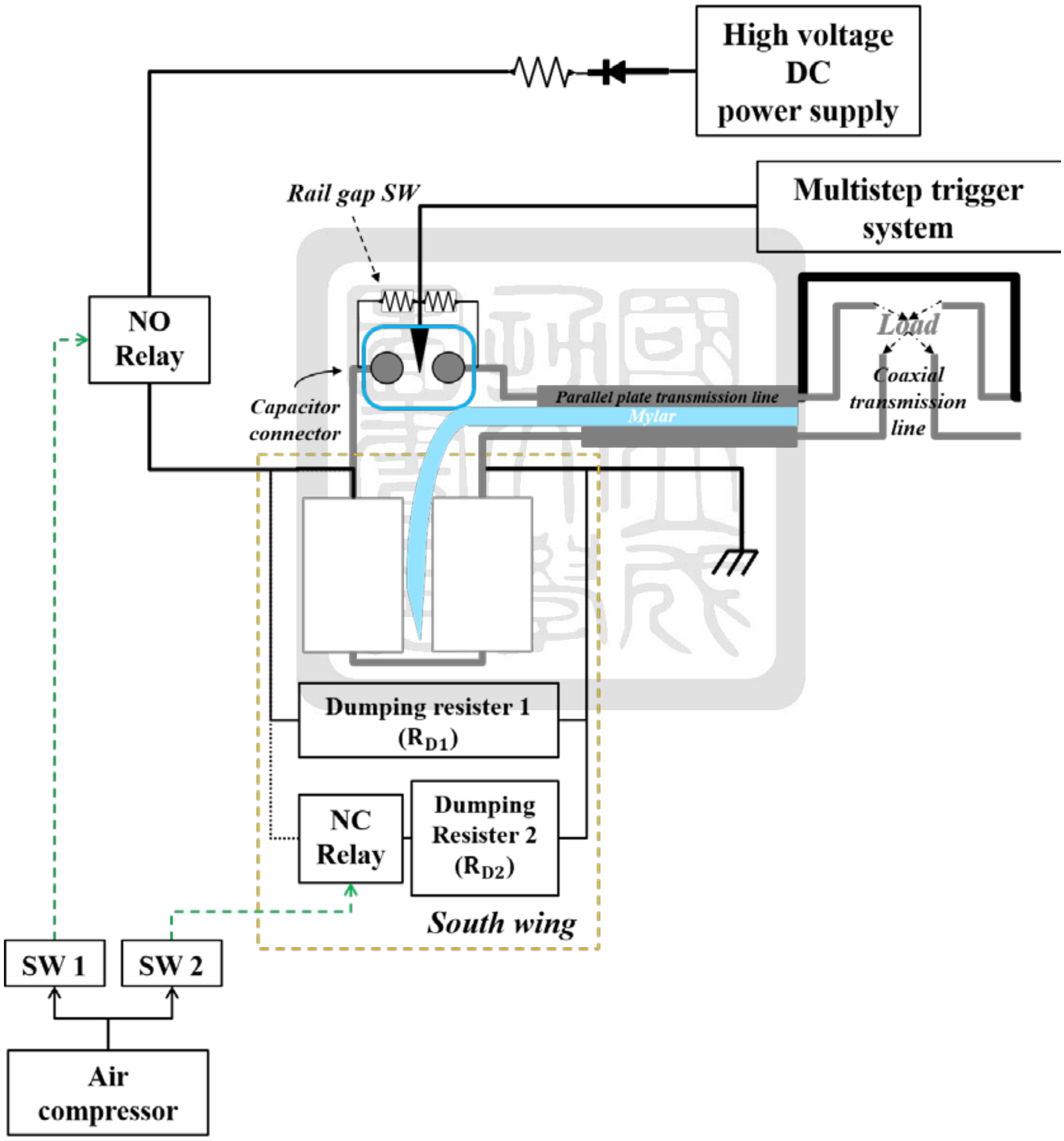

Figure 2.8: The experimental setup diagram of the south wing pulsed-power system.

doi:10.6844/NCKU201900671

Chapter 3 Compressed air systems

To keep gas clean in switches, stabilize the function of switches, and keep capacitors in an environment with low humidity to avoid high voltage breakdown in the system, we built two different compressed air systems. One is a compressed gas cylinder. The other one uses a compressor. In section 3.1, the dry air using a compressed gas cylinder for switches is introduced. In section 3.2, a compressed air system to drive relays and for the dryer is introduced.

3.1 Dry air using the compressed gas cylinder

The dry air provided by the compressed air cylinder is to provide dry air for rail gap switches and the Marx generator. The architecture of the flowing dry air system is shown in Figure 3.1. The dry air source is a compressed gas cylinder contenting compressed dry air. From left to right are a main valve, a control valve, a switch which is a ball valve, a flow controller valve, and a flowmeter. This system is going to provide the dry air continuously and take away the dust from electrodes generated from discharge in switches.

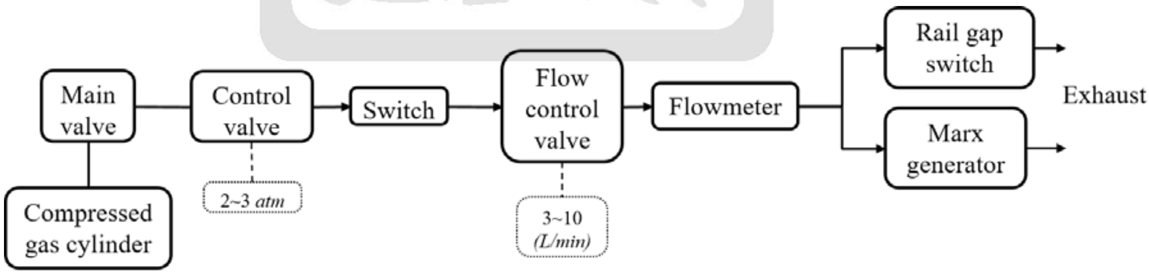

Figure 3.1: The architecture of the flowing dry air system to supply dry air for switch and Marx.

To determine how long we need to wait after the gas is being supplied, we calculated the fraction of new gas in volume to the whole volume using different flow rates under different supplying times as shown in Table 3.1 and Table 3.2. For example, if the total volume is 7000 cm^3, the flow rate is 3 L/min, and a portion of

doi:10.6844/NCKU201900671

new gas is 58% in the box after two minutes, as explained below.

This table is calculated with the following assumption: (1) the dry gas flows into the box at a flow rate of x L/min; (2) the inlet and the outlet have the same pore size and flow rate; (3) the internal gas is uniform; and (4) the volume of the box is V cm^3. Assume that the new gas has a volume y(t) cm^3 inside a box. We have the following equation:

$$dy = x * dt - \left(\frac{y}{V}\right) * x * dt \ .$$

It means that the increased volume of the new gas is equal to the amount of new gas that flows in (1^{st} term on the right-hand side of the equal sign) subtracting the portion that leaves the box after mixing(the 2^{nd} term on the right-hand side of the equal sign). We can get the equation:

$$\frac{dy}{1-\frac{y}{V}} = x * dt \equiv -V\frac{dY}{Y} \quad \text{with} \quad Y \equiv 1 - \frac{y}{V} \ .$$

Therefore, the ratio of new gas in the box is

$$\frac{y}{V} = e^{-\frac{x}{V}t} \ .$$

The operating procedures of dry air using the compressed gas cylinder are shown in Table 3.3 and Table 3.4. Figure 3.2 are the components used in this system.

doi:10.6844/NCKU201900671

Table 3.1: Flowmeter parameter reference table using 7000 cm^3 volume.

Volume is 7000 cm^3								
Time \ Flow rate (L/min) %	3	4	5	6	7	8	9	10
2 min	58	68	76	82	86	90	92	94
3 min	72	82	88	92	95	97	98	99
4 min	82	90	94	97	98	99	99	100
5 min	88	94	97	99	99	100		
6 min	92	97	99	99	100			
7 min	95	98	99	100				
8 min	97	99	100					
9 min	98	99	100					
10 min	99	100						

Table 3.2: Flowmeter parameter reference table using 14000 cm^3 volume.

Volume is 14000 cm^3								
Time \ Flow rate (L/min) %	3	4	5	6	7	8	9	10
2 min	35	44	51	58	63	68	72	76
3 min	47	58	66	72	78	82	85	88
4 min	58	68	76	82	86	90	92	94
5 min	66	76	83	88	92	94	96	97
6 min	72	82	88	92	95	97	98	99
7 min	78	86	92	95	97	98	99	99
8 min	82	90	94	97	98	99	99	100
9 min	85	92	96	98	99	99	100	
10 min	88	94	97	99	99	100		

doi:10.6844/NCKU201900671

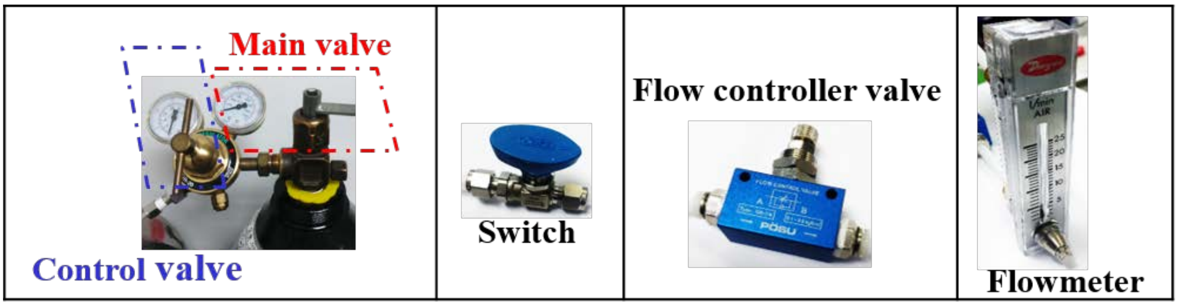

Figure 3.2: Picture components.

Table 3.3: Open operation of the flowing dry air using the cylinder.

Open operation of the flowing dry air using the cylinder	
Step	**Check &execute**
1	**Switch status:** Closed **Action:** Open the main valve clockwise
2	**Switch status:** Closed **Action:** Slowly open the control valve counterclockwise and adjust to 2~3 atm.
3	**Switch status:** Closed → Open **Action:** Open the switch
4	**Switch status:** Open **Action:** Use a flow controller valve to adjust the flow rate to 3 to 10 liters per minute.

Table 3.4: Closed operation of the flowing dry air using the cylinder.

Closed operation of the flowing dry air using the cylinder	
Step	**Check &execute**
1	**Switch status:** Open **Action:** Closed the main valve counterclockwise
2	**Switch status:** Open **Action:** Wait for the control valve to return to zero
3	**Switch status:** Open **Action:** Closed the control valve clockwise
4	**Switch status:** Open → Closed **Action:** Closed the switch

doi:10.6844/NCKU201900671

3.2 A compressed gas system using a compressor

We need compressed gas to drive two different systems: (1) pneumatic high voltage relays and (2) a dryer. Therefore, we built a compressed gas system using a compressor. Shown in Figure 3.3 is a schematic of the whole system. Corresponding parts are shown in Figure 3.4. The pressure control valve (PCV 1) controls the output pressure for relays. In principle, a flow control valve is needed to regulate the flow rate into switches. However, the flow rate is limited by the long tube so that the FCV1 is not used. Each relay then can be controlled by each switch ($SW_1 \sim SW_4$).

On the other hand, the dryer and relays use different working pressure. The pressure control valve (PCV2) is used to control the output pressure for the dryer. The flow control valve is used to control the flow speed, which avoids excessive flow and causes the upstream pressure drops. Finally, the dryer provides the dry air to the acrylic boxes that contain the south and the north wings for insulation. The operation flow of this system and setting each component are shown in Table 3.5 and Table 3.6.

doi:10.6844/NCKU201900671

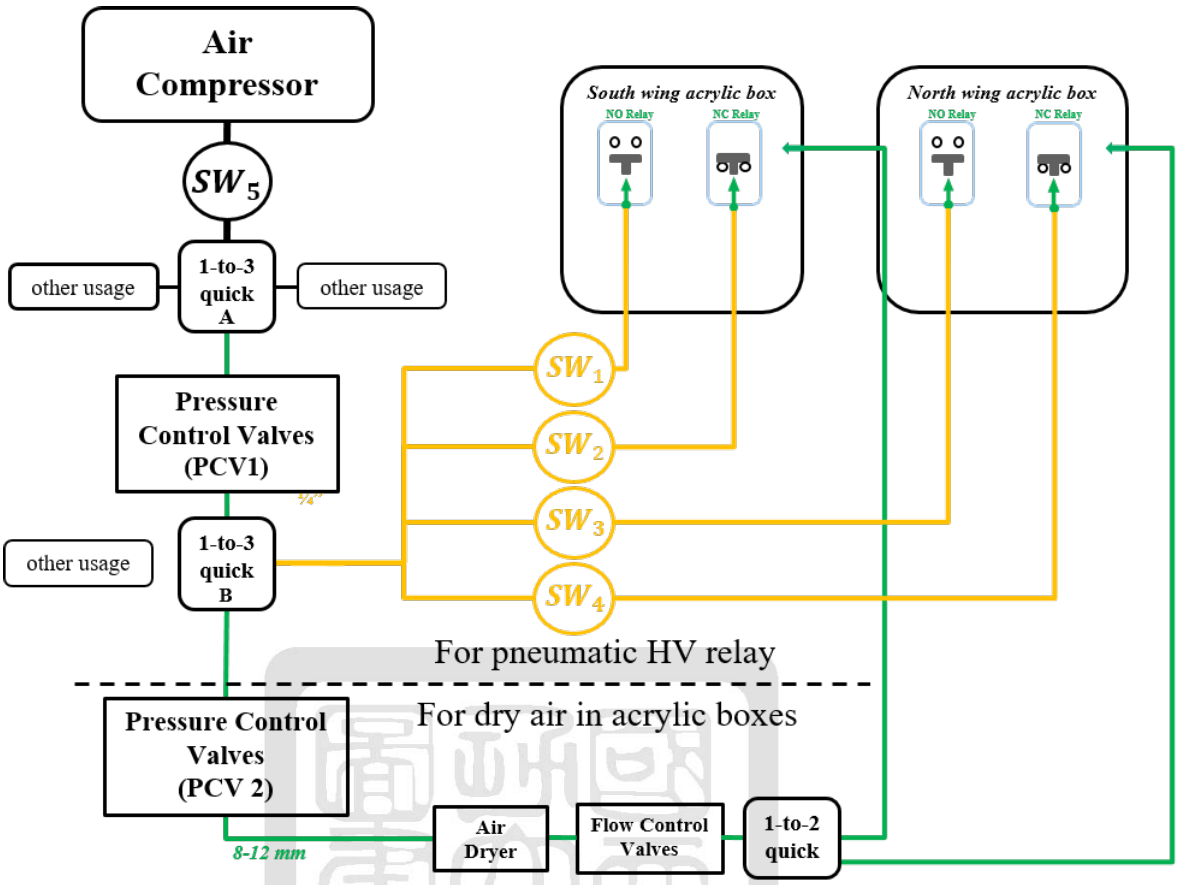

Figure 3.3: Air compressor is used to push relays and supply gas to the dryer.

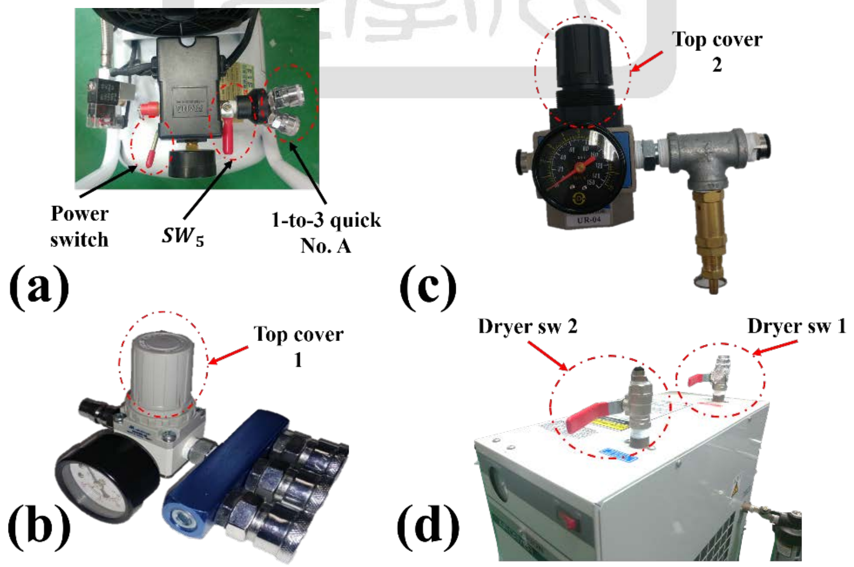

Figure 3.4: Air compressor is used to push relays and supply gas to the dryer.

doi:10.6844/NCKU201900671

Table 3.5: Open operator of the compressor system.

The open operator of a compressed gas system using a compressor	
Step.	Action
1.	Make sure switches SW_1~SW_4 are closed.
2.	Make sure the switch SW_5 on the compressor is closed.
3.	Turn on the compressor's power.
4.	Turn on the power switch, as shown in Figure 3.4(a), on the compressor.
5.	Waiting for compressor compressed air to 8 atmospheres and it will stop to compressing the air by it self.
6.	Pull up the top cover 1, which is shown in Figure 3.4(b)
7.	Turn the top cover 1 counterclockwise to set the pressure to zero.
8.	“Slowly” open the switch (SW_5) on the compressor.
9.	“Slowly” turn the top cover 2 clockwise to set the pressure to 3 atm.
10.	Press down the top cover 1.
11.	Make sure PCV 2 is not connected to the system.
12.	Pull up the top cover 2, which is shown in Figure 3.4(c)
13.	Turn the top cover 2 counterclockwise to set the pressure to zero.
14.	Close Dryer sw 1 and Dryer sw 2 on the dryer, as shown in Figure 3.4(d)
15.	Connect PCV 2 to the 1-to-3 quick B.
16.	Slowly turn the top cover 2 clockwise to set the pressure to 1 atm.
17.	Press down the top cover 1.
18.	Turn off the Flow Control Valves counterclockwise
19.	Open the power of the Dryer and wait for 3 minutes.
20.	“Slowly” switch the Dryer sw 2 on.
21.	“Slowly” switch the Dryer sw 1 on.
22.	“Slowly” turn off the Flow Control Valves clockwise.

doi:10.6844/NCKU201900671

Table 3.6: Closed operator of the compressor system.

The closed operator of a compressed gas system using a compressor	
Step.	Action
1.	Make sure the voltage of all capacitors is the safe voltage.
2.	Turn off the compressor's power supply.
3.	Turn off the power switch, as shown in Figure 3.4(a).
4.	Wait for the dryer to exhaust the gas in the air compressor.
5.	“Slowly” closed the Dryer sw 1.
6.	“Slowly” closed the Dryer sw 2.
7.	Turn off the power of the Dryer.
8.	Closed the switch (SW_5) on the compressor.
9.	Open the switch which is at the bottom of the air compressor. Exhaust residual air and water from the air compressor.
10.	Closed the switch which at the bottom of the air compressor.

doi:10.6844/NCKU201900671

Chapter 4 Pneumatic high voltage relay

The relay switches the system between different states. One of the states is separate high voltage DC power supply from the system after charging is completed. Another one is used to control the dumped resistor so that the residual energy of the capacitor in the system is dissipated by the dumped resistor.

The simplified schematic diagram of the pulsed-power system can be represented in Figure 4.1. The relay S_1 is connected in series with the power supply and the capacitor to protect the power supply by the switch off; Relay S_2 is connected in series with a dumped resistor and in parallel with the capacitor. The resistor is used to dump remaining energy in the capacitor.

In section 4.1, the conditions required for the relay in PPCB are introduced. In Section 4.2, the mechanism design of the relay is introduced.

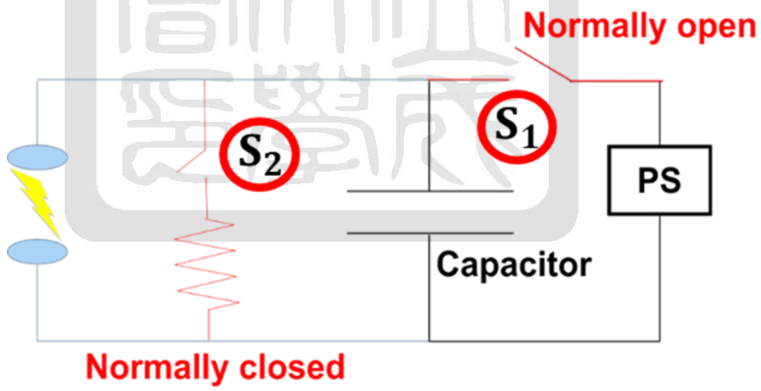

Figure 4.1: Simple PPCB circuit diagram with two switches

4.1 Requirements of relays

The relay has two simple styles, as shown in Figure 4.2. One is a normally-open (NO) relay. There are no contacts between when it is not activated. The other one is a normally-closed (NC) relay. Electrodes contact with each other when the relay is not activated. As shown in Table 4.1, depending on the states suitable relays are used. Relay S_1 is open in both the initial state and the end state, so that normally open (NO)

doi:10.6844/NCKU201900671

relay is suitable for S_1. Relay in S_2 is closed in both the the initial state and the end state so that normally closed (NC) relay is suitable for S_2. Both NO and NC relay are needed in PPCB so that we design both types of relays.

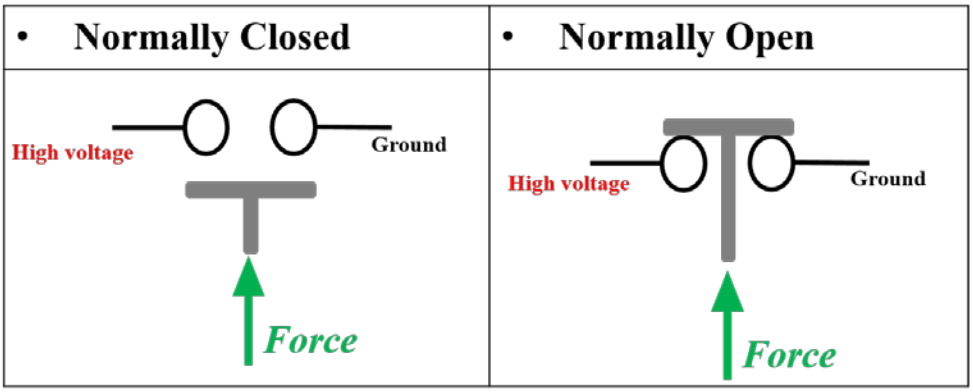

Figure 4.2: The normally closed relay and the normally open relay.

Table 4.1: Relay status during the experiment and suitable relays.

Opportunity / Switch	S_1	S_2
Initial state	Open	Closed
Charging state	Closed	Open
In experiment state	Open	Open
End state	Open	Closed
Switch type	NO	NC

The relay is connected between the high voltage and the ground. In order to hold high voltages, the distance between each electrode of the relay must be far enough to avoid breakdown between any two electrodes. On the other hand, insulator used in the relay need to avoid surface flashover. The relay I designed uses one metal plate to impact two cylinder electrodes for electrical contacts. To avoid breakdown and surface flashover between any two electrodes, we use some physical mechanisms in the support frame. First, we use the empirical formula from Northstar Research Corporation[6]

$$\frac{V}{d} = E = 24.5P + 6.7\left(\frac{P}{R_{eff}}\right)^{1/2} \ \text{kV/cm}$$

doi:10.6844/NCKU201900671

, and used it to determine the distance between each electrode to avoid breakdown. In the formula, R_{eff} = 0.23R, where R is the radius of the cylinder electrode in cm, P is pressure of abient gas in atm, d is distance between two electrodes in cm, V is the voltage betweent two electrodes in kV. The capacitors of PPCB will be charged to 50 kV in the future. Also, we set the voltage safety factor of the relay to be 1.6 times. Therefore, assuming that capacitors are charged to 80 kV, the required length d is 22.3 mm. The distance between any two conductors must be greater than 22.3 mm.

4.2 Design of relays

As shown in Figure 4.3, the relay consists of four basic parts:

(1) The support frame: it is made of strong plastic poles to support cylindrical electrodes.

(2) The spring support frame: it fixes the spring between the plastic plate and the metal plate.

(3) The rod of the pneumatic valve: it uses the extension rod to increase the distance between electrodes and the pneumatic valve. Since the extension rod is made of plastic, a cylindrical frack is used to strengthen the extension rod.

(4) The air cylinder holder: it is used to insulate pneumatic valves.

doi:10.6844/NCKU201900671

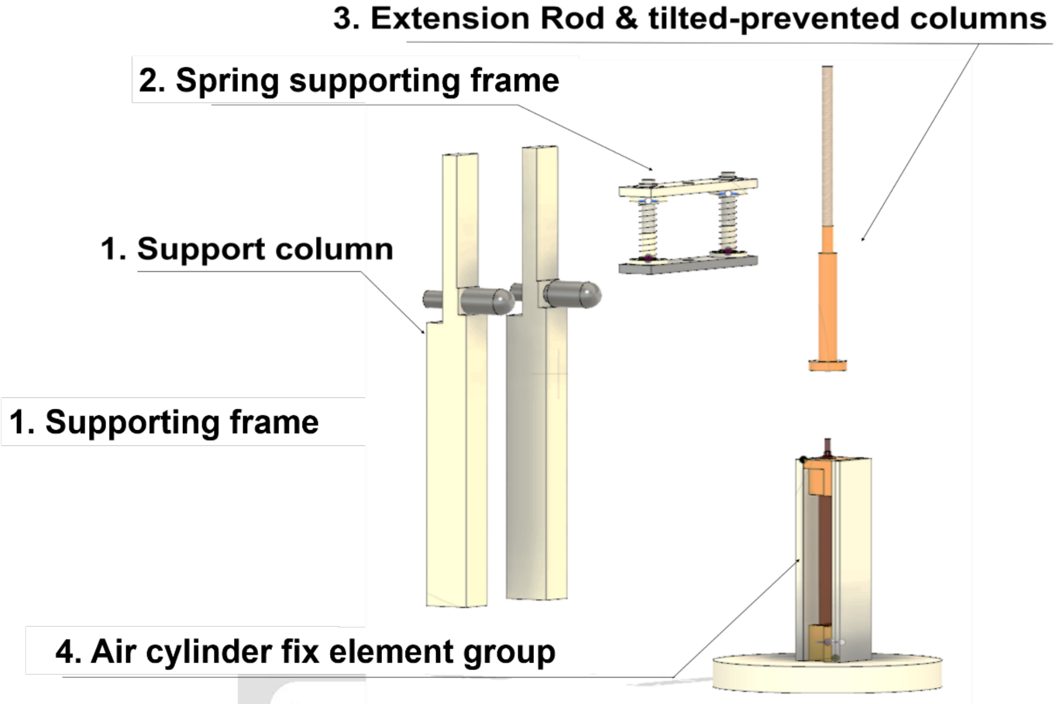

Figure 4.3: The relay design is a combination of four parts

The starting point of the design is the air cylinder [SMC:NCMKB075-0400S] which is made of metal, so it needs to be insulated by plastic first. The electrode will be hit by metal plate every time it is used so the pole used to support the electrode must have a sufficiently strong structure. The pneumatic valve position is in the middle of the support frame so that the distance between two electrodes on the support frame will be longer than the width of the air cylinder holder. The spring restoring force make the metal plate and electrodes contact with each other firmly.

4.2.1 The air cylinder holder

Both NO and NC relays have the same air cylinder holder which consists of an upper block, a rear board, a front board, a lower block, a bottom plate, and an air cylinder, as shown in Figure 4.4. The bottom plate is the base and there is a hole for connecting the gas pipe with the air cylinder. The upper block is used to attach with the tilted-prevented columns(In section 4.2.2). Except the air cylinder, components are made of polyethylene.

doi:10.6844/NCKU201900671

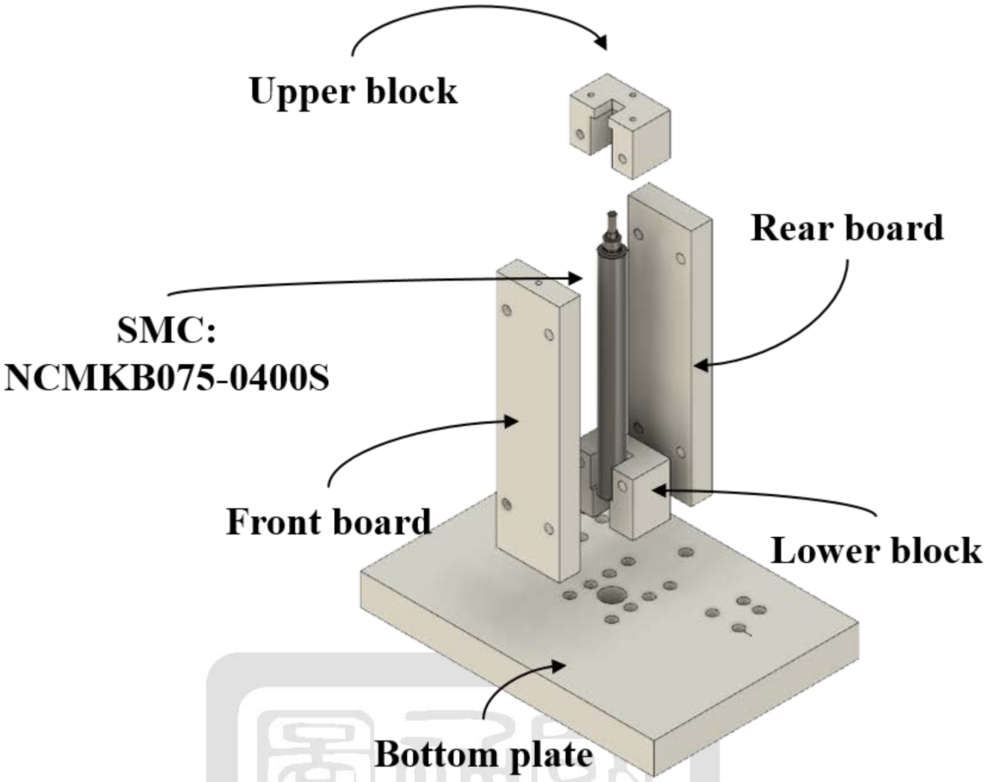

Figure 4.4: The constitution of the pneumatic valve holder.

4.2.2 The rod of the pneumatic valve

Both NO and NC relays have rods for extending the length. The rod of the air cylinder consists of an extension rod, a connecting rod, and tilted-prevented columns, as shown in Figure 4.5. All of that is made of polyethylene. The NC relay has longer rods because it needs more space for other components. The tilted-prevented column is used to provide a track to make the rod move straightly. The connecting rod is used to connect with the air cylinder and the extension rod. The extension rod provides more working range for the spring supporting frame.

doi:10.6844/NCKU201900671

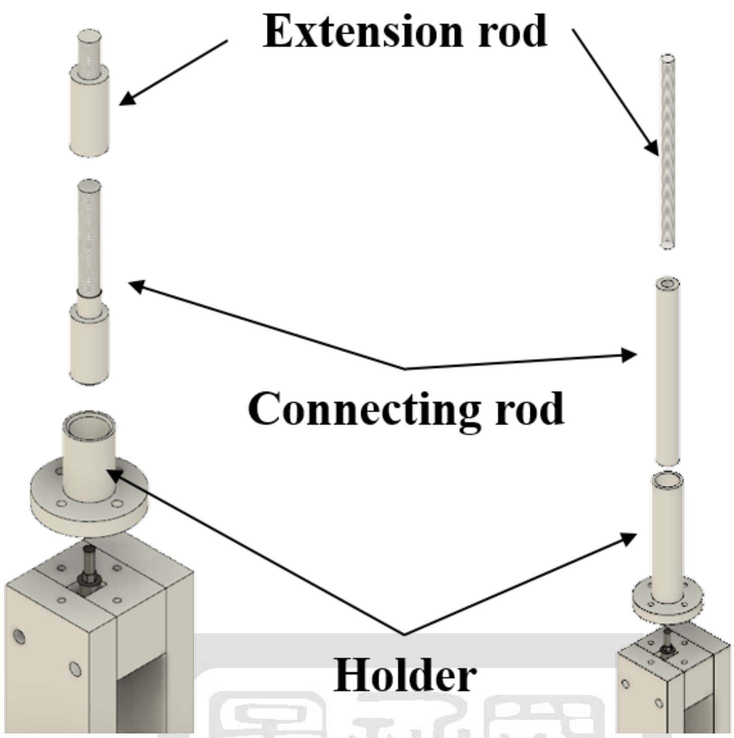

Figure 4.5: The constitution of the rod of the pneumatic valve. On the left is the NO relay and on the right side is the NC relay.

4.2.3 The supporting frame

Each relay (NO and NC) has different design of the supporting frame. The supporting frame consists of two cylindrical electrodes made of aluminum alloy, two electrode beds, two main supports and two structural beams, as shown in Figure 4.6. Except for the electrode, they are made of polyethylene. The main support is attached with the bottom plate, an electrode bed, the cylindrical electrode, and the structural beam. As shown in Figure 4.7(a) and (c), the electrode and the electrode bed are locked to the main support. When the electrode is struck by the metal plate, the bed is used to increase the support of the electrode. As shown in Figure 4.7(b) and (d), the main support and the structural beam are screwed to each other firmly. This is because the PE column after machining is usually bent. By attaching two together, they become flat. The supporting frame has some grooves on it to increase the surface path, as shown in Figure 4.6. This design is to avoid surface flashover.

doi:10.6844/NCKU201900671

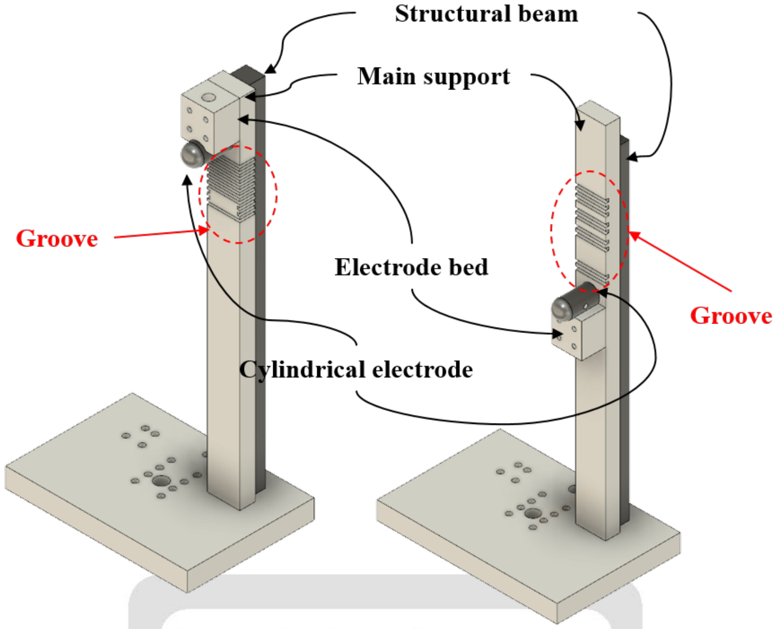

Figure 4.6: The constitution of the rod of the support frame. On the left is the NO relay and on the right side is the NC relay.

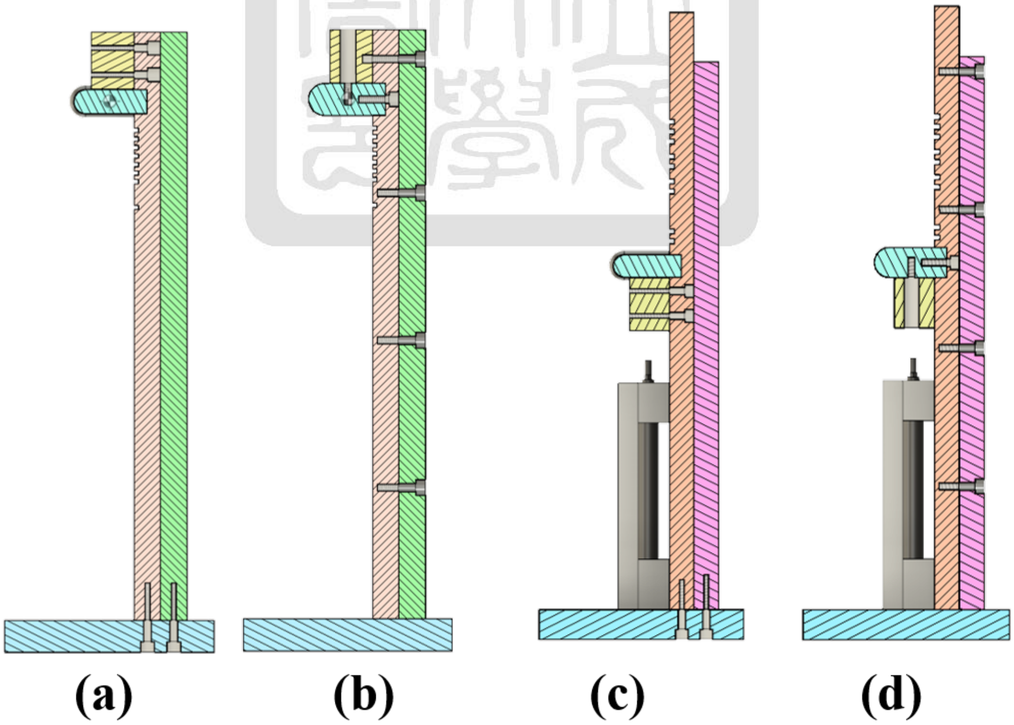

Figure 4.7: Sections of two relays. (a)and(b) is section of the NO relay in different deep. (c)and(d) is section of the NC relay in different deep.

doi:10.6844/NCKU201900671

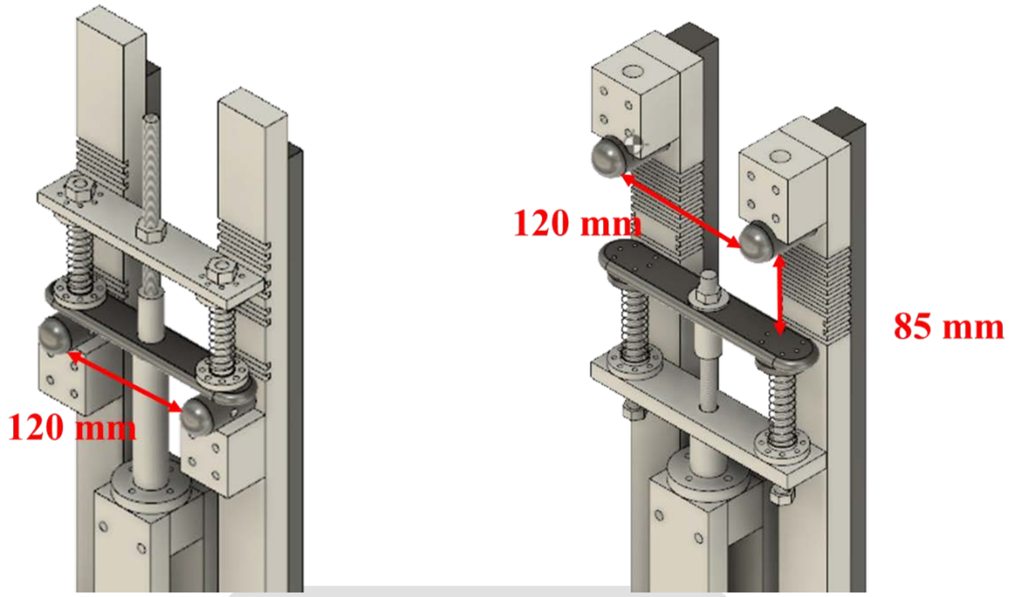

Figure 4.8: The distance between two electrodes is bigger than 22.3 mm. On the left is the NO relay and on the right side is the NC relay.

4.2.4 The spring supporting frame

The spring force is used to strengthen the contact between electrodes and the metal plate. It consists of a metal plate, a plastic plate, two convex flanges, two framing flange, two spring, and two fully threaded rod. The spring is fixed between the convex flange and the framing flange. The convex flange is screwed on the metal plate. The framing flange is screwed on the plastics plate. Nuts are used to adjust the distance between the metal plate and the plastic plate or the distance between the metal plate and two electrodes.

The length of the spring is longer than the distance between the plastic plate and the metal plate, as shown in Figure 4.10, the spring supporting frame is designed slightly swaying to allows the metal plate to make stronger contact with electrodes.

doi:10.6844/NCKU201900671

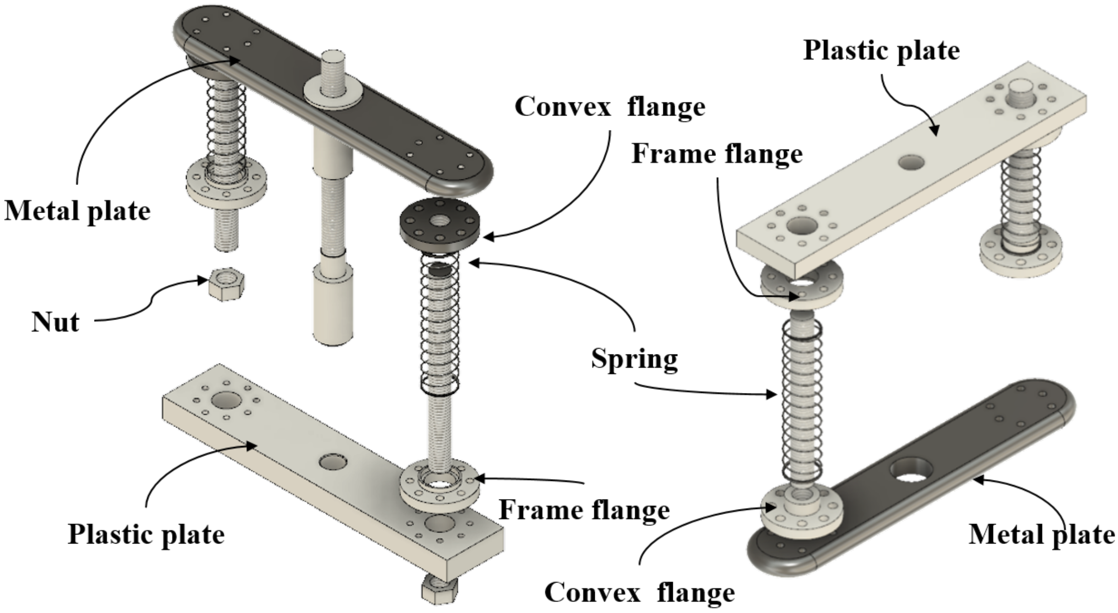

Figure 4.9: The constitution of the rod of the spring support frame. On the left is the NO relay and on the right side is the NC relay.

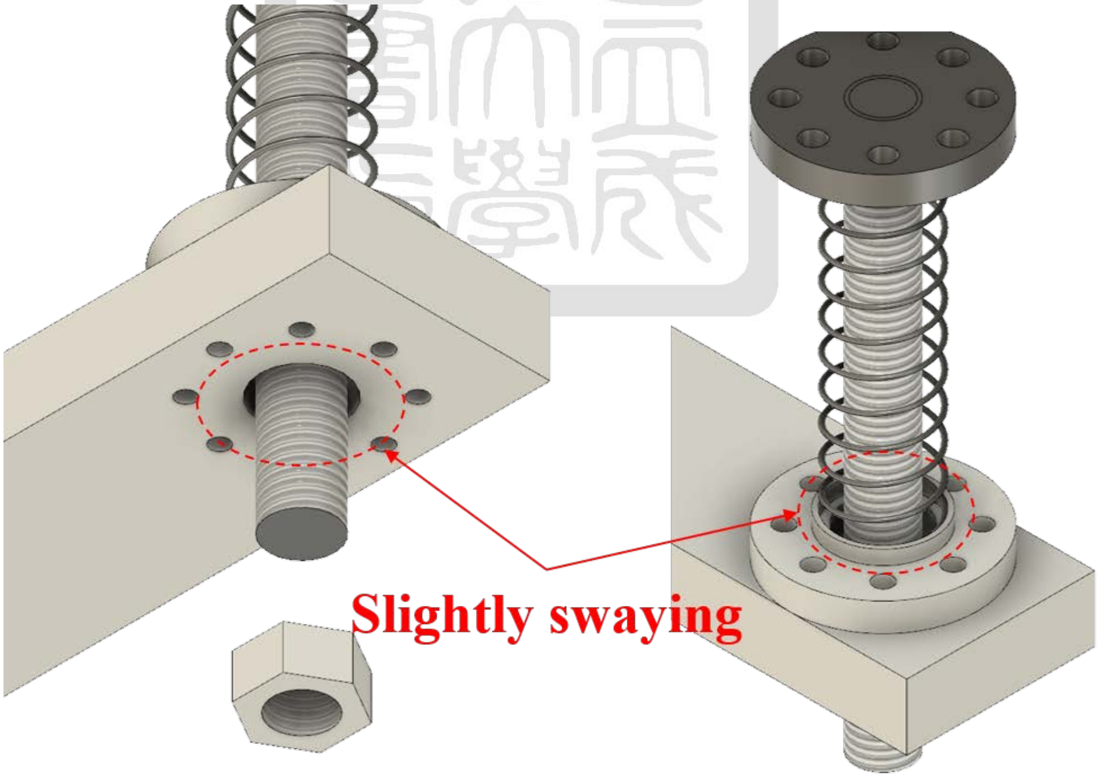

Figure 4.10: Special design of the spring frame for strong contact.

doi:10.6844/NCKU201900671

4.2.5 Operation of relays

When the air cylinder is driven by the compressed gas, the relay is activated. The metal plate will make contact with or be away from two electrodes. Show in Figure 4.11 is how the NO relay and the NC relay look like when it is deactivated or activated.

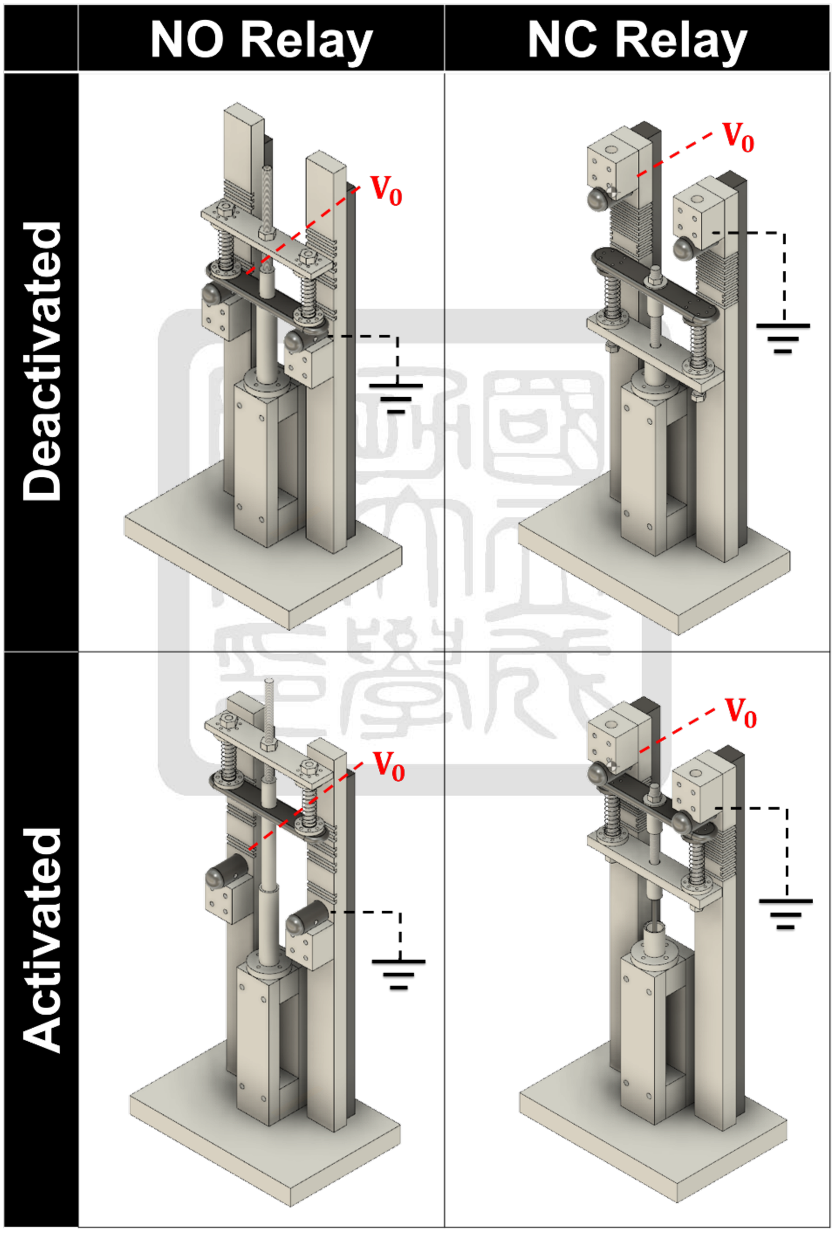

Figure 4.11: NO relay and NC relay in deactivated and activated

doi:10.6844/NCKU201900671

Chapter 5 Multistep triggering system

The fast trigger pulse is generated from a Marx generator. It is used to trigger the rail-gap switch forming the multichannel discharge in the switch. The requirement of the fast trigger pulse generator is to provide a trigger pulse with a rising speed > 5 kV/ns[7]. Therefore, we use a multistep triggering system consisting of an improved small pulse generator[3] and a Marx generator introduced in section 5.1. In section 5.2, the general Marx generator and one used in our lab are introduced. We use a different gap distance and different electrodes to optimize the Marx generator. The process is introduced in section 5.3. In section 5.4, we show the data and the optimized parameters.

5.1 Multistep triggering system

The multistep triggering system divides the triggering process into several stages (1) to avoid the possibility of arcing between the power ground and the earth ground. (2) to prevent the system current transmitted back to the instrument, and (3) to deliver energy with the required amplitude and the rising (falling) speed for triggering the rail-gap switch.

As shown in Figure 5.1, the transistor-transistor logic(TTL) signal is converted from the fiber transmitter into an optical signal which is transmitted to the receiver in the trigger-pulse system. The optical signal is then converted back to the electrical signal to activate the trigger-pulse system. The trigger-pulse system sends a -17-kV pulsed signal with a rising time of 55 μs[2,3]. The pulse is too slow. Therefore, this is used to trigger the Marx generator providing a -40-kV pulse with a rising time of 5 ns, i.e., a falling time of 5 ns, to trigger the rail-gap switch.

doi:10.6844/NCKU201900671

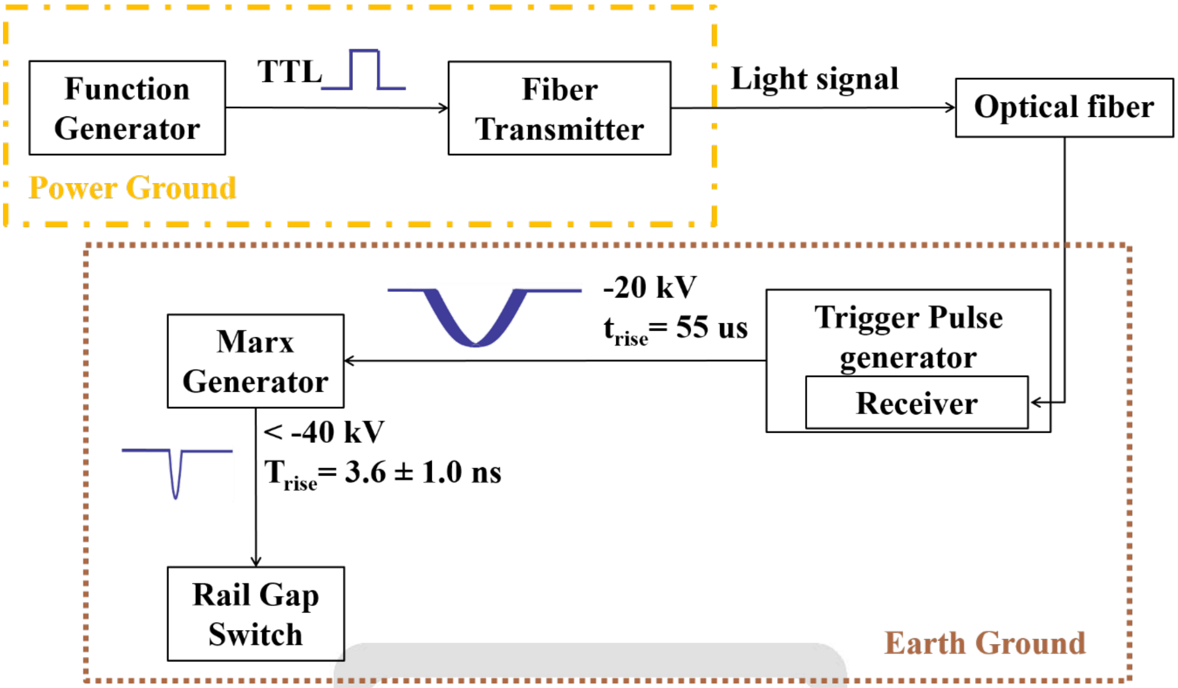

Figure 5.1: the operation of the multistep trigger system is shown.

5.1.1 The battery-powering trigger-pulse generator

In the original trigger-pulse generator[3], the power supply of the receiver is connected to the power ground. In other words, the earth ground and the power ground were connected to each other leading to some EMP issues. To cut off the connection between the power ground and earth ground, we replaced the AC-to-DC converter to a 24V battery connecting to a DC-to-DC converter (V_{in} =18~36 V, V_{out}=15 V). The DC-to-DC converter provides a steady DC output of 15 V even the voltage of the battery drops over time. The ground of the battery floats with the chassis ground. Therefore, there is no arcing between the power ground and the earth ground. Furthermore, there is no path to conduct a current back to any instruments through the ground wire.

As shown in Figure 5.2, the power of the trigger-pulse generator is a 24-V battery which connected with a DC-to-DC converter to provide a 15-V DC power for the IGBT. Everything remains the same except that the ground potential of the trigger-

doi:10.6844/NCKU201900671

pulse generator floats with the earth ground.

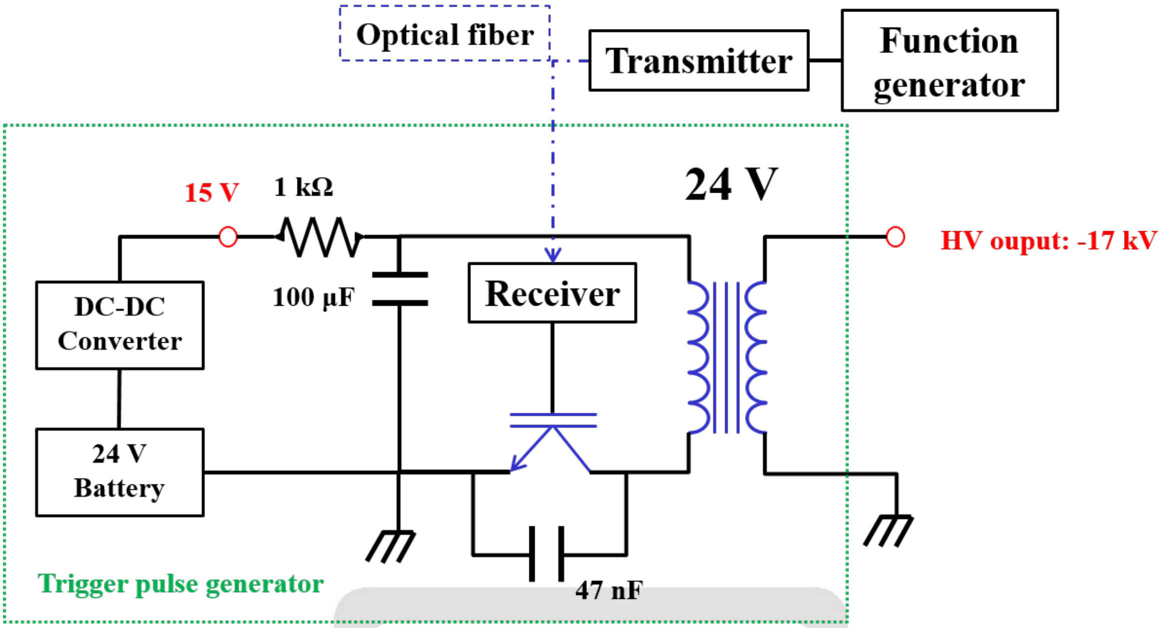

Figure 5.2: The trigger-pulse generator using a 24 V battery.

5.2 The Marx generator

A Marx generator is used to generate a pulse output with a voltage several times of the input DC voltage a DC power supply. As shown in Figure 5.3, a Marx generator has many capacitors connected in parallel when they are charged to V_0. Each pair of electrodes, i.e., each switch in each stage can hold the high voltage V_0. When each switch in each stage is activated, sequentially, capacitors are discharged as connected in series. The system then provides a pulse output with a voltage several times of V_0.

doi:10.6844/NCKU201900671

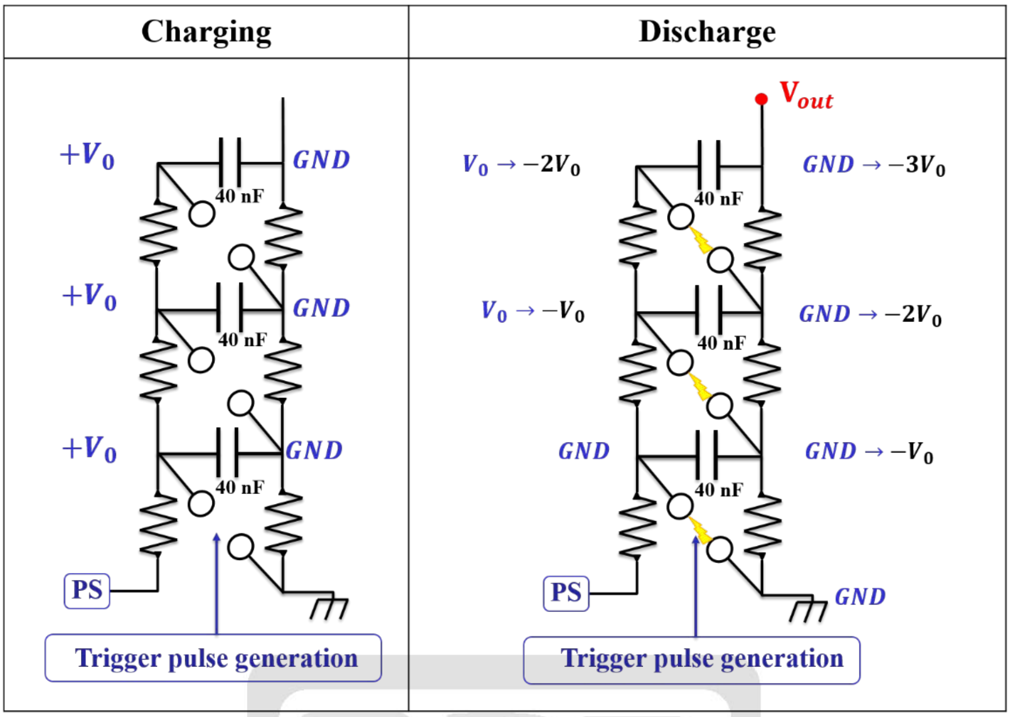

Figure 5.3: The charging and discharging of the Marx generator.

As shown in figure 5.3, the Marx generator in our lab uses three capacitors. The capacitance is 40 nF. The three-stage Marx is used. The fourth switch, called the peaking switch, is used to filter out low voltage signals and increase the rising time (falling time in reality since it is a negative output).

The 1st switch is a Trigatron switch, where disk electrodes are used. The gap distance is 10 mm. Trigatron has two main electrodes, the anode and the cathode with an insulated trigger embedded in the cathode, as shown in Figure 5.4.

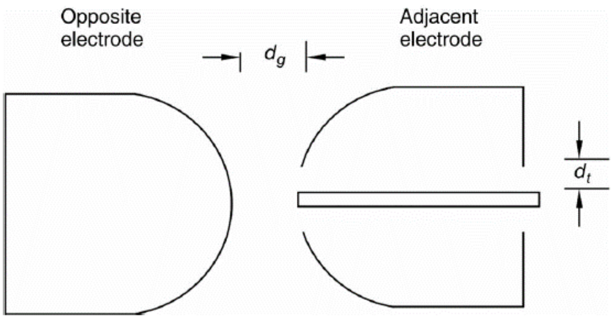

Figure 5.4: A Trigatron switch has a trigger pin embedded in one of the electrodes.

doi:10.6844/NCKU201900671

The 2nd and the 3rd switches are self-breakdown switches which use M8 Cap nuts as electrodes. From Table 1.2, we know the Paschen's curve of the M8 cap nut. Therefore, we can determine the gap distance based on Table 1.2. The gap distance is 7 mm.

The 4th switch is a peaking switch which uses the disk electrode to increase the falling speed of the output signal. From Table 1.2, we know the Paschen's curve of the disk electrode. Therefore, we can determine the gap distance based on Table 1.2. The gap distance is 10 mm.

The output of the 4th switch is connected to the earth ground through a 100 Ω resistor as the load so that the output (test point in Figure 5.5(b)) is at the ground before the switch is closed.

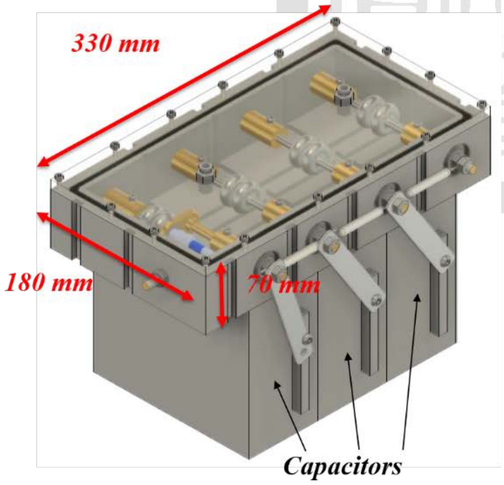

(a)

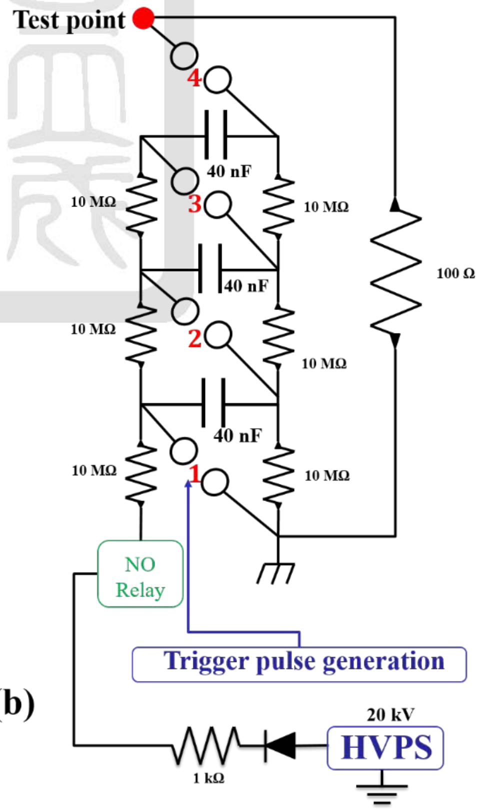

(b)

Figure 5.5: The (a) the top view of the Marx generator. (b) the circuit diagram of the Marx generator.

doi:10.6844/NCKU201900671

5.3 Optimization of the Marx generator

The goal is to generate pulse signals with a rising speed of > 5 kV/ns. In this case, they are fast enough to trigger the rail-gap switch forming the multichannel discharge. The output of our Marx has two peaks before the main pulse, as shown in Figure 5.6. The falling speeds of those two peaks are slow and the amplitudes are low. The amplitudes are not high enough to trigger the rail-gap switch. Nevertheless, we still want to eliminate the effect from those two peaks.

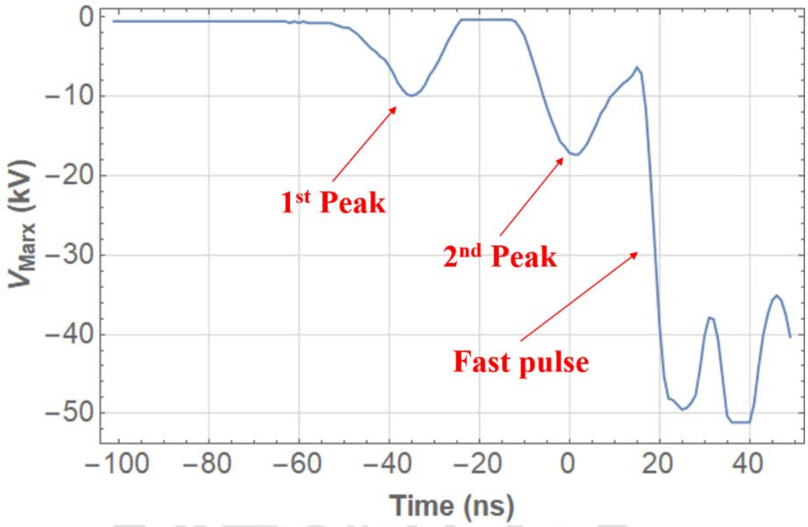

Figure 5.6: the pulse waveform of the Marx generator

We suspected the following factors that affect the output signal of the Marx generator: (1) the UV light generated from discharges of each switch will affect discharges of other switches; (2) resistance of the load makes the difference; (3) each switch has a different breakdown voltages, and equivalent capacitance; (4) electrodes with different shapes have different equivalent capacitances.

We have designed a series of experiments, shown in Table 5.1, to explore dependences of these factors of the output signal of the Marx generator.

In Comparison 1, in order to confirm the dependences of UV light, we placed black acrylic plates as blockers between each stage to block UV light, as shown in Figure 5.7. In Comparison 2, in order to confirm the dependence of resistance of the

doi:10.6844/NCKU201900671

load resistor, two resistors, 100 Ω and 1 kΩ, were used. In Comparison 3, M8 cap nuts were used for the 4th switch. Three gap distance, 10 mm, 14 mm, and 18 mm were tested. In Comparison 4, the gap distance of the 4th switch was kept 10 mm. We used two different type electrodes for that switch. In Comparison 5, the gap distance of the 4th switch was kept 18 mm. We used two different types of electrodes for that switch.

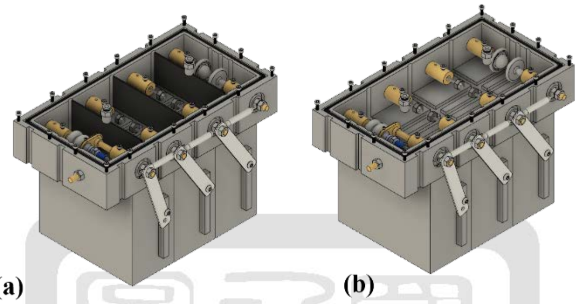

Figure 5.7: (a) The Marx with blockers. (b) Without blockers.

We measured the signal characteristics of the Marx generator including the rise speed and the rise time under different conditions listed above.

Table 5.1: the various parameters experiments.

Comparison	Test	Shading or not	Resistance	Gap distance	Electrode	Result
1	1	Blocker	100 Ω	10 mm	Disk	No Shading
	2	No Blocker	100 Ω	10 mm	Disk	
2	3	Blocker	1k Ω	10 mm	Disk	100 Ω
	4	Blocker	100 Ω	10 mm	Disk	
3	5	Blocker	100 Ω	10 mm	Disk	10 mm
	6	Blocker	100 Ω	14 mm	Disk	
	7	Blocker	100 Ω	18 mm	Disk	
4	8	Blocker	100 Ω	10 mm	M8 Cap nut	Disk electrode
	9	Blocker	100 Ω	10 mm	Disk	
5	10	Blocker	100 Ω	18 mm	M8 Cap nut	
	11	Blocker	100 Ω	18 mm	Disk	

5.4 Experimental Results

Results of different comparison in Table 5.1 are as following:

(1) Comparison 1: as shown in Figure5.8, the black points are the case

doi:10.6844/NCKU201900671

without no blockers, and the red points are data with blockers. There is no significant difference between experiments with and without acrylic blocking UV light between switch. Both the 2nd peak with using blockers were higher than -20 kV. However, the 2nd peak is higher without blockers than with blockers. Therefore, we decided not to use blockers.

(2) Comparison 2: shown in Figure5.9 is the comparison of using two different load resistors. The black data points are from the experiment using 100 Ω and the red data points are from the experiment using 1 kΩ. The delay time between the 1st peak and the 2nd peak shows that $\Delta t_{100\Omega} < \Delta t_{1\,k\Omega}$. Therefore, the 100 Ω resistor will be used.

(3) Comparison 3: shown in Figure 5.10 is a comparison of using disk electrodes with three different gap distance. The data of red points is from using the 10-mm gap. The data of gray points is from using the 14-mm gap. The data of yellow points is from using the 18-mm gap. All data is shifted onin time so that the second peaks of each data overlap with each other roughly. There are two significant differences. One is the delay time Δt between the 1st peak and the 2nd peak. The delay time between these two peaks Δt_{10} is the shortest when 10 mm gap distance is used. The other thing is that with a longer gap distance, output voltage V is lower and the falling time Δt_{fall} is longer. Therefore, the best option is to use a 10-mm gap.

(4) Comparison 4 and 5: shown in Figure 5.11 is the comparison of using two different electrodes while keeping the gap distance of the 4th switch10 mm. The data of red points are from using disk electrodes. The data of gray points are from using M8 cap nut. Again, data is shifted in time so that those second peaks

doi:10.6844/NCKU201900671

are overlapped. It shows that the delay between two peaks is shorter when disk electrodes are used. Similar results for using 18 mm gaps are obtained, as shown in Figure 5.12. Therefore, disk electrodes will be used.

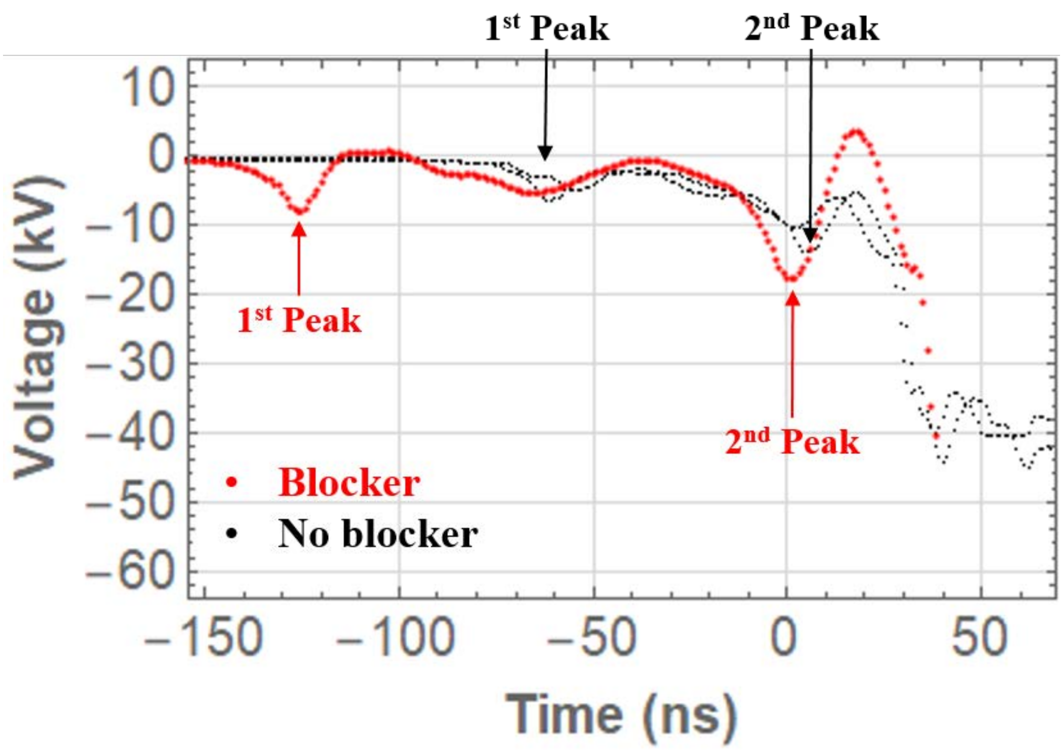

Figure 5.8: Blocker(Red) or not blocker(Black)

doi:10.6844/NCKU201900671

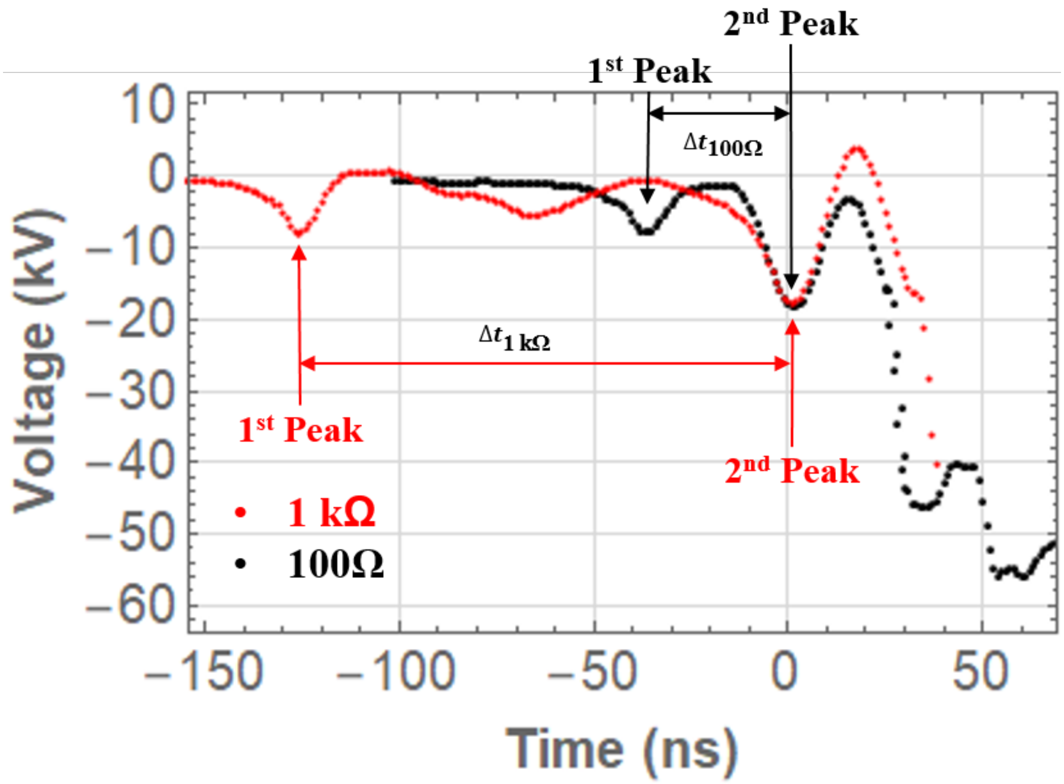

Figure 5.9: 1 kΩ(Red) and 100 Ω(Black)

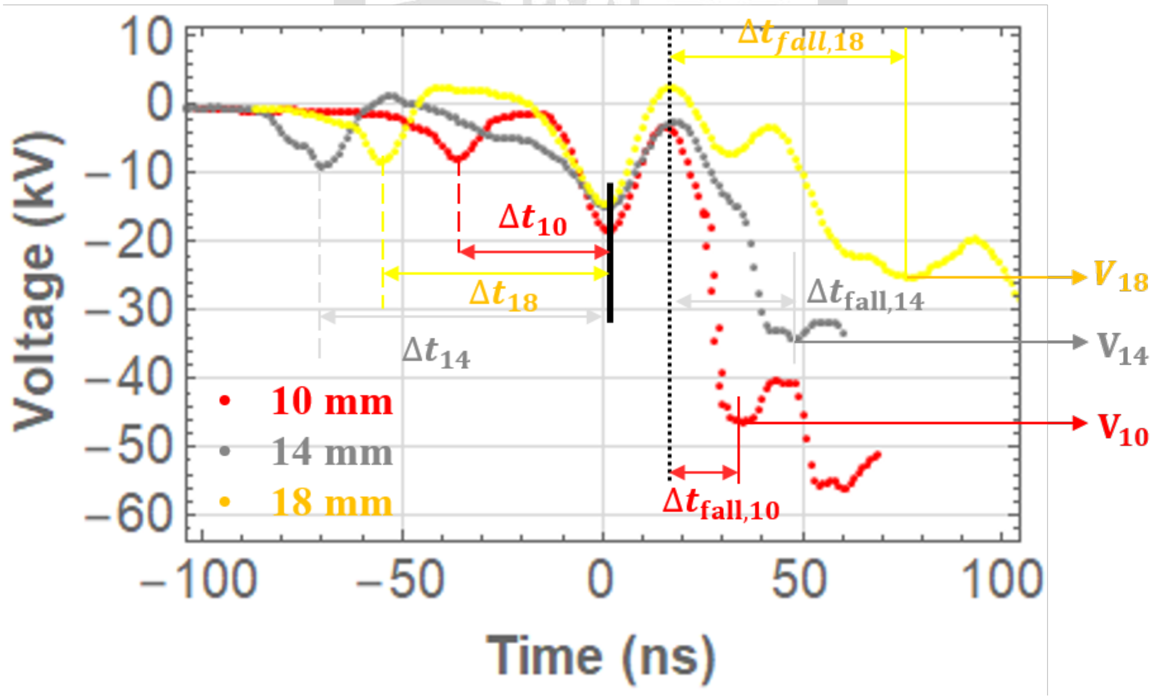

Figure 5.10: the experiment of three different gap distance.

doi:10.6844/NCKU201900671

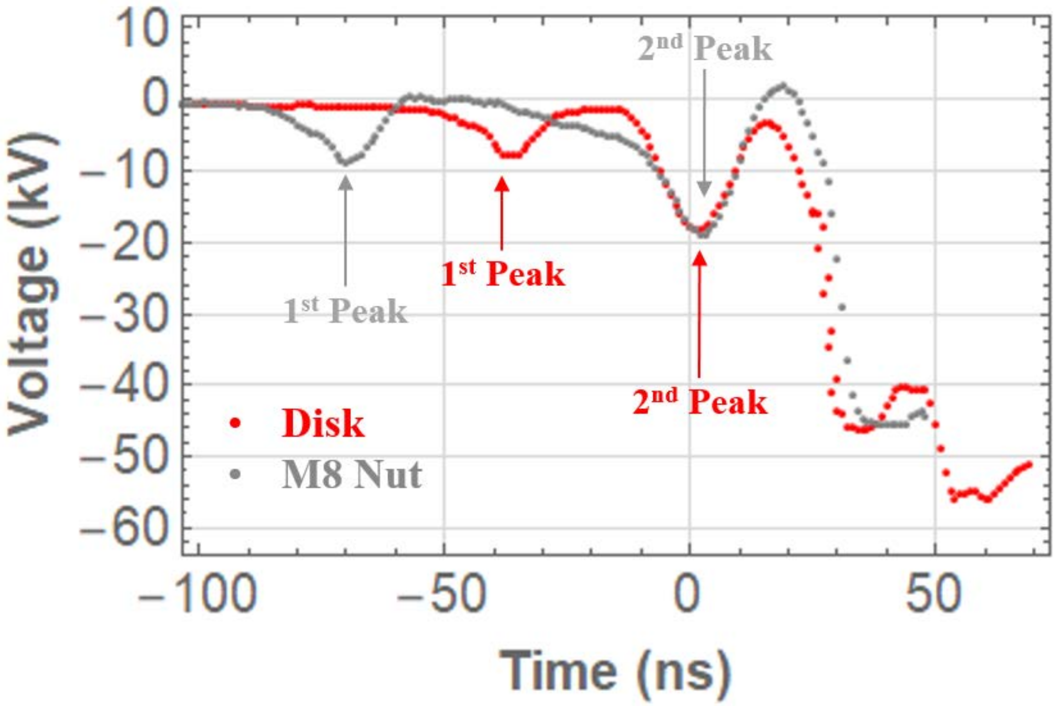

Figure 5.11: 10 mm gap distance experiments: the data of disk is red. The data of the M8 cap nut is gray.

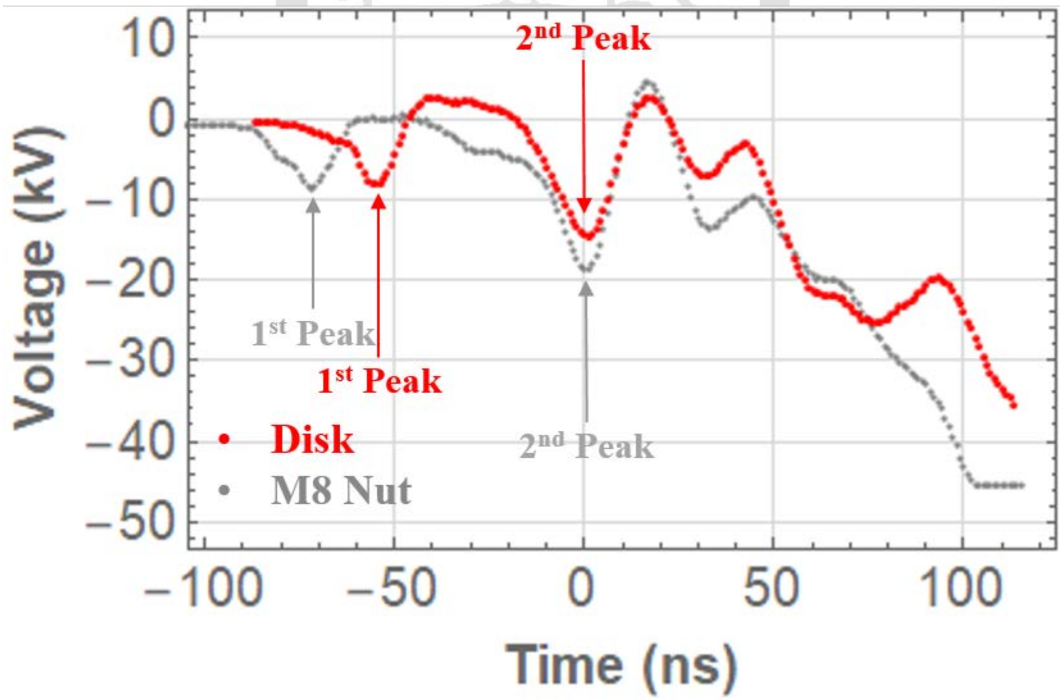

Figure 5.12: 18 mm gap distance experiments: the data of disk is red. The data

doi:10.6844/NCKU201900671

of the M8 Nut is gray.

After these tests, the best conditions are : (1) without using blockers; (2) 10-mm gap, and (3) using disk electrodes in the peaking switch. We also measured the performance of the Marx generator, which is the falling speed of voltage. We measured the output voltage 5 times. In each data, 5 data points shown in Figure 5.13 were used. A straight line fitted to those 5 data points in each experimental result. The slope is the falling speed. The 5 times fitting results are shown in Table 5.2. The falling speed of the Marx generator is -6.6 ± 0.4 kV/ns. It meats the requirement of generating a pulse with a rising speed of > 5 kV/ns for triggering rail-gap switches.

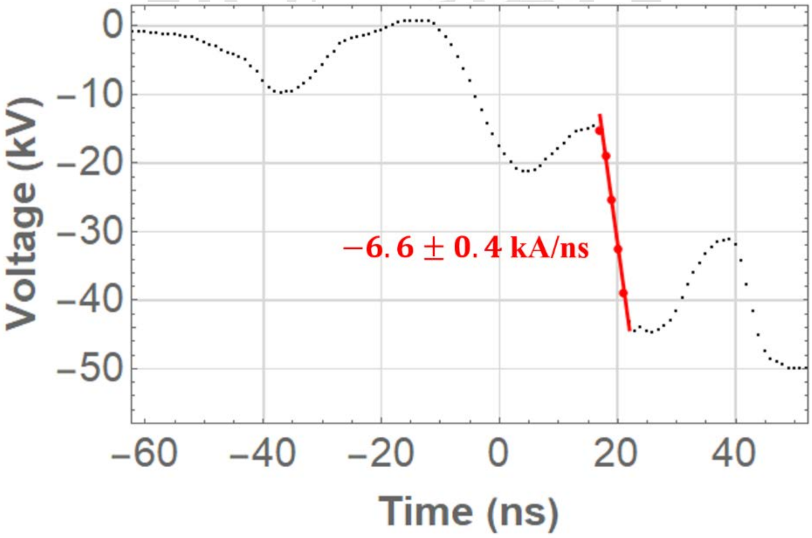

Figure 5.13: the five data point used to fit the falling speed of the voltage.

Table 5.2: Fitting data of five times experiment and the result of an average and the standard deviation is shown.

Data	1	2	3	4	5	avg	std
Falling speed [kV/ns]	-6.46	-7.08	-6.44	-7.	-6.24	-6.6	0.4

doi:10.6844/NCKU201900671

Chapter 6 The rail-gap switch testing

In PPCB, low inductance switch, the rail gap switch is used. The inductance of the rail-gap switch is indirectly obtained by fitting the discharge current to the RLC oscillation equation. Therefore, we set up experiments that included a rail-gap switch, different numbers of bricks of capacitors and some wires with fixed inductances. Through analyzing data, we can obtain the inductances of capacitors and switches. In section 6.1, the general rail-gap switch and parameters of the rail-gap switch in our lab are introduced. The total inductance of the experimental system is analyzed by fitting the discharge current to the RLC oscillation. We use it to get the inductance of the rail gap switch and one-brick capacitor. This experimental setup are introduced in section 6.2. In section 6.3, the process of analyzing data was introduced. The result is shown in section 6.4.

6.1 Rail-gap switches

A rail gap switch is one of the most critical instruments in PPCB. It consistently holds a high voltage when the system is being charged. It becomes conductive in a short period time the discharge current from capacitors. Multichannel discharge of the rail-gap switch can conduct the discharge current uniformly distributed ling the rail-type electrode achieving a small inductance. To initiate multichannel discharge in the rail-gap switch, a fast high voltage trigger pulse with a rising speed >5 kV/ns is required. The trigger pulse was generated using the multistep triggering system introduced in Chapter 5.

A rail gap switch is like a spark gap. However, its electrodes are two long cylinders parallel to each other to promote multichannel. As shown in Figure 6.1(a), the rail-gap switch has three electrodes. They are anode and cathode and a knife edge

doi:10.6844/NCKU201900671

electrode(E_1, E_2, and T,). The anode and the cathode are rail-like. The rounded shape provides a small field enhancement. Contrarily, the knife edge electrode highly enhances the field by a edge and is triggered by a fast-rising trigger pulse (>5kV/ns) [7]. The gaseous insulating mediums like SF6, N2, Ar, or mixtures of these at pressures of a few atmospheres are used generally.

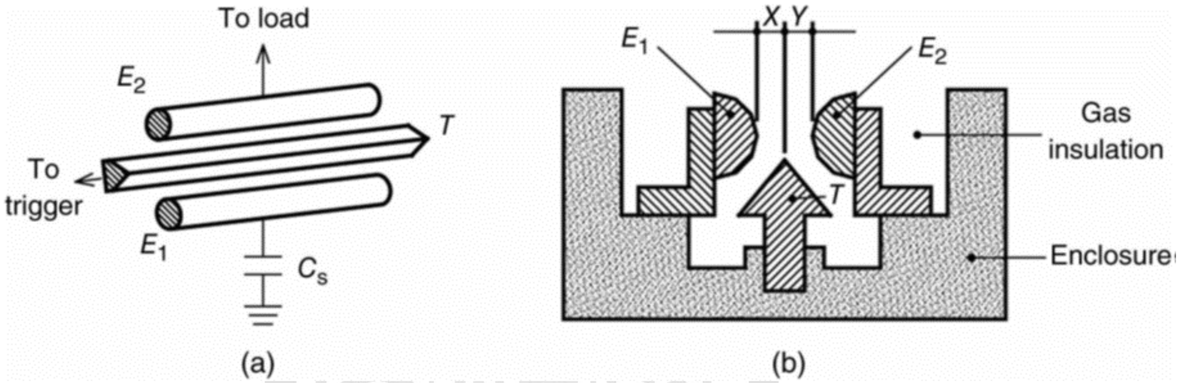

Figure 6.1: (a)A rail gap switch has long electrodes to encourage multichannel. (b)A typical mounting arrangement for an electrically triggered rail gap.[8]

The rail-gap switch which used in our lab, shown in Figure 6.2, consists of two rail-like electrodes, a knife edge electrode, a trigger pin, two bridges, two connectors, and a cover box. Two rail-like electrodes, the knife edge, two bridges are made of stainless steel. The trigger pin and two connectors are made of brass. The box of the rail-gap switch is made of polyformaldehyde (POM) and the top of the box is made of acrylic. The trigger pin receives the pulsed trigger signal and passing it to the knife edge electrode so that the signal triggers the rail-gap switch. A rail-like electrode, a bridge, and a connector are connected by stainless-steel screws. The function of the bridge is used to adjust the parallelism and the height between the knife edge electrode and two rail-like electrodes, and also the distance of the gap between two rail-like electrodes. To keep the breakdown voltage stable and clean in the box, a

doi:10.6844/NCKU201900671

compressed dry air provided by the compressed gas cylinder keeps flowing through the switch with a flow rate of 8 L/min. The same flow goes through the Marx generator in the multistep triggering system.

Shown in Figure 6.3 is the side view of the rail-gap switch. $\boldsymbol{A_1}$ and $\boldsymbol{A_2}$ are axes of two rail-like electrodes in the plane $\boldsymbol{S_{E\_axis}}$. $\boldsymbol{P_{knife}}$ is the ridgeline of the knife edge electrode which in on the plane $\boldsymbol{S_{E\_axis}}$ as well. $\boldsymbol{S_{E\_bottom}}$ is the plant tangential to the bottom of two electrodes. $\boldsymbol{S_{knife}}$ is the upper plane of the base of the knife edge electrode.

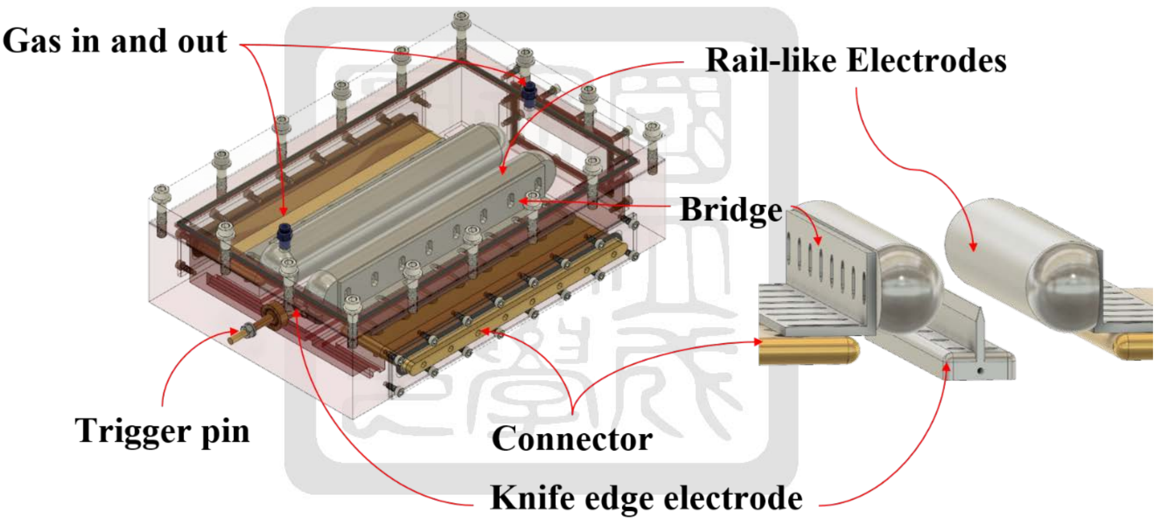

Figure 6.2: Schematics of the rail gap switch.

doi:10.6844/NCKU201900671

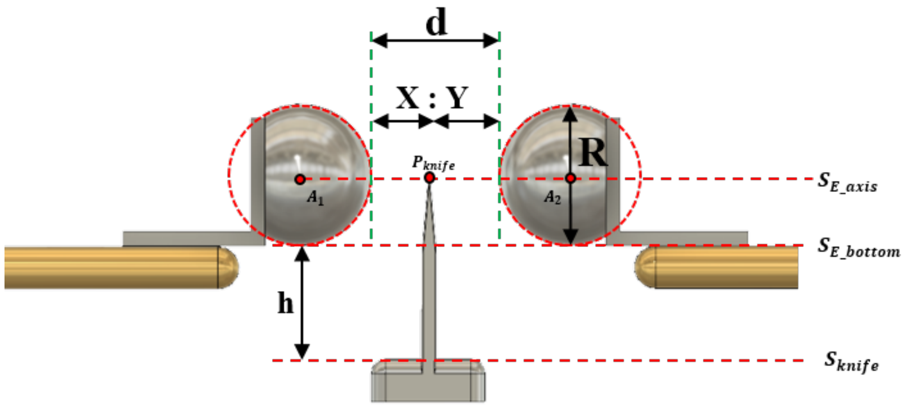

Figure 6.3: Relative position relationship of components in the rail gap switch.

The distance of the gap between two electrodes is critical for the breakdown voltage. Thus, spacer A, as shown in Figure 6.4, was build to fix the gap distance with 21 mm between two electrodes. The gap is too wide for 20 kV. Therefore, we only used spacer A to obtain the parallelism between $\boldsymbol{A_2}$and $\boldsymbol{A_2}$, and the height between $\boldsymbol{S_{E\_bottom}}$ and $\boldsymbol{S_{knife}}$ to ensure the $\boldsymbol{P_{knife}}$ is on the plane $\boldsymbol{S_{E\_axis}}$.

The breakdown voltage of the rail-gap switch with the ratio of Y=3 mm to X=6 mm in Figure 6.3 at 1 atm is 29.4 ± 0.9 kV, as shown in Figure 6.5. To make the rail-gap switch hold a higher breakdown voltage, 1 mm was added to each gap between the knife-edge electrode and each rail-like electrodes. Therefore, the total distance we used was 11 mm. Therefore, I designed spacer B, as shown in Figure 6.6, which is made of three plates with different thickness.

In order to trigger the rail-gap switch by the multistep-triggering system smoothly, the gap distance between the knife edge electrode and the rail-like electrodes with high voltage terminal is 7 mm and the other side is 4 mm. Therefore, the center plate of spacer B is 5 mm, which has the same thickness as the knife edge. The others are 4.5 mm and 1.5 mm, respectively, so that the ratio of X:Y is 7 mm to

doi:10.6844/NCKU201900671

4 mm. The actual measured values are 4.36 mm and 1.4 mm. Therefore, the electric field from the fast trigger pulse is highly enhanced by the knife edge electrode.

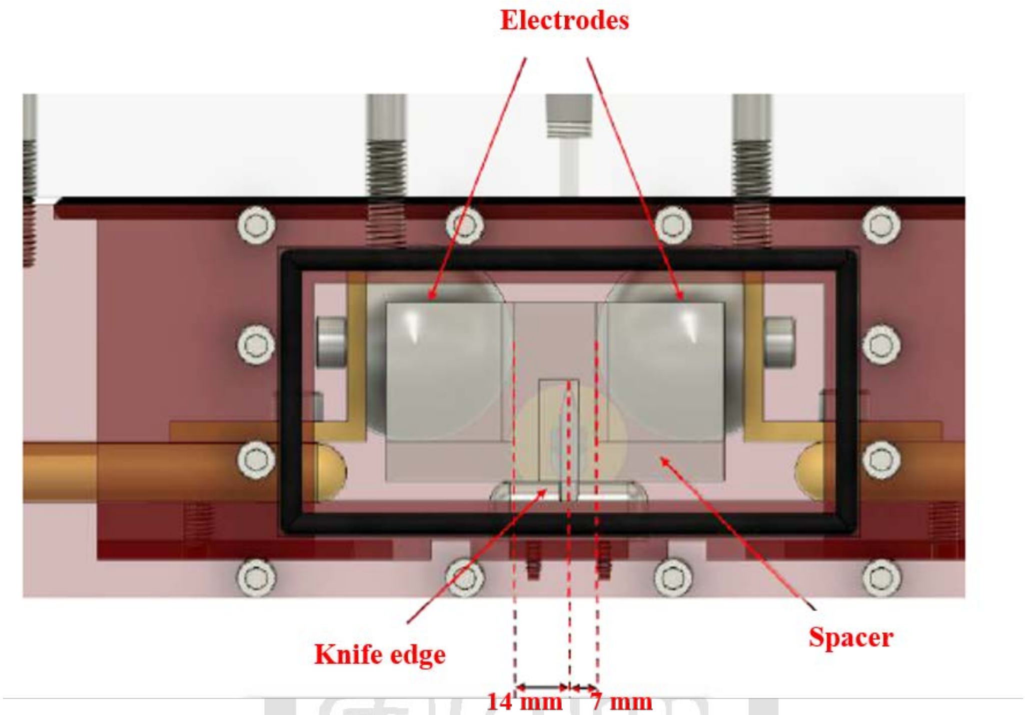

Figure 6.4: Spacer A with the gap distance between the knife edge and the electrode with a high voltage terminal and other gap distance are 7 mm and 14 mm.

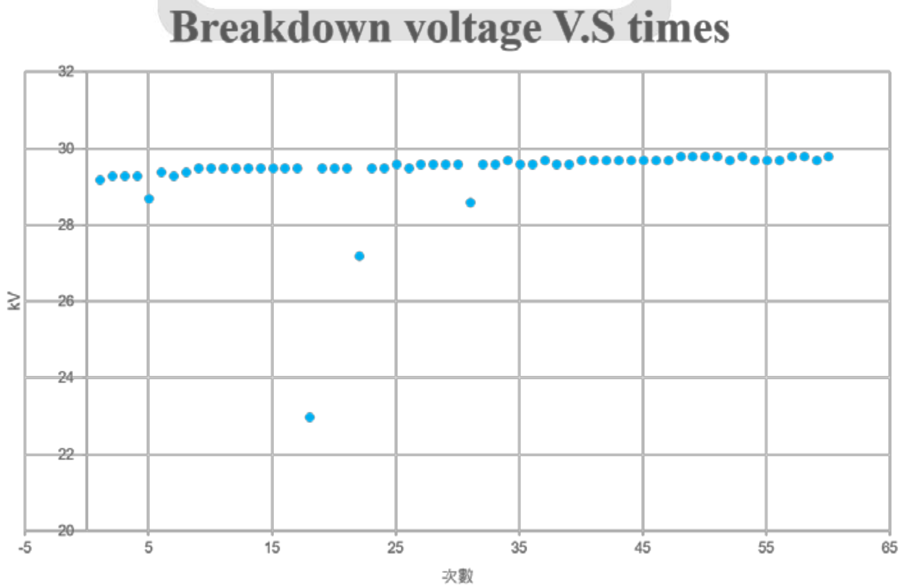

Figure 6.5: The test data of the rail gap switch with a ratio of 6 mm to 3 mm.

doi:10.6844/NCKU201900671

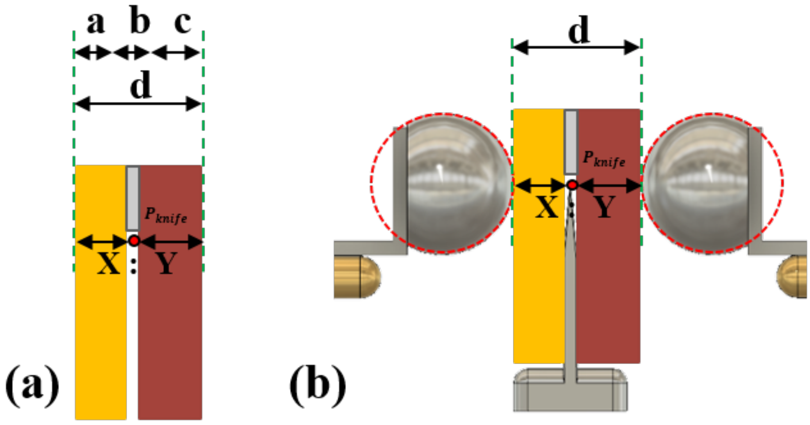

Figure 6.6: Spacer B consists of three different thickness plate. The mid palate is 5 mm, which is the same as a knife edge.

6.2 Experimental setup

To measure the inductance of the rail gap switch, we set up discharge experiments with the rail-gap switch and N-brick capacitor, shown in Figure 6.7. The number od brick is from 1 to 5. All bricks are connected in parallel. In experiments, the N-brick capacitor and capacitors of the Marx generator are charged to 20 kV and measured by using the high voltage probe (HVP). The charging voltage is measured using the HVP and the oscilloscope. The multistep trigger-pulse generator is used to trigger the rail-gap switch. When the rail gap switch is triggered, the output current is measured by a Pearson current Monitor (Model(301X)) and the voltage of the N-brick capacitor was measured using HVP.

Notice that the oscilloscope is powered by a 24-V battery (YUASA: SMF 55B24L) connecting to a DC24V-TOAC110V converter (WM: TS-1000). The ground of the battery, i.e., the ground of the oscilloscope floats with the system ground. If to prevent arcing in the oscilloscope due to the voltage difference between the system

doi:10.6844/NCKU201900671

ground and the power ground. Pneumatic high voltage relay was used to separate the power supply before the rail-gap switch was triggered to protect the power supply. Please refer section 3.2 for the functions and procedures of relays. The system is placed in a ground fence.

doi:10.6844/NCKU201900671

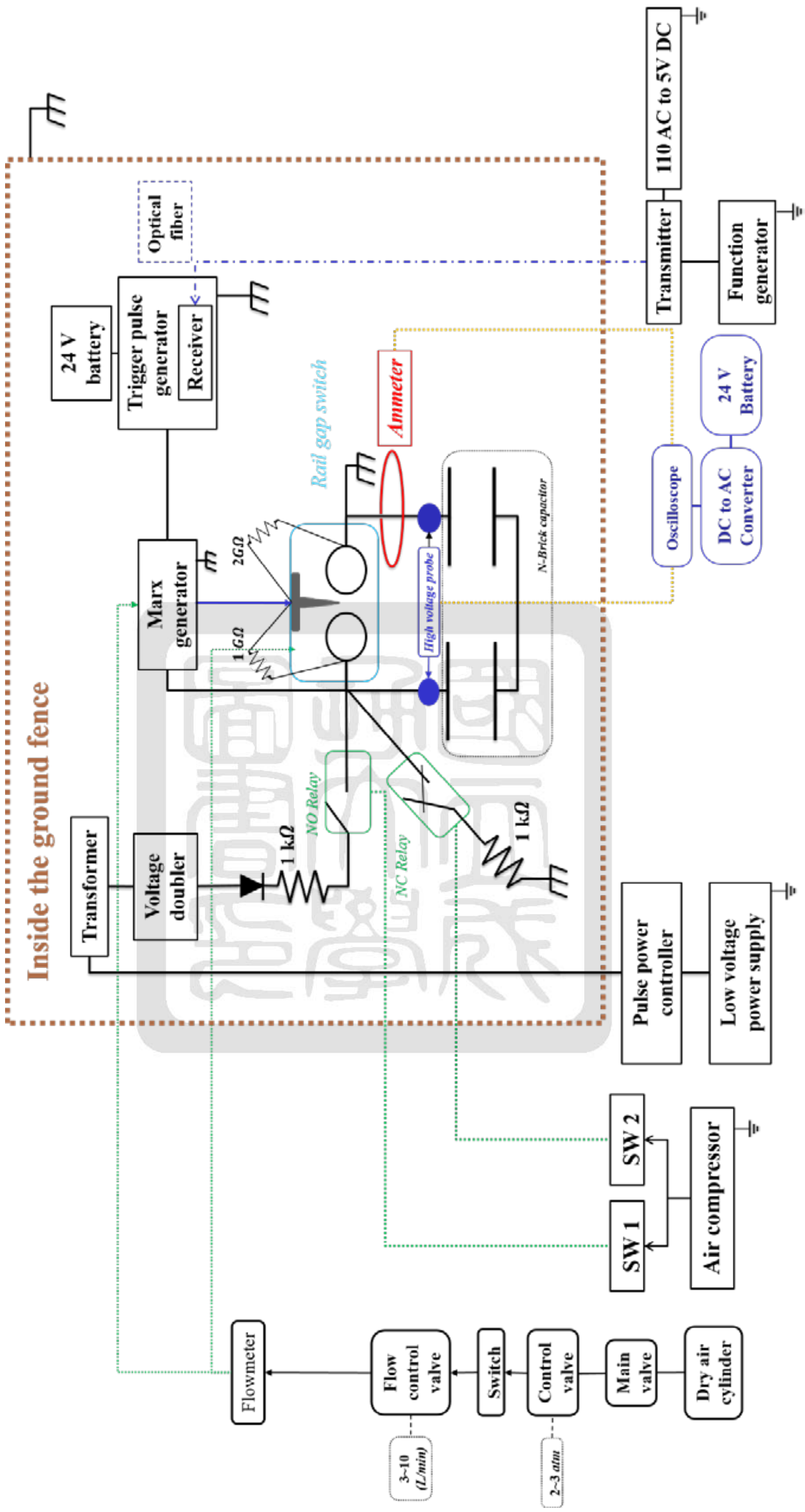

Figure 6.7: Architecture diagram of the N-brick discharge experiment.

doi:10.6844/NCKU201900671

6.3 Analysis method

Output signals of our discharge experiments are underdamped RLC oscillation, as shown in Figure 6.8, so that we can get parameters of the total inductance and the total resistance. We can fit any data using the current formula of the RLC underdamped response:

$$I_{(t)} = \frac{V_{charge}}{\sqrt{\frac{C}{L} - (\frac{R}{2})^2}} e^{-\frac{R}{2L}t} \sin\left(\left[\sqrt{\frac{1}{LC} - (\frac{R}{2L})^2} \right] t \right).$$

Therefore, the function,

$$I_{(t)} = \alpha e^{-\frac{(t-b)}{\gamma}} \sin[\beta * (t-b)],$$

was used to fit the data, while α, β, γ, and b are variables in this curve fitting. The inductance can be solved as

$$L = \frac{1}{C_{N-brick}} \frac{1}{\left(\frac{1}{\gamma}\right)^2 + (\beta)^2} .$$

And the resistance is

$$R = \frac{2L}{\gamma} .$$

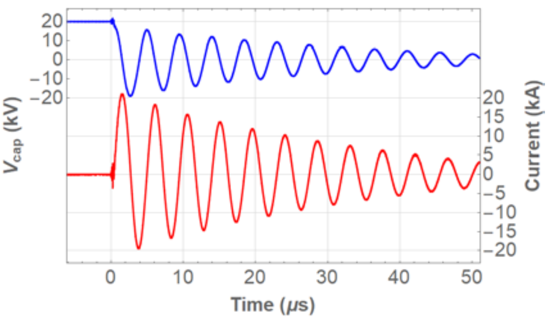

Figure 6.8: The discharge experiment of the one-brick capacitor and the rail-gap switch. The blue data is the voltage of the capacitor. The red data is current.

doi:10.6844/NCKU201900671

The total inductance includes the rail-gap switch, N-brick capacitors and transmission lines. The transmission line consists of 2 pair of straight wires connected in series where each pair consists of straight wires two lines connected in parallel. The inductance of each line is 100 nH [9] so that the total inductance of transmission lines is $\frac{100}{2} * 2 = 100$ nH, as shown in Figure 6.9. To find the inductance of the one-brick capacitor, a sequence of capacitors test discharges with gradually adding more bricks of capacitors were conducted. The capacitor has N-brick capacitors connected in parallel so that the inductance of capacitors is $\frac{L_{1-Brick}}{N}$, where $L_{1-Brick}$ is the inductance of the one-brick capacitor and N is from 1 to 5. Therefore, the total inductance of each discharge experiment is

$$L_{N-total} = (L_{SW} + L_{line}) + \frac{L_{1-Brick}}{N} \ldots \text{Eq (1)}$$

where L_{sw} is the inductance of the rail-gap switch and the total inductance of the transmission line L_{line} is 100 nH. We conducted 5 experiments with different numbers of the one-brick capacitor and measured the total inductance using the curve fitting. Finally, the relationship between total inductance $L_{N-total}$ and N is fitted by using Eq (1). Therefore, L_{SW} and $L_{1-Brick}$ can be obtained.

doi:10.6844/NCKU201900671

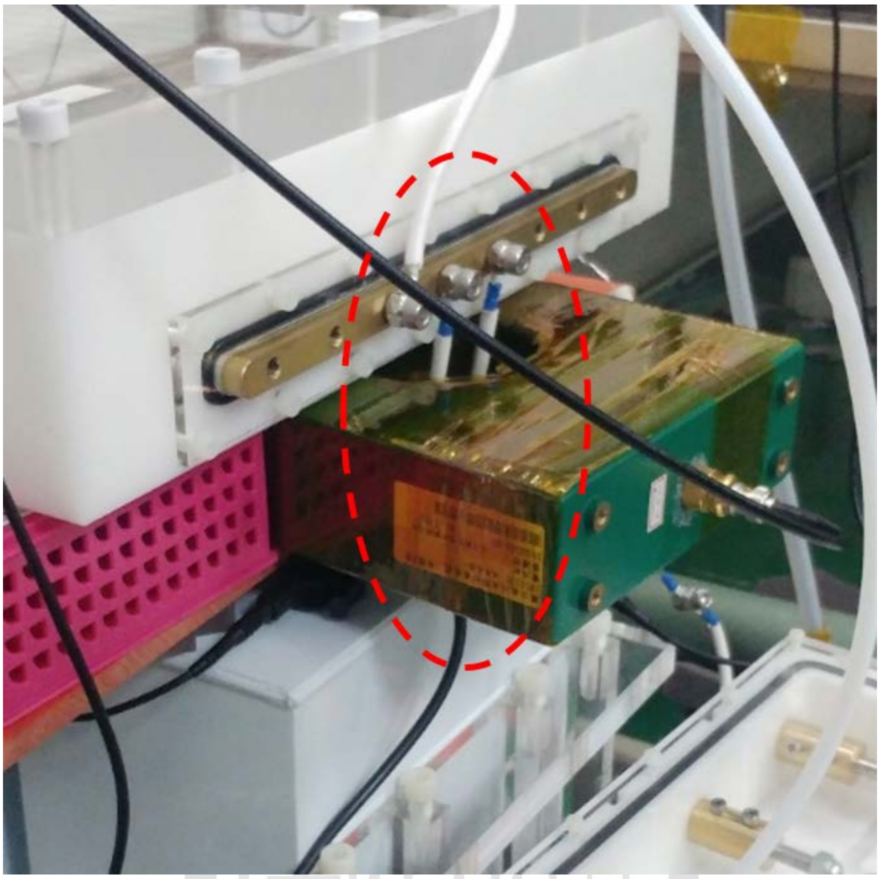

Figure 6.9: The transmission line.

6.4 Experimental Results

The discharge curve with different numbers of brick of the capacitors are shown in Figure 6.10 to Figure 6.14. The averaged fitted parameters are shown in Table 6.2. Note that each condition was repealed more than 10 times. Each current are shown in Figure 6.15. The relationship of L_{total} and N is shown in Figure 6.16 and it is fitted using Eq (1). The peak current is the maximum point of the fitting curve.

doi:10.6844/NCKU201900671

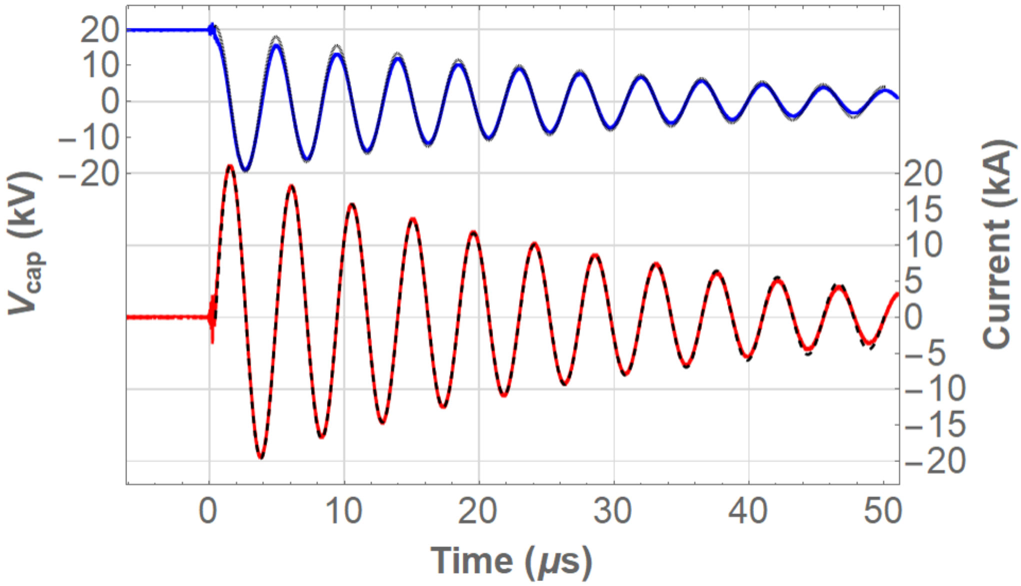

Figure 6.10: The discharge experiment with the one-brick capacitor.

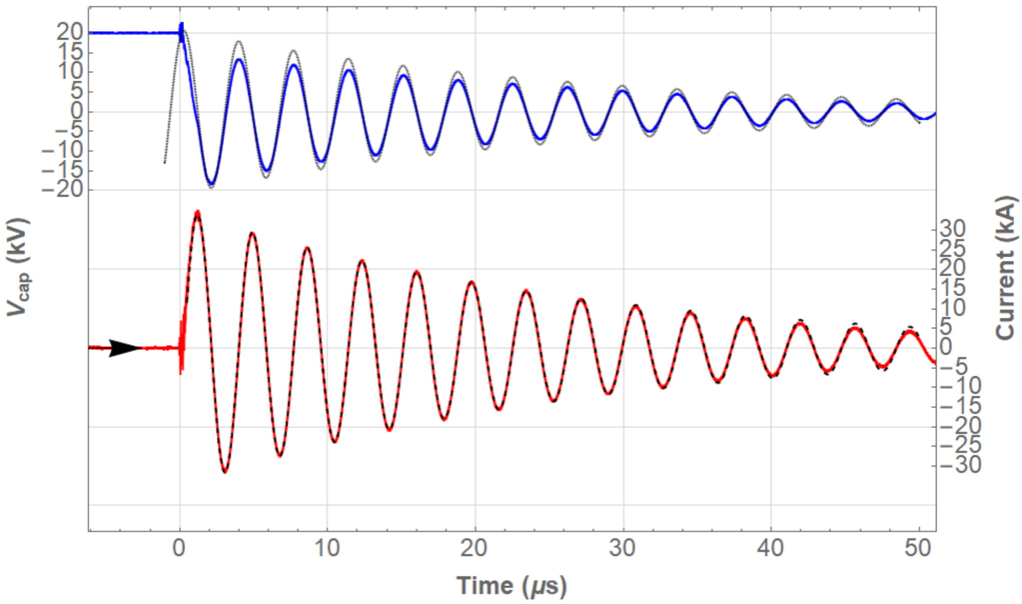

Figure 6.11: The discharge experiment with the two-brick capacitor.

doi:10.6844/NCKU201900671

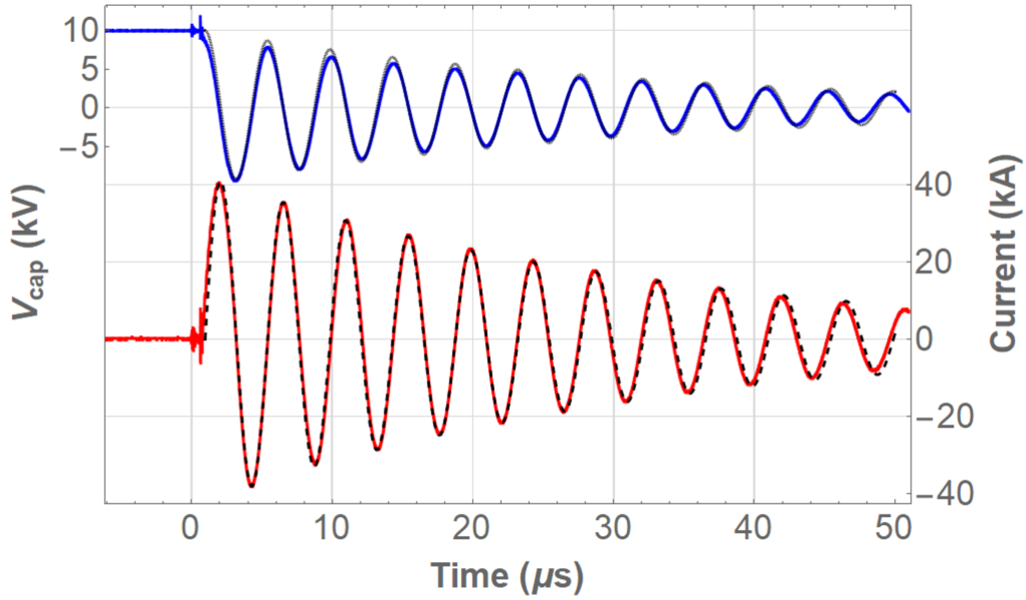

Figure 6.12: The discharge experiment with the three-brick capacitor.

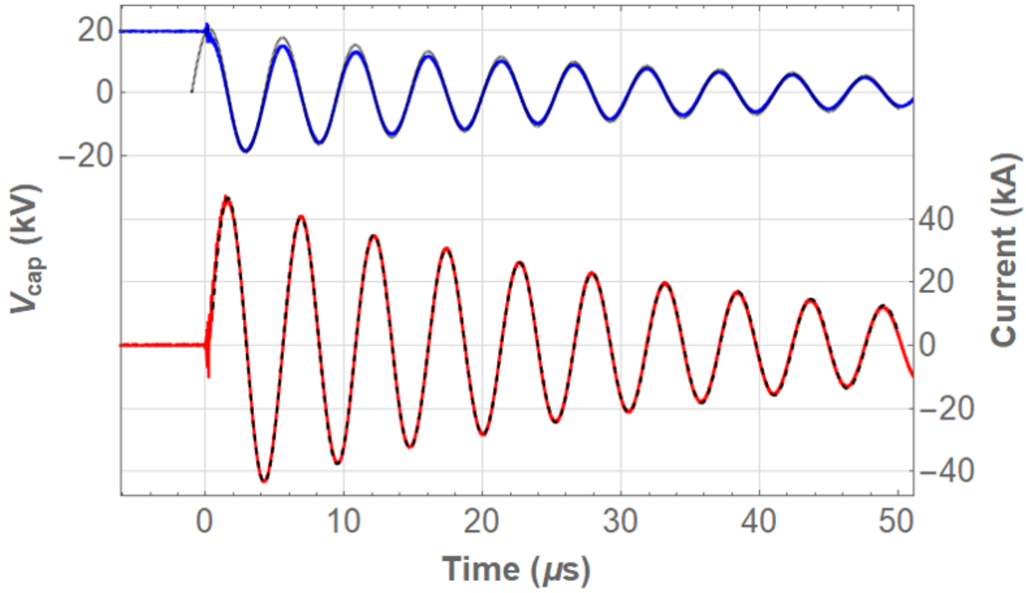

Figure 6.13: The discharge experiment with the four-brick capacitor.

doi:10.6844/NCKU201900671

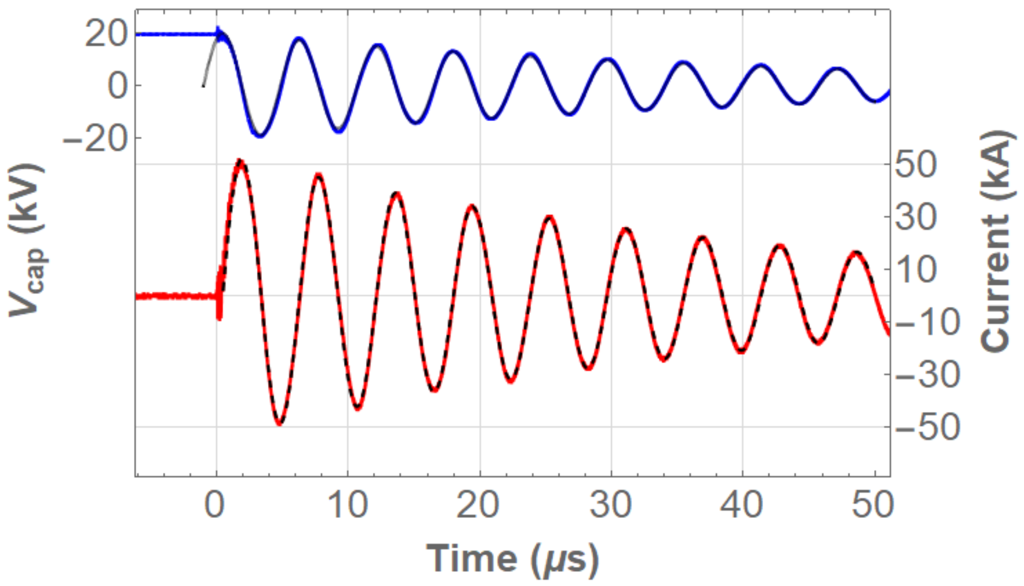

Figure 6.14: The discharge experiment with the five-brick capacitor.

The fitting result is shown in Figure 6.15 and Table 6.1. The fitting result is $L_{total} = (330 \pm 10) + \frac{70\pm20}{N}(\mathrm{nH})$. That means 330 nH is the sum of the inductance of the rail gap switch and the transmission line (100 nH) so that the inductance of the rail gap switch is 230 ± 10 nH. On the other hand, the inductance of the one-Brick capacitor is 70 ± 20 nH.

Table 6.1: The discharge experiment with N-brick.

			Fitting parameter				Solved result		Maximum curve
N-Brick	Data		α	b	γ	β (MHz)	L (nF)	R (mΩ)	Peak current
1	10	Avg	21.0	0.2	19.7	2.2	403	41	20.3
		Std	0.3	0.0	0.4	0.0	5	1	0.2
2	10	Avg	34.5	0.3	25.8	1.7	356	27.6	33.3
		Std	0.3	0.0	0.4	0.0	4	0.7	0.4
3	10	Avg	43.2	0.8	31	1.4	337	21.7	41.7
		Std	0.6	0.3	1	0.0	4	0.9	0.6
4	7	Avg	48.4	0.4	36.5	1.2	350	19.2	46.7
		Std	0.8	0.1	0.5	0.0	4	0.5	0.8
5	8	Avg	53.5	0.4	40.4	1.1	351	17.4	51.6
		Std	0.8	0.1	1.2	0.0	6	0.8	0.7

doi:10.6844/NCKU201900671

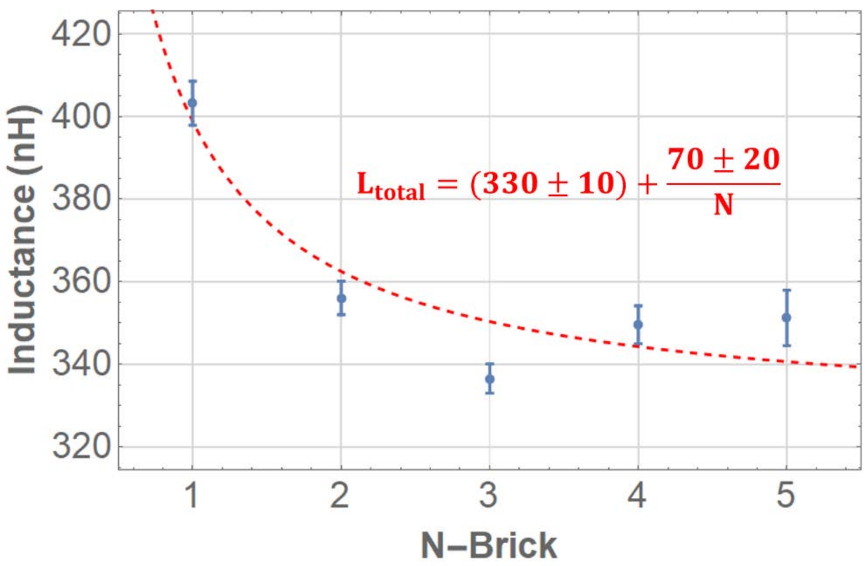

Figure 6.15: The average data of each experiment is used to fit the curve.

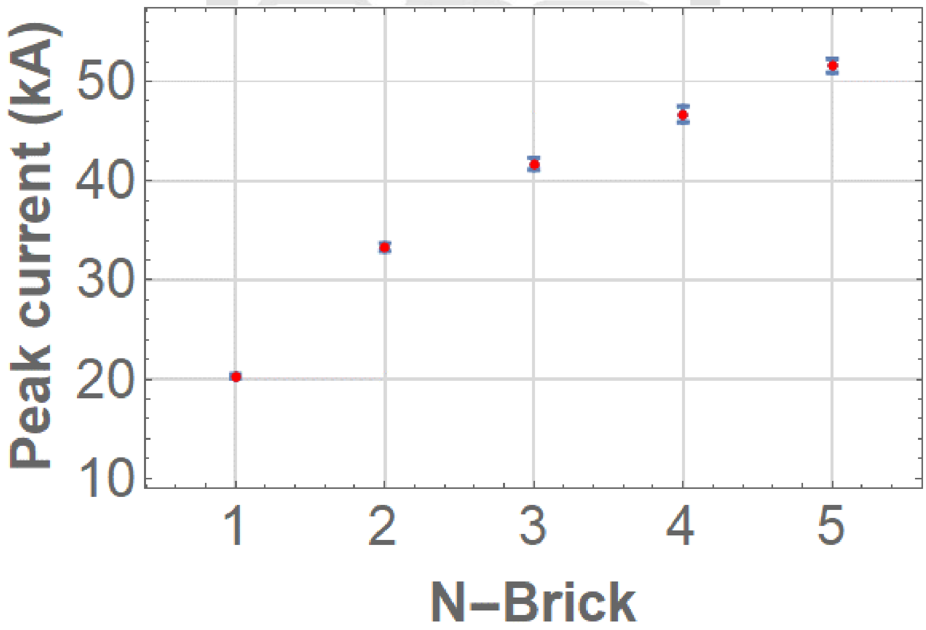

Figure 6.16: The peak current of each experiment.

Table6.2: The parameter of 5-brick capacitor with a rail-gap switch.

	Estimate	Standard Error	t-Statistic	P-Value
Inductance of L_{sw} + 100 [nH]	330	10	34	0.00005
Inductance of one-brick [nH]	70	20	4	0.03

doi:10.6844/NCKU201900671

Chapter 7 The south wing pulsed power system testing

In order to build the PPCB step by step, we built the south wing of the PPCB and measured its discharge characteristics. We need to measure the peak current, the inductance, and the jitter of the south wing so that we can estimate the final performance of the PPCB. The jitter needs to be small enough so that both the north wing and the south wing of the PPCB can be synchronized. Using the same method in section 6.3, we can component inductances of the south wing. Finally, we analyze the jitter between the peak current and the trigger-pulse signal. In section 7.1, the construction of the south wing is introduced. In section 7.2, the experimental setup is introduced. In section 7.3, the data analysis is introduced. The peak currents and the inductance are also given. In section 7.4, the jitter is defined and given. In section 7.5, the result is given.

7.1 The south wing

The south wing pulsed- power is shown in Figure 7.1 which is basically half of the PPCB. It consist of the coaxial transmission (14 nH), a parallel plate transmission line (8 nH), a capacitor connector (95 nH) , a rail-gap switch and N-brick capacitor where N is 1, 3, or 5. Therefore, the capacitance of this system is 0.5, 1.5, or 2.5 uF CORRESPONDING TO N=1, 3, 5, RESPECTIVELY, and the total inductance with N-Brick capacitor can be shown as

$$L_{N-total} = (L_{sw} + L_{load} + L_{Others}) + \frac{L_{1-Brick}}{N}$$

where $L_{others} = 8 + 95 + 14 = 117$ nH. The high voltage DC power supply is used to charge the N-brick capacitor and capacitors of the Marx generator to 20 kV. The multistep trigger system is used to trigger the rail gap switch.

doi:10.6844/NCKU201900671

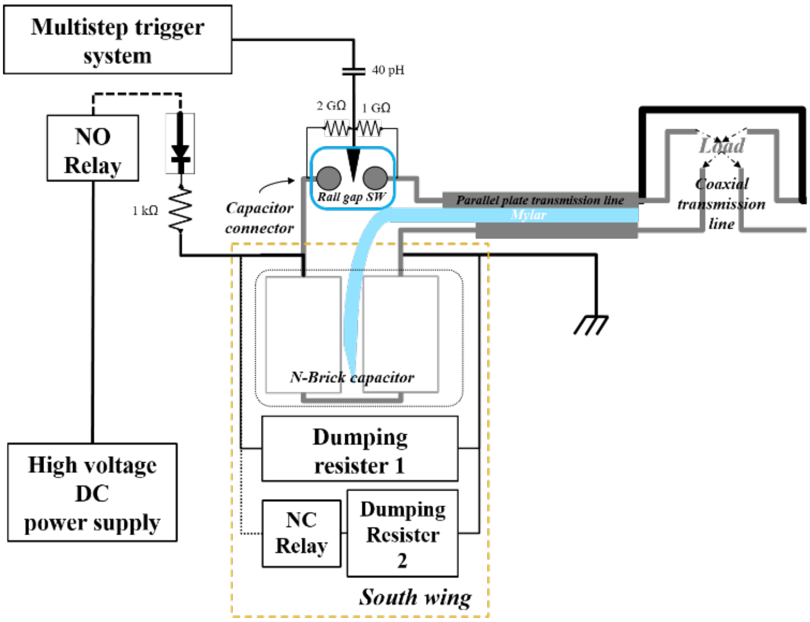

Figure 7.1: The composition of the south wing pulsed-power system.

7.2 Experimental setup

To find the inductance of PPCB, we built the south wing first and tested it with different numbers (1, 3, and 5) of the one-brick capacitor. All capacitors were connecting in parallel. As shown in Figure 7.2, the load consisted of 8 straight wire connected in parallel. Each wire was 35 cm long and the diameter of each wire was 1.7 mm (AWG16). There were two high voltage probe, where HVP1 was used to measure the voltage of the capacitor, and the HVP2 was used to measure the output signal of the Marx generator. The discharge current of the south wing was measured by the Pearson current monitor (Model: 301X). Each experiment with different numbers of the one-brick capacitor was tested 20 times.

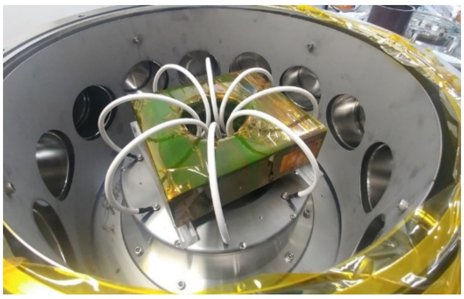

Figure 7.2: The load consisted of 8 straight wire connected in parallel.

doi:10.6844/NCKU201900671

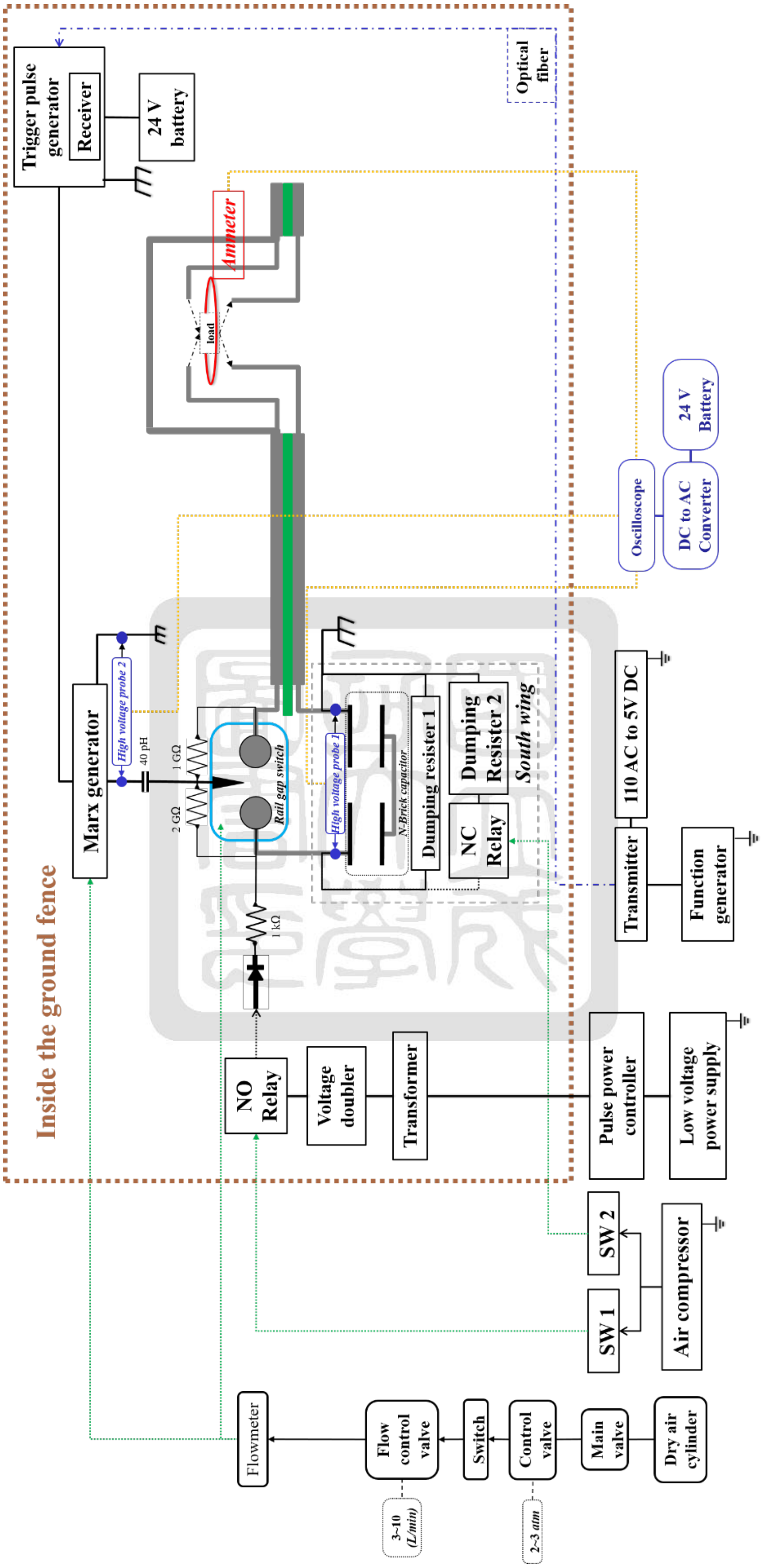

Figure 7.3: Experimental setup to test the discharge in the south wing.

doi:10.6844/NCKU201900671

7.3 Analysis method

The output signal of discharge experiments, as shown in Figure 7.4, are used to find the total inductance and resistance of the system. The total inductance includes a rail gap switch, N-brick capacitor, a parallel plate transmission line (8 nH), a coaxial transmission (14 nH), a capacitor connector (95 nH), a rail gap switch (L_{sw}) and N-brick capacitor($\frac{L_{1-Brick}}{N}$) where N is 1, 3, or 5, and a load. The load consists of 8 wires connecting in parallel where each wire is 35 cm long and the diameter of each wire is 1.7 mm so that the inductance of each wire is 418 Nh [9]. Therefore, we assume that the inductance of the load is 53 nH. [9]. Therefore, the total inductance of each test is

$$\mathrm{L_{N-total}(nH) = (L_{SW} + 170) + \frac{L_{1-Brick}}{N}}$$

where 170 is the sum of L_{load} (53 nH)and L_{other}(8+14+95 nH). We conducted experiments using different numbers of the one-brick capacitor.

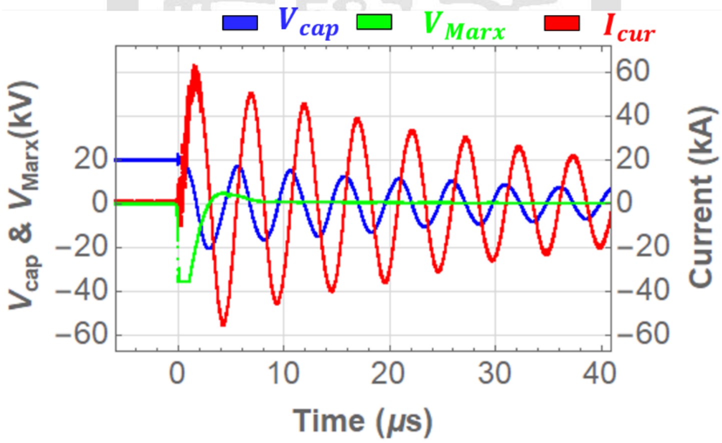

Figure 7.4: The output signal of discharge experiments

The total inductance in experiments was obtained using the same method in section 6.3. By fitting Eq (1) to the relationship between the total inductance and N, we can find the inductance of the rail gap switch and the one-brick capacitor. Each experiment with different numbers of the one-brick capacitor was repeated 20 times.

doi:10.6844/NCKU201900671

Each fitted data are shown in Figure 7.5 to Figure 7.7.

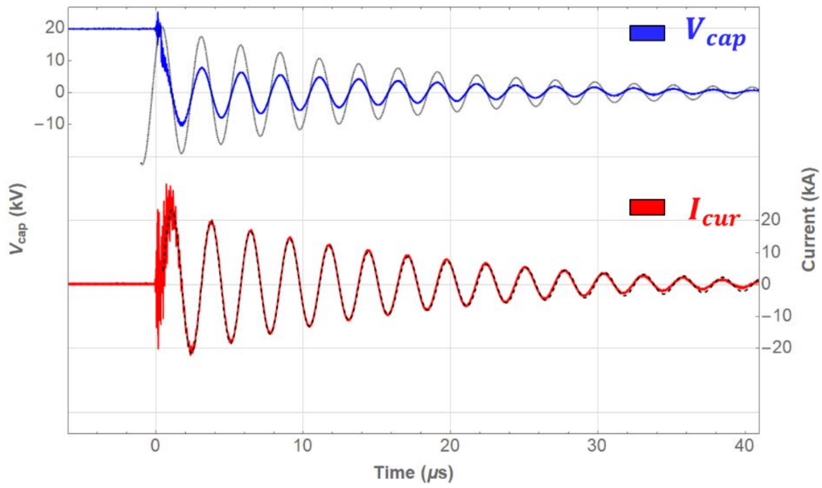

Figure 7.5: South wing discharge experiment using the one-brick capacitor.

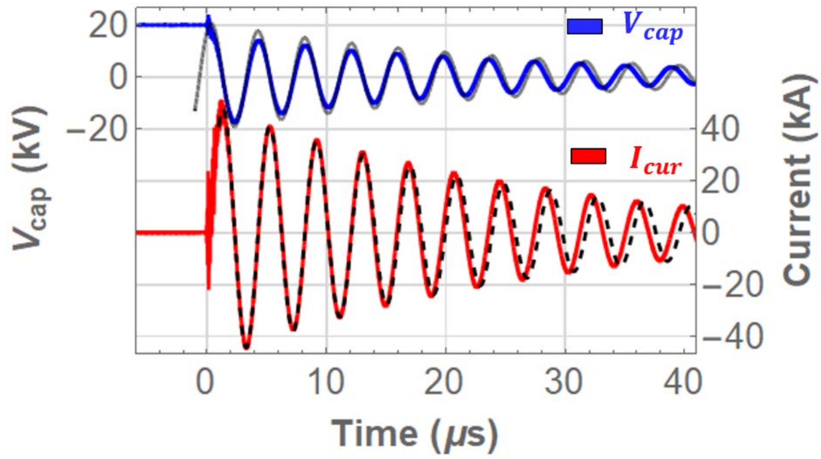

Figure 7.6: South wing discharge experiment using the three-brick capacitor.

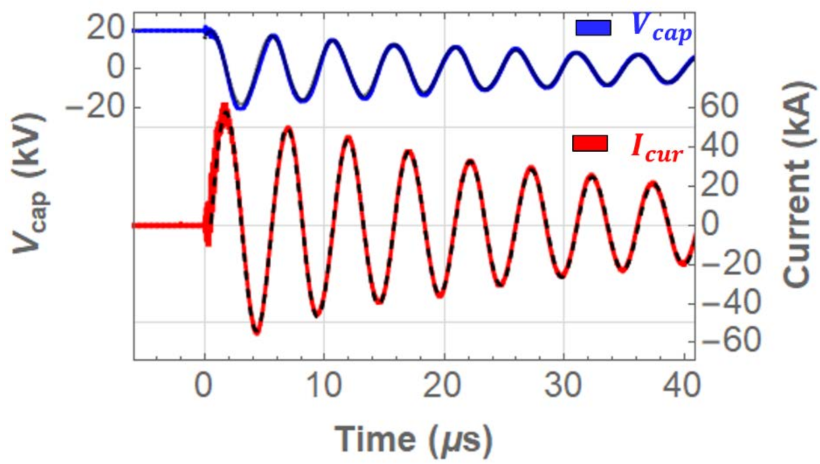

Figure 7.7: South wing discharge experiment using the five-brick capacitor.

doi:10.6844/NCKU201900671

The averaged discharge parameters in each experiment are shown in Table 7.1. Eq (1) was used to fit the averaged inductance of each experiment respect to N. The result of the fitting curve, shown in Figure 7.8, is $230 \pm 20 + \frac{120\pm30}{N}$. Therefore, we got the inductance of the rail gap switch of 60 ± 10 nH, and the inductance of the one-brick capacitor is 120 ± 30 nH.

Table 7.1: The discharge parameters in each experiment and the calculated inductance and resistance.

			Fitting parameter				Solved result		Maximum curve
N-Brick	Data		α	b	γ	β (MHz)	L (nF)	R (mΩ)	Peak current
1	23	Avg	24.2	0.6	16.0	2.36	360	50	23.22
		Std	0.4	0.2	0.6	0.02	5	2	0.35
3	23	Avg	49.5	0.4	24	1.59	263	22	47.5
		Std	0.6	0.2	1	0.02	5	1	0.6
5	20	Avg	60.0	0.5	35	1.22	269	16	57.8
		Std	0.8	0.1	1	0.01	5	1	0.8

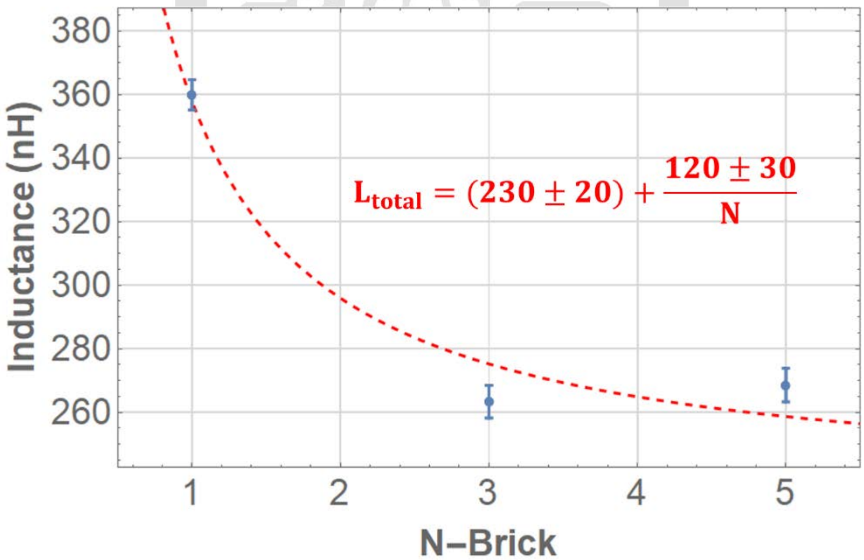

Figure 7.8: The average value of the inductance obtained by each experiment and the result of curve fitting.

doi:10.6844/NCKU201900671

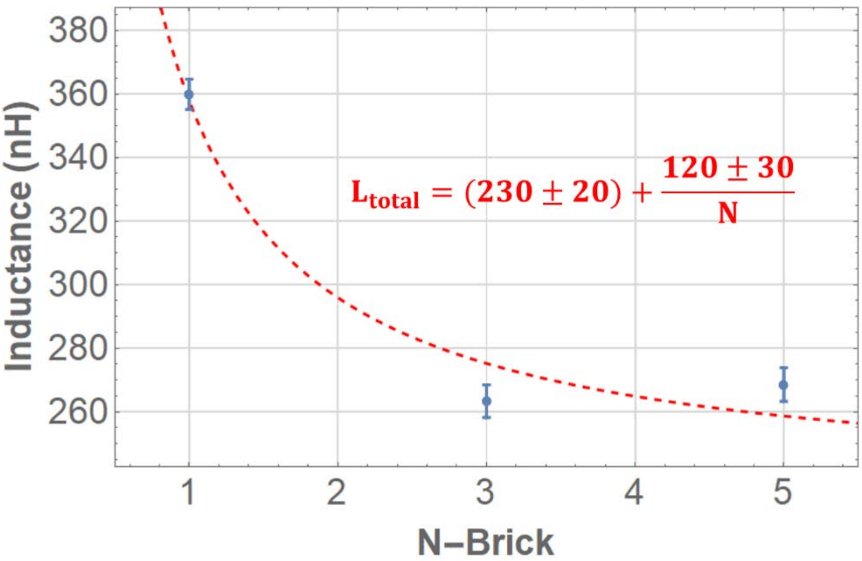

Figure 7.9: The peak current of N-brick experiment in the south wing.

Table 7.2: Curve fitting parameters with N-brick.

	Estimate	Standard Error	t-Statistic	P-Value
Inductance of $L_{sw} + 170$ [nH]	230	20	14	0.04
Inductance of one-brick [nH]	120	30	4	0.13

7.4 Jitter of the south wing

Jitter and the delay time are important parameters in PPCB. The parallel plate capacitor bank is asymmetrical energy bank design. The trigger pulse from the Marx generator (multistep triggering system) triggers a rail-gap switch in each wing. Therefore, the energy in capacitors of each wing flows into the load. After a delay time, the current through the load which is the superposition of two pulsed currents from each wing reaches the peak value. Therefore, the delay time is defined as the time difference between the trigger pulse and the peak current. To make the two current waves form each wing perfectly superimpose, the delay time needs to be consistent. Experimentally, the degree of the uncertainty of this delay time is called jitter. In other words, the smaller the jitter, the more perfect the superposition of currents from the two wings.

To obtain jitters, we need to define when a trigger pulse is delivered and when

doi:10.6844/NCKU201900671

the current through the load reaches the peak value. We measured the voltage of the Marx generator using HVP 2. The current was measured using Pearson current monitor.

The characteristics voltage signal of the Marx generator is shown in Figure 7.10. It has three features which are two minimum peaks in red, and a fast falling edge in green so that we define three reference points. Each minimum peak is defined by the minimum point, P_1 and P_2, in each part,. If there are multiple minimum values, their average is used.

The time reference point defined in the green section is as following:

(1) The point T is defined as the maximum point after the second peak. If there are multiple values, the average of those is used. The point D is defined as the first minimum point after point T. If there are multiple values, the average of those is used.

(2) As shown in Figure 7.11, V_{Top} and V_{Down} are defined as $V_{Top} \equiv V_T - 0.2|V_D - V_T|$ and $V_{bottle} \equiv V_T - 0.8|V_D - V_T|$. We find the data points between between T_T and T_D in time and V_{Top} and V_{Down} in voltage 20% to 80% of $|V_D - V_T|$.

(3) Yellow points are those we picked on step (2). They are fitted a line by which marked as L_{Marx}. The slope of this line is defined as the rising(falling) speed of the Marx generator, which are shown in Table 7.3.

(4) The intersection of L_{Marx} and V_{Top} is defined as the initial point M_1 of the rising(falling) edge. The intersection of L_{Marx} and V_{Down} is defined as the end M_2 of the rising(falling) edge. The rise time is then be defined as the time difference and recorded in Table 7.3. The third reference point P_{Marx} is the middle point of those two points, as shown in Figure 7.14.

doi:10.6844/NCKU201900671

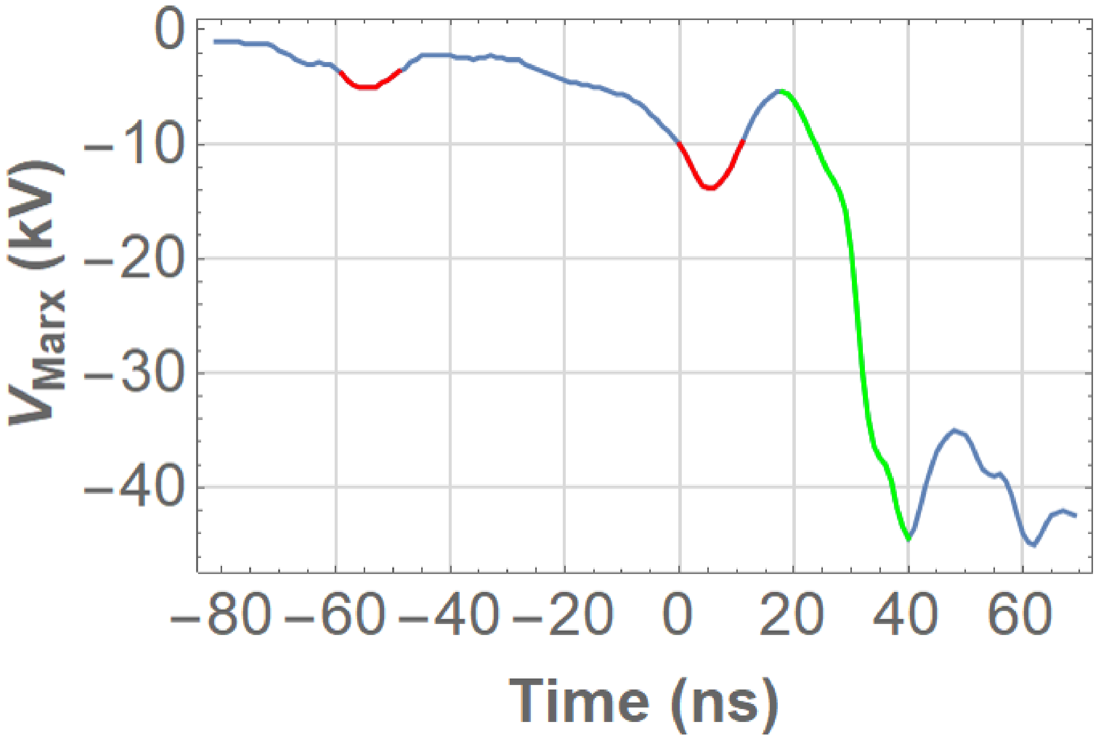

Figure 7.10: There are three significant waveforms in the pulse signal from the Marx generator.

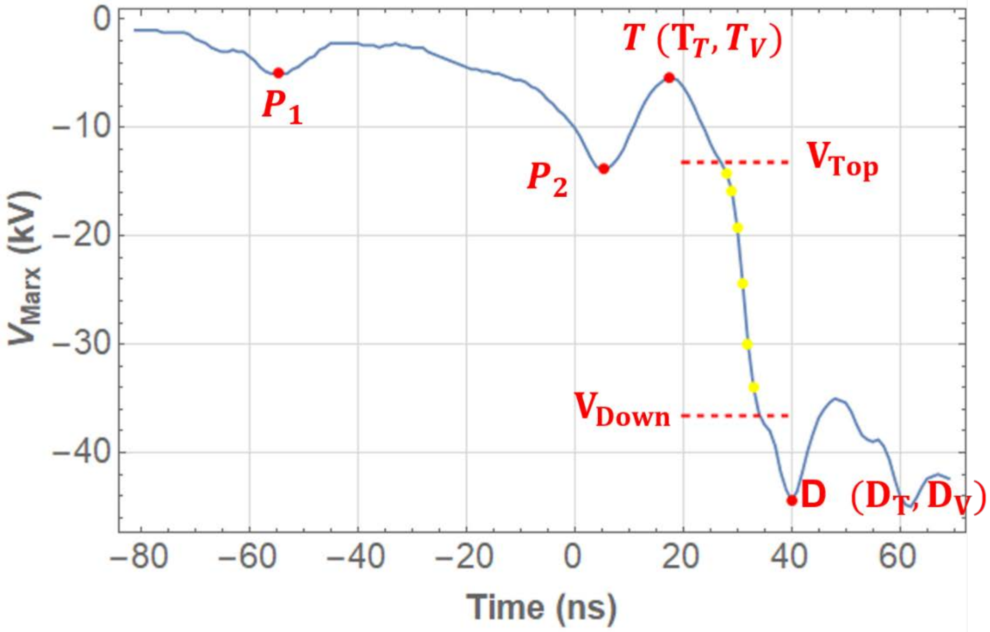

Figure 7.11: The region extremum defines two reference points. Defines the range of usage data for the third reference point.

doi:10.6844/NCKU201900671

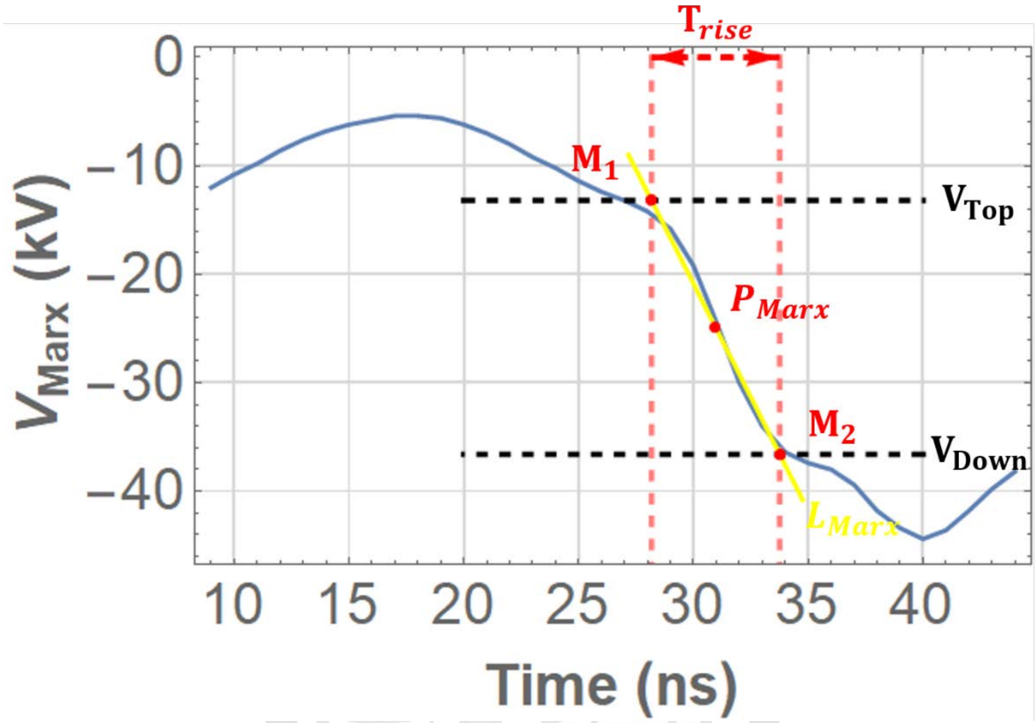

Figure 7.12: The rising(falling) time and the rising(falling) speed of the Marx generator are defined.

Table 7.3: The rise speed and the rise time of the Marx generator in this experiment.

	Rise speed [kV/ns]	Rise time [ns]
T0023	**-4.19**	**5.58**
T0024	**-3.34**	**6.12**
T0025	**-4.08**	**5.21**
T0026	**-3.48**	**5.83**
T0028	**-3.84**	**4.97**
T0022	**-4.60**	**2.63**
T0020	**-5.28**	**2.00**
T0019	**-3.46**	**3.45**
T0018	**-2.82**	**4.28**
T0017	**-3.78**	**3.11**
Avg	**-3.9**	**4.3**
Stdev	**0.7**	**1.4**

doi:10.6844/NCKU201900671

To define the time of the peak current occurs, the discharge current data in the first quarter cycle will be selected and curve fitted with a quadratic function. As shown in Figure 7.13, data within 10% to 90% of in the first half cycle is used for curve fitting. The maximum point of this fitting is defined as the peak current, which marked as P_{cur}. Finally, all reference points are ploted together in Figure 7.14 .

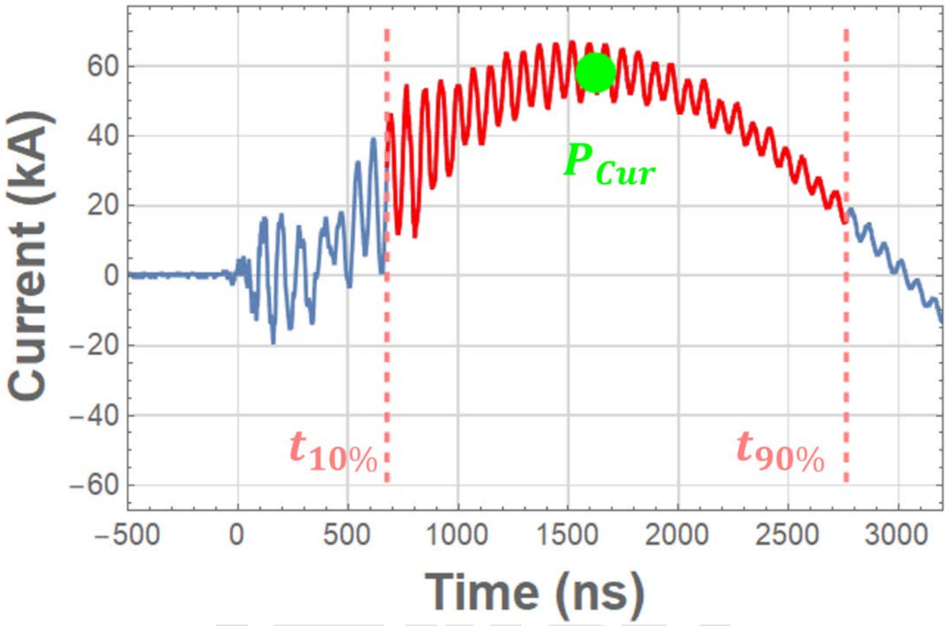

Figure 7.13: The current data is used to define the point P_{cur}.

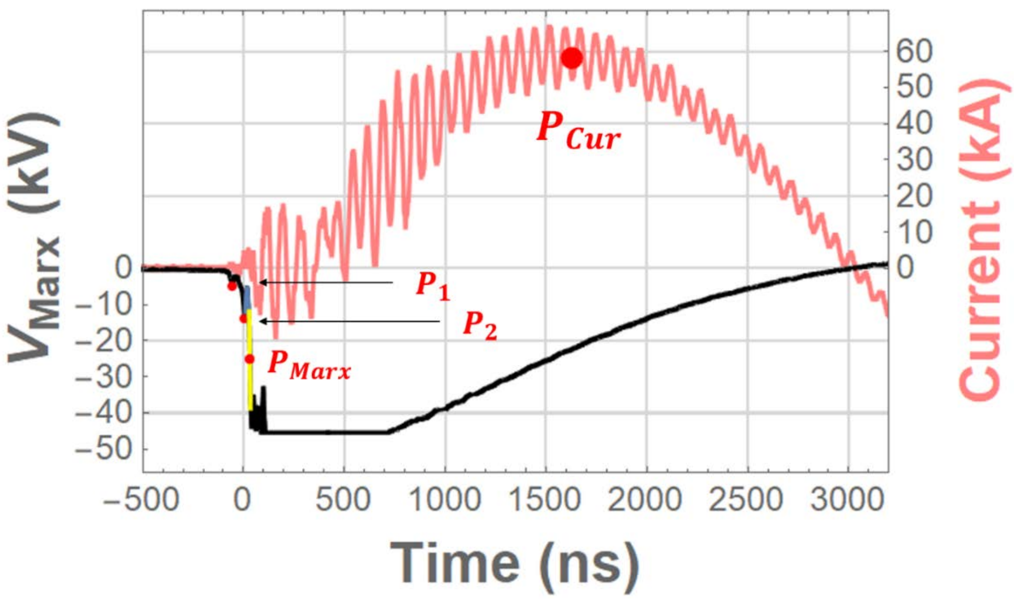

Figure 7.14: Each data provided 5 points and those are used to find the delay time.

doi:10.6844/NCKU201900671

We analyze the data and record the time of P_1, P_2, P_{Marx}, and P_{cur}. We define three delay times as (1) D_1 is the delay time between P_1 and P_{cur}, (2) D_2 is the delay time between P_2 and P_{cur}, and (3) D_{Marx} is delay time between P_{Marx} and P_{cur}. Those delay times are shown in Table 7.4. Jitters are defined as the standard deviation of the delay time. We alos used different rang of the data which is 25% to 75% of the half period to find the point P_{cur}, as shown in Table 7.5. Those jitters are in same order and are not significant distinctive with using the range of 10% to 90% result meaning that the analysis is robust. The percentage of the jitter over a quarter of a cycle (cuttent rise time) is about 17%.

Table 7.4: The three delay time are shown, fitting range of P_{cur} is 10% to 90% of the half period.

Data	D_1	D_2	D_{Marx}
T0023	1681	1621	1596
T0024	1669	1606	1579
T0025	2182	2117	2078
T0026	2222	2156	2113
T0028	1657	1596	1564
T0022	1846	1770	1730
T0020	2158	2099	2075
T0019	1908	1814	1770
T0018	1765	1678	1636
T0017	1755	1674	1627
Avg	1884	1813	1777
Stdev	224	226	225
%	17	17	17

doi:10.6844/NCKU201900671

Table 7.5: The jitter by using the point P_{cur} which fitting range is 25% to 75% of the half period.

Data	D_1	D_2	D_{Marx}
T0023	1663	1603	1578
T0024	1637	1574	1547
T0025	2170	2105	2066
T0026	2200	2134	2091
T0028	1645	1584	1552
T0022	1846	1770	1730
T0020	2158	2099	2075
T0019	1908	1814	1770
T0018	1765	1678	1636
T0017	1755	1674	1627
Avg	1875	1804	1767
Stdev	225	227	225
%	17	17	17

7.5 Summaries

In the discharge test of the south wing, we find the inductance of the rail gap switch is 60 ± 10 nH and the inductance of the one-brick capacitor is 120 ± 30 nH. The jitter of the south wing is more than 200 ns, which is 17% of the rise time of the current. The jitter may be too long to synchronize discharge current from two sings. We need to improve jitter.

doi:10.6844/NCKU201900671

Chapter 8 Optimization of the south wing

In order to make the system more stable and with smaller jitter, we designed a shorter rail-like electrode for the rail-gap switch and round electrodes for the peaking switch in the Marx generator. The new electrodes are inducted in section 8.1. The design of the experiment process is shown in section 8.2. The results are presented in Section 8.3.

8.1 Shorter electrodes for the rail gap switch

After many discharges, the erosion spots on the rail-like electrodes of the rail gap switch, as shown in Figure 8.1(a)~(c), are intense at the junction of the hemisphere and the cylindrical surface which is also closed to the end of the knife edge electrode, as shown in Figure 8.1 (d) and Figure 8.2. Even everything was within tolerance, the radius of the junction is slightly larger than that of the cylindrical. The electric field is enhanced at the junction of the rail-like electrode and the end of the knife edge electrode. Therefore, we make the rail-like electrode shorter to keep those two parts farther away and prevent discharge between those two parts. The new electrode is 25 mm shorter than the original electrode on each, i,e., the junction is 25 mm away from the end of the knife edge electrode.

The round electrode, as shown in Figure 8.3, on the other hand, is for the peaking switch of the Marx generator. The round electrode with a spherical surface makes the electric field slightly stronger. A pair of round electrodes has a smaller equivalent capacitance than a pair of disk electrodes. We expect that the round electrode with a spherical surface can provide faster-falling speed and shorter falling times.

Experiments with of all combinations are conducted to find the best performance in terms of small jitter for the south wing pulsed-power system.

doi:10.6844/NCKU201900671

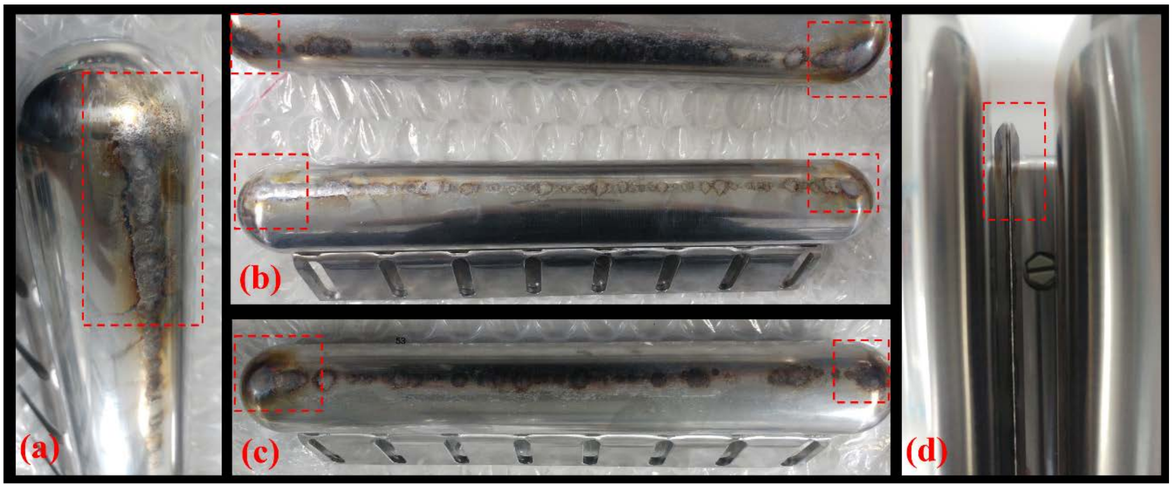

Figure 8.1: (a)~(c) The scar on the rail-like electrode are dense in specific locations. (d) The scar is dense on the end of the knife edge.

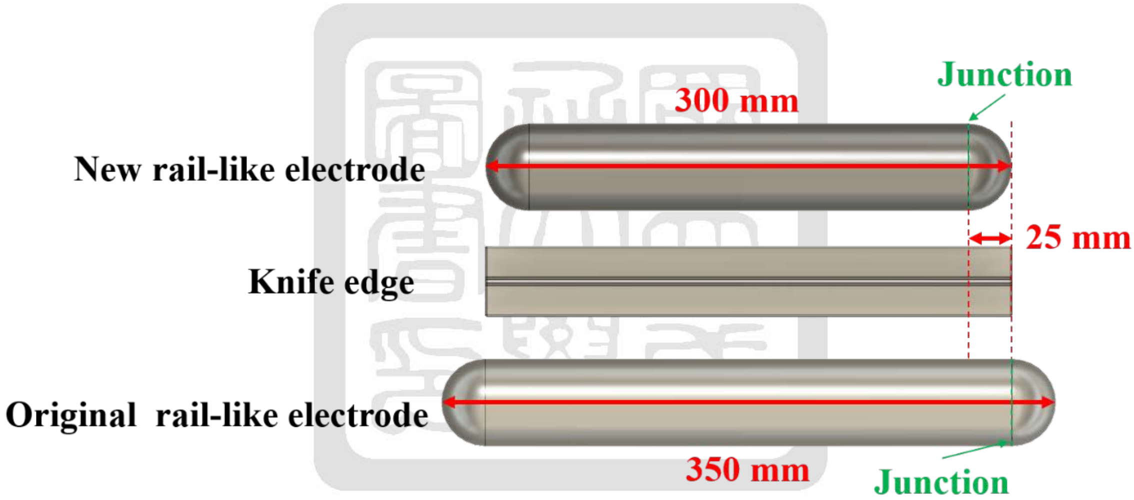

Figure 8.2: Top view: The rail-like electrode with 350 mm and 300 mm and the knife edge with 300 mm.

doi:10.6844/NCKU201900671

	Shape	Profile and specifications
Round electrode		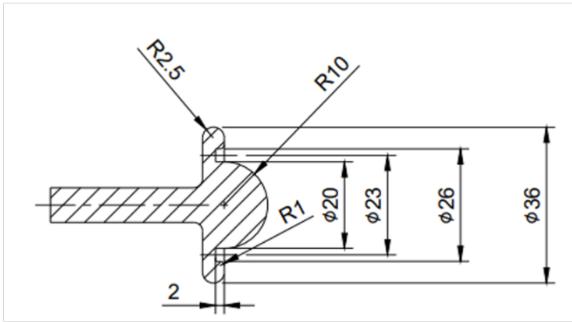
Disk electrode		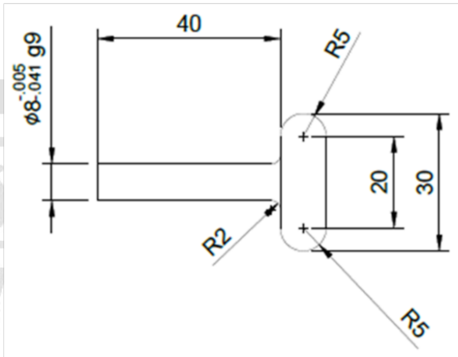

Figure 8.3: The round electrode and the disk electrode for the Marx generator.

8.2 The design of the experiment

There are four kinds of tests A, B, C, and D, as shown in Table 8.1. They are in different conditions using different electrodes separately. The electrodes of the rail gap switch have two options: length of 350 mm and 300 mm. The electrodes of the peaking switch in the Marx generator have two options: the disk electrodes and the round electrodes. Experiment D was finished in chapter 7. We conduct B, C, and D to compare those four experiments with each other. The parameters will be shown. We will discuss with the total inductances, the peak currents, jitters, Energy efficiencies, the power of the south wing and the falling speed and the falling time of the Marx generator.

doi:10.6844/NCKU201900671

Table 8.1: All combined experiments are tested.

Exp	Rail-like electrode (mm)	Marx (shape)
D	350 mm	Disk
A	350 mm	Round
B	300 mm	Round
C	300 mm	Disk

8.3 Data analysis

Shown in Table 8.2 is data of each delay time and jitter. The definitions of delay times and jitters are the same to section 7.4. When experimental condition moved from D to A, the delay and jitter are shorter. When experimental condition moved from 350 mm(D and A) to 300 mm (B and C), jitters are shorter and even less than 1% of a quarter of a cycle(current rise time), as shown in Table 8.3. It is quite an excellent performance.

Table 8.2: Each delay time and jitter of all experiments.

Exp	Rail-like electrode (mm)	Marx (shape)	D_1 (ns)	D_2 (ns)	D_{Marx} (ns)	$Jitter_1$ (ns)	$Jitter_2$ (ns)	$Jitter_{Marx}$ (ns)
D	350 mm	Disk	1884	1813	1777	224	226	225
A	350 mm	Round	1601	1566	1548	57	58	59
B	300 mm	Round	1516	1483	1466	12	11	11
C	300 mm	Disk	1517	1483	1456	14	11	12

Table 8.3 shows that the shorter rail-like electrodes make a smaller inductance of the south wing. The standard deviation of the inductance is also smaller. That is to say, the junction on the surface of the 350-mm rail-like electrodes causes the concentrated discharge between the junction of the rail-like electrodes and the end of the knife edge electrode.

doi:10.6844/NCKU201900671

Table 8.3: The period of RLC oscillation and the percentage of jitter in a quarter cycle those are analyzed from all experiments.

Exp	Rail-like electrode (mm)	Marx (shape)	T (ns)	$\frac{Jitter_1}{T/4}$(%)	$\frac{Jitter_2}{T/4}$(%)	$\frac{Jitter_{Marx}}{T/4}$(%)
D	350 mm	Disk	5164.46	17.32	17.47	17.40
A	350 mm	Round	5142.96	4.46	4.49	4.61
B	300 mm	Round	5116.55	0.92	0.83	0.86
C	300 mm	Disk	5121.35	1.10	0.87	0.95

Table 8.4 and Table 8.5 are used to calculate the Energy Efficiency. The power of the discharge of the south wing are shown in Table 8.6. The energy in the capacitor with capacitance C is when the capacitor is charged to voltage V. When the capacitor is fully discharged and the current reaches the maximum value I_{peak}, the enenagy in the system is $\frac{1}{2}LI_{peak}{}^2$, where L is total inductance and the I_{peak} is the peak current. We can use the average inductance in Table 8.4 for L and use the peak cuttent in Table 8.5 for I_{peak} so that the enenagy of the south wing is calculated. The enenagy is divided by a quarter period to get the averaged power of the south wing.

Proof of $\frac{1}{2}LI_{peak}{}^2$ is the enenagy of the south wing is following:

Our parameters are from the result of fitting curve

$$\mathrm{I_{(t)}} = \frac{\mathrm{V_{charge}}}{\sqrt{\frac{\mathrm{L}}{\mathrm{C}}-(\frac{\mathrm{R}}{2})^2}}\mathrm{e}^{-\frac{\mathrm{R}}{2\mathrm{L}}\mathrm{t}}\ \sin(\ [\sqrt{\frac{1}{\mathrm{LC}}-\left(\frac{\mathrm{R}}{2\mathrm{L}}\right)^2}\ ]\ \mathrm{t})\ \ .$$

The peak current is the maximum point of the fitting curve which occurs at the first quarter cycle. So, let t = T/4, where T is the period of the RLC response. Here, T is solved from

$$\mathrm{T} = \frac{2\pi}{\sqrt{\frac{1}{LC}-\left(\frac{R}{2L}\right)^2}}.$$

The formula becomes

$$\mathrm{I_{(T/4)}} = \frac{\mathrm{V}}{\sqrt{\frac{\mathrm{L}}{\mathrm{C}}-(\frac{\mathrm{R}}{2})^2}}\mathrm{e}^{-\frac{\mathrm{R}}{2\mathrm{L}}*\frac{\mathrm{T}}{4}}.$$

doi:10.6844/NCKU201900671

The data shows that

$$\frac{L}{C} \gg \left(\frac{R}{2}\right)^2, \text{ and } \mathbf{e}^{-\frac{\mathbf{TR}}{\mathbf{8L}}} \approx \mathbf{e}^{-\frac{\mathbf{1}}{\mathbf{1000}}} \approx 1.001 = 1.$$

So that can become

$$I_{peak} \cong \frac{V}{\sqrt{\frac{L}{C}}}.$$

That is also the conservation equation

$$\frac{1}{2} L {I_{peak}}^2 = \frac{1}{2} C V^2 \ .$$

On the left-hand side of the equal sign, the averaged parameter of the total inductance L and the peak current I_{peak}. On the right-hand side is the capacitance C (2.5 uF) of the south wing and the charging voltage V (20 kV). If the system has no energy loss, the equation holds. The power efficiency is defined as

$$\frac{LI^2}{CV^2} * 100 \ \ [\%] \ .$$

Shown in Table 8.6 shows that the loss of energy is less than 10%. The power of the south wing is between 351 to 364 MW. The best result is C which has the 93.2% power efficiency and 364 MW power. The beat result is C which has 93.2% power efficiency and 364 MW power.

The falling speed and the falling time of the Marx generator are shown in Table 8.7. That shows that the Marx generator using the peaking switch with the round electrode has the faster-falling speed and the shortest falling time.

Table 8.4: The total inductance of each experiment.

Exp	Rail-like electrode (mm)	Marx (shape)	L (nH)	L_stdev
D	350	Disk	270	5
A	350	Round	268	6
B	300	Round	265	3
C	300	Disk	266	3

doi:10.6844/NCKU201900671

Table 8.5: The peak current of each experiment.

Exp	Rail-like electrode (mm)	Marx (shape)	Peak current (kA)	Pcur_stdev
D	350 mm	Disk	57.9	1.0
A	350 mm	Round	58.5	0.6
B	300 mm	Round	59.2	0.7
C	300 mm	Disk	59.2	0.6

Table 8.6: Estimate the power efficiency and power of the south wing pulsed-power system using the average of the experimental data

Exp	Rail-like electrode (mm)	Marx (shape)	L (nH)	Peak Current (kA)	Energy $\frac{1}{2}LI^2$ (J)	Ideal Energy $\frac{1}{2}CV^2$ (J)	Power Efficiency (%)	T (ns)	Power (MW)
D	350	Disk	270	57.9	453	500	90.5	5164	351
A	350	Round	268	58.5	459	500	91.7	5143	357
B	300	Round	265	59.2	464	500	92.9	5117	363
C	300	Disk	266	59.2	466	500	93.2	5121	364

Table 8.7 The falling speed and the falling time in each experiment.

Exp	Rail-like electrode (mm)	Marx (shape)	Falling speed (kV/ns)	Std (ns)	Falling time (ns)	Std (ns)
D	350	Disk	-3.9	0.7	4.3	1.4
A	350	Round	-9.3	0.5	2.7	0.1
B	300	Round	-7.7	1.4	3.1	0.7
C	300	Disk	-6.8	1.4	3.6	1.0

Those experiments show that using the 300-mm rail-like electrodes in the rail gap switch and using the round electrodes in the peaking switch of the Marx generator have the best performance for the smallest jitter, smaller inductance and more stable falling time of the Marx generator.

doi:10.6844/NCKU201900671

Chapter 9 The negative output of the south wing

In order to make the south wing provide a negative output, the chamber is connected to the ground and a suitable resistor is used, as shown in figure 9.1. When its state is ‘‘In experiment’’ which is shown in Table 2.3, the output voltage is the opposite. The resistance of R_{D1}, R_{D2} and R_{div} are 50 MΩ, 1 kΩ and 50500 Ω, respectively. In section 9.1, we introduced the measurement method of the experiment. In section 9.2, the peak current, the total inductance, and the jitter of the south wing with negative output are shown.

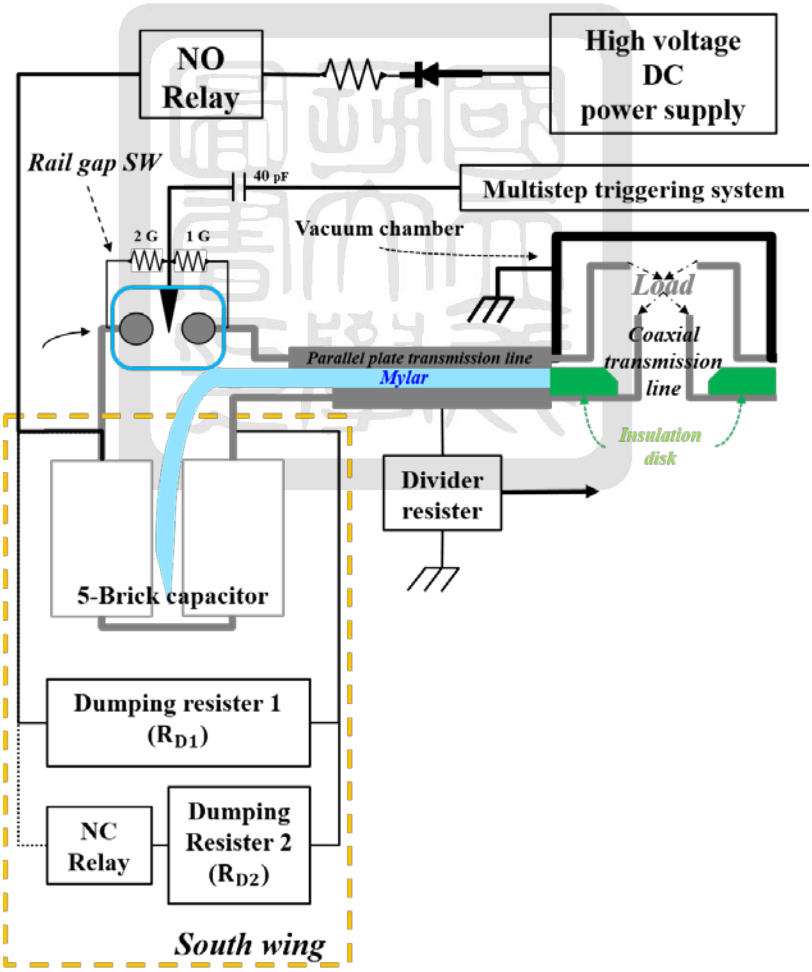

Figure 9.1: Setup of the negative output of the south wing

doi:10.6844/NCKU201900671

9.1 The measurement method of the experiment

We measured the voltage signal of the Marx generator and capacitors with two high voltage probes (P6015A). Those ground terminus both probes were connected to the same point which is the green circle in Figure 9.2. We used the current monitor (Pearson 301X) to measure the current signal of the load. To confirm that the instrument was safe on the top plate of the parallel-plate transmission line, we also measured the voltage of the point between “Test 1” and “Ground”, as shown in Figure 9.2. In order to understand whether the new and old electrodes have the same characteristics, we compared jitters using two different electrodes. After 10 discharge experiments, we replaced the old electrode by the new one and conducted experiments for 30 times. We measured the voltage of the load once.

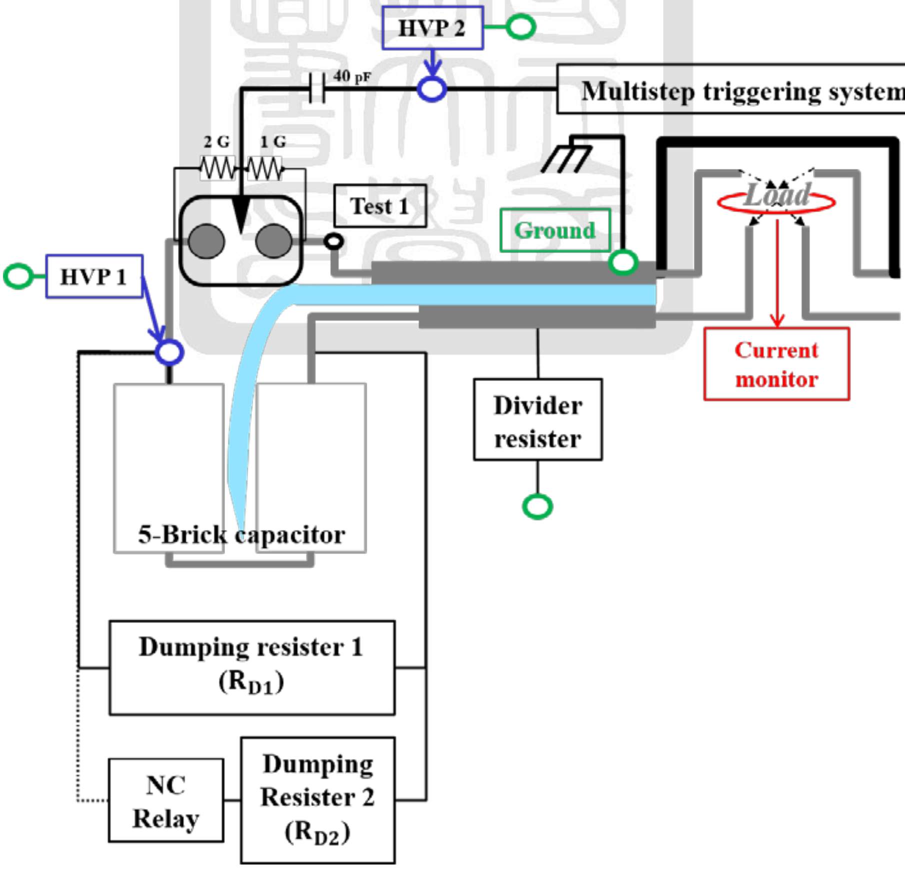

Figure 9.2: Measuring instrument configuration diagram.

doi:10.6844/NCKU201900671

9.2 The negative output result

The result of the voltage of the point between ‘‘Test 1’’ and ‘‘Ground’’ is shown in Figure 9.3. Instruments placed on the top plate of the parallel-plate transmission line require 200 volts of insulation. Figure 9.4 and Figure 9.5 is one data of the old electrode which continued using after experiments in chapter 8 and 10 times in this chapter. Figure 9.6 and Figure 9.7 is one data of experiments using new rail-like electrode. We tested it 30 times. As shown in Table 9.1 and Table 9.2, there is no noticeable difference in results. The pulsed-power system using the south wing has jitter below 5% of the quarter period. Shown is Figure 9.8 is a record of delay time for each experiment. In the first 30 discharge experiments, the change in delay time was within 55 ns of the standard deviation. Shown is Figure 9.9 is the voltage signal of capacitors and the load. The maximum voltage between capacitors and ground is 13.0 volts, which is 65.2% of the charging voltage. The maximum voltage of the load is 4.5 volts, which is 22.4% of the charging voltage. Therefore, the plasma provided in our system is not suitable for the diode method.

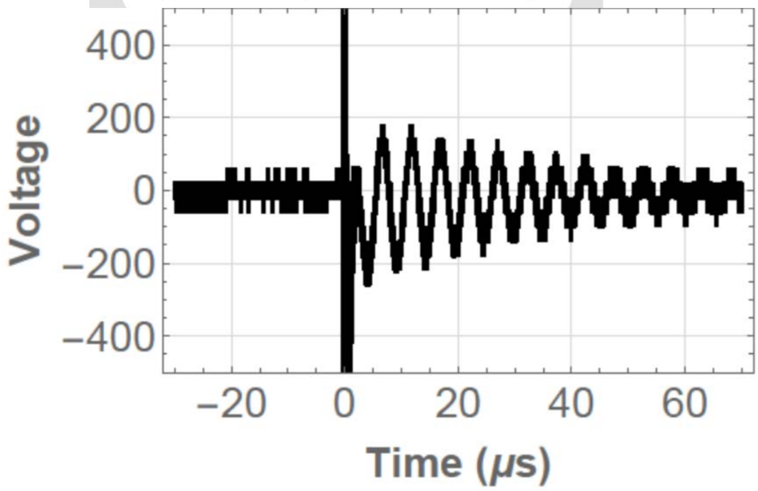

Figure 9.3: the voltage signal of the point between ‘‘Test 1’’ and ‘‘Ground.’’

doi:10.6844/NCKU201900671

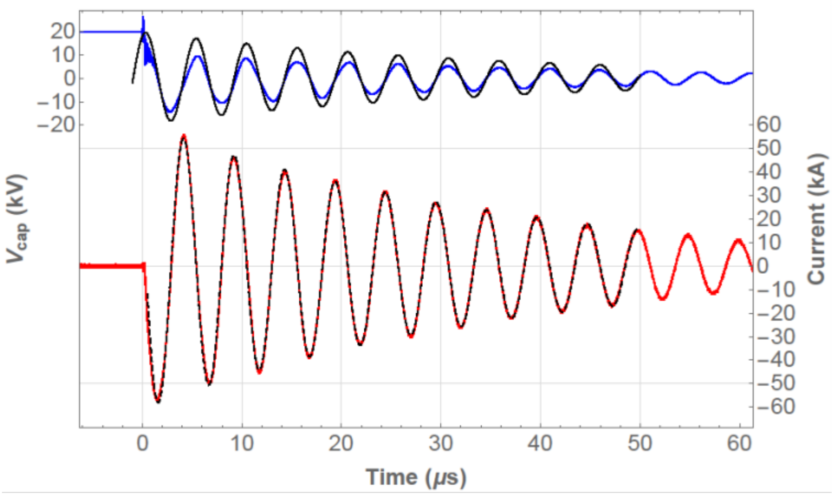

Figure 9.4: Current curve fitting result of the old electrode.

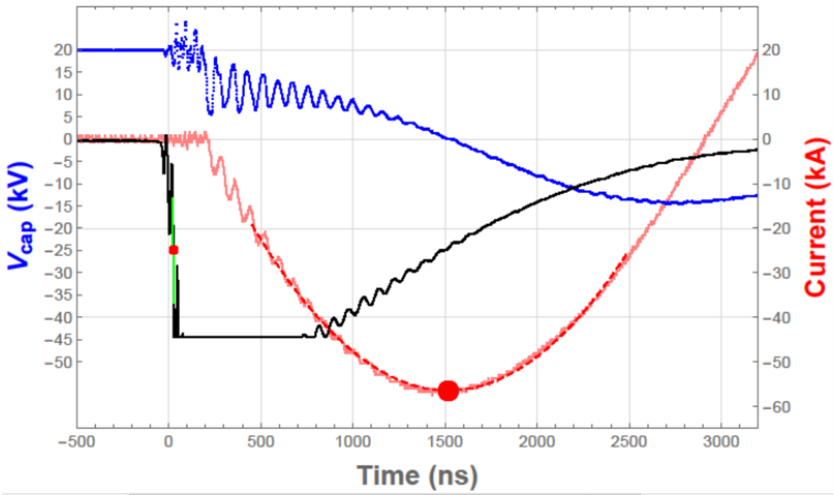

Figure 9.5: Trigger, voltage and current signal analysis result of the old electrode.

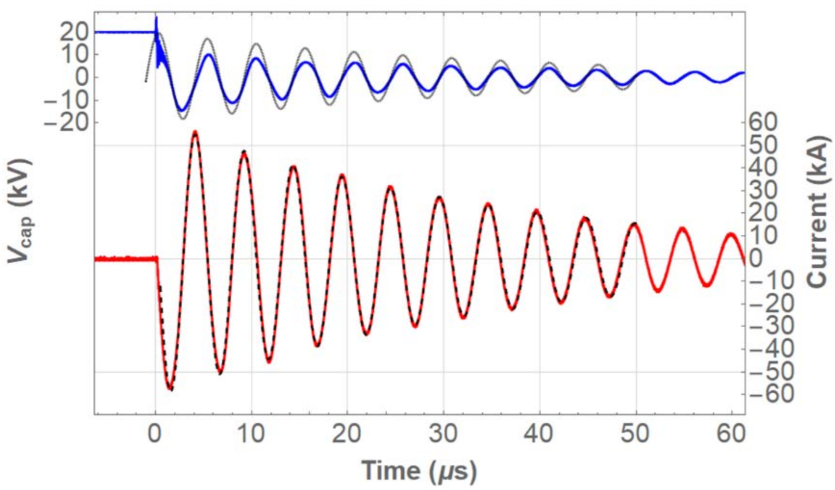

Figure 9.6: Current curve fitting result of the new electrode.

doi:10.6844/NCKU201900671

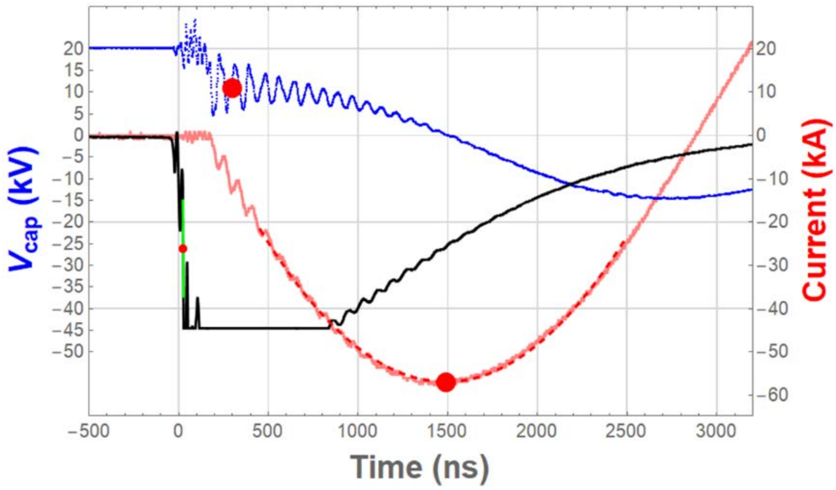

Figure 9.7: Trigger, voltage and current signal analysis result of the new electrode.

Table 9.1: Analysis result of the peak current, total inductance, and Marx signal.

Electrode	Time	Peal Current [kA]	T [ns]	L [nH]	Falling Speed [kV/ns]	Falling Time [ns]
Old	10	58.8 ± 0.7	5050 ± 30	263 ± 3	-6.3 ± 0.9	3.7 ± 0.6
New	30	58.4 ± 0.6	5080 ± 20	260 ± 2	-6.1 ± 1.0	3.8 ± 0.7

Table 9.2: Analysis result of the delay time and jitter.

Electrode	Time	T [ns]	DelayTime [ns]	Jitter [ns]	Jitter [%]
Old	10	5050 ± 30	1469 ± 38	38	3.0
New	30	5080 ± 20	1520 ± 60	55	4.3

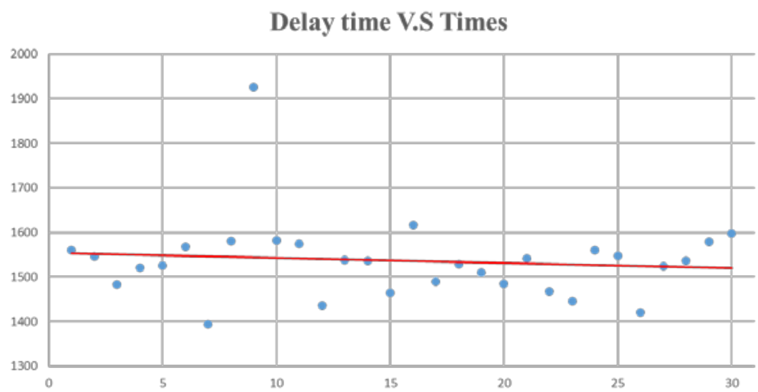

Figure 9.8: Record of delay time for each experiment.

doi:10.6844/NCKU201900671

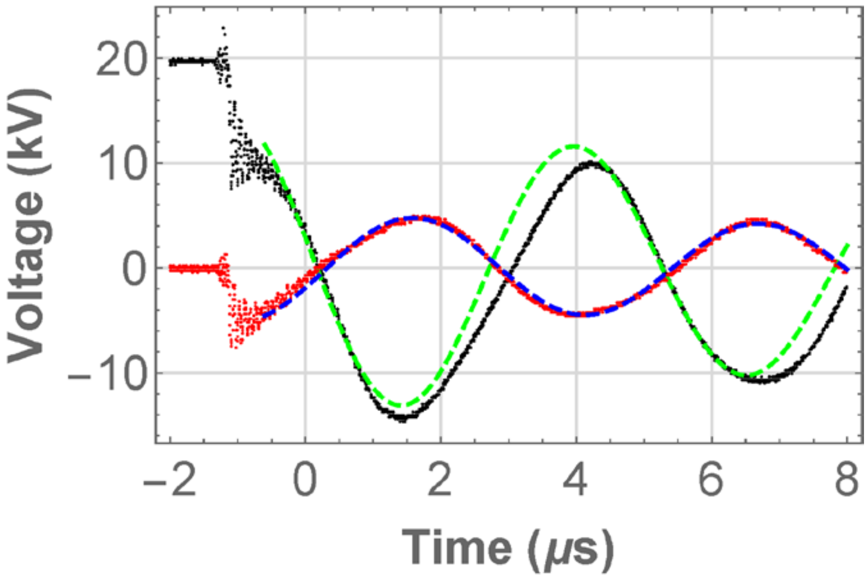

Figure 9.9: The voltage signal of capacitors and the load.

doi:10.6844/NCKU201900671

Chapter 10 Summary

The south wing of the PPCB was built. The PPCB includes 20 capacitors with a total capacitance of 5μF, 2 rail-gap switches, multistep-triggering system, parallel plate and coaxial transmission lines, high-voltage power supply, and compressed air system. The south wing is half of the system. It stores 500 J when it is charged to 20 kV. It provides an output with the power of ~400 MW.

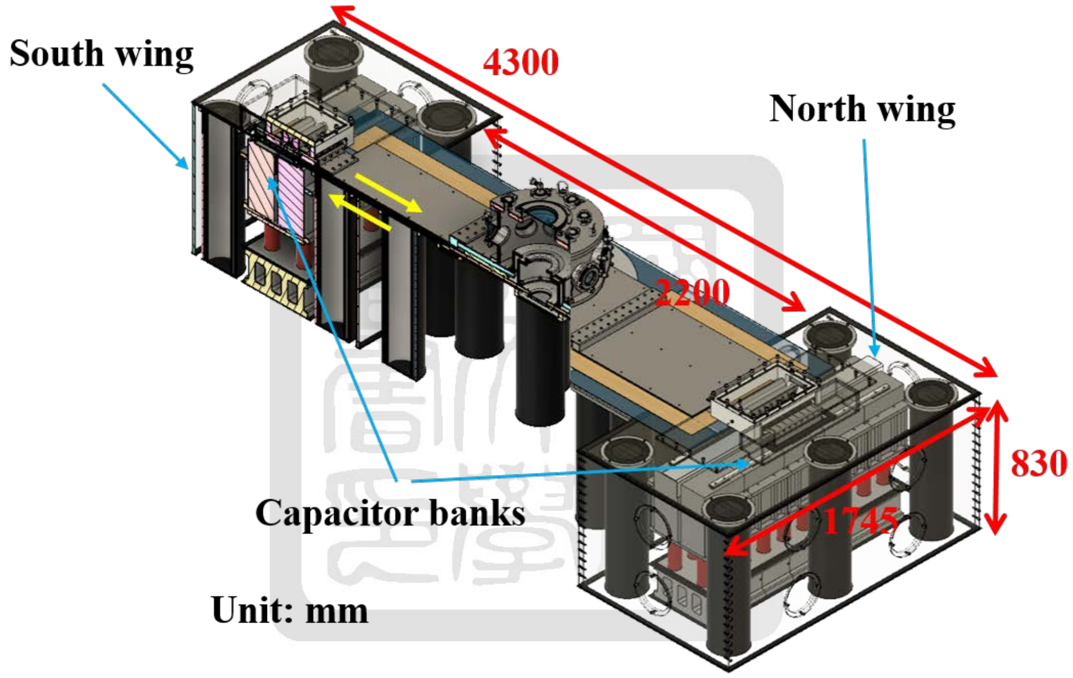

Figure 10.1: The parallel plate capacitor bank pulsed-power system

The rail-gap switch uses the 300-mm long rail-like electrodes. The gap distance between rail-like electrodes and the knife-edge electrode are 6.86 mm to 3.90 mm, as shown in Figure 9.2(a). The gas in the rail gap switch is 1 atm flowing dry air. To trigger the rail-gap switch, the multistep-triggering system was built. The 3-stage Marx generator in the system, as shown in Figure 9.2(b), was used. Each stage of the Marx generator has a 40-μF capacitor and charged to 20 kV. When round electrodes

doi:10.6844/NCKU201900671

are used for the peaking switch in the Marx generator, a -40 kV pulse with a falling speed of -7.7 ± 1.4 kV/ns and the falling time of 3.4 ± 0.7 ns was generated. It meets the requirement of using a pulse with a rising speed > 5 kV/ns to initiative multichannel in the rail-gap switch.

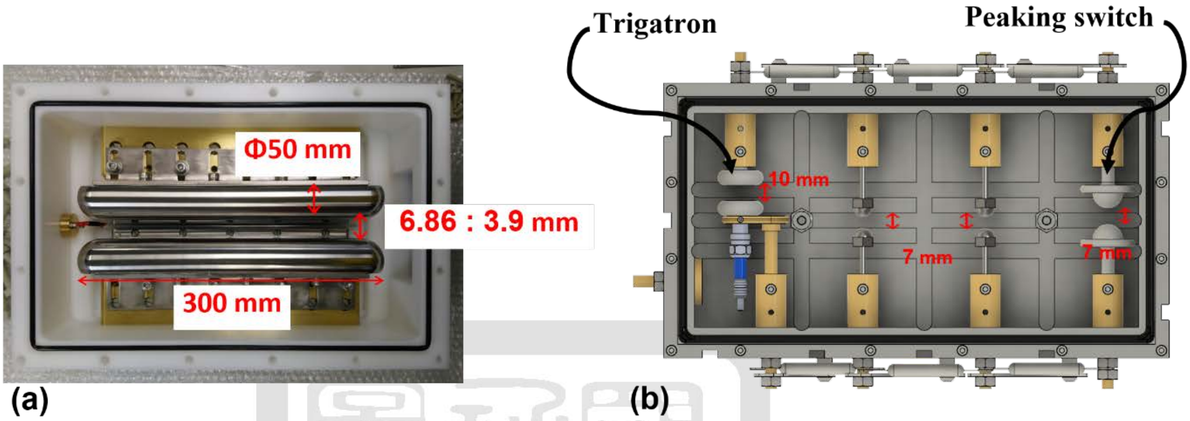

Figure 10.2: (a) The rail-gap switch used in our lab. (b) The Marx generator used in our lab.

The south wing was built and optimized. The total inductance was 265 ± 2 nH (with a 53-nH load). The curve-fitting results showed that the inductance of the rail-gap switch was 60 ± 20 nH and the inductance of the one-brick capacitor was 120 ± 30 nH. The optimized south wing provided a peak current of 59.2 ± 0.7 kA with a rising time of 1280 ± 10 ns and power was 363 MW. The jitter respect to the trigger pulse was only 11 ns, 1% of the rise time. Therefore, we can synchronize the north wing and the south wing within the accuracy of 1%. Therefore, we are expecting a peak current of ~120 kA when the full PPCB is built in the near future. We summarize all results of the system in Table 9.1.

doi:10.6844/NCKU201900671

	South wing	PPCB	
# of capacitor	10	20	
Capacitance/each	1 uF		
Total Capacitance	2.5 uF	5 uF	
Voltage	20 kV	20 kV	50 kV
Total energy	0.5 kJ	1 kJ	6.25 kJ
Current rise time (ns)	1280 ± 10	~1280	
Peak current (kA)	59.2 ± 0.7	~120 kA	~300 kA
Inductance (nH)			
Total (with 53-nH load)	265 ± 3 nH	~130 nH	
The rail-gap switch	60 ± 20		
One-brick capacitor	120 ± 30		
Jitter	11 ns		
$\frac{\text{Jitter}}{T_{rise}}$	1 (%)		
Power	363 ± 7 MW	~ 0.8 GW	
Marx			
Falling speed (kV/ns)	-7.7 ± 1.4		
Falling time (ns)	3.1 ± 0.7		

Table 10.1: The result of the south wing.

doi:10.6844/NCKU201900671

Bibliography

[1] Yasushi Hayashi, Plasma Sources Sci. Technol. 13 675 (2004)

[2] Mei-Feng Huang. ‘’rust remover using small pulsed-power system’’. Master Thesis, July 2017.

[3] Sheng-Hua Yang, Master Thesis, National Cheng Kung University (2018)

[4] https://en.wikipedia.org/wiki/Paschen

[5] Lucy-Ann McFadden and Torrence Johnson and Paul Weissman, ed., Encyclopedia of the Solar System, 2nd Ed. (Academic Press, 2006).

[6] Northstar Research Corporation[6]

[7] R.Verma etc., Rev. Sci. Instrum. 85, 095117 (2014)

[8] Foundations of Pulsed Power Technology

[9] https://www.eeweb.com/tools/wire-inductance

doi:10.6844/NCKU201900671

A1 Circuit diagram of the trigger pulse generator

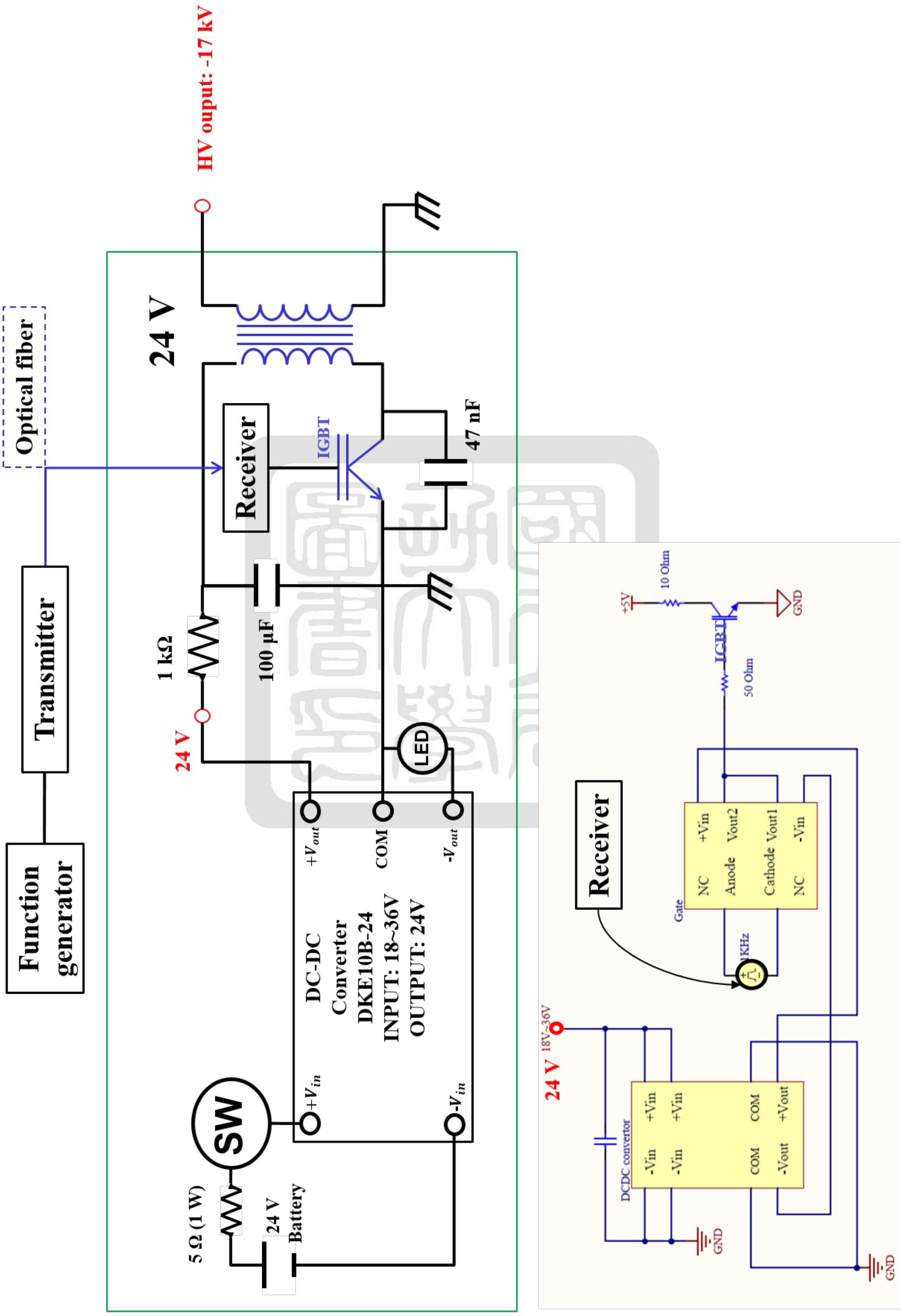

doi:10.6844/NCKU201900671

A2 Drawings of the normally open (NO) relay

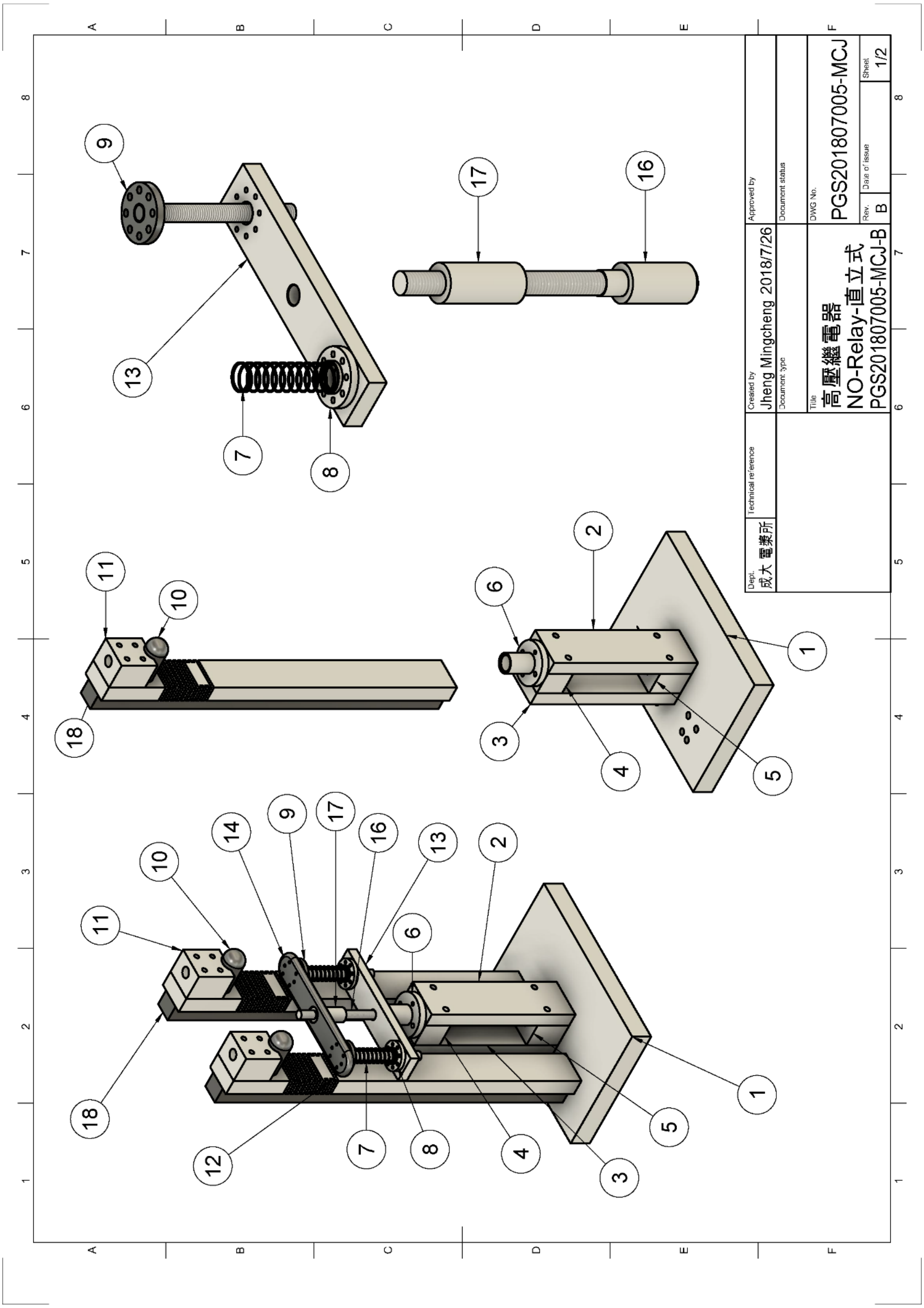

doi:10.6844/NCKU201900671

明細表

項目	數量	零件名稱	零件工程圖號	Rev	材料	說明
0	1組	NO-Relay 總圖	PGS201807005-MCJ	B		
1	1	底板	PGS201806001-MCJ	B	PE	
2	1	氣動閥固定架-上基板	PGS201806002-MCJ	A	PE	
3	1	氣動閥固定架-下基板	PGS201806003-MCJ	A	PE	
4	1	氣動閥固定架-頭	PGS201806004-MCJ	A	PE	
5	1	氣動閥固定架-後	PGS201806005-MCJ	A	PE	
6	1	NCM KB 075-0400S	無			
7	2	彈簧-85-13-19.5*17.5-1	無			
8	2	彈簧固定架-下	PGS201806008-MCJ	A	PE	
9	2	彈簧固定架-上	PGS201806009-MCJ	A	PE	
10	2	NO電極	PGS201806006-MCJ	A	鋁合金5	
11	2	電擊架配件	PGS201806007-MCJ	A	PE	
12	2	NO電極架	PGS201807001-MCJ	B	PE	
13	1	NO-彈簧架-板	PGS201806014-MCJ	A	PE	
14	1	NO-電擊板	PGS201806015-MCJ	A	鋁合金5	
15	1	NO-延長-支撐架	PGS201806016-MCJ	A	PE	
16	1	延長桿1號	PGS201806017-MCJ	A	PE	
17	1	延長管2號	PGS201806018-MCJ	A	PE	
18	2	NO直立式加強柱	PGS201807003-MCJ	B	PE	

Dept.	Technical reference	Created by	Approved by
成大 電機所		Jheng Mingcheng 2018/7/26	
		Document type	Document status
		Title: NO-Relay-直立式	DWG No.: PGS201807005-MCJ
			Rev.: B; Date of issue: ; Sheet: 2/2

doi:10.6844/NCKU201900671

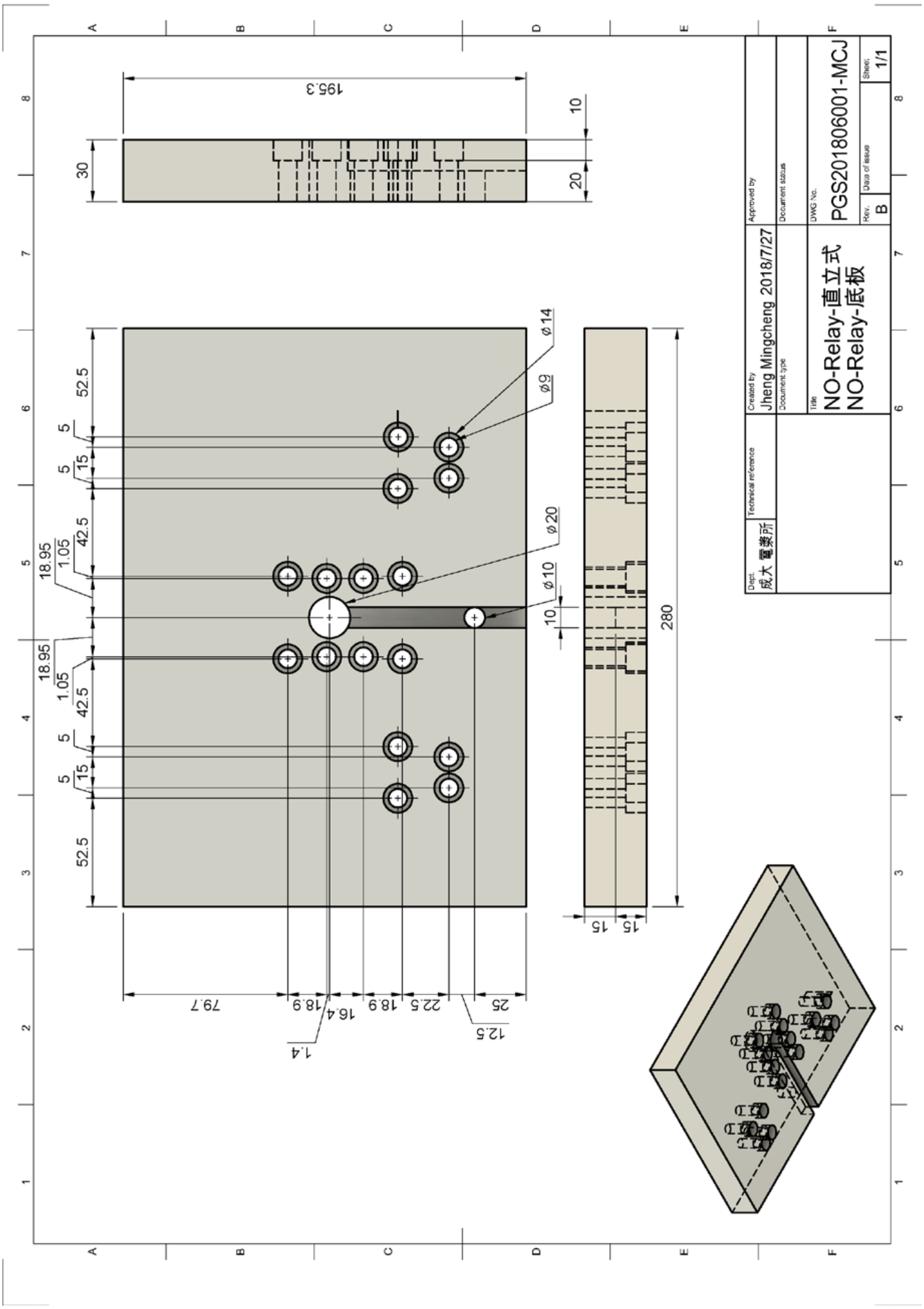

doi:10.6844/NCKU201900671

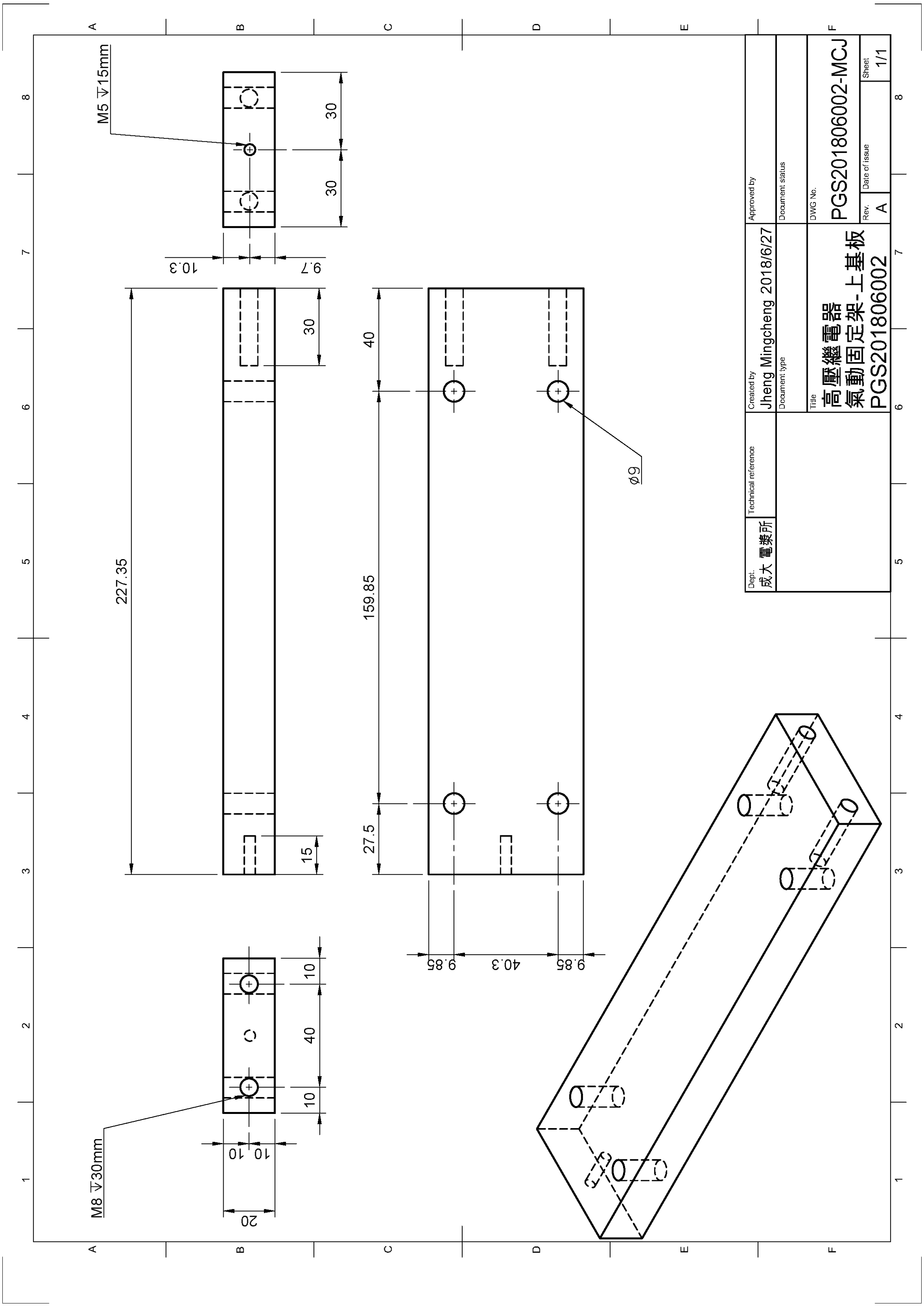

doi:10.6844/NCKU201900671

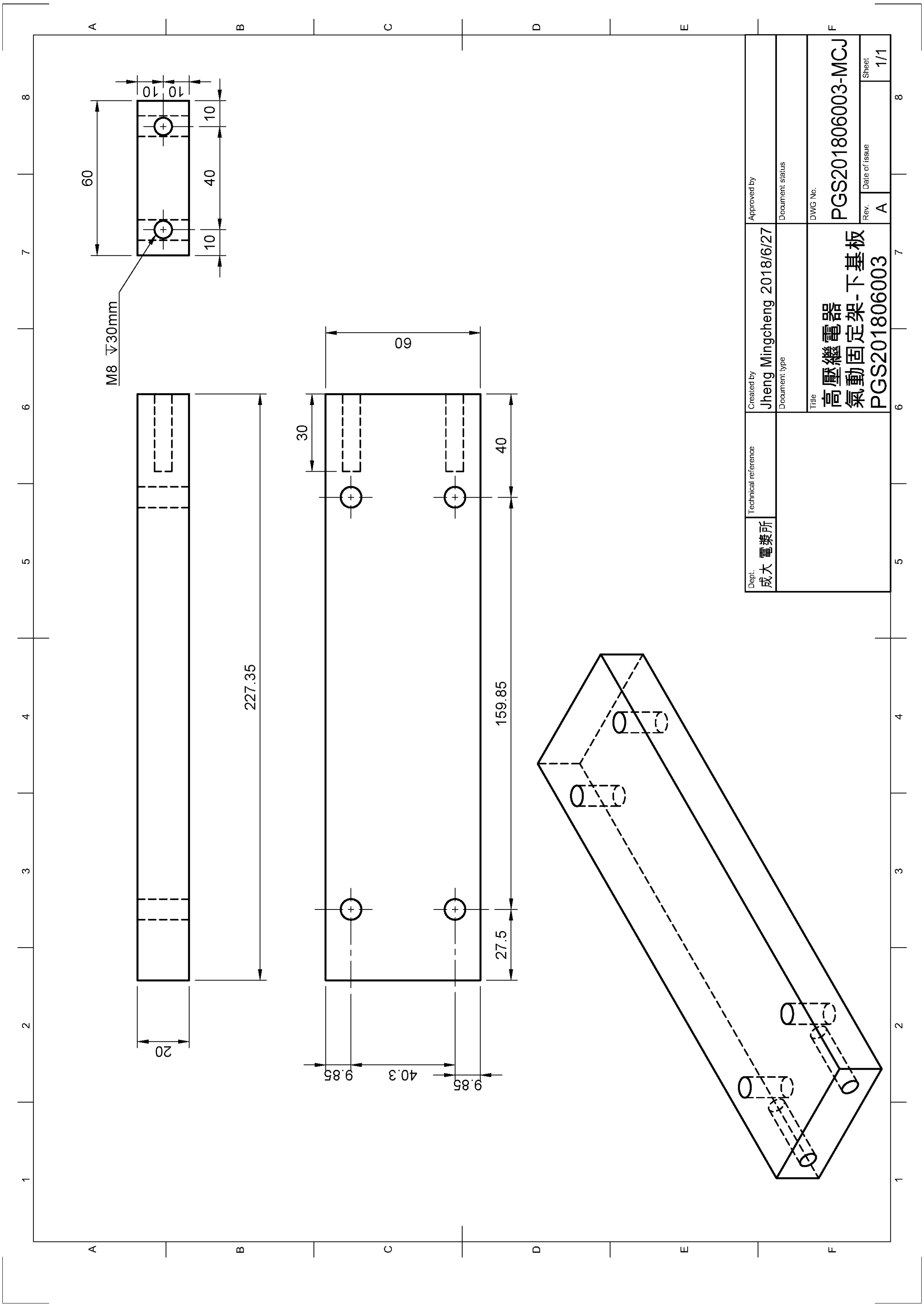

doi:10.6844/NCKU201900671

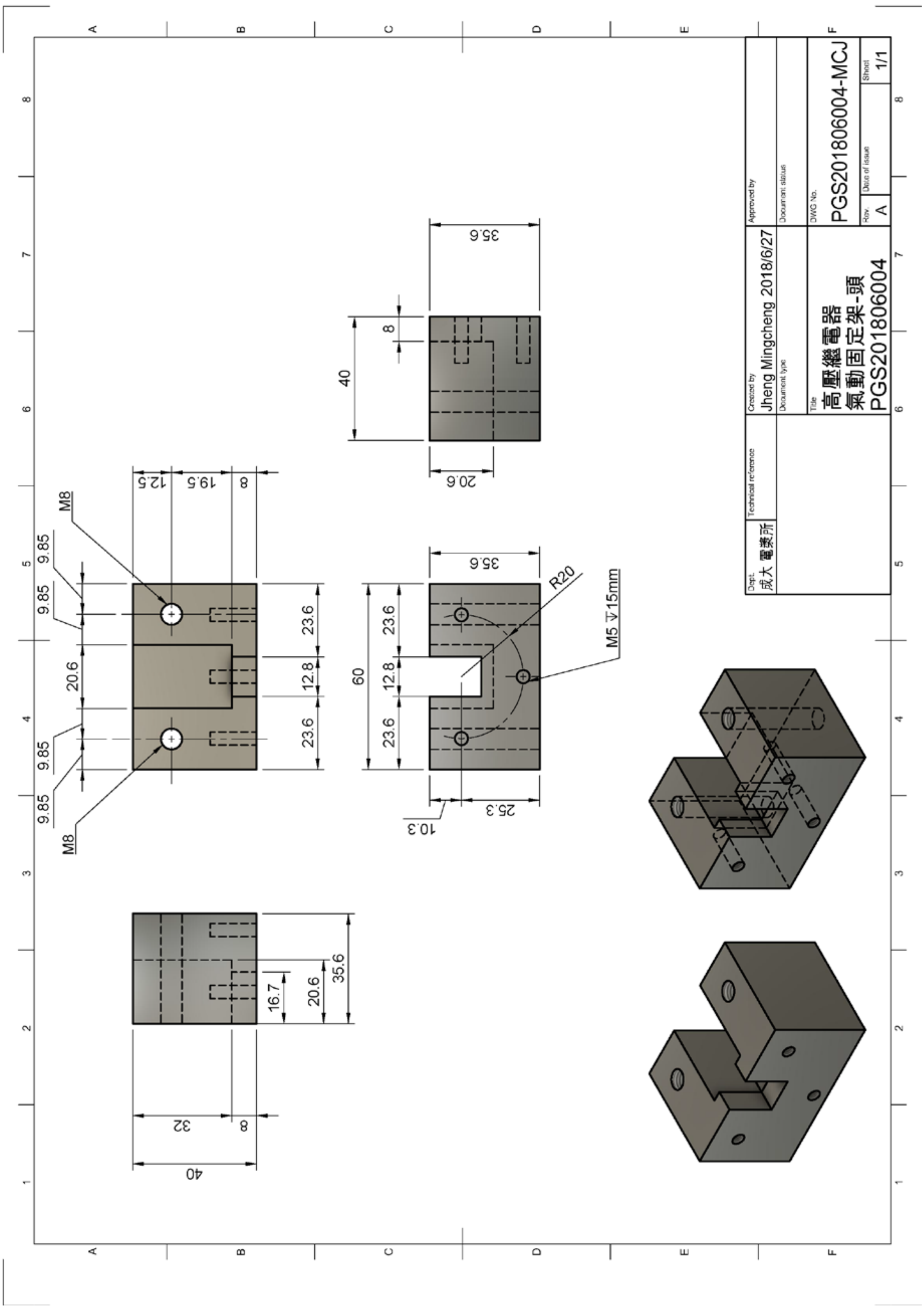

doi:10.6844/NCKU201900671

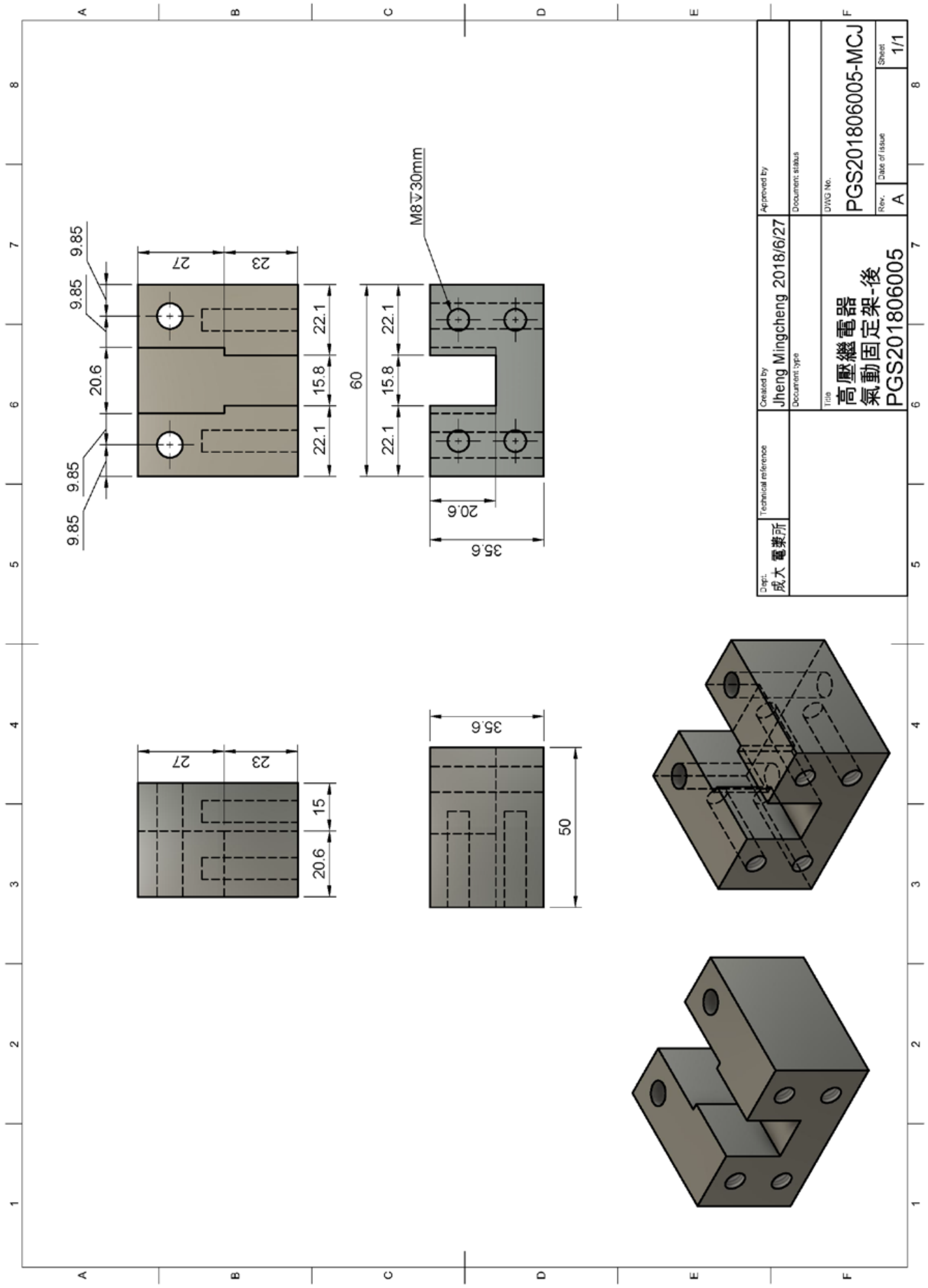

doi:10.6844/NCKU201900671

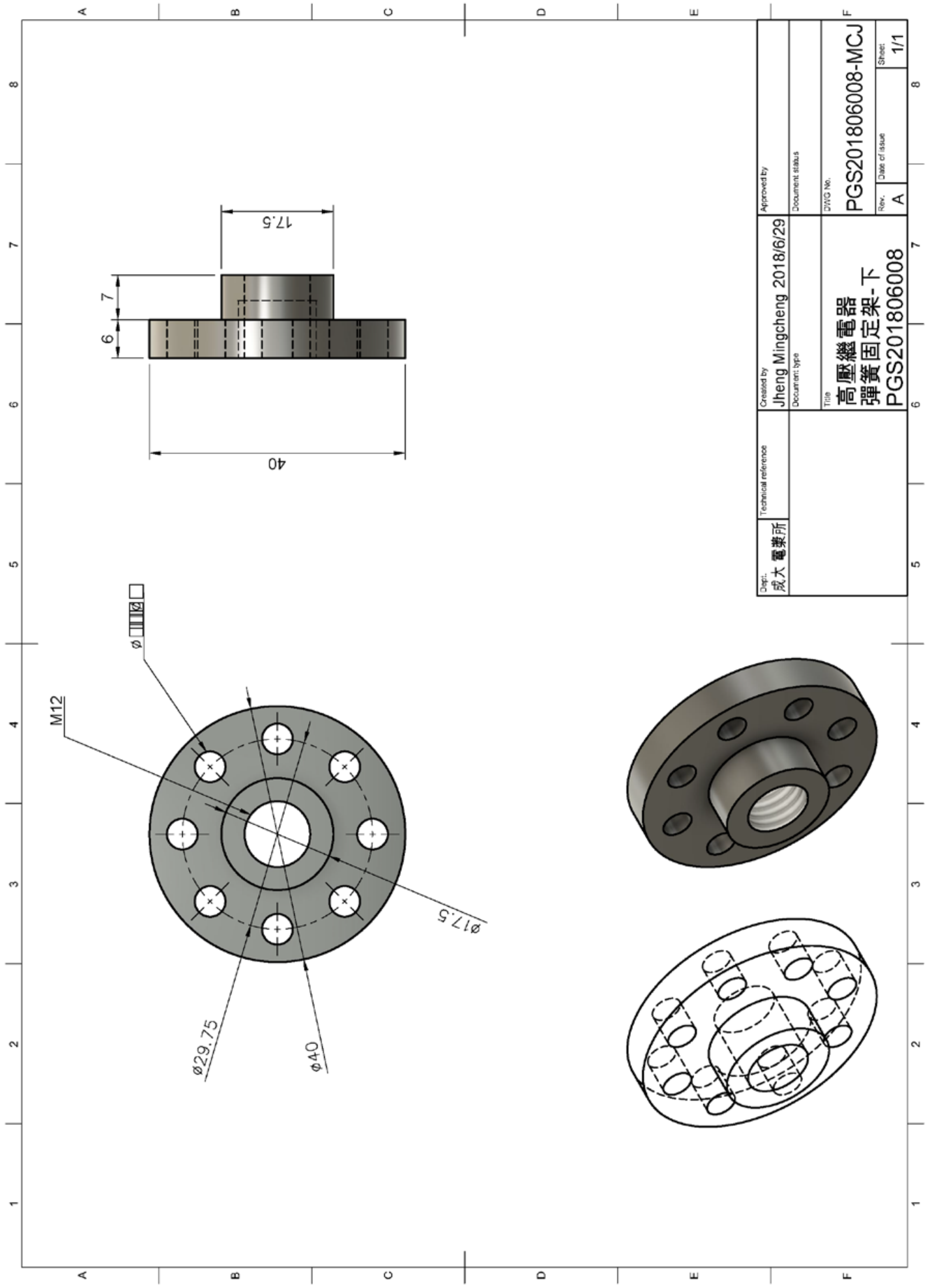

doi:10.6844/NCKU201900671

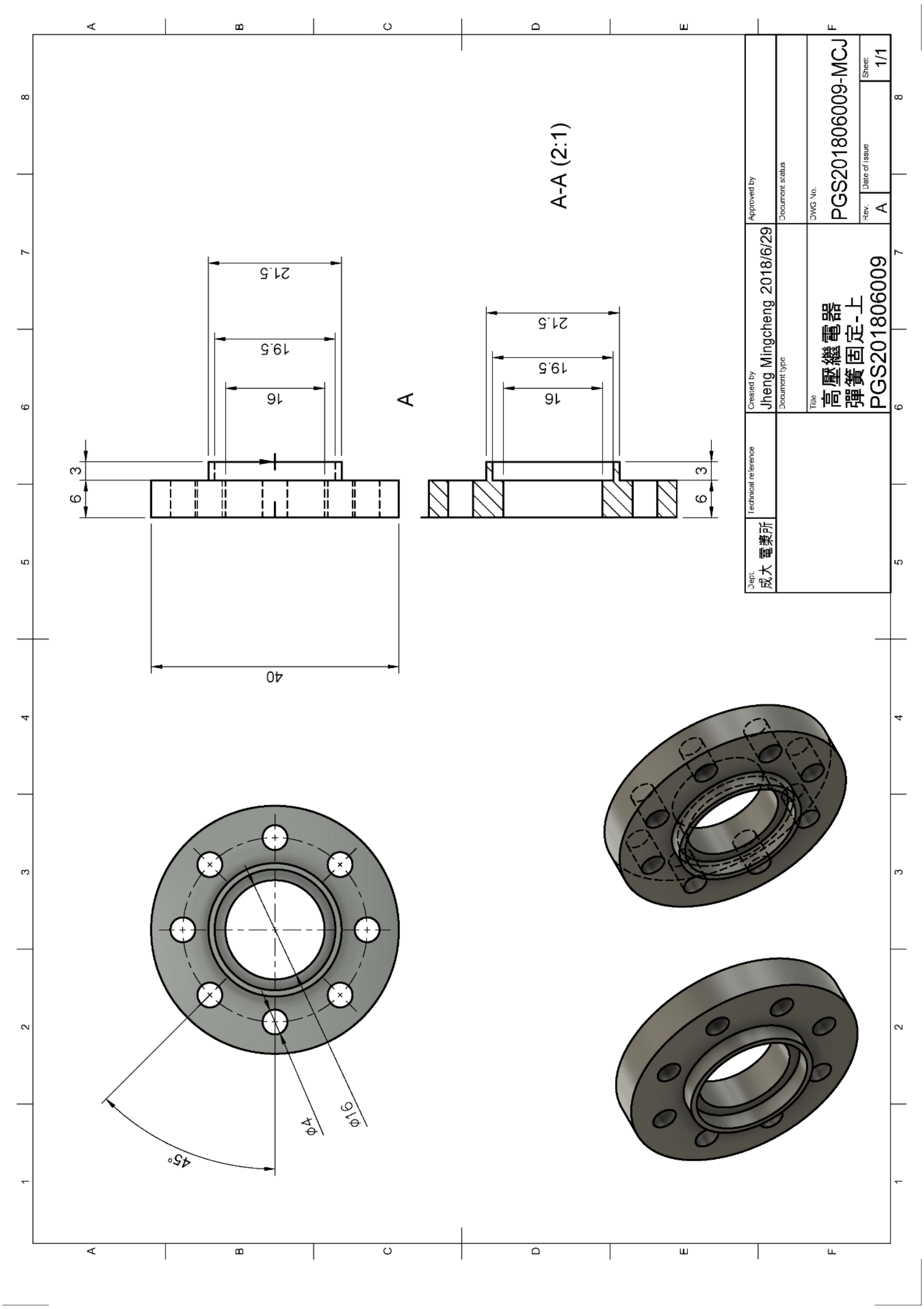

doi:10.6844/NCKU201900671

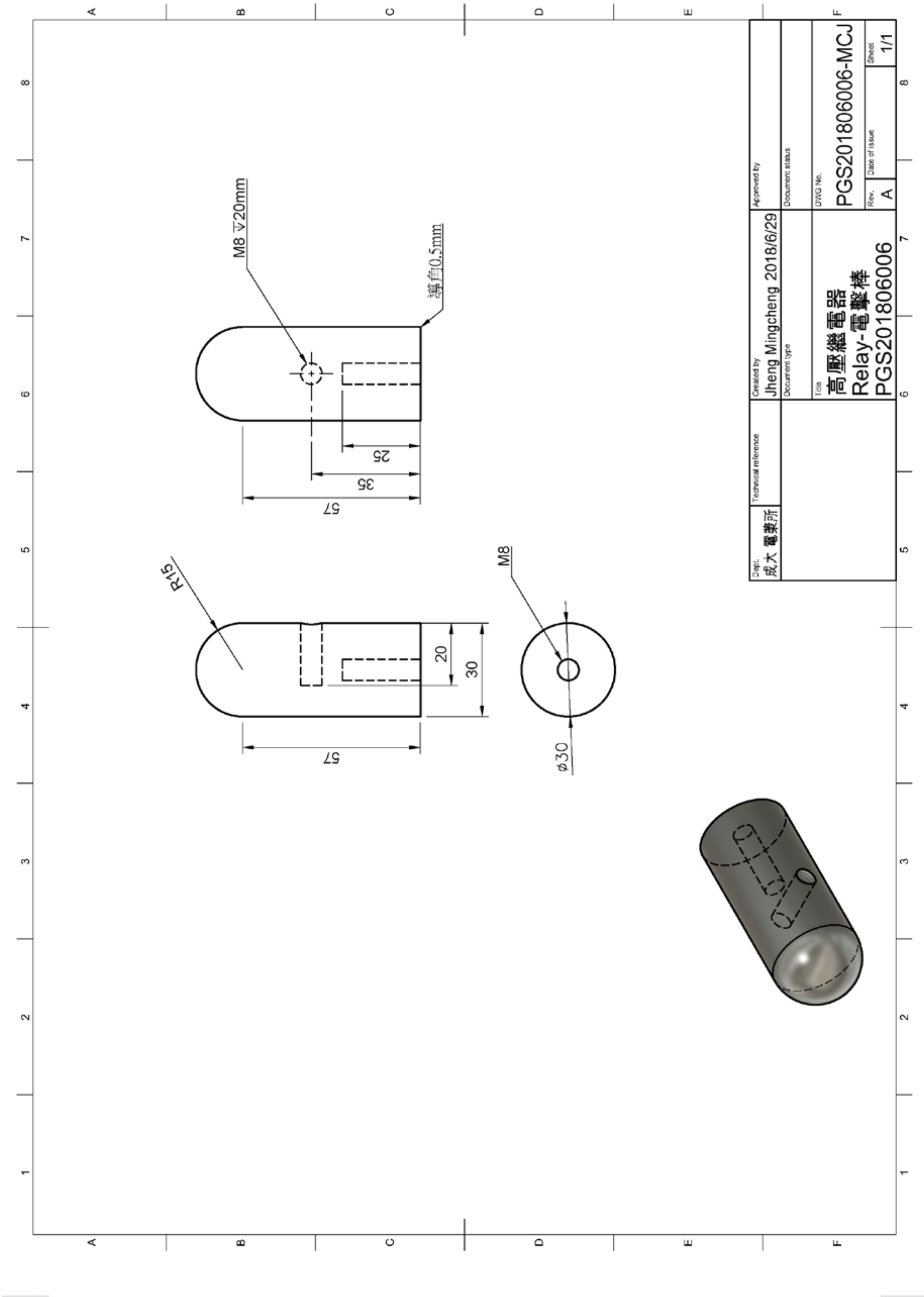

doi:10.6844/NCKU201900671

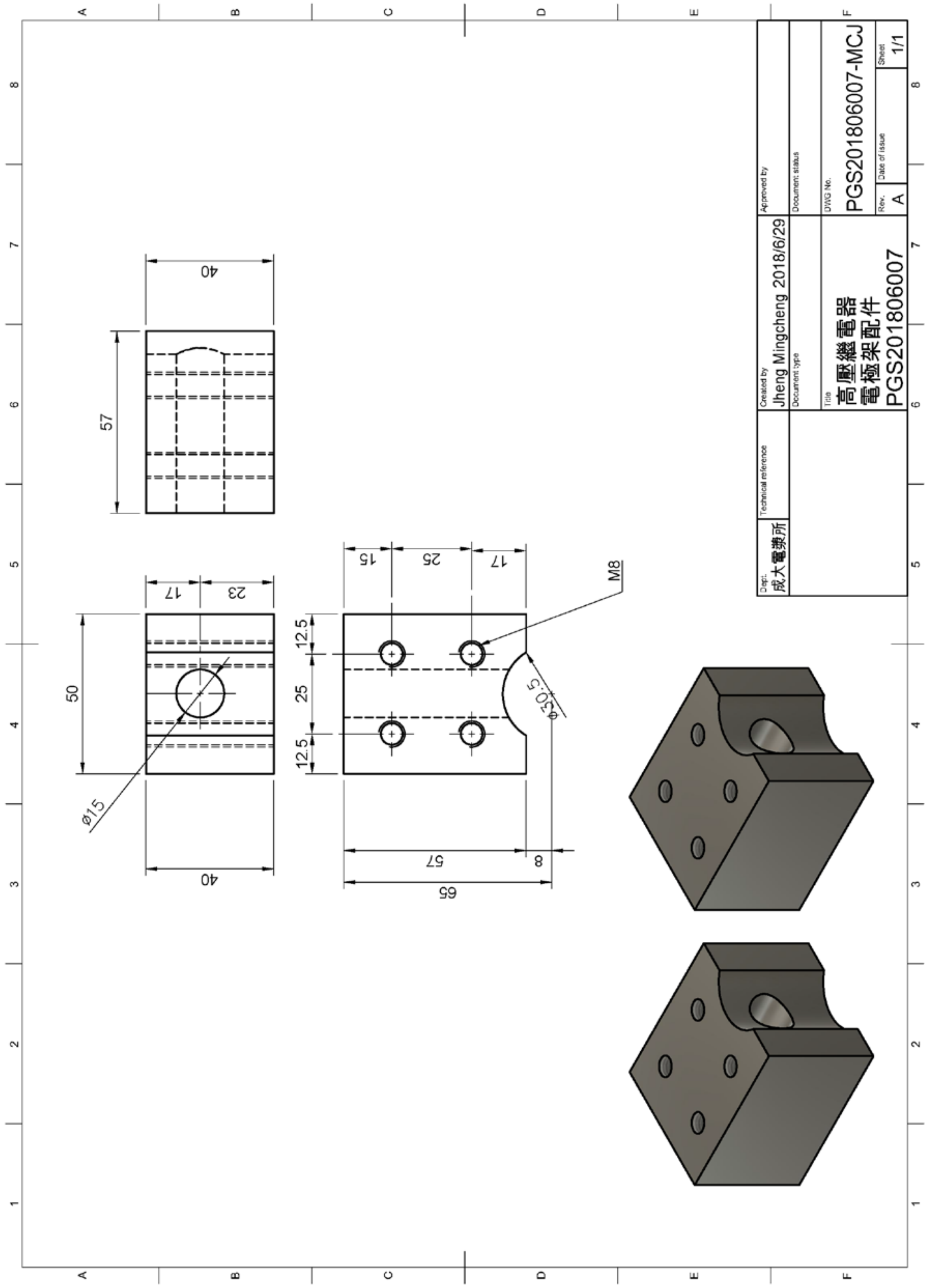

doi:10.6844/NCKU201900671

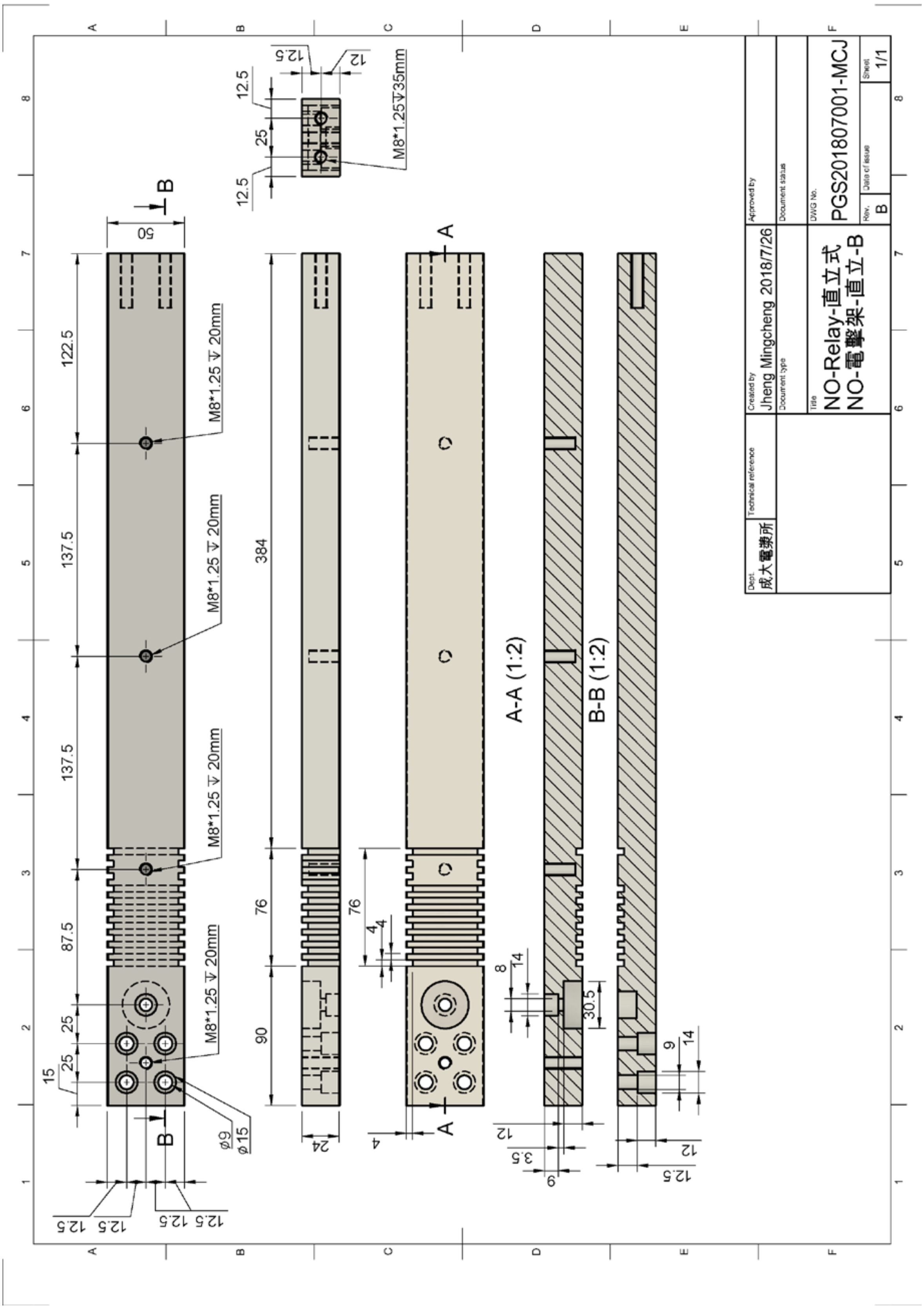

doi:10.6844/NCKU201900671

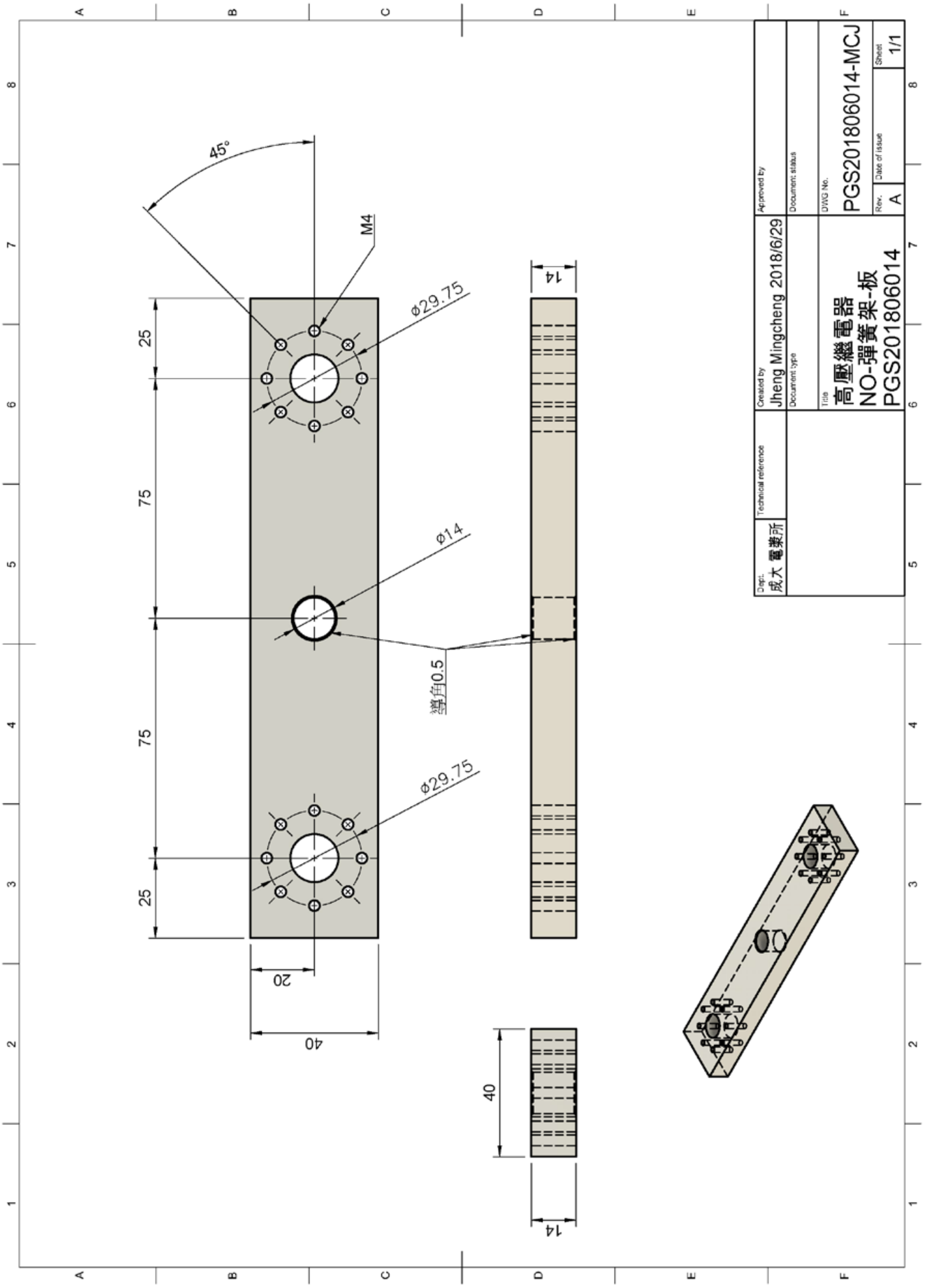

doi:10.6844/NCKU201900671

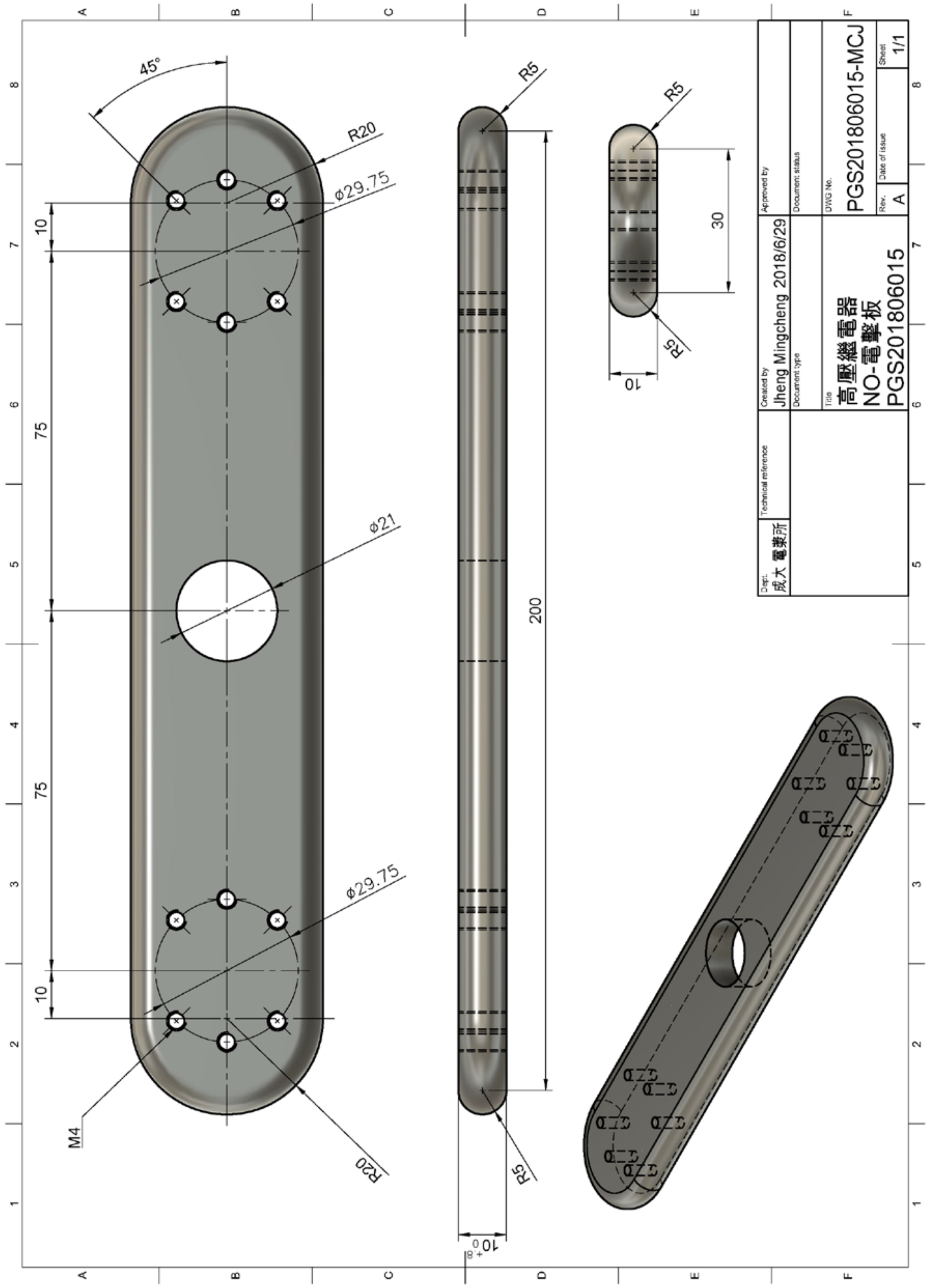

doi:10.6844/NCKU201900671

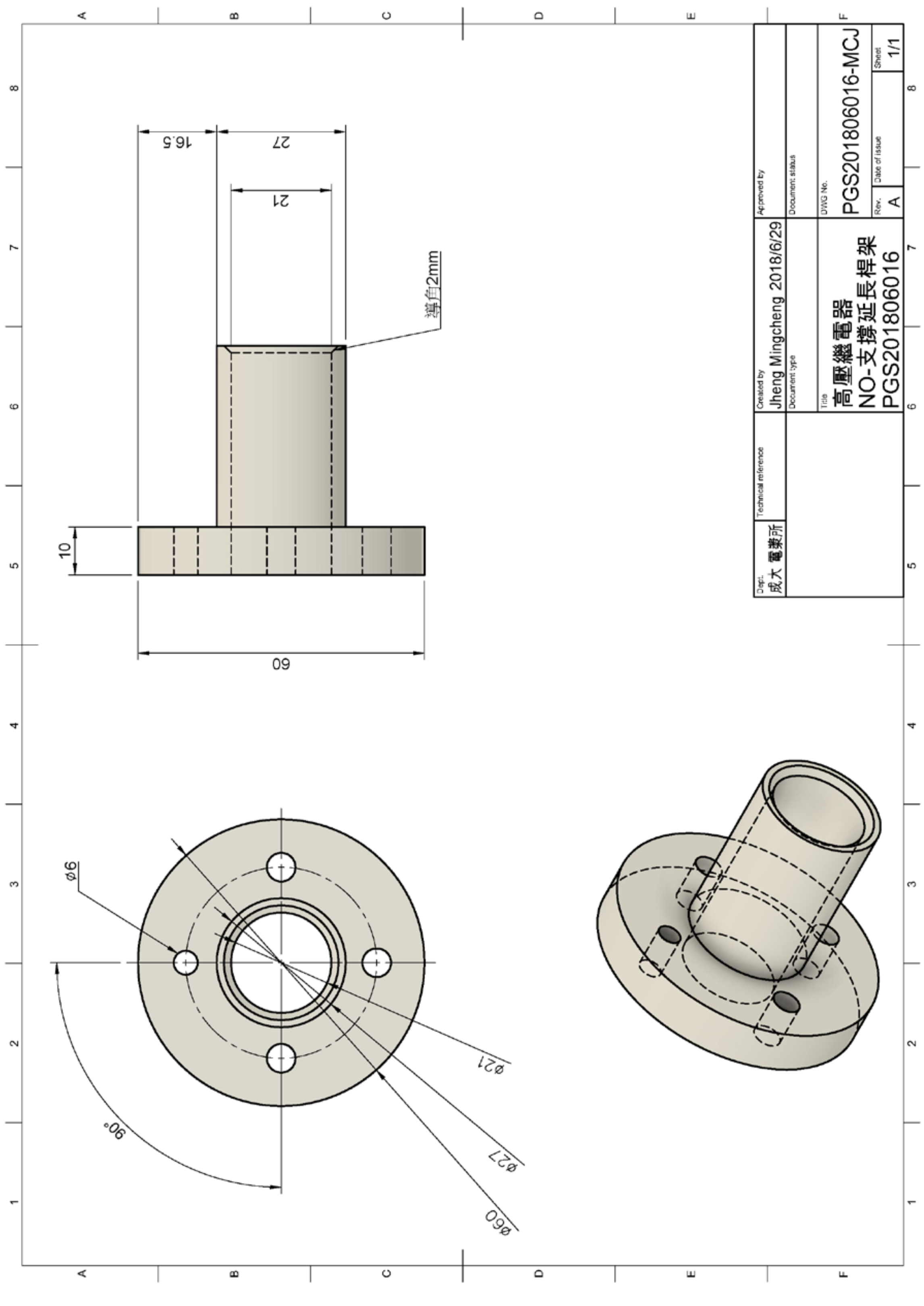

doi:10.6844/NCKU201900671

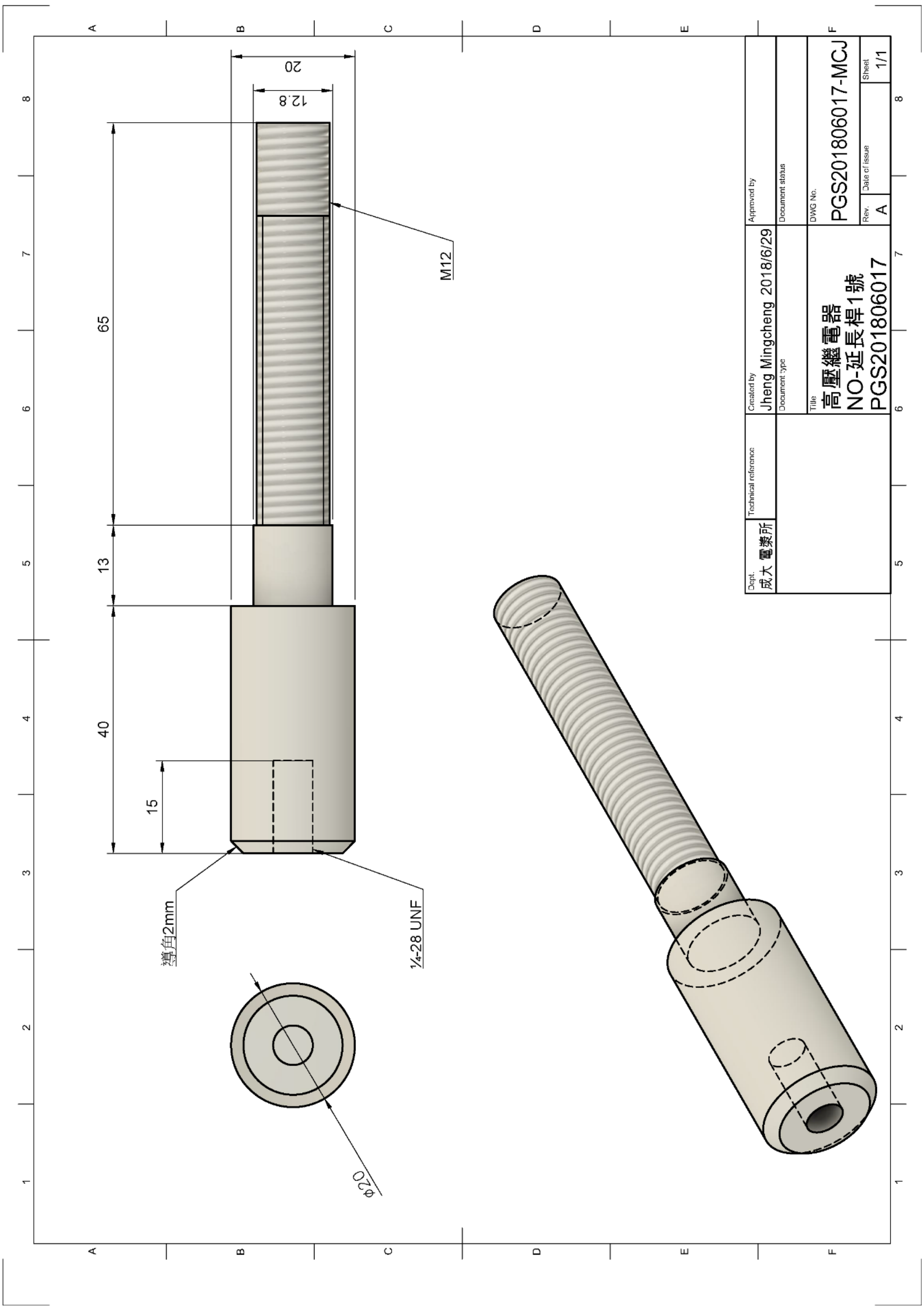

doi:10.6844/NCKU201900671

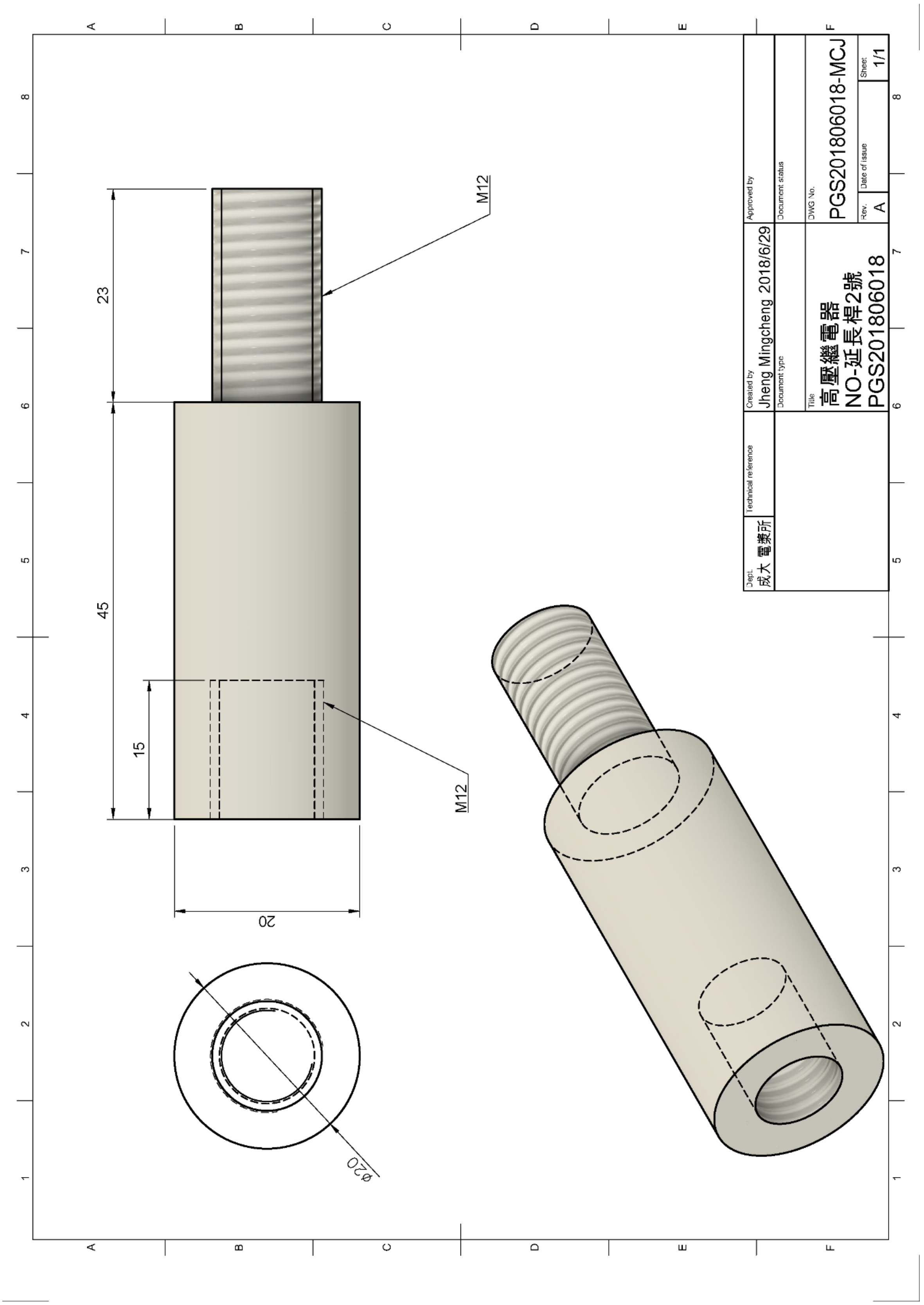

doi:10.6844/NCKU201900671

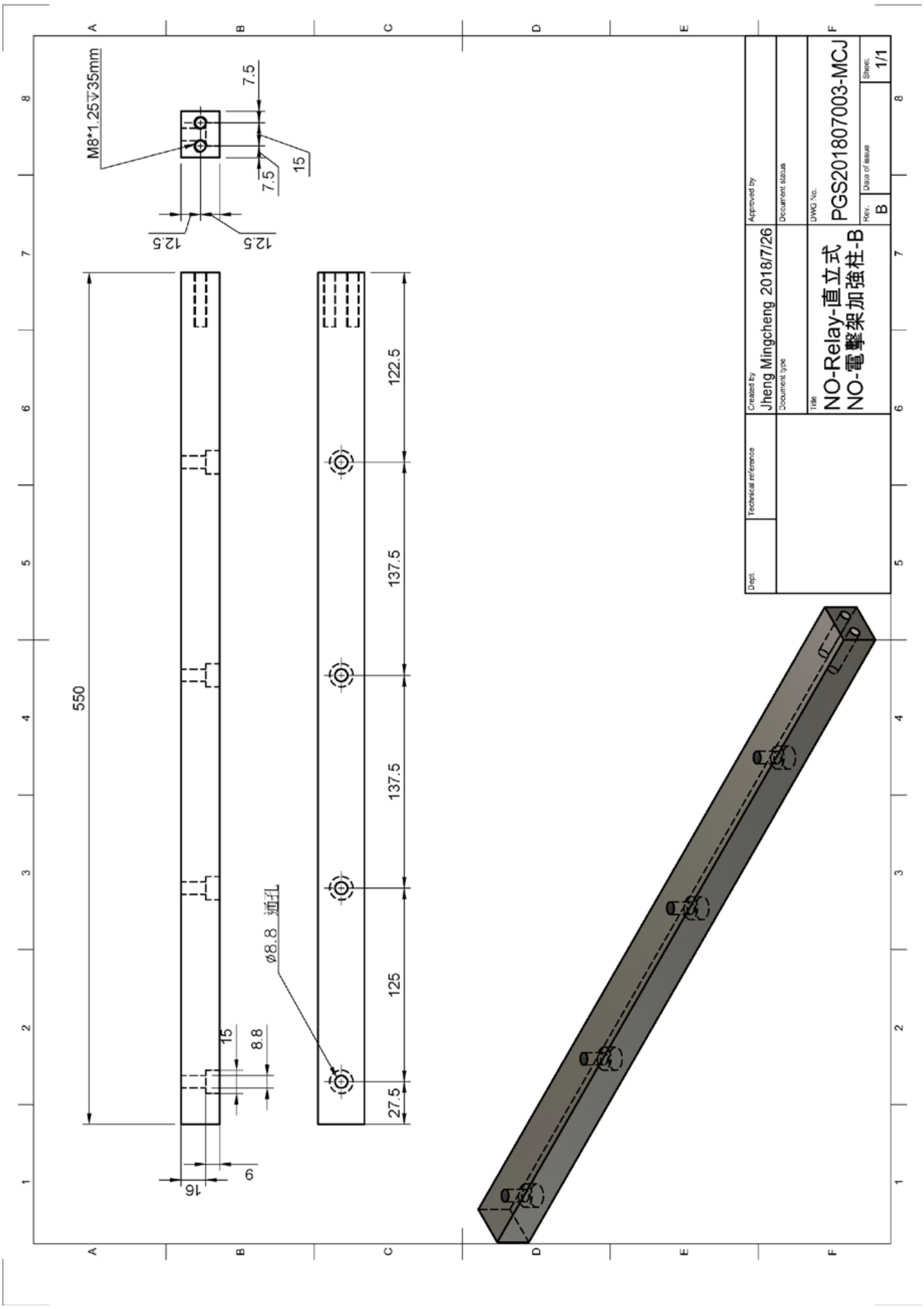

doi:10.6844/NCKU201900671

A3 Drawings of the normally closed (NC) relay

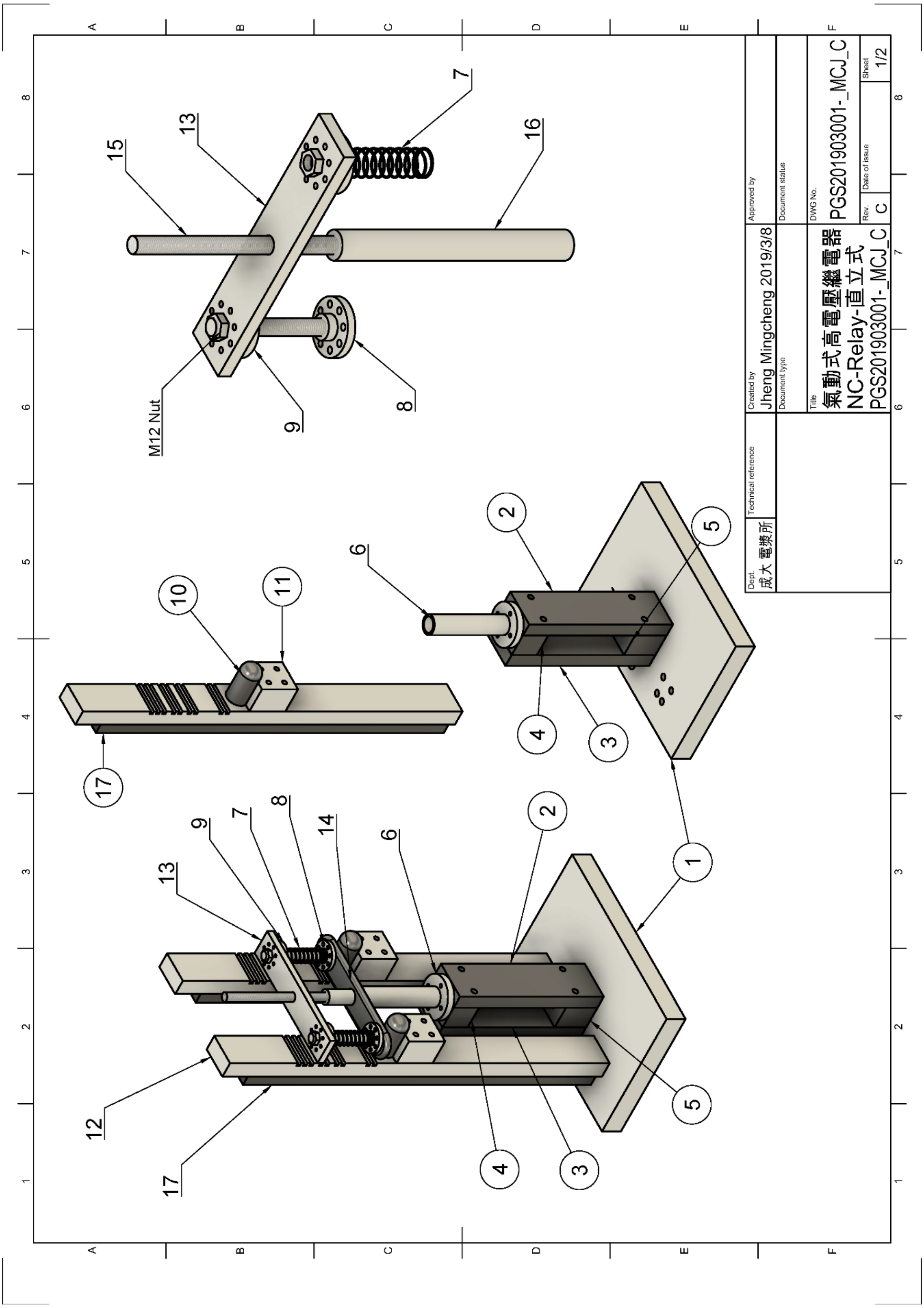

doi:10.6844/NCKU201900671

明細表

項目	數量	零件名稱	工程圖號	Rev	材料	備註
0	1組	NC-Relay總圖	PGS201903001-_MCJ_C	C		
1	1	底板	PGS201806001-MCJ		PE	
2	1	氣動閥固定架-上基板	PGS201806002-MCJ		PE	
3	1	氣動閥固定架-下基板	PGS201806003-MCJ		PE	
4	1	氣動閥固定架-頭	PGS201806004-MCJ		PE	
5	1	氣動閥固定架-後	PGS201806005-MCJ			
6	1	NCM KB 075-0400S	無			
7	2	彈簧-85-13-19.5*17.5-1	無			
8	1	彈簧固定座-下	PGS201806008-MCJ		PE	
9	1	彈簧固定座-上	PGS201806009-MCJ		PE	
10	2	NC電極	PGS201806006-MCJ		PE	與NO共用
11	2	電極架配件	PGS201806007-MCJ		PE	
12	2	NC-電擊架	PGS201807002-B-MCJ		PE	
13	1	彈簧支撐架-板	PGS201806013		PE	
14	1	NO-電擊板	PGS201806015-MCJ		PE	
15	1	NC延長桿	PGS201806010-A-MCJ			
16	1	NC-延長桿支撐架	PGS201806011-A-MCJ-			
17	2	NC直立式加強柱	PGS201807004-A-MCJ		PE	

Dept.	Technical reference	Created by	Approved by
		Jheng Mingcheng 2019/3/8	
		Document type	Document status
		Title: 氣動式高電壓繼電器 NC-Relay-直立式 PGS201903001-_MCJ	DWG No.
			Rev. C / Date of issue / Sheet 2/2

doi:10.6844/NCKU201900671

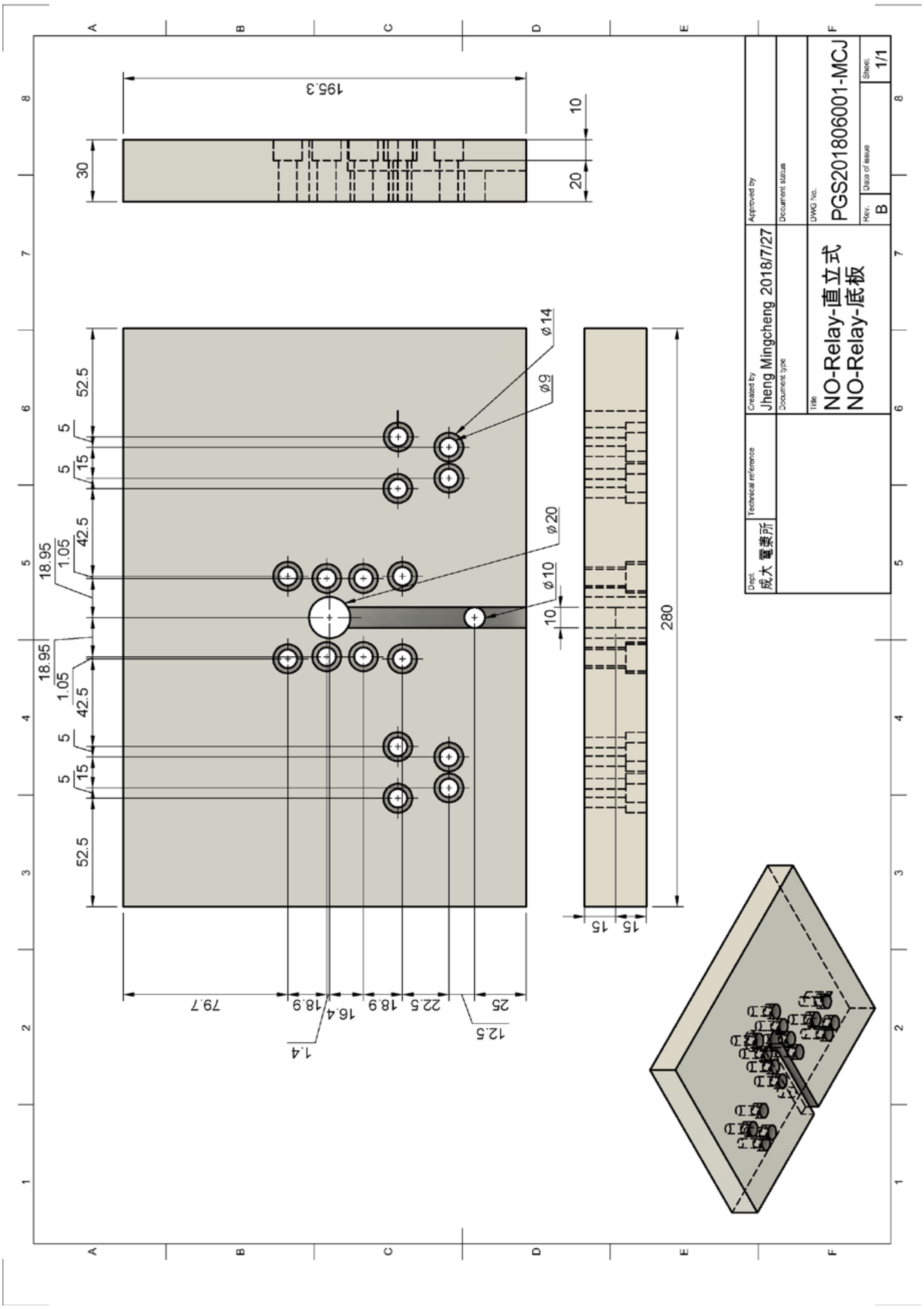

doi:10.6844/NCKU201900671

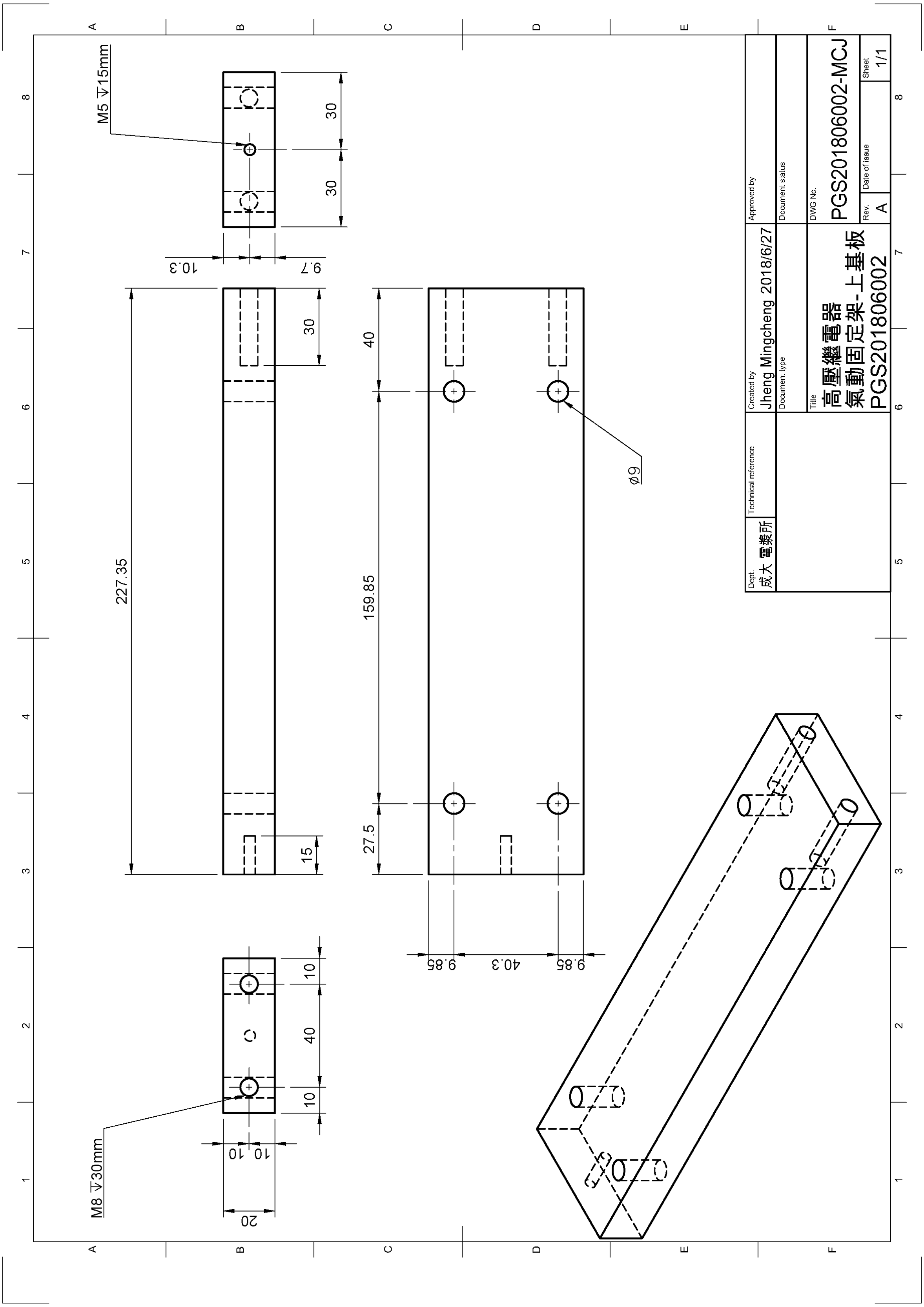

doi:10.6844/NCKU201900671

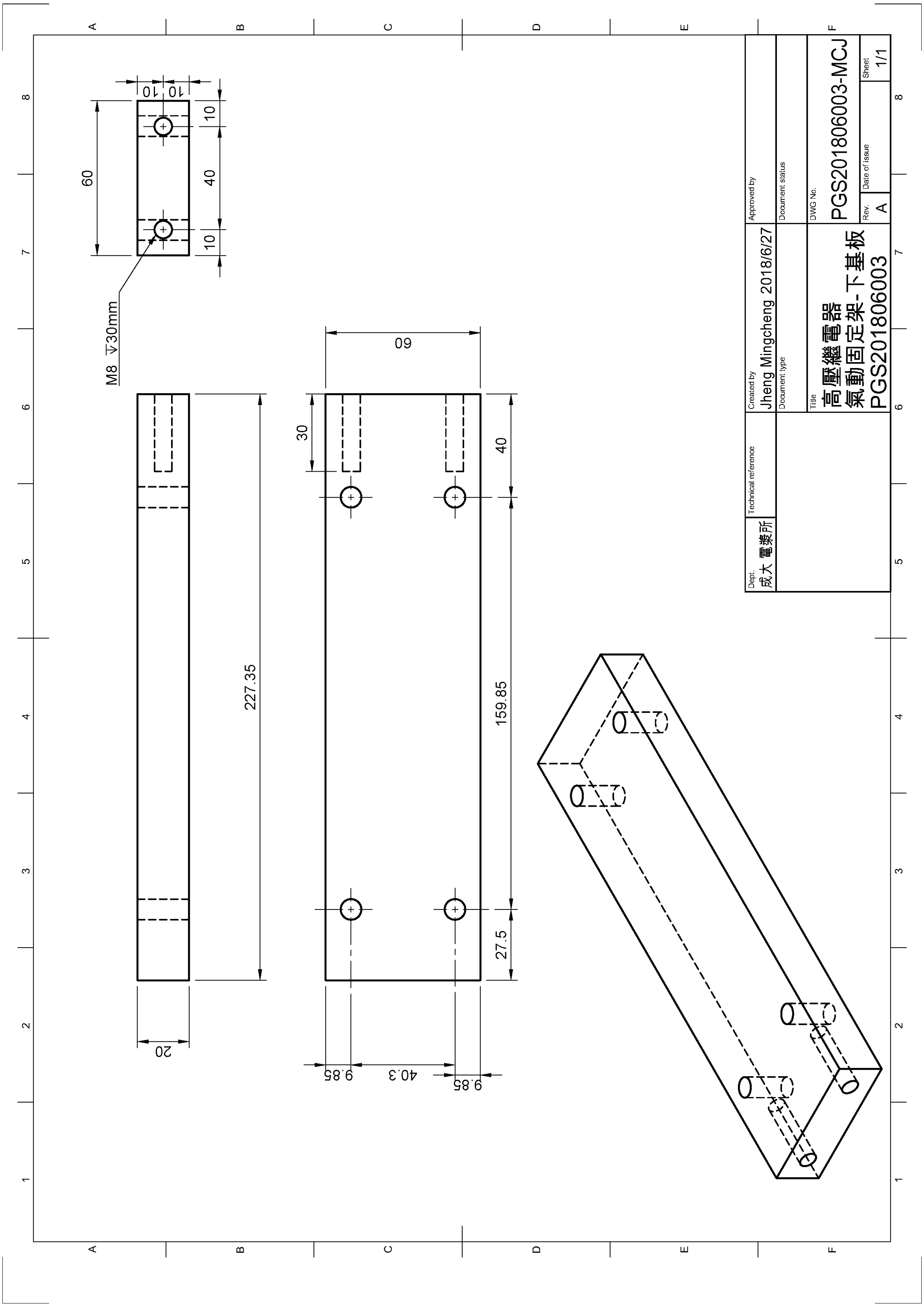

doi:10.6844/NCKU201900671

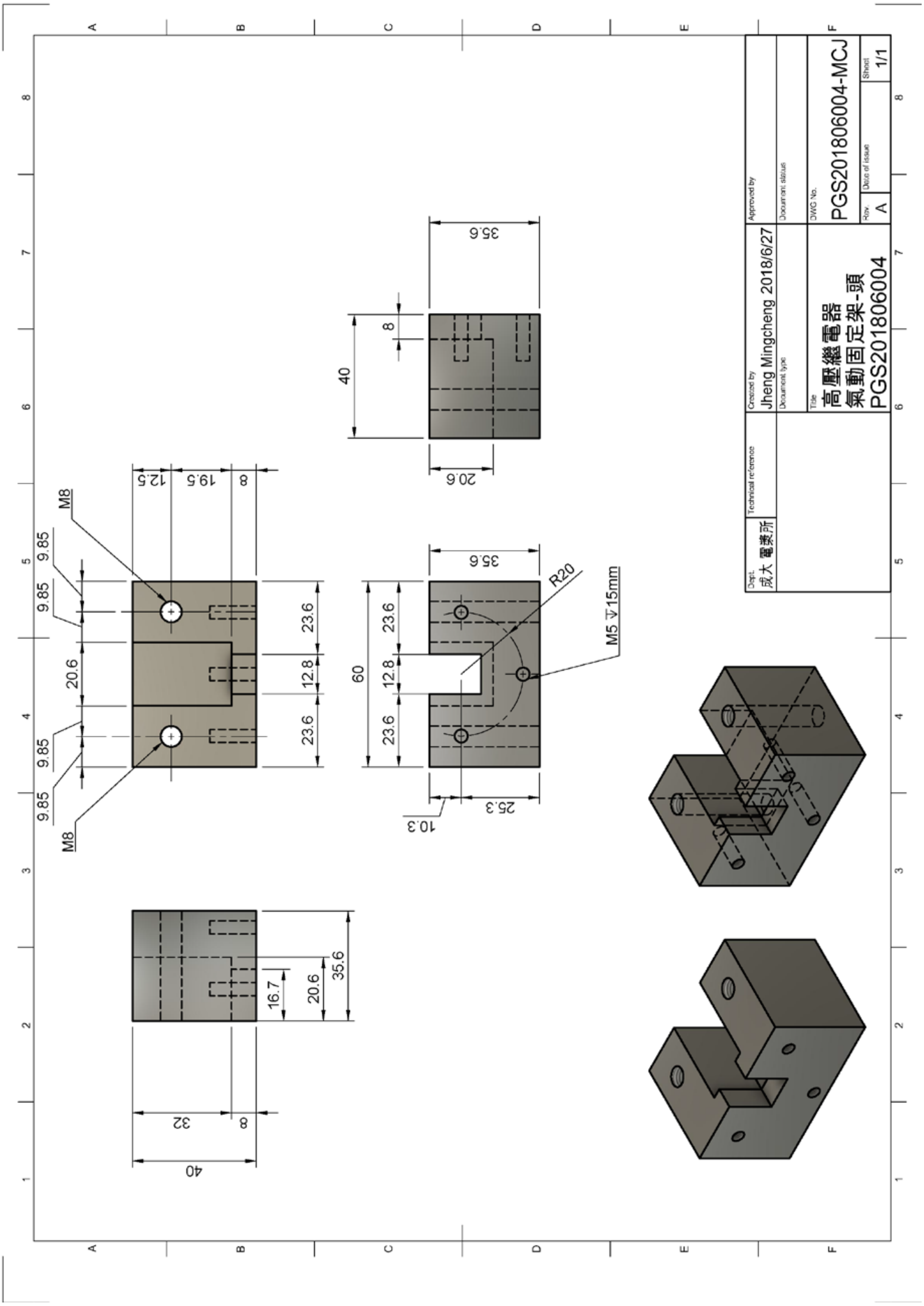

doi:10.6844/NCKU201900671

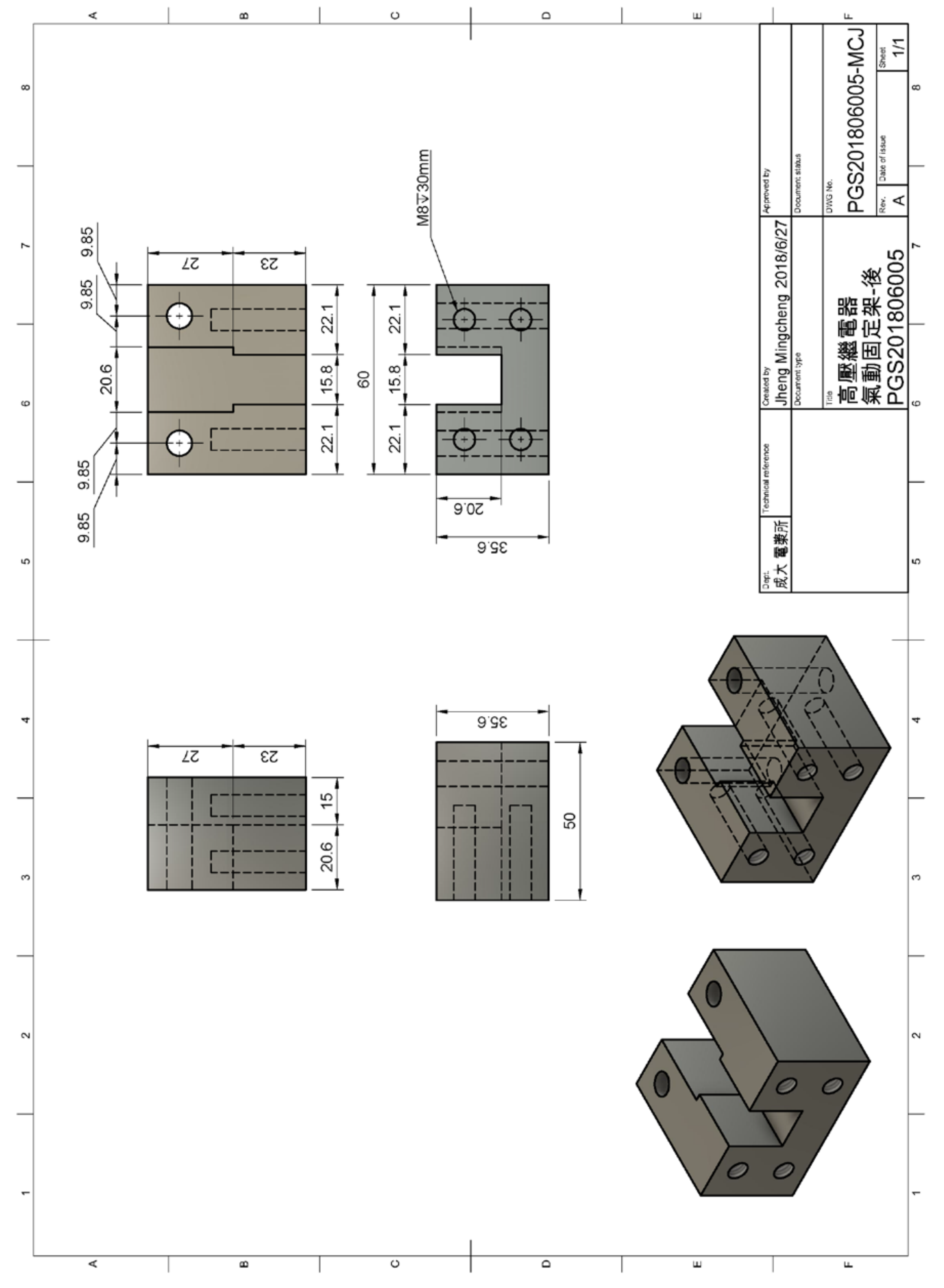

doi:10.6844/NCKU201900671

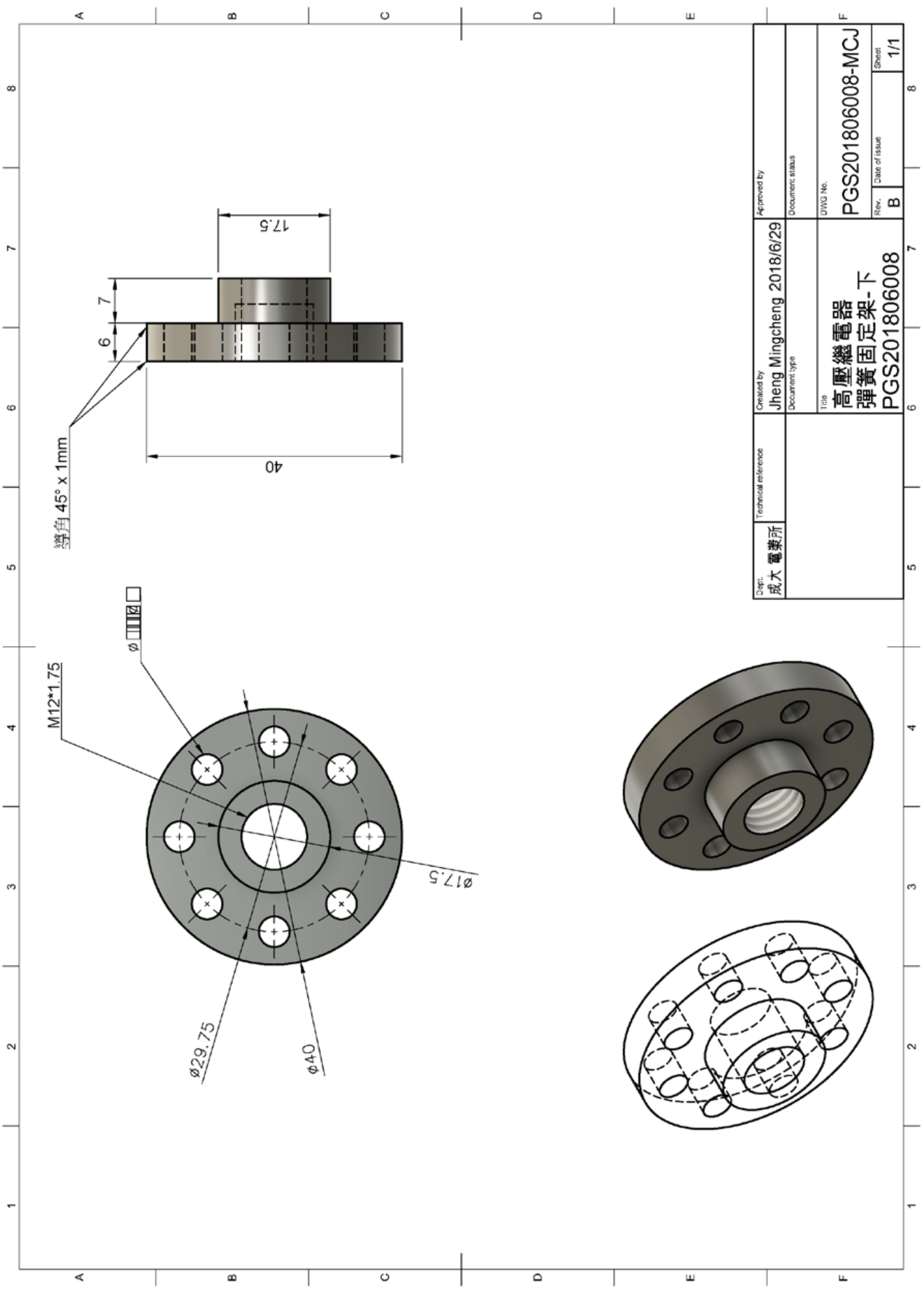

doi:10.6844/NCKU201900671

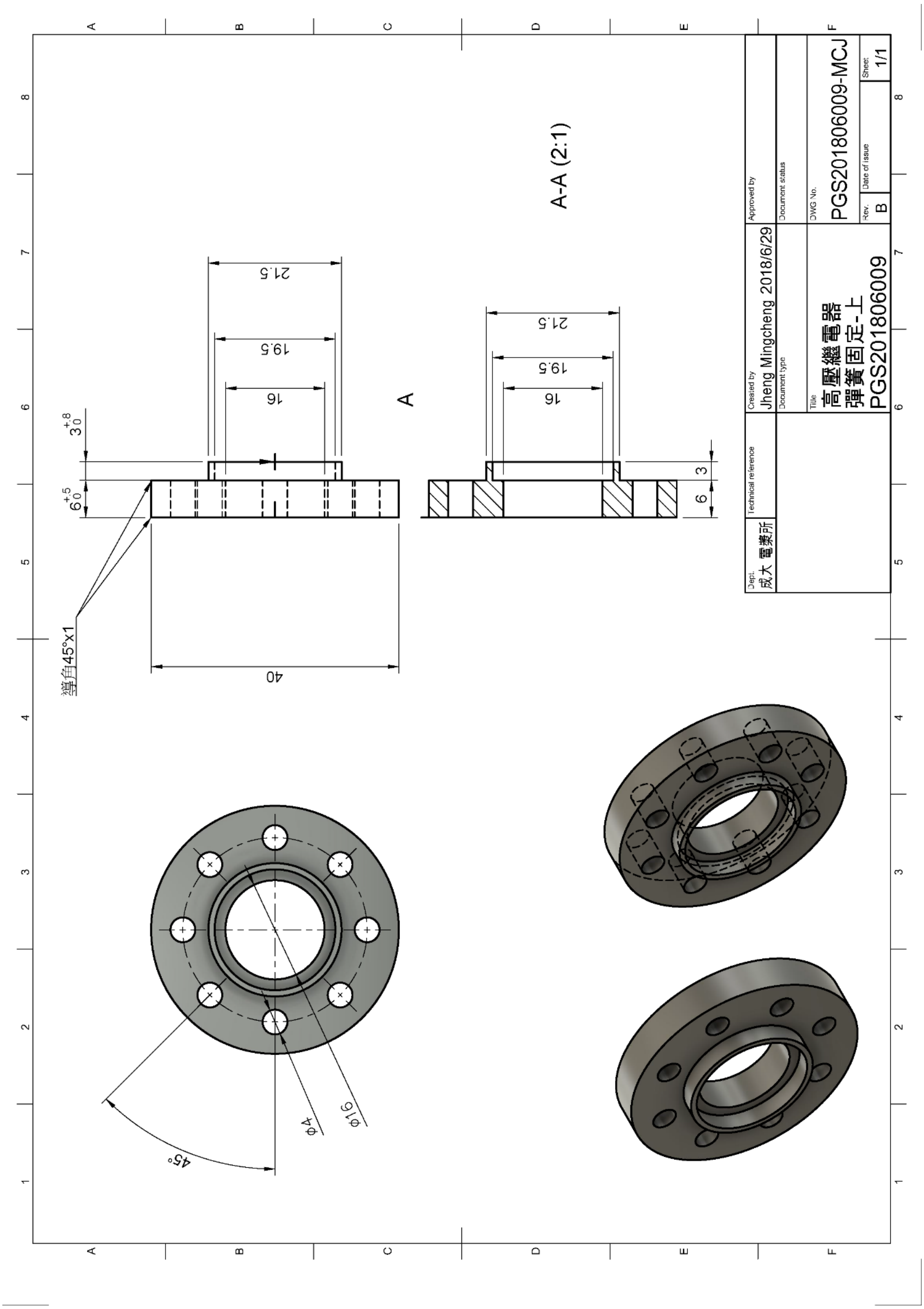

doi:10.6844/NCKU201900671

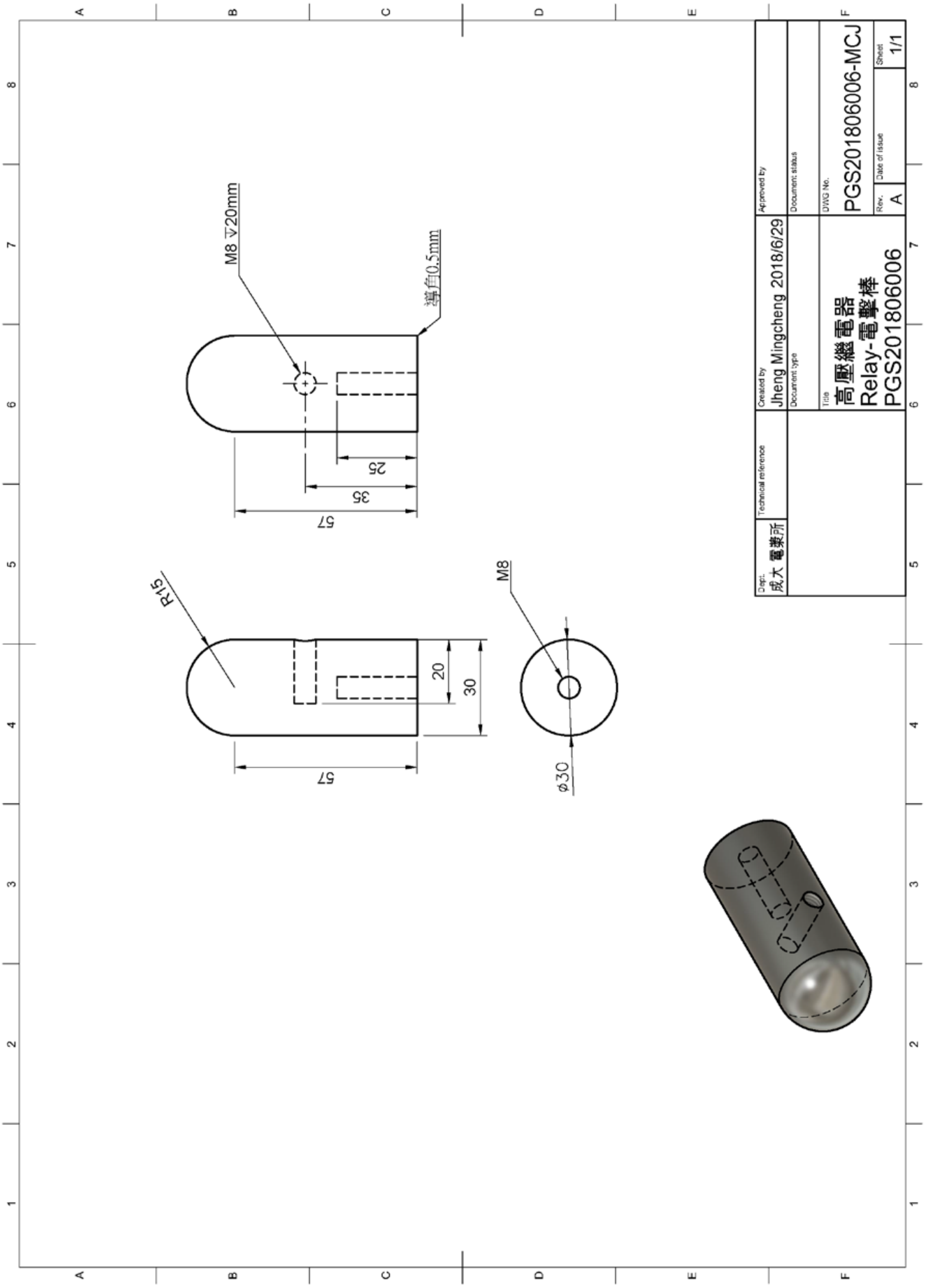

doi:10.6844/NCKU201900671

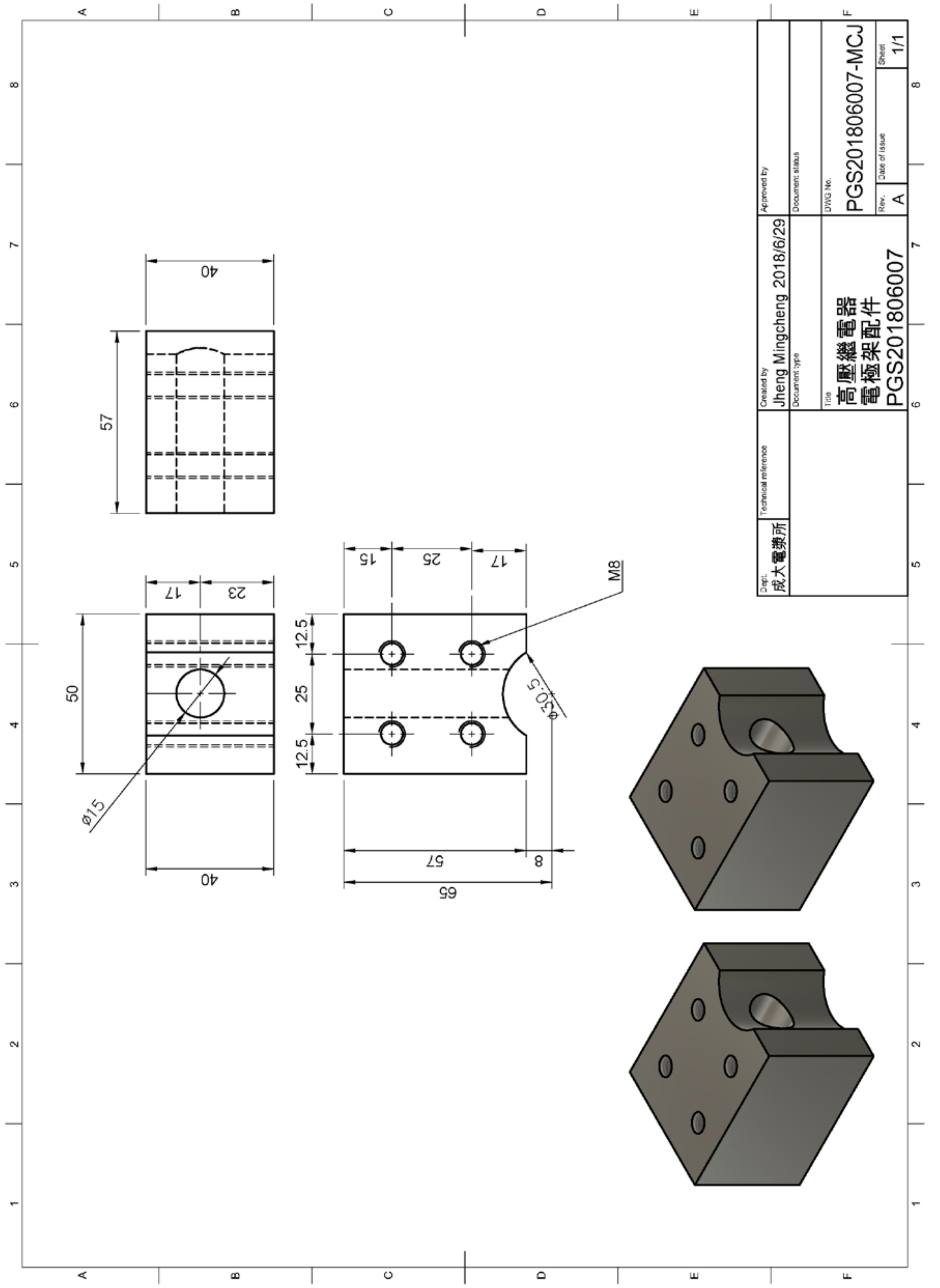

doi:10.6844/NCKU201900671

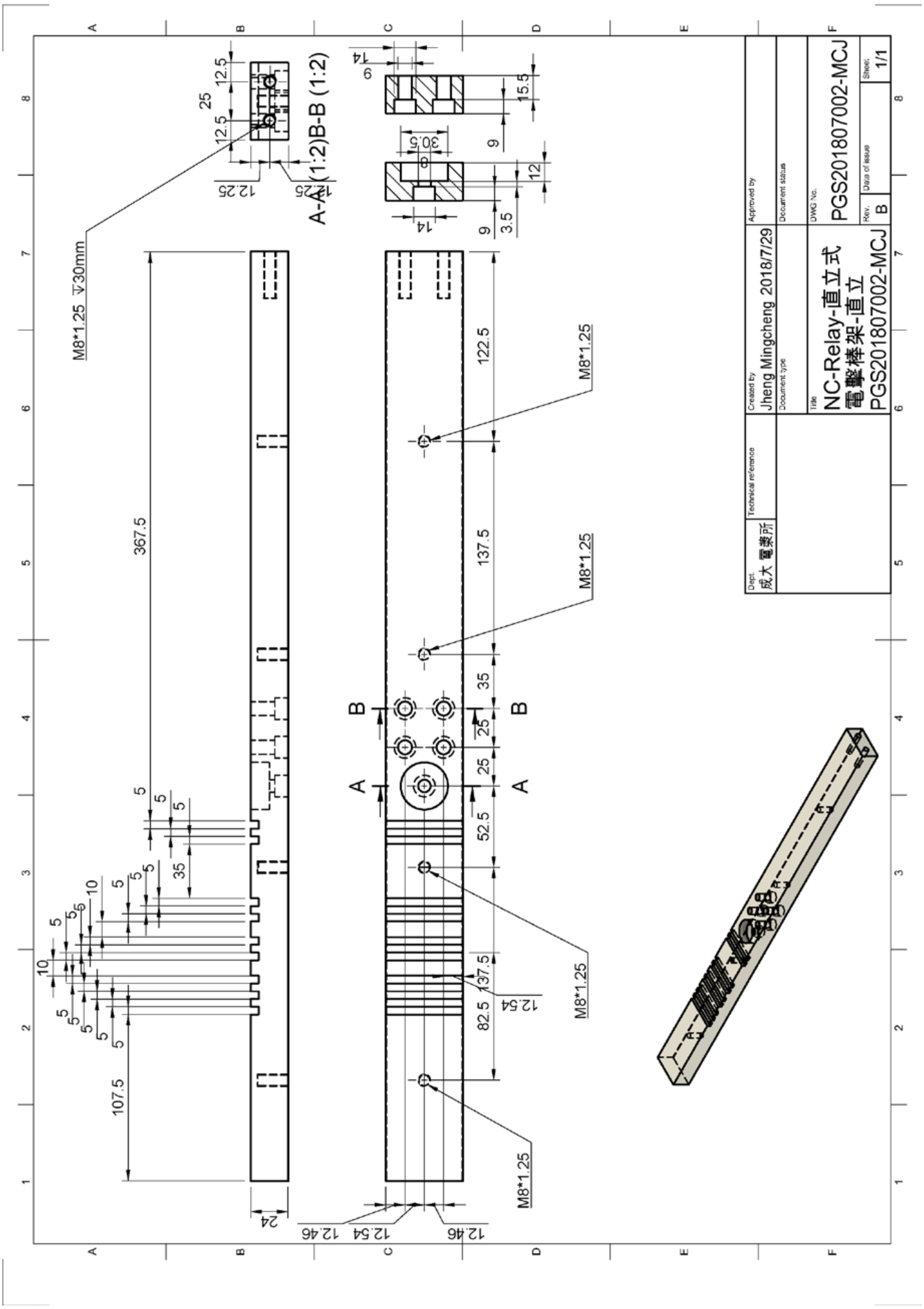

doi:10.6844/NCKU201900671

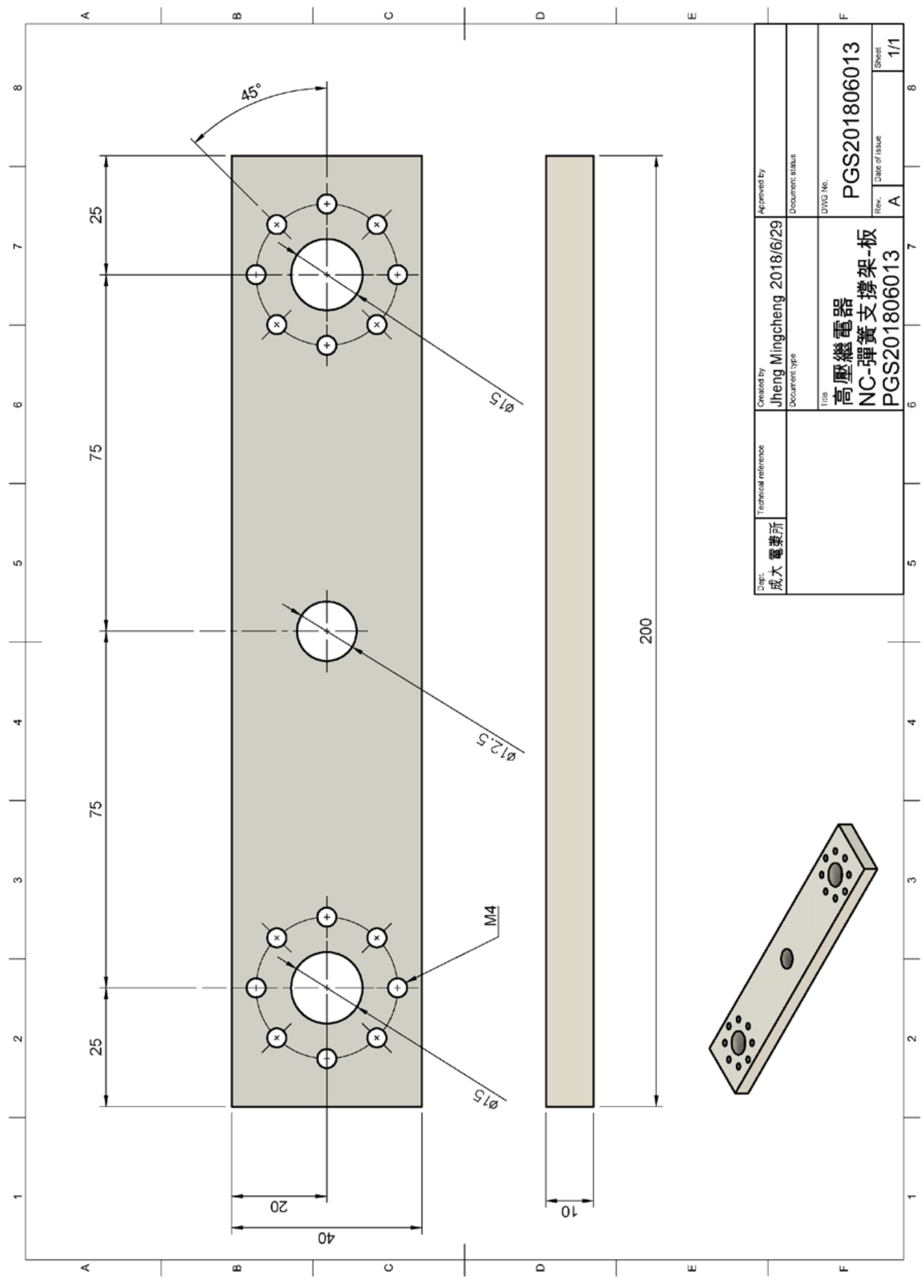

doi:10.6844/NCKU201900671

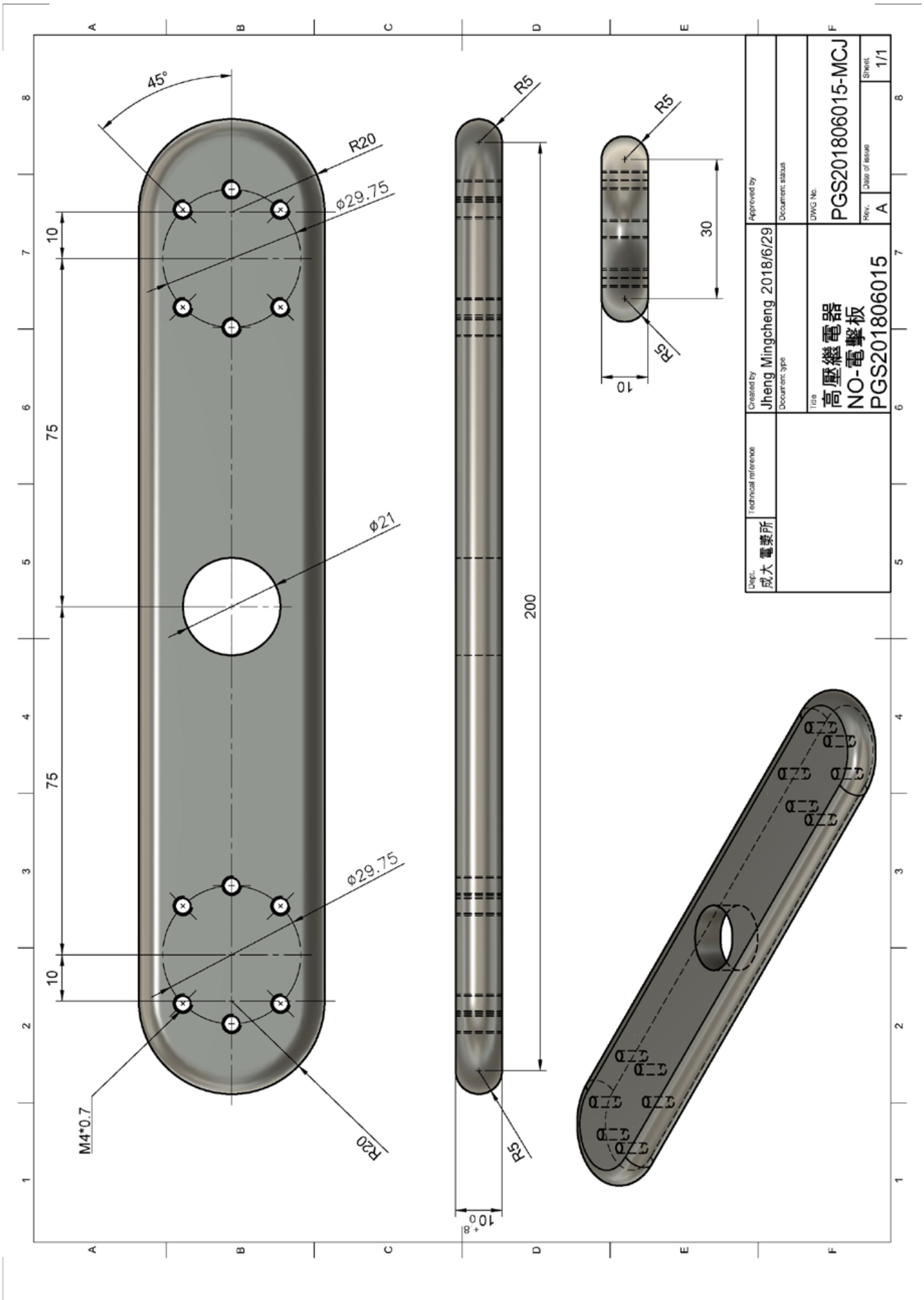

doi:10.6844/NCKU201900671

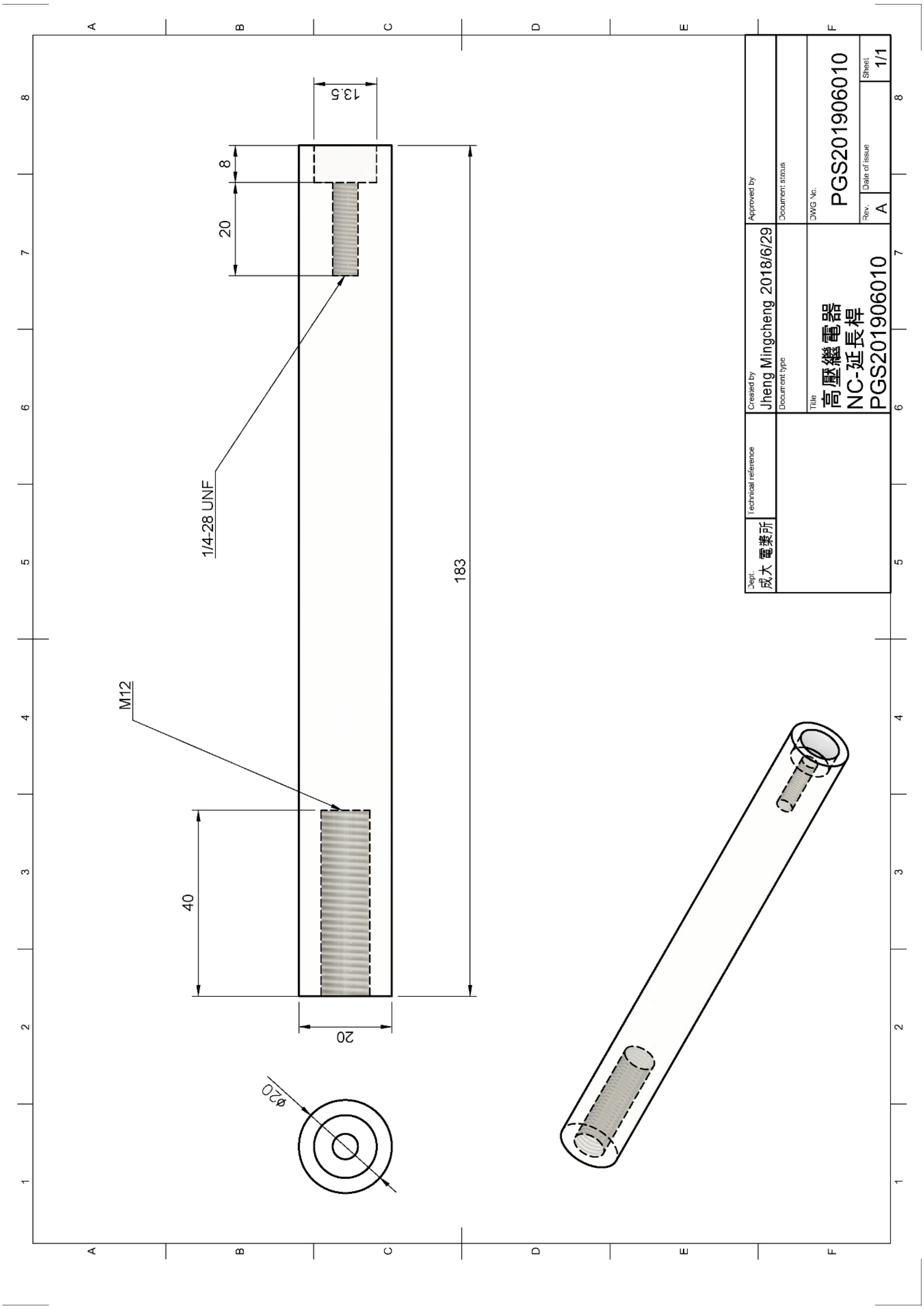

doi:10.6844/NCKU201900671

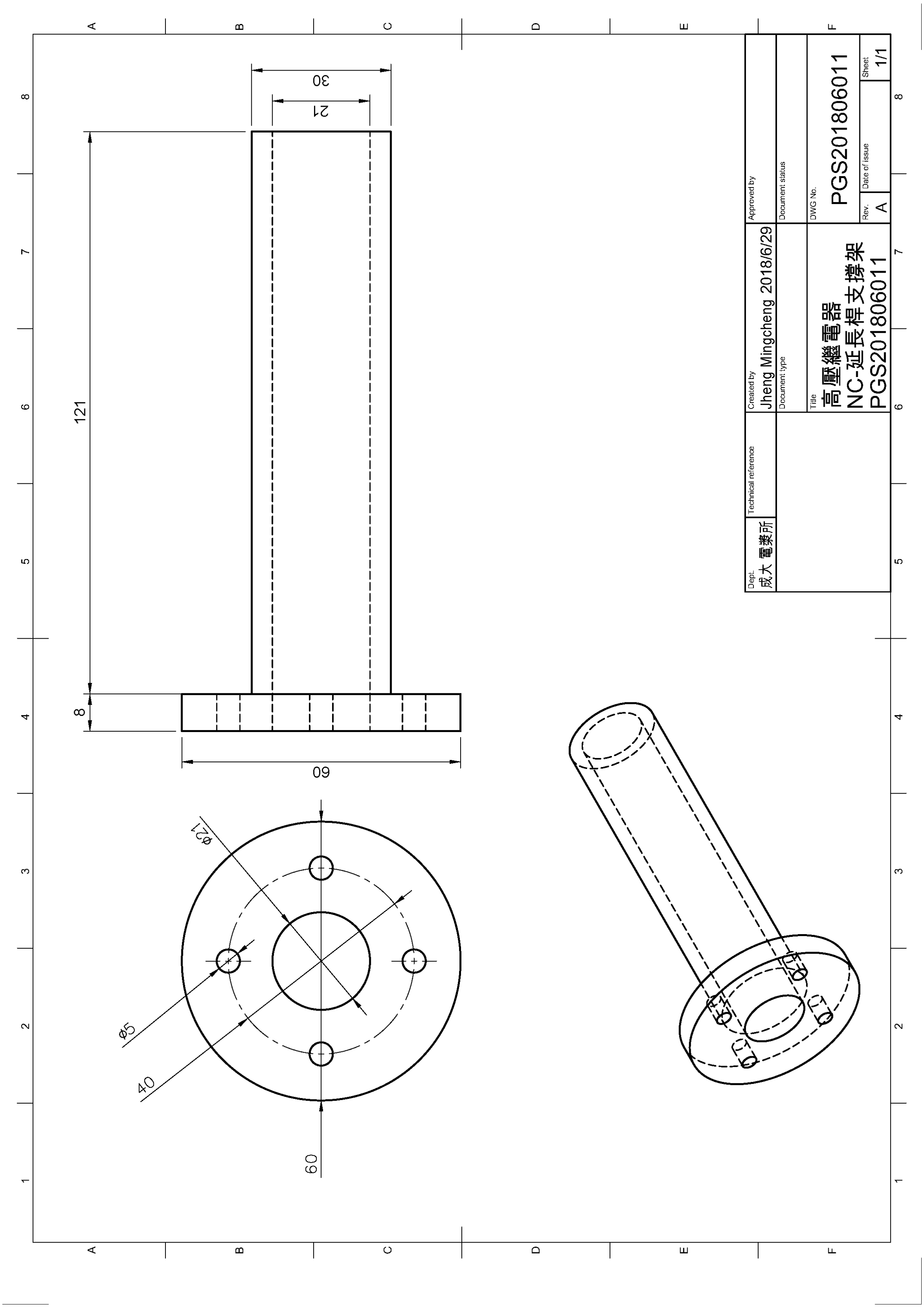

doi:10.6844/NCKU201900671

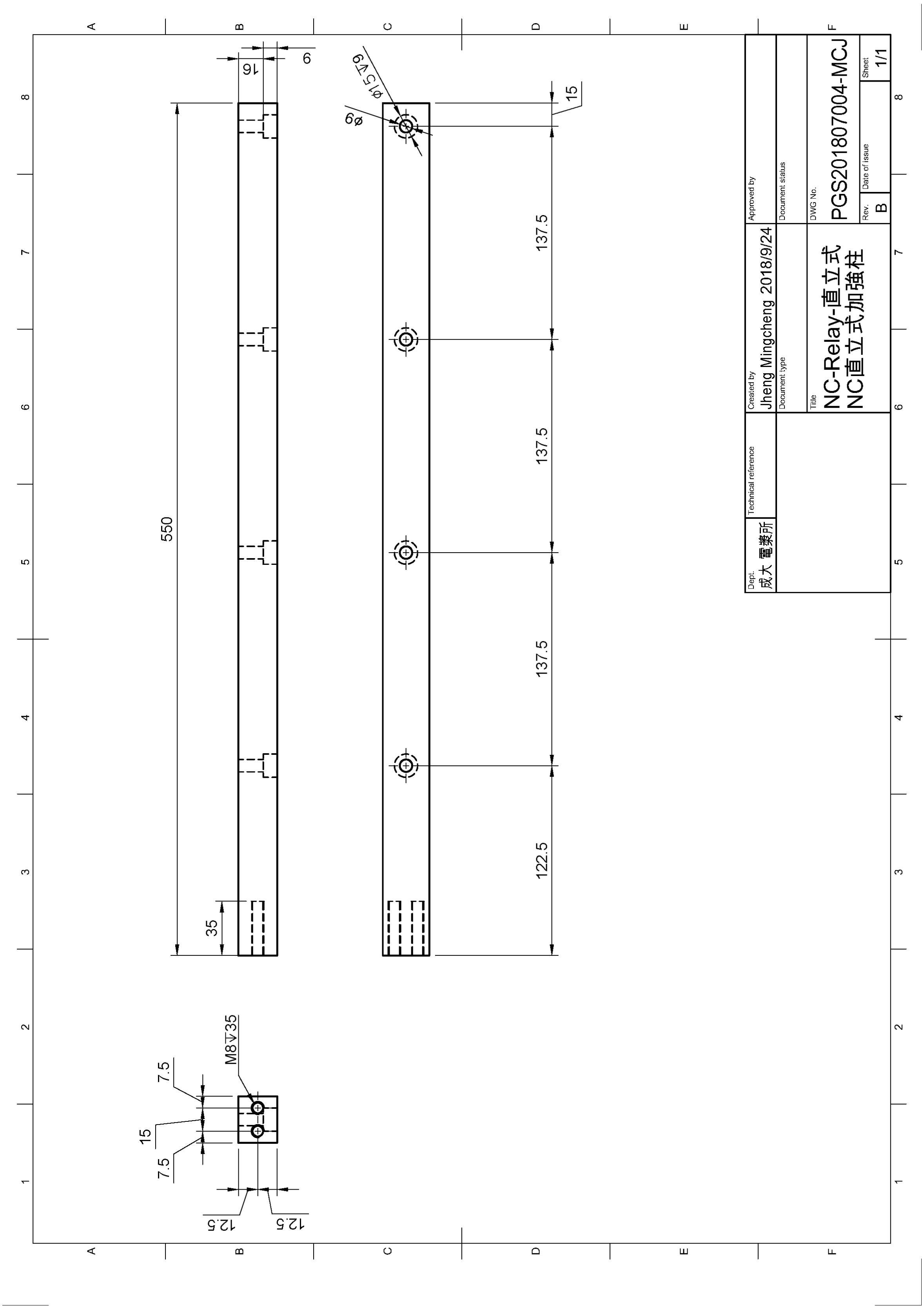

doi:10.6844/NCKU201900671

A4 Drawings of Trigatron

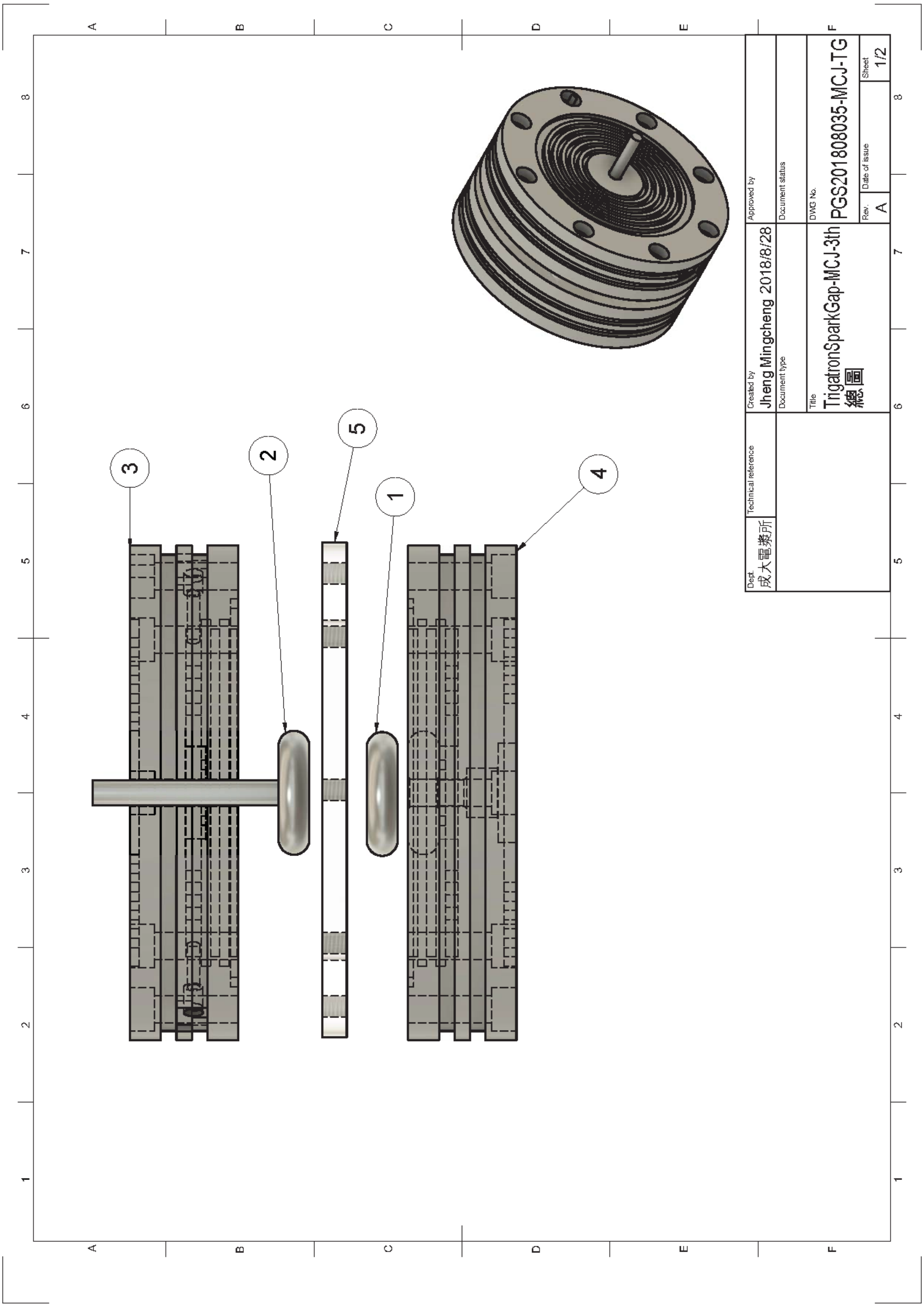

doi:10.6844/NCKU201900671

明細表					
項目	數量	工程圖圖號	中文名稱	英文名稱	材質
1	1	PGS201808030-MCJ-TG	電極M10	Electrode-M10	不鏽鋼
2	1	PGS201808031-MCJ-TG	電極M8	Electrode-M8	不鏽鋼
3	1	PGS201808032-MCJ-TG	上蓋	CaseUp	POM
4	1	PGS201808033-MCJ-TG	下蓋	CaseDown	POM
5	1	PGS201808034-MCJ-TG	隔板	Gasket-8mm	POM

Dept.	Technical reference	Created by	Approved by
成大電機所		Jheng Mingcheng 2018/8/28	
		Document type	Document status
		Title: TrigatronSparkGap-MCJ-3th 總圖	DWG No.
			Rev. A / Date of issue / Sheet 2/2

doi:10.6844/NCKU201900671

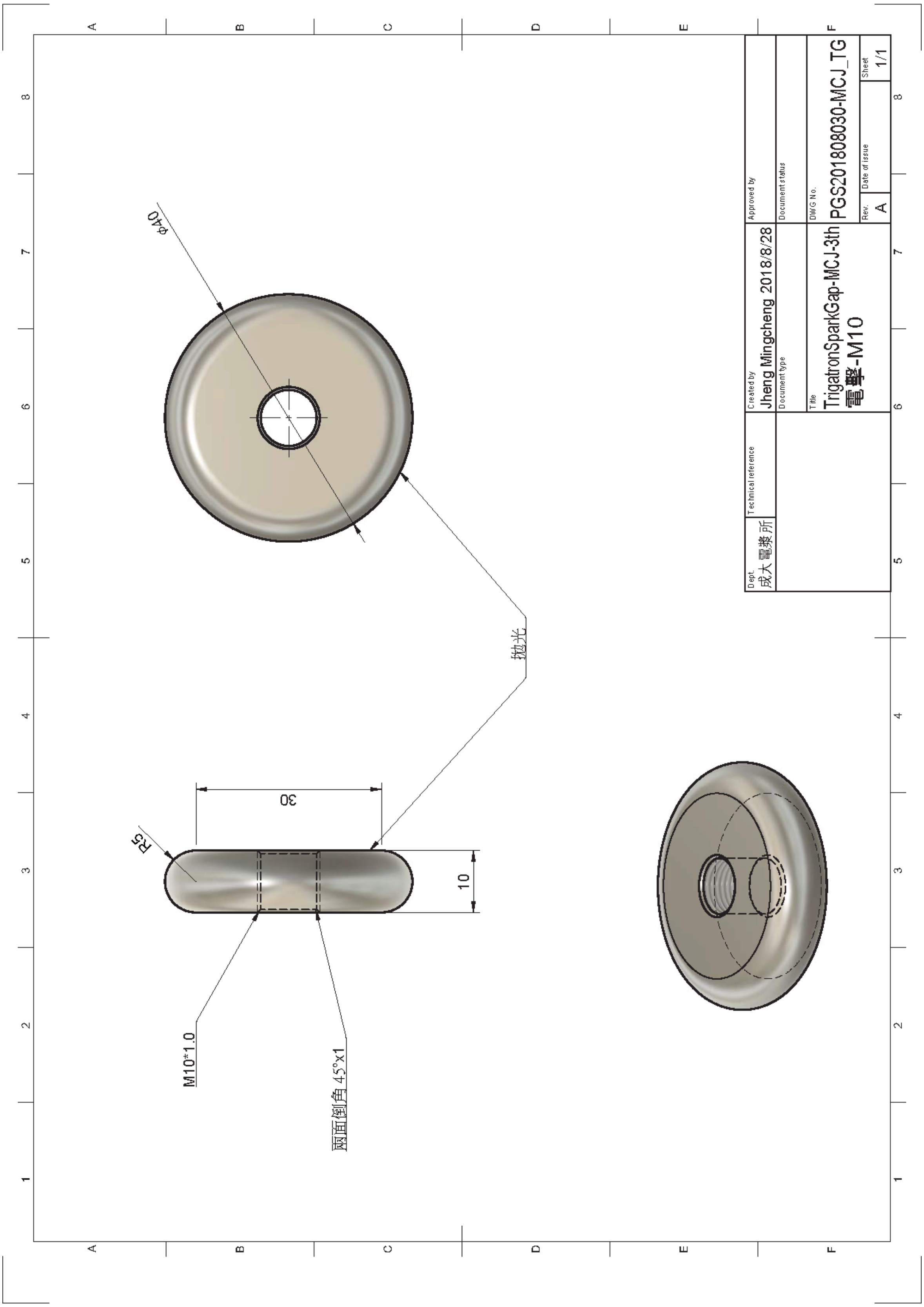

doi:10.6844/NCKU201900671

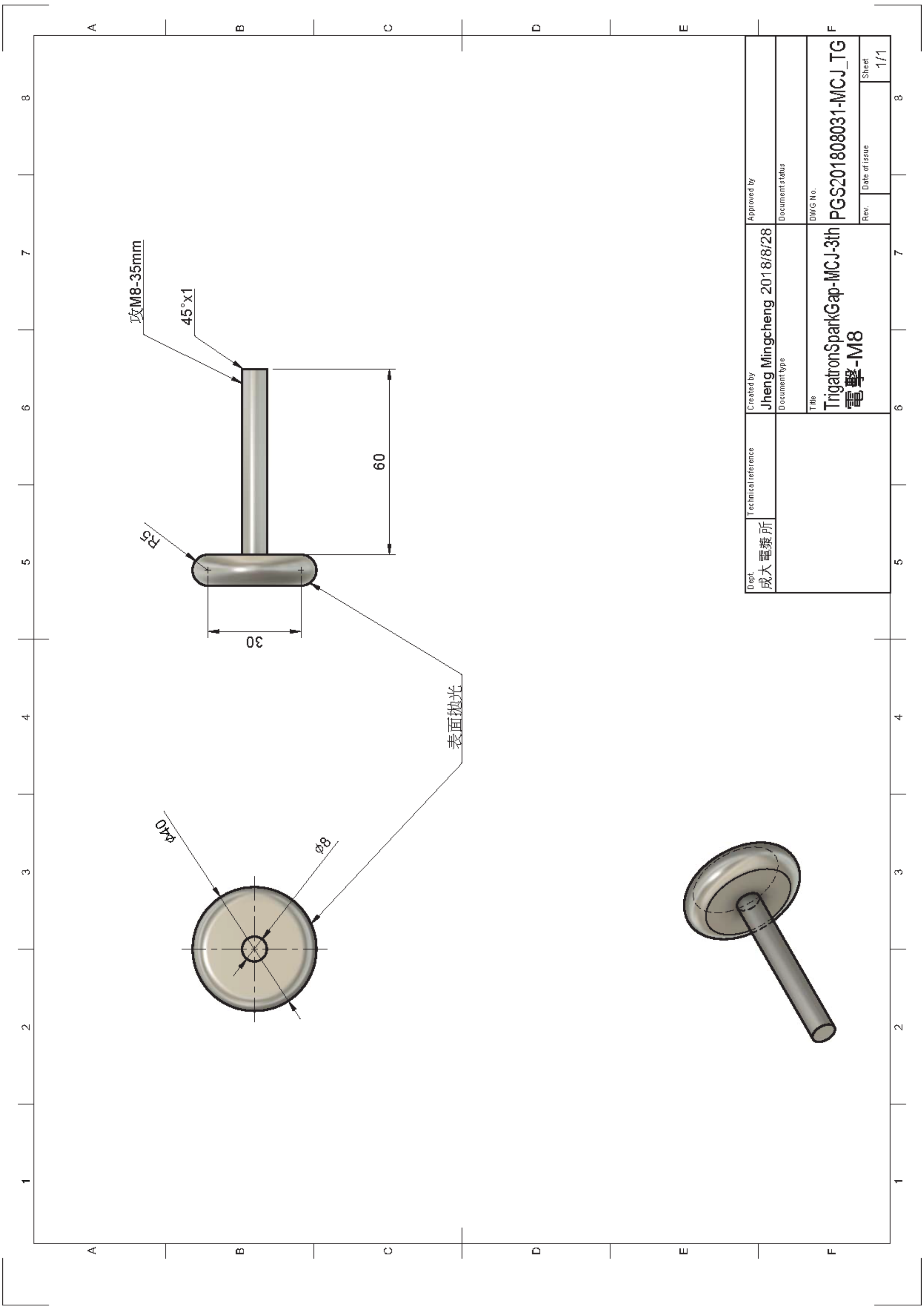

doi:10.6844/NCKU201900671

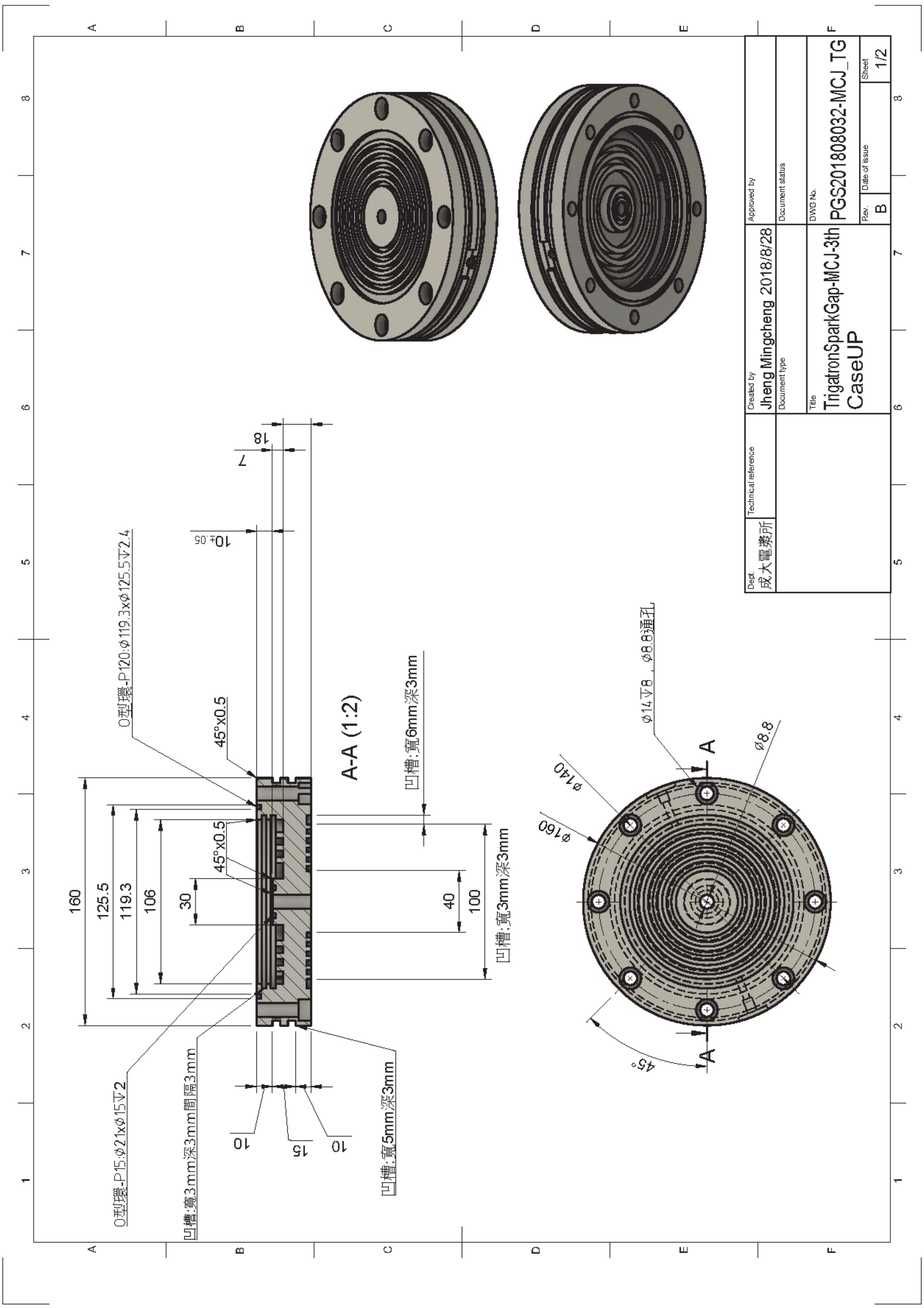

doi:10.6844/NCKU201900671

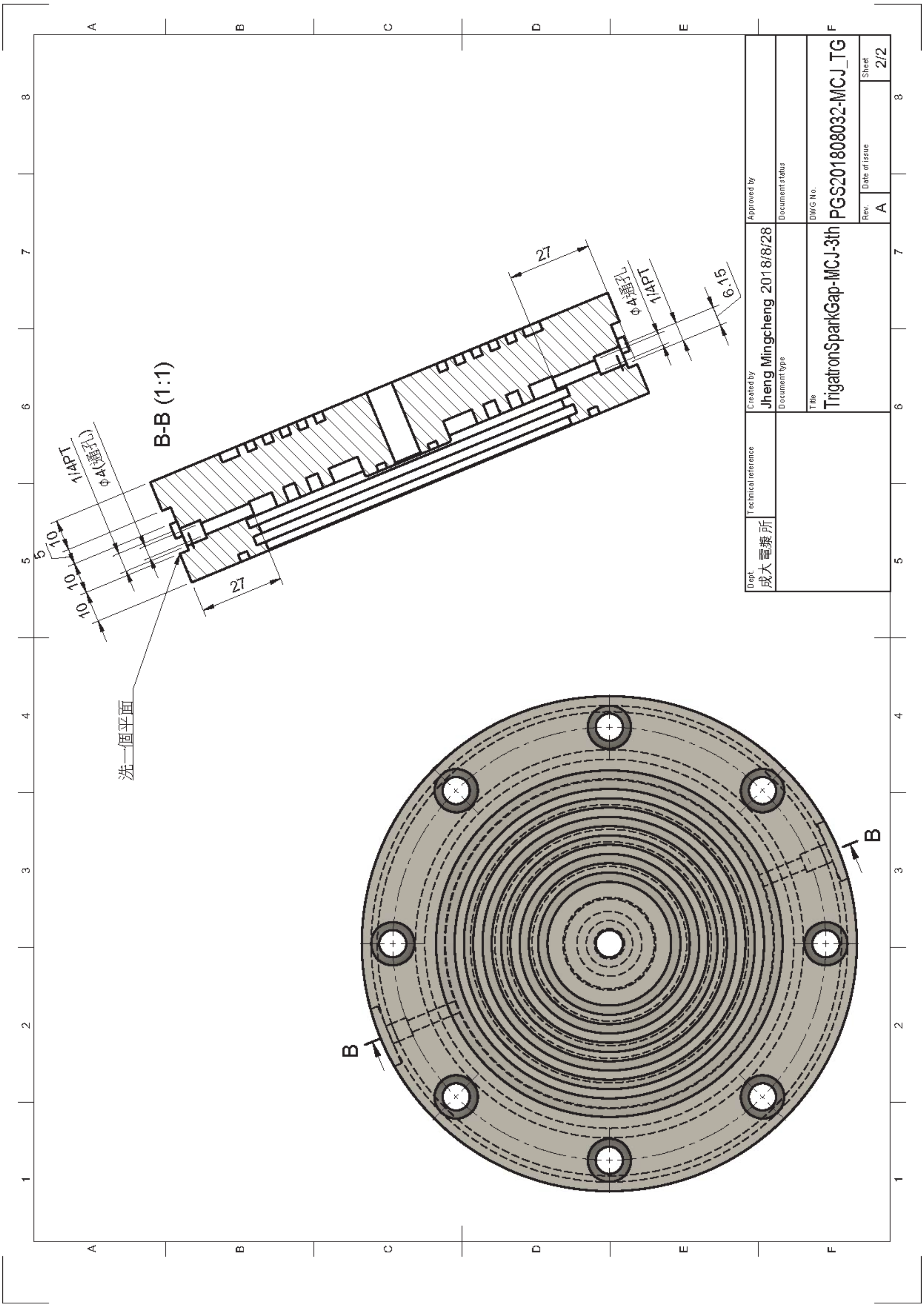

doi:10.6844/NCKU201900671

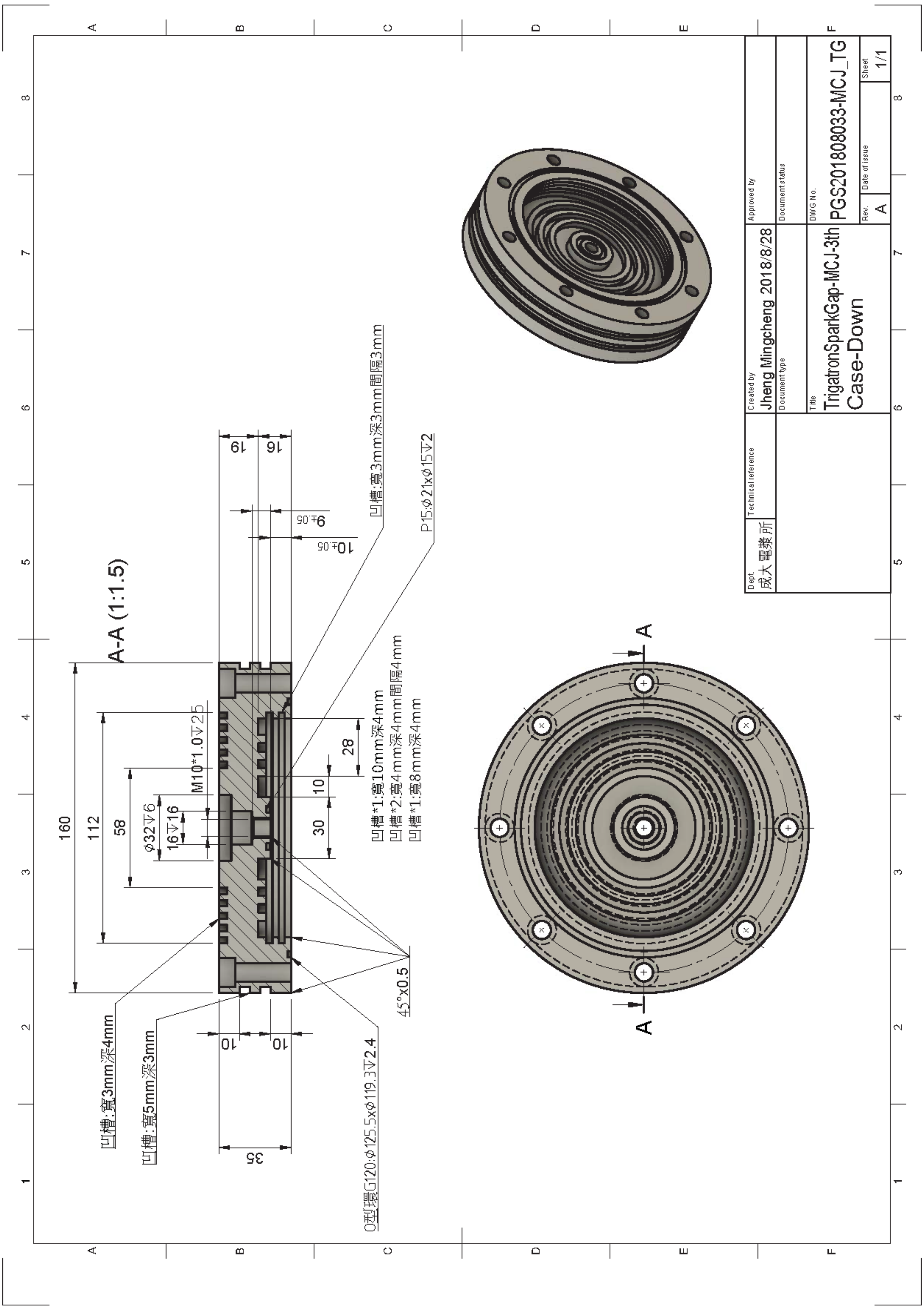

doi:10.6844/NCKU201900671

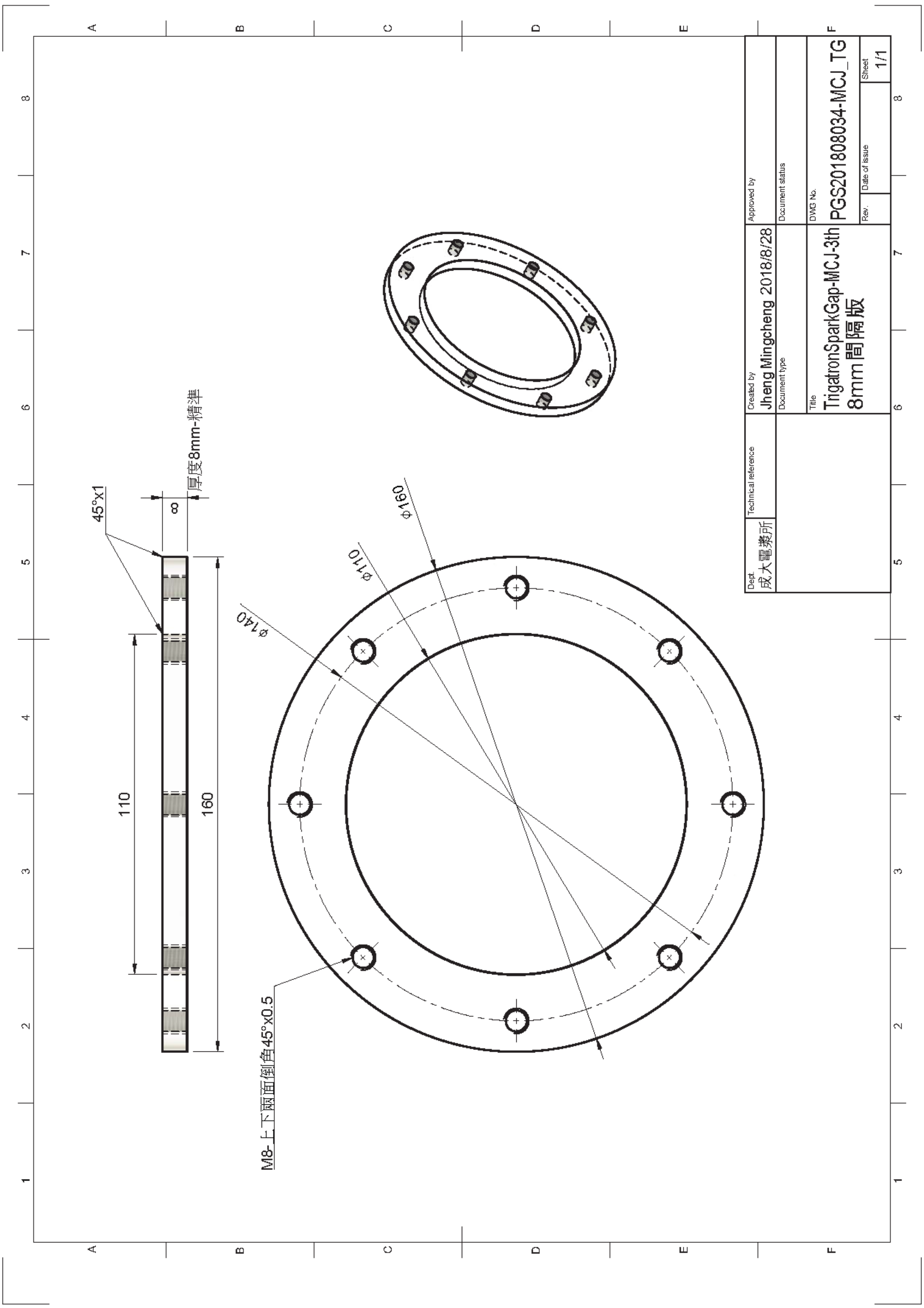

doi:10.6844/NCKU201900671

A5 Drawings of the round electrode

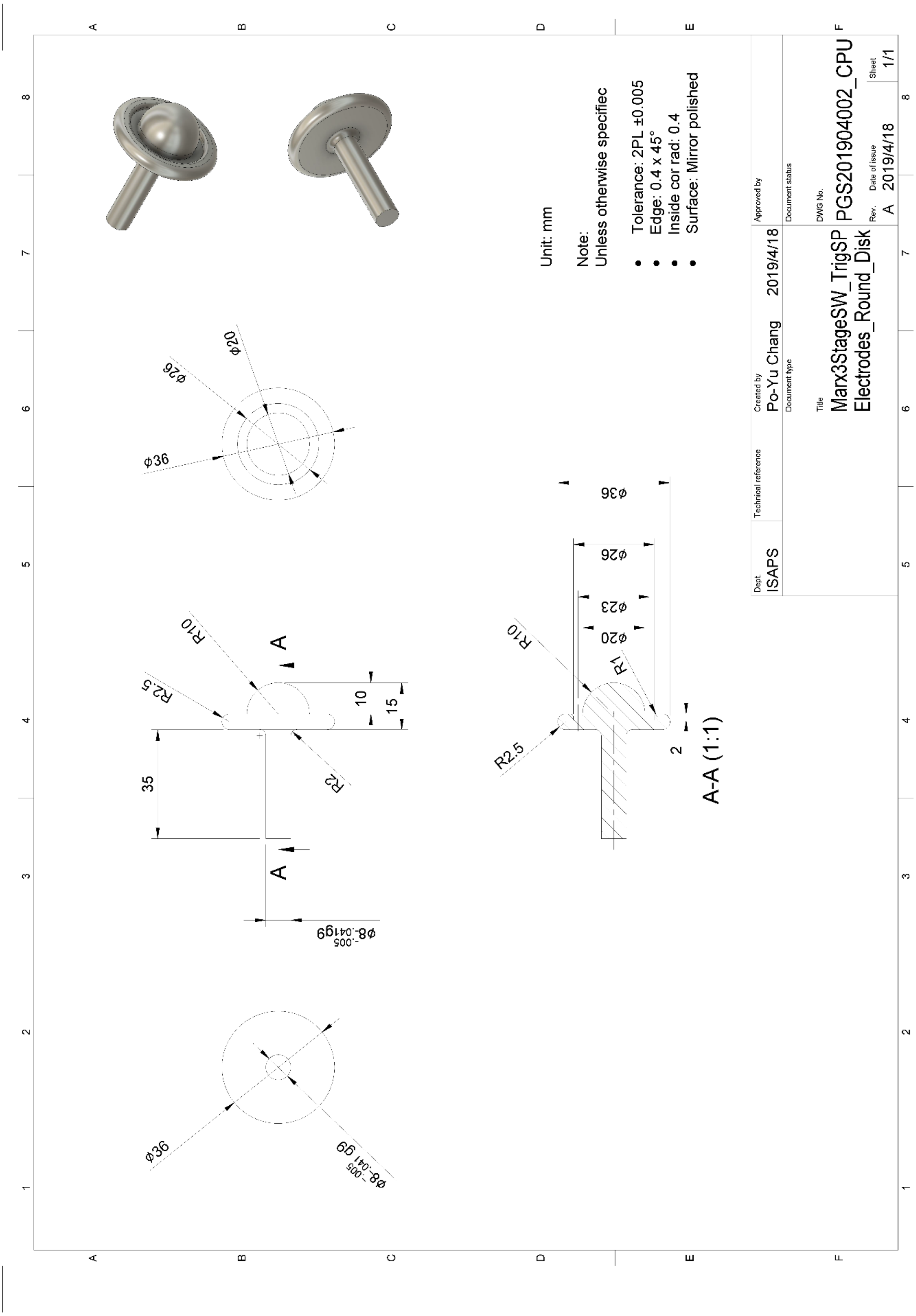

doi:10.6844/NCKU201900671

A6 Operation of the pulsed-power system

Step1: Setting two compressed air systems as shown in Chapter3.

Step1-2: Setting refers to Section 3.1, and get “the delay time” of each experiment.

Step1-2: Setting refers to Section 3.2, then you can change the state of relays according to the experimental state as shown in Table 2.2.

System status	States of the relay	
	NO relay	*NC relay*
Initial state	Open	Closed
Charging	Closed	Open
In experiment	Open	Open
End	Open	Closed

Table 2.2: The different situation of the south wing pulsed-power system working by each relay.

Figure A6-1: Low voltage power supply.

Figure A6-2: Pulse power controller.

doi:10.6844/NCKU201900671

Step2: Open the high voltage power supply (shown in Figure A6-3)

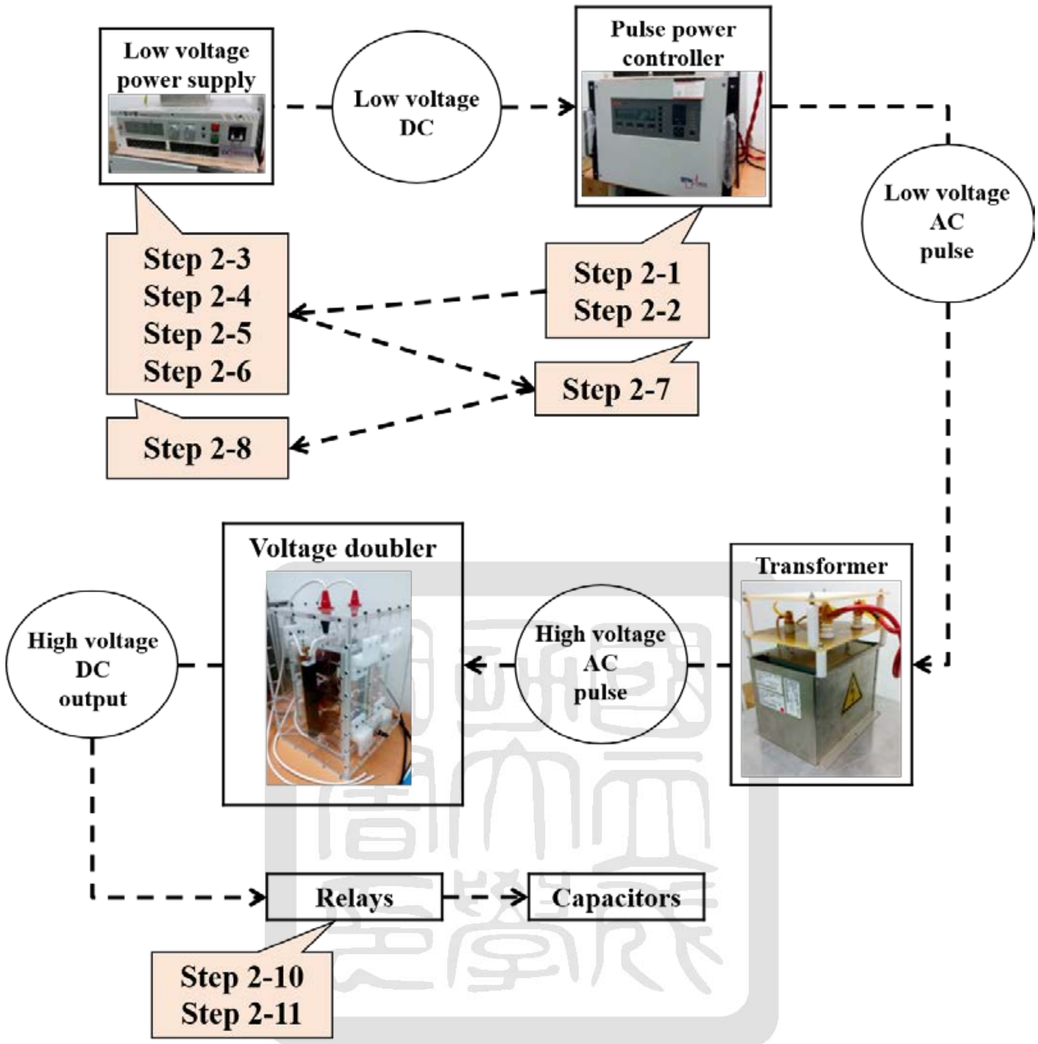

Figure A6-2: Open operation of the HVPS.

Step 2-1	Turn the main power of the pulse power controller as shown in Figure A6.2.
Step 2-2	Set the control panel of the pulse power controller for $T_{ON+} = 15$, $T_{ON-} = 15$, $T_{OFF+} = 35$, $T_{OFF-} = 35$.
Step 2-3	Turn the main power of the low voltage power supply as shown in Figure A6.1.
Step 2-4	Switch counterclockwise to the voltage and current of the low voltage power supply as shown in Figure A6.1.
Step 2-5	Press "the Power Output" of the low voltage power supply, as shown in Figure A6.1.
Step 2-6	Switch clockwise a quarter turn of the current of the low voltage

doi:10.6844/NCKU201900671

	power supply as shown in Figure A6.1.
Step 2-7	Press ‘‘the Power Output’’ of the pulse power controller.
Step 2-8	Switch clockwise turn of the voltage of the low voltage power supply until the voltage you needed.
Step 2-9	Confirm the required experimental status as shown in Table 2.2.
Step 2-10	Change the state of the NO relay to charge capacitors.
Step 2-11	After changing capacitors, controll relays to cut off circuit refers to the experimental status as shown in Table 2.2.

Step3: Close the high voltage power supply

Step 3-1	Press the ‘‘Power Output ’’ of the pulse power controller as shown in Figure A6.2.
Step 3-2	Press the ‘‘Power Output ’’ of the high voltage power supply as shown in Figure A6.1.
Step 3-3	Press the ‘‘Main Power’’ of the pulse power controller as shown in Figure A6.2.
Step 3-4	Switch counterclockwise to the end of the voltage and current of the pulse power controller as shown in Figure A6.2.
Step 3-5	Turn off ‘‘Main Power’’ of the high voltage power supply as shown in Figure A6.1.

doi:10.6844/NCKU201900671

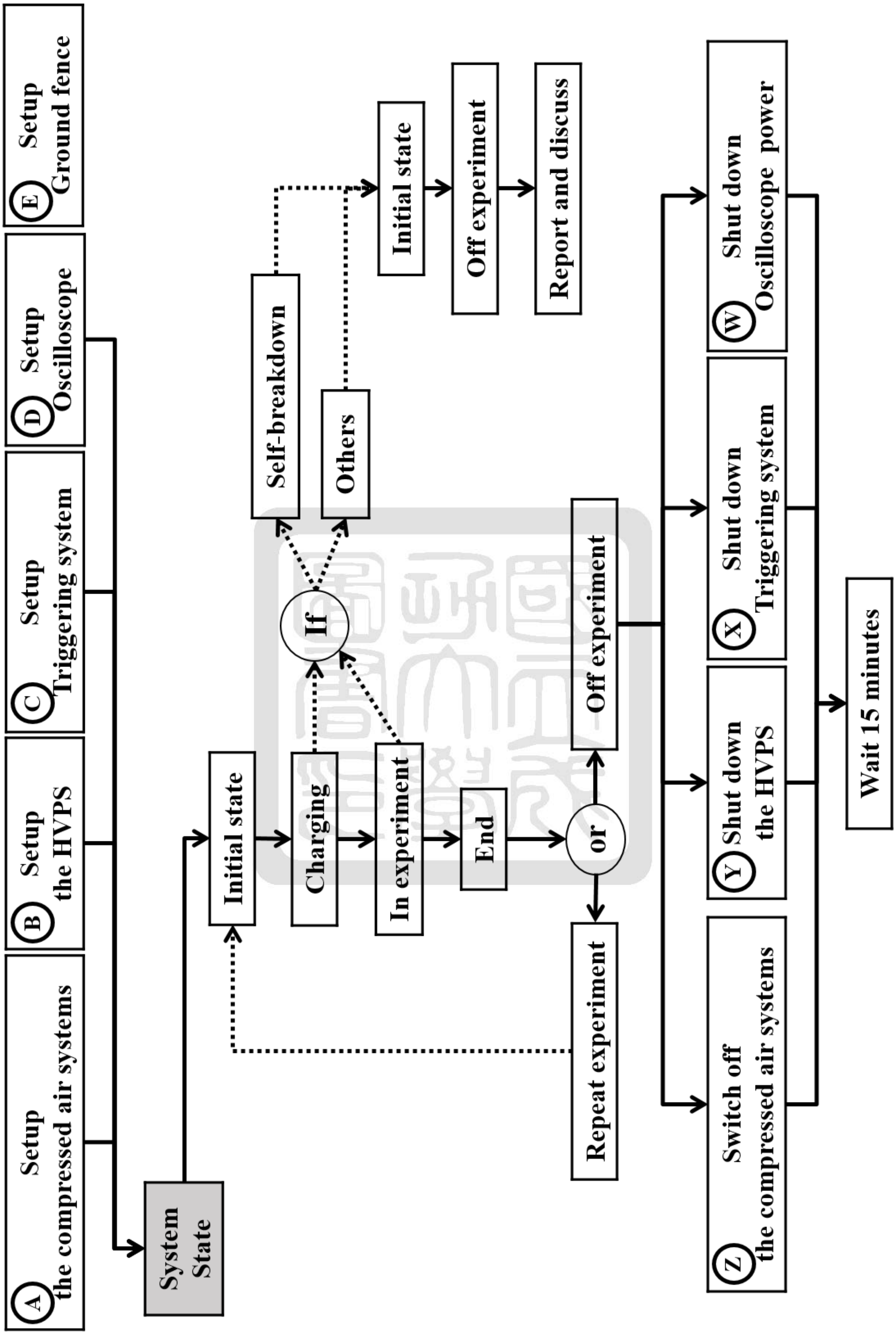

Figure A7-1: The fundamental operation of the pulsed-power system.

doi:10.6844/NCKU201900671

A7 Circuit diagram of the trigger pulse generator

公司名稱	地址	電話
盛新配管材料股份有限公司		
欣陸興業有限公司	http://www.neoway-chem.com	
威正塑膠有限公司	台南市仁德區忠義路 662 號	06-2700852
嘉興實業社	台南市安南區長和路一段 949 巷 320 之 16 號	06-2627338
三峰鐵工廠	嘉義市民雄鄉文隆村鴨母坔 1-107 號	05-2207466
景頎科技	台南市永康區大灣路 1102 巷 17 弄 43 號	06-2071430
三川金屬有限公司	台南市永康區中正南路 70 號	06-2827123
財成五金行	台南市永康區永大路二段 980 號	06-2055939
順鴻空油壓五金行	台南市永康區國光六街 51 號	06-2710715
金全通鋁材有限公司	台南市歸仁區和順路一段 296 號	06-2721167
日源倉儲設備有限公司	台南市東區農路 805 號(營業處)	06-2345577
台南電池	台南市中西區成功路 307 號	06-220-3838
大億水泥園藝行	台南市東區東門路三段 34 號	06-2670969
資峰塑膠有限公司	台南市永康區中正南路 416 號	06-2420594
大海彈簧	台南市中西區民族路三段 214 號	
邁提斯企業有限公司	露天拍賣: maddishshop2014	05-233-3663
UCI 電子	露天拍賣: mada1283	

實驗室之設施設備	購買公司/委託製造
Rail-gap switch	三峰鐵工廠
Marx generator	三峰鐵工廠/景祈科技股份有限公司
Trigatron	威正塑膠有限公司
塑膠螺絲/工程塑膠	嘉興實業社
空壓元件	順鴻空油壓五金行
高壓電源供應器之設備架	金全通鋁材有限公司
接地網的角鋼支撐架	日源倉儲設備有限公司

doi:10.6844/NCKU201900671

Equipment	Modle	Specification	
High voltage probe	HVP40	1000X Output resistance: 1000 MΩ DC to 75 MHz Max peak voltage: 40 kV DC, 20 kV peak pulse	
Current monitor	301X	Sensitivity: 0.01 Volt/Ampere +1/-0% Output resistance: 50 MΩ Maximum peak current: 50 kA Maximum rms current: 400A	
High power wire wound resistor		Resistance	Power
	TE1000B10RJ	10 Ω	1000 W
	TE1500B100RJ	100 Ω	1500 W
	TE1500B1K0J	1 kΩ	1500 W
Coaxial Cable	URM67		
Pneumatic Roundline Cylinder	NCMKB075-0400S	Work pressure: 25~250 PSI Piston speed: 50 to 500 mm/sec	

doi:10.6844/NCKU201900671

A8 Folder position

Experiment	**Location: Experiment//**
Discharge of the capacitors and thr rail-gap switch	
Marx generator	20181126_TPG_24V_inMarx&Marx(BandC)output
	20181127-Mart B&D
	20181128-Mart B&ACD
	20181129-Mart OUTPUT
One-stage discharge	20181227_one_stage
Two-stage discharge	20190102_one_stage
	20190116_two_stage_L&H_Current_with_tape
1~2 stage	20190117_trigger_one-stage
One-stage discharge	20190214_One-stage_PS500W_3_Part-test
	20190215_one-stage_衰減器
Two-stage discharge	20190218_two-stage_withTwoRogroski
Test with the south wing	
One-brick discharge	20190307_one-brick_discharge_in_gundBox
Two-brick discharge	20190308_two-brick_discharge_in_gundBox
3-brick discharge	20190311_Three-brick_discharge
	20190312_three-brick_discharge
	20190314_3-brick_discharge
4-brick discharge	20190315_for-brick_discharge
5-brick discharge	20190319_5-brick_discharge

doi:10.6844/NCKU201900671

South wing pulsed-power system	
One-brick discharge	20190412_1-brick_discharge_via_chamber
3-brick discharge	20190415_3-brick_discharge_via_chamber
5-brick discharge	20190417_5-brick_discharge_via_chamber
Marx output	20190423_MarxOutput
	20190424_MarxTest
	20190429_Marx_20kVoutput
	20190507_Marx_2-3-4-Round_electrode
Rail-gap switch	20190509_Short_Rail_gap_electrode
	rail gap switch 耐壓測試
Negative output of the south wing	20190715_5-brick_負高壓_5M&500ohm
	20190715_5-brick_負高壓_5M&500ohm-New-rail-gap

doi:10.6844/NCKU201900671

A9 Picture of the discharge

Figure A10.1: Before discharge.

doi:10.6844/NCKU201900671

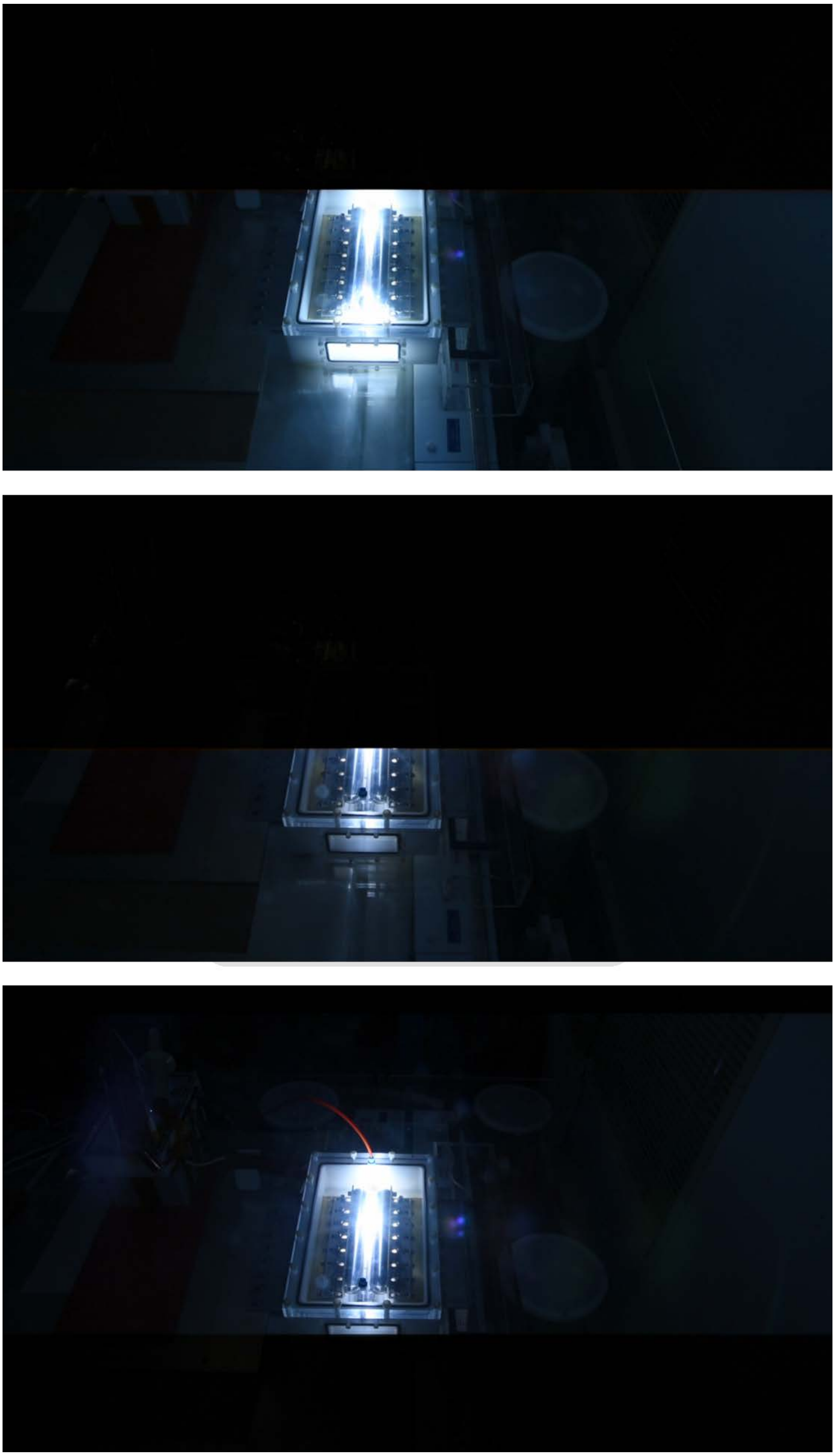

Figure A10.2: One of discharge test.

doi:10.6844/NCKU201900671

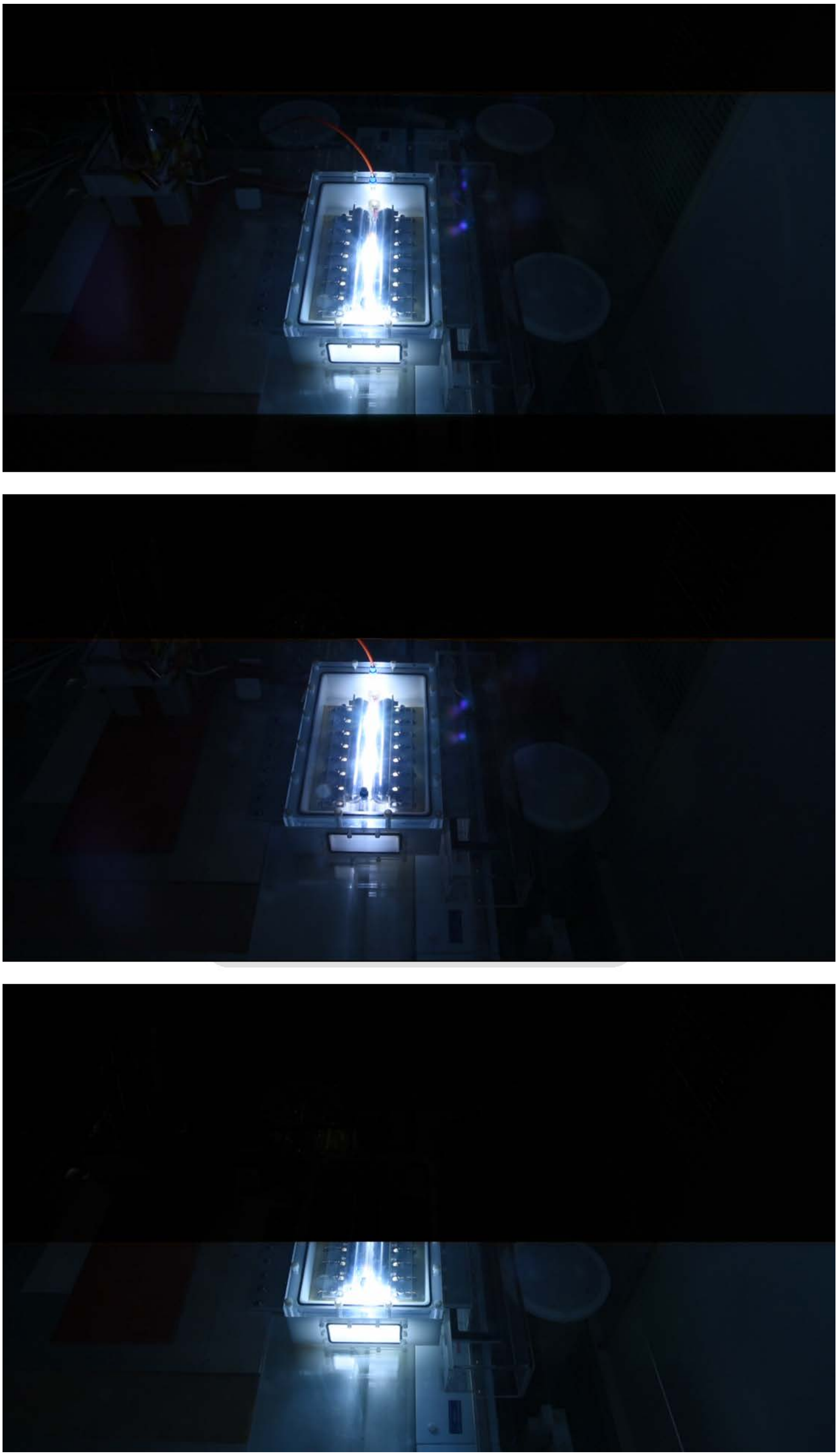

Figure A10.3: One of discharge test.

doi:10.6844/NCKU201900671

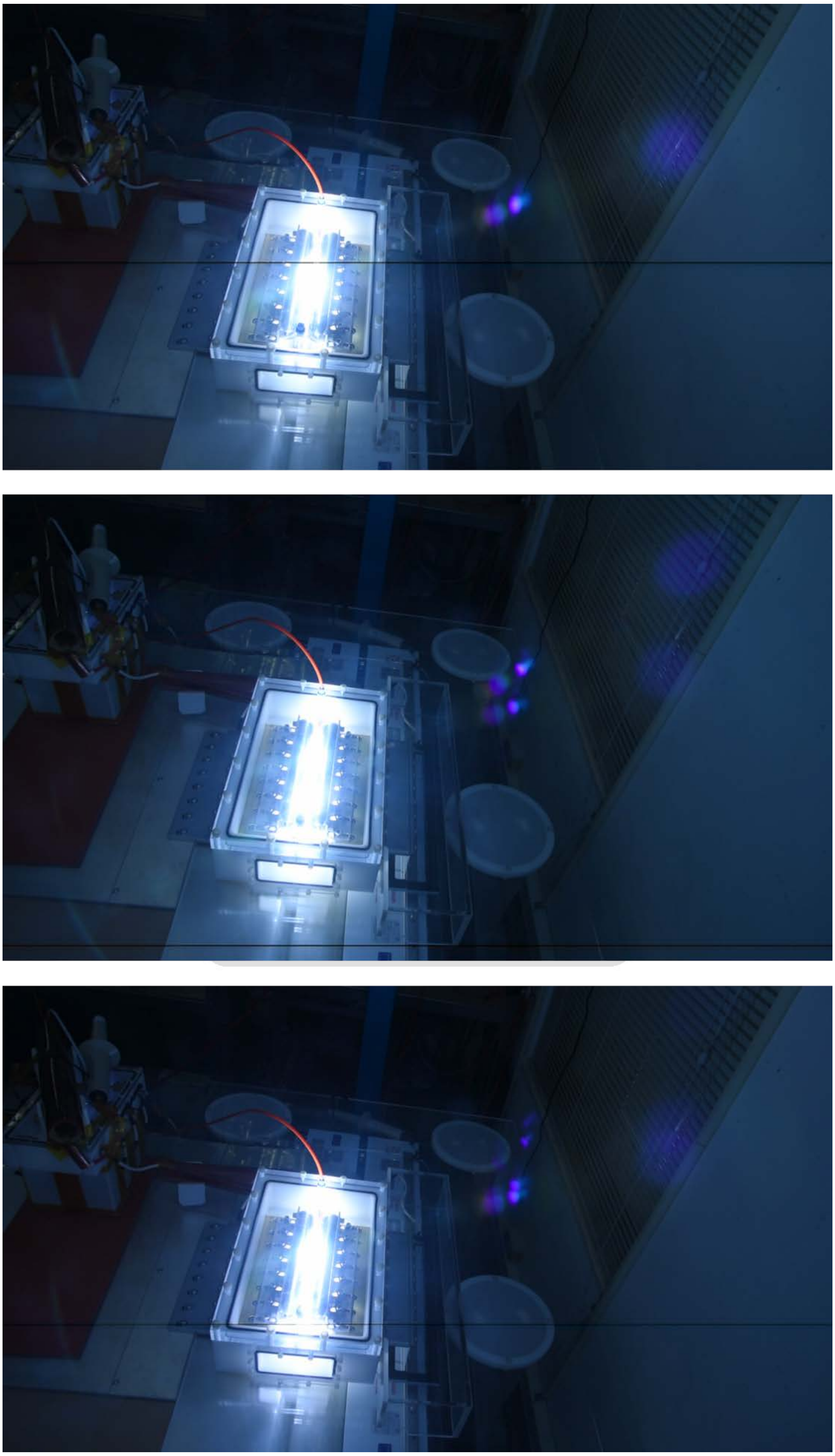

Figure A10.4: One of discharge test.

doi:10.6844/NCKU201900671